Active surge control of centrifugal compression systems

Theoretical and experimental results of drive actuation

Bjørnar Bøhagen

Active surge control of centrifugal compression systems

Theoretical and experimental results of drive actuation

Thesis for degree of philosophiae doctor

Trondheim, June 2007

Norwegian University of Science and Technology
Faculty of Information Technology, Mathematics and Electrical Engineering
Department of Engineering Cybernetics

NTNU
Norwegian University of Science and Technology

Thesis for degree of philosophiae doctor

Faculty of Information Technology, Mathematics and Electrical Engineering
Department of Engineering Cybernetics

ISBN 978-82-471-2761-2 (printed ver.)
ISBN 978-82-471-2775-9 (electronic ver.)
ISSN 1503-8181
ITK Report 2007-2-w

Thesis at NTNU, 2007:126

Summary

This thesis addresses modeling and active surge control of a simple compression system, using only the drive system of the compressor for actuation. Theoretical results are validated by experiments on a test rig that was built as a part of this work. Control laws are derived in two stages. First all system states, such as pressure mass flow and impeller speed, are assumed as available signals. All the resulting control laws require feedback from mass flow. However, transient measurement of this variable is not available. Observers are therefore developed for this purpose.

The laboratory that was build and from which experimental data are gathered, consists of a compressor, plenum volume, control valve, in between ducting and drive system. The centrifugal compressor stage compresses air from ambient conditions, discharging into a duct connecting compressor and plenum. The plenum discharges over the valve. The drive system consists of a electric motor and drive.

Controllers and observers are derived on the basis of the so-called variable speed Greitzer model. This model contains the compressor map, which in many cases involves some uncertainty. Uncertainty can be caused by varying ambient conditions and change of map due to wear and tear. For this reason it was investigated whether it was possible to express the compressor map by measurements. It is shown that this can be done if one has a sufficient length of duct upstream or downstream the compressor.

Two control strategies are presented. One considers the impeller speed and the other considers applied torque as control variable. As previously mentioned, all control laws require feedback from mass flow, and must be combined with an observer for implementation. Furthermore, torque control laws involve the compressor map. In view of modeling results, this map can be implemented by a model or a measurement in the case of sufficient duct lengths. Experimental validation of control laws indicate that torque control

is better than speed control for the setup in question, in terms of it ability to stabilize surge. The reason for this can be explained by the internal loop of the drive system, offering a faster response for torque than for speed control. It is shown by experiments that torque control can extend mass flow range of the machine by more than 15 to 20 percent relative to the point for which surge occurs for the open loop system. These numbers corresponds to two different impeller speeds, where 20 percent increase was achieved at a lower impeller speed than that of 15 percent. It is also shown experimentally that speed control is able to stabilize a operating point for which surge occurs for the open loop. However, this strategy was not able to considerably increase the operating range

Three type of observes are derived. These are reduced order observers for mass flow, pressure and mass flow observers, and pressure, mass flow and impeller speed observers. Furthermore, the observers vary among themselves in the way one compensates for the compressor map, model or measurement. The main purpose of these observes is to offer a estimate of mass flow, so that the derived control laws can be implemented. However, these observers can also offer disturbance rejection for pressure and impeller speed measurements. Reduced order observers for mass flow and observers for pressure and mass flow are validated experimentally. It is shown that the mass flow estimates are within an accuracy of 10 percent compared to measured mass flow, and that the pressure estimates offers disturbance rejection. The observers are derived on the basis of the compression system model, not taking the specific control law into account, and can therefore be used for any control law derived on the basis of the Greitzer model.

Contributions in work leading to this thesis are considered to be:

- Planning and building of a compression system laboratory for active surge control by means of drive system.
- Extending the Greitzer model by introducing a measurement for the compressor map. Theoretical derivation and experimental validation.
- Extending a previously presented active surge control law, when considering impeller speed as control variable. Theoretical derivation, stability analysis and experimental validation.
- Deriving novel control laws for active surge control when considering

impeller drive torque as control variable. Theoretical derivation, stability analysis and experimental validation.

- Deriving novel observers for variable speed Greitzer model. Theoretical derivation, stability analysis and experimental validation.

The work contained in this thesis has partially been published in six papers:

- Bøhagen B. and J.T. Gravdahl, Control laws for active surge control of centrifugal compressors using drive torque, accepted for publication in Automatica, May 2007

- Bøhagen B. and J.T. Gravdahl, Circle criterion observer for a compression system, to appear in Proceedings of the 2007 American Control Conference, New York, July 2007

- Bøhagen B. and J.T. Gravdahl, Active surge control using drive torque: dynamic control laws, Proceedings of the 45th IEEE Conference on Decision and Control, San Diego, December 2006

- Bøhagen B. and J.T. Gravdahl, Active control of compression systems using drive torque; a backstepping approach, Proceedings of the 44th IEEE Conference on Decision and Control, Seville, December 2005

- Bøhagen, B., O. Stene and J.T. Gravdahl, A GES mass flow observer for compression systems: Design and experiments, Proceedings of the 2004 American Control Conference, Boston, June 2004

- Bøhagen, B. and J.T. Gravdahl, On active surge control of compressors using a mass flow observer, Proceedings of the 41st IEEE Conference on Decision and Control, Las Vegas, December 2002

Preface

The research presented in this thesis is the result of my doctoral studies from 2002 to 2007 at the department of Engineering Cybernetics (ITK) at the Norwegian University of Science and Technology (NTNU) under the guidance of Professor Jan Tommy Gravdahl. My funding was mainly provided by NTNU, and partially by The Gas Technology Center and ITK.

This work would never have been conducted by me without the encouragement, support and patience of my supervisor Jan Tommy Gravdahl. I am grateful for his deep and detailed knowledge of compressor control from which he has shared willingly, as well as his ability to focus on the big picture when needed. Also, I am thankful for his efforts to organize so that I could focus on research.

During my studies I spent six months at The Dynamics and Control Technology group at the department of Mechanical Engineering of Eindhoven University of Technology as a visiting scientist. I appreciate the hospitality of this group, and would especially like to thank associate Professor Bram de Jager and Jan van Helvoirt for inviting me. Especially, I would like to thank Jan van Helvoirt for invaluable discussions of compressor modeling and control.

I would like to thank all my colleagues at the department of Engineering Cybernetics for providing a good environment for research. Especially, I appreciate the discussions and company of Roger Skjetne and Svein Hovland of whom I have shared office with during these years, Erik Kyrkjebø and Johannes Tjønnås for insightful and challenging discussions of various control topics. I would also like to direct a special thank Hans Jørgen Berntsen, Terje Haugen and Arvid Lervold at the department workshop for always offering their help and insight in putting theory to practice. Finally, I would like to thank Tove K. Johansen and Eva Amdahl for clearing all the administrative issues and letting me focus on my research.

I would also like to thank ABB for the cooperation, Svein Vatland for providing electric motor and drive and Morten Heggem for his enthusiasm in helping us with specifying and setting up the drive system.

Trondheim, May 2007 Bjørnar Bøhagen

Contents

Chapter 1

Introduction

Gas compressors are explained as follows in the encyclopedia Britannica:

> *A compressor is device for increasing the pressure of a gas by mechanically decreasing its volume. Air is the most frequently compressed gas but natural gas, oxygen, nitrogen, and other industrially important gases are also compressed ...*

This explanation can be further detailed by evaluating the ideal gas law

$$p = \rho RT$$

where p is pressure, ρ is density, R is the gas constant and T is temperature. Density can be expressed as $\rho = \frac{m}{V}$, where m is mass and V is volume, and it follows that a reduction of volume is equivalent with an increase of density for a given amount of mass. Hence, a compressor can alternatively be defined as a devise that increases pressure by increasing density.

Several types of compressors exists, where their differences lies in how compression for a gas is achieved. Some examples include centrifugal compressors, axial compressors, reciprocating compressors, scroll compressors and diaphragm compressors. The three latter compressors work by reducing the physical volume occupied by the gas. An application of the reciprocating compressor, familiar to most people, is found in the car combustion engine. The majority of these engines use a cylinder and piston to reduces the volume of a fixed amount of mass prior to the cylinder ignition.

Centrifugal and axial compressors, collectively called turbo compressors, works by a fundamentally different principle than the other mentioned examples. The compression from these machines can be considered as a result of two steps. First the fluid velocity is increased, and then the fluid kinetic energy is converted to pressure by reducing velocity. The second step can be illustrated by the Bernoulli equation

$$p_1 + \frac{1}{2}\rho v_1^2 = p_2 + \frac{1}{2}\rho v_2^2$$

for steady frictionless incompressible flow along streamline.[1] Let the subscript 1 refer to the state of high fluid velocity and subscript 2 to the state of low fluid velocity. It then follows from the relation that p_2 is larger than p_1. The energy consuming part of turbo compressors is that of increasing fluid velocity, when the machine needs some drive unit for this task. Fluid deceleration is achieved by means of redirecting and/or diverging fluid flow using the mechanical construction of the compressor.

Turbo compressors are sometimes also called continuous flow compressors. These compressors supply a steady mass flow and pressure, in contrast to e.g. the reciprocating compressor which supplies mass flow and pressure in a more pulsating fashion.

Compression systems using turbo compressors are subject to the phenomena of surge and rotating stall. Surge is characterized by oscillations of mass flow and pressure. These oscillations can be observed in any part of the system, such as upstream and downstream ducting as well as in the compressor itself. Stall is characterized by locally reduced or blocked flow in the compressor. This phenomenon is only observed only in the compressor, meaning that flow upstream and downstream the compressor can be steady even though the compressor is stalling. Hence, surge can be regarded a system phenomenon whereas stall is a phenomenon restricted to the compressor itself. Both of these phenomena constitute undesirable operation for the compressor and compression system. For large machinery the surge oscillations can be violent enough to damage upstream and downstream components. Furthermore, the reduced efficiency resulting from these instabilities can result in temperatures high enough to seriously alter or even melt mechanical compressor components.

[1] Assuming incompressible flow violates the previously stated properties of gas compression, but is made to illustrate conversion to pressure by means of a simple expression. Furthermore, this assumption is valid for relatively low fluid velocities.

Control of surge and rotating stall can be divided in two main approaches: avoidance and active control. Avoidance control ensures that the system only operates in regions for which the instabilities do not occur. This is the industrial standard. Active control, on the other hand, aims at stabilizing these phenomenons. In terms of control terminology, surge and rotating stall are observed for the open loop system. The avoidance approach use feedback in order to ensure operation in the open loop stable region, whereas the active control uses feedback in order to stabilize open loop unstable operating points in addition to ensure stability of the open loop stable region.

1.1 The centrifugal compressor

The centrifugal compressor consists of mainly three parts: impeller, diffuser and volute/collector. Figure 1.1 shows a picture of such a compressor, where part of the casing has been cut away. The impeller, which can be recognized as the bladed wheel, increases the fluid velocity by spinning at a relatively high speed. Note that fluid enters the impeller axially, with respect to the shaft driving it, and leaves radially. This gives rise to the name radial compressor, also used for the centrifugal compressor. There is no dedicated diffuser in this example. However, when fluid flows in the collector, from impeller exit to compressor exit (open pipe in top of picture), this forms a diverging channel. Hence, the casing serves as both diffuser and collector in this case. An integrated gear box, placed between the impeller and the black driving wheel, can also be recognized for this unit. The compressor in Figure 1.1 is called a single stage centrifugal compressor, which comes from using one impeller. Multi stage compressors can be considered as several single stage compressors mounted in series, sharing one drive shaft. The collector from the first stage then guides the fluid to the impeller of the second stage and so forth.

A principal sketch of various definitions related to the compressor is shown in Figure 1.2, accompanied by a picture of the impeller. Fluid enters the compressor through the inducer, also called impeller eye. The inducer is a region restricted by the compressor inlet radius and hub radius, for which the entering fluid is exposed to the impeller blades. The hub is simply a region of the impeller wheel dedicated to the shaft driving it. When leaving the impeller, the fluid enters the diffuser. The task of this component is

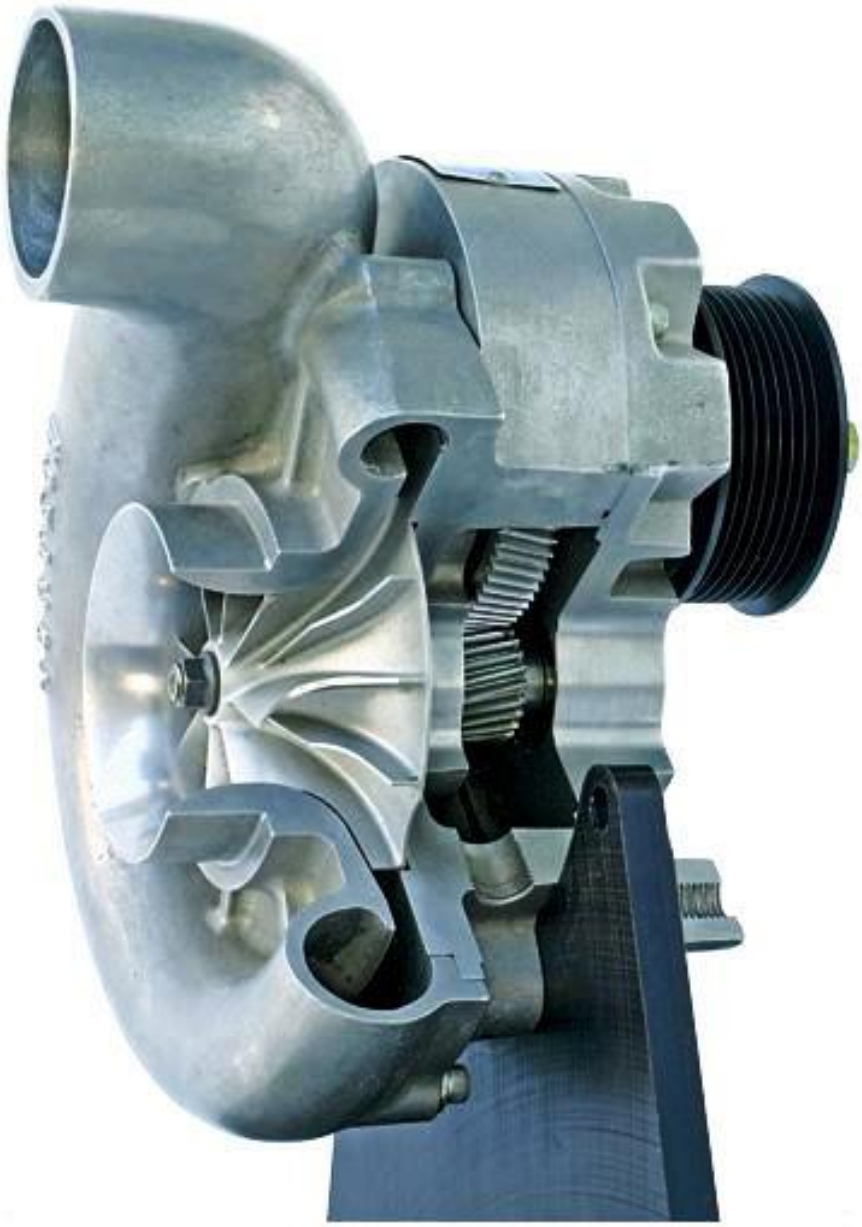

Figure 1.1: Single stage centrifugal compressor (Photo: Vortech, www.vortechsuperchargers.com)

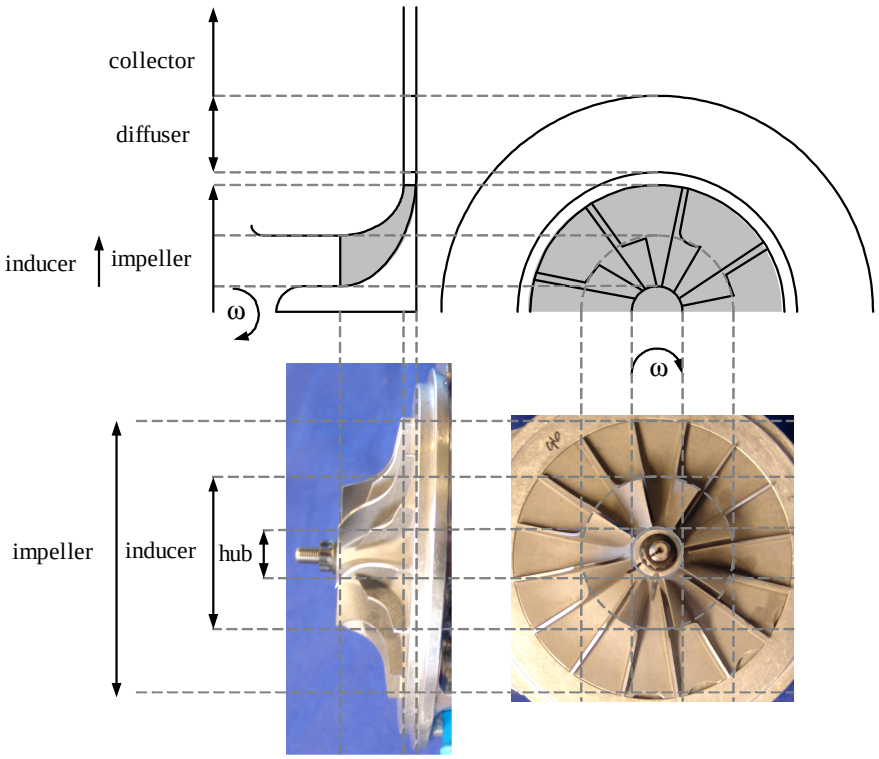

Figure 1.2: Components of the centrifugal compressor

to reduce the fluid velocity in order to gain pressure. Finally, the flow is gathered by the collector and guided to the compressor exit. As was commented in discussion of Figure 1.1, the collector can also serve as a diffuser.

Centrifugal compressors have had and still have a wide-spread area of application, [1]. Two examples include turbocharger/supercharger for the combustion engine and transportation of gas in pipelines. Figure 1.3 shows pictures of a turbocharger and a general purpose multi stage centrifugal compressor, left and right respectively. Turbochargers can generally be divided in three parts: a filter at compressor inlet, a compressor and a gas turbine which is driving the compressor. For the turbocharger in Figure 1.3, an air filter can be identified to the far left. The compressor can be identified as

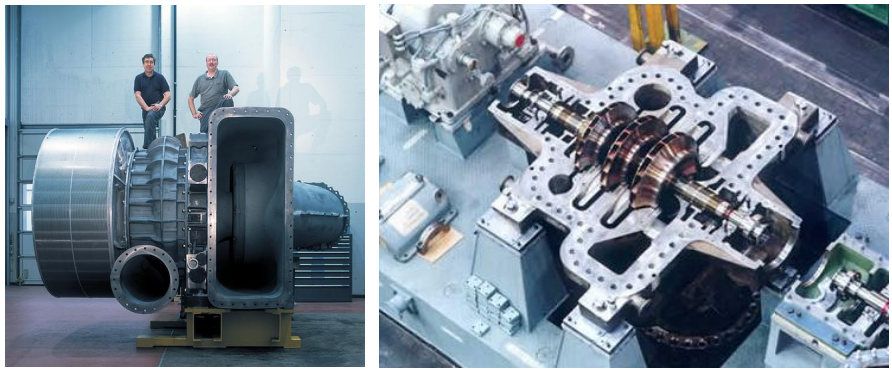

Figure 1.3: Turbocharger and general purpose three stage centrifugal compressor (Photo left: ABB, www.ABB.com and Photo right: MAN TURBO, www.manturbo.com)

the component below the man in dark blue T-shirt. This is a centrifugal compressor similar to that of Figure 1.1, with inlet at the left, through the air filter, and outlet through the circular pipe facing the reader. The gas turbine can be identified as the component below the man in light blue T-shirt. The multi stage centrifugal compressor of Figure 1.3 consists of three impellers mounted on one shaft, giving it the name three stage centrifugal compressor. Gas enters the compressor from the right, or more specifically it enters the compressor from below and is guided to the inducer of the impeller to the right. Here it traverses the first impeller and the diverging cannel connecting the first and second impeller, which completes the first stage. Then this procedure is simply repeated two more times before the gas leaves the compressor. It follows that a multi stage compressor is a series of single stage compressors. The motivation for this is simply found in that with a higher inlet pressure, the single stage compressor is able to produce a higher outlet pressure. Also, the pressure levels reached with a single stage relatively large impeller can also be produced with a few stages of smaller impellers.

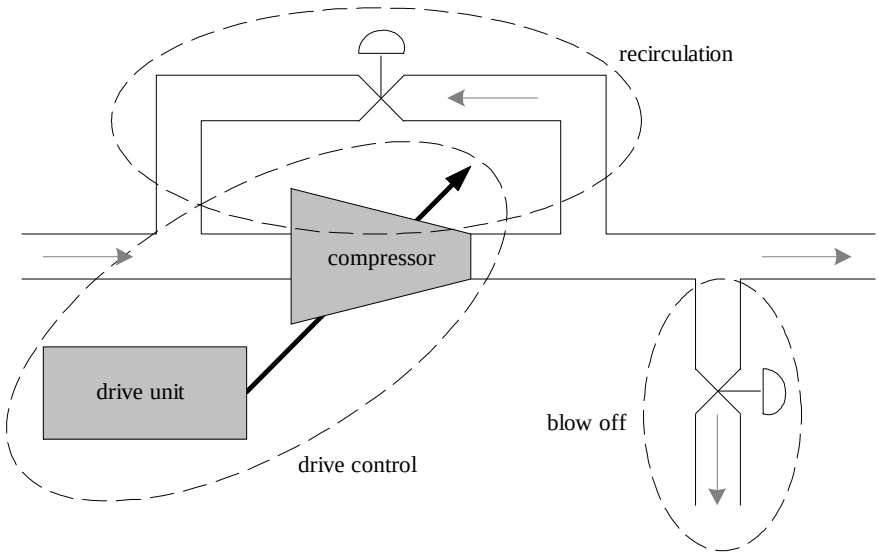

Figure 1.4: Principal sketch of some surge control approaches

1.2 Motivation

Figure 1.4 illustrates two of the approaches used for surge control, in addition to drive control. Controlling surge by a recirculation loop involves feeding compressed gas from downstream the compressor back to upstream compressor. The major disadvantage of this approach is that "the same gas" is compressed several times, consuming energy from the driving unit each time it is compressed. Controlling surge by blow off involves, as the name indicates, blowing off compressed gas downstream the compressor and into the surroundings of the compression system. Since the compressed gas is blown into the surroundings, this approach is first and foremost restricted to applications of air compression. The major disadvantage of this approach is that the compressed gas, which has consumed energy from the driving unit, is completely wasted.

Using the drive unit to control surge in the compression system has potentially several advantages. First of all, the drive unit is already present in the system and must be so in order to drive the impeller. This implies that no additional components are needed for this approach. In the ideal

case one can consider the drive unit being able to control/stabilize the entire operating range of the compression system. In which case the recirculation loop and blow off branch can be removed, being present in the compression system for the objective of control only. However, a more realistic scenario would be that the drive unit is able to control/stabilize parts of the open loop unstable region for the compression system. By then combining drive control and the other approaches, the amount of gas recycled and/or blown off can possibly be reduced compared to the situation where the drive is not used for active surge control.

This approach is probably most relevant when the compressor is driven by an electric motor. Electric motors are relatively fast and easy to control in comparison to e.g. a gas turbine, often used as drive unit for the compressor.

1.3 Approach

This thesis is divided into two parts. The first part consists of theoretical considerations on modeling and control of a simple compression system, whereas the second parts seek to evaluate the theoretical findings in of the first part by means of experiments.

Chapter 2 introduces the so-called variable speed Greitzer model, which is a widely used dynamic model of a simple compression system using turbo compressors. In order to form a richer fundament for feedback control, this model is extended by introducing pressure measurements to the model.

Chapter 3 derives control laws for active surge control of the Greitzer model by considering impeller speed or impeller torque as the only control input for the system.

Chapter 4 derives observers for the Greitzer model. The main objective of this chapter is to derive observers for mass flow, since this variable is needed in control laws and can not be measured. Reduced order observers for mass flow are derived as well as observers for mass flow, pressure and impeller speed.

Chapter 5 briefly presents the laboratory used for experimental validation of theory.

Chapter 6 describes model identification, static and dynamic, of the laboratory in view of the theoretical considerations in Chapter 2.

Chapter 7 evaluates the observers from Chapter 4 experimentally.

Chapter 8 evaluates some of the control laws from Chapter 3 experimentally.

Chapter 9 gives some concluding remarks as well as suggestions for further work.

This thesis do not contain simulations of control laws or observers. The reason for this is the rather extensive use of experimental data, which is considered to a better means of evaluating theory than simulations. However, not all observers and control laws are experimentally tested. For simulation of these, the reader is referred to the related published papers.

Part I

Theory

Chapter 2

Mathematical model

2.1 Introduction

The literature reports a rather extensive amount of work published on compressor and compression system modeling, [2], [3], [4] and [5]. Modeling of compression systems can be divided in two categories; those that capture the phenomenon of surge and those that captures the phenomena of both surge and rotating stall. As discussed Chapter 1, surge is a system phenomenon resulting in all system states entering a limit cycle. A model for this phenomenon can in general be described by a set of ordinary differential equations of various system states, where it is required from the model that it can reproduce both steady and transient behavior for states, such as pressure and flow, in accordance with that of the experimentally observed. Rotating stall is fundamentally different from surge in the sense that this is a phenomenon appearing locally in the compressor and is not necessarily reflected through system states. To illustrate this point one can consider flow through the compressor to be a system state. Assume that the compressor initially is operating un-stalled with a given through flow. Assume then that the compressor enters stall for some reason. If flow in the un-stalled impeller passages now increases, the overall compressor flow can appear to be the same as in the un-stalled case. Hence, the very nature of compressor stall implies hat this phenomenon should be modeled using partial differential equations. Models including rotating stall will not be further commented on when this work is limited to control of surge. For extensive studies on this topic the reader is referred to the famous Moore and Greitzer

model [6] and [7], and the more resent results reported in [8] and [9].

An early result on compression system surge model was reported in [10]. Due to its linear nature this model is limited to simulating relatively small surge oscillations. A model extensively used for surge analysis and control is the so-called Greitzer model, giving dynamic equations for mass flows and pressure in a compression system. The theoretical derivation is reported in [11] and experimental validation is given in [12]. The Greitzer model was originally derived for axial compressors, but shown to also be applicable for the centrifugal compressor in [13] by theoretical and experimental studies. In [14] the model of Greitzer was extended to include also a dynamic equation for compressor rotor speed, originally derived for impeller speed of a centrifugal compressor, where both theory end experiments was presented. The variable speed compression system model was also extensively discussed in [2], with a more theoretical approach of describing both compressor characteristic and torque set up by the spinning impeller.

This chapter starts by introducing dynamic equations for the variable speed Greitzer model in Section 2.2. The material presented in this section is a brief summary of previous work, for which the interested reader is referred to the already referred literature and references therein for a more detailed description. Section 2.3 discusses in some more detail the compressor stage and its model. In Section 2.4 the original Greitzer model is extended to include pressure measurements at well defined locations. Section 2.5 discusses and states model properties for the compression system. Equilibrium points and open loop stability of the compression system is discussed in Section 2.6.

2.2 Compression system dynamic model

A compression system for which the main components are a compressor, a plenum volume and a throttle is considered. The compressor and throttle are placed in upstream and downstream ducts of the plenum respectively. Furthermore, inlet conditions for the duct containing the compressor and outlet conditions for the duct containing the throttle are assumed to be that of a ambient pressure reservoir. This system is illustrated in Figure 2.1.

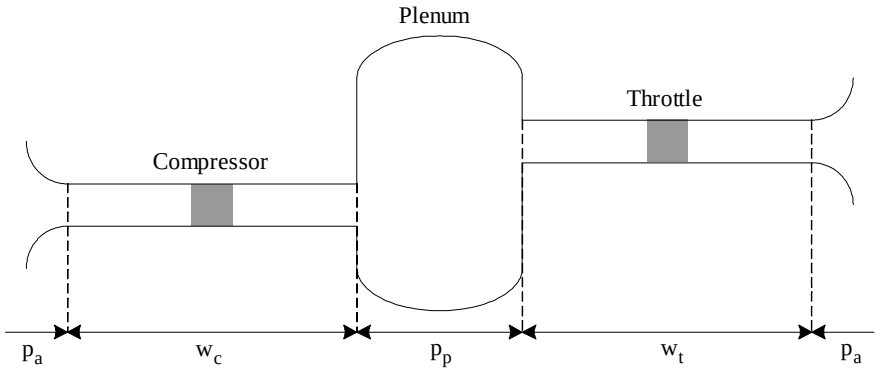

Figure 2.1: Simple compression system

2.2.1 Plenum pressure dynamics

The dynamic equation for plenum pressure is derived by evaluating the mass balance. By considering a fixed control volume and assuming uniform density, the volume integral of the mass balance is rewritten

$$\frac{d}{dt}\int_{V_p(t)} \rho_p dV = \frac{d\rho_p}{dt}\int_{V_p} dV = V_p \frac{d\rho_p}{dt},$$

where the subscript p refers to plenum. By further assuming ideal gas and isentropic process in the plenum results in the relation $dp_p = c_p^2 d\rho_p$, where $c_p = \sqrt{\kappa_p R T_p}$ is the speed of sound in plenum. Plenum pressure can now be expressed as

$$\dot{p}_p = \frac{c_p^2}{V_p}(w_c - w_t) \tag{2.1}$$

where w_c is the mass flow entering the plenum from the duct containing the compressor and w_t is the mass flow leaving plenum into the duct containing the throttle.

2.2.2 Duct mass flow dynamics

The dynamic equations for duct mass flows are derived by evaluating the linear momentum balance. By considering a fixed control volume and modeling the flow as incompressible and one dimensional for a constant area

duct, constant density and uniform axisymmetric fluid velocity, the volume integral of the linear momentum balance is rewritten

$$\frac{d}{dt}\int_{V_c(t)} \rho_c v_c dV = \rho_c A_c \frac{dv_c}{dt}\int_{L_c} dl = \frac{dw_c}{dt} L_c,$$

where the subscript c refers to the duct containing the compressor. The momentum flux of this system equals zero, $\sum_{in/out} \rho_c v_c^2 A_c = 0$, due to the stated assumptions of one dimensional and incompressible flow. The forces acting on this system is modeled by surface pressure forces and a resultant force of which the compressor can be considered the main contributor $\sum F = p_a A_c - p_p A_c + F_c'$, where the subscript a refers to ambient conditions. Mass flow in the duct containing the compressor can now be expressed as

$$\dot{w}_c = \frac{A_c}{L_c}\left(p_a - p_p + F_c\right) \tag{2.2}$$

where $F_c = \frac{1}{A_c} F_c'$ is defined for notational convenience. Note that this definition of F_c gives it the SI unit Pascal, $N/m^2 = Pa$. Mass flow in the duct containing the throttling device is modeled in the same manner, resulting in

$$\dot{w}_t = \frac{A_t}{L_t}\left(p_p - p_a - F_t\right) \tag{2.3}$$

where the subscript t referees to the duct containing the throttle. The sign convention of the forces considers F_c working along the flow direction whereas F_t is working against it. To this end it can be noted that flow in the duct containing the compressor is considered is defined positive when flowing from ambient to plenum and positive flow in duct containing throttle is considered positive when flowing from plenum to ambient.

2.2.3 Impeller speed dynamics

The dynamic equation for impeller speed is derived by evaluating the angular momentum balance for the spinning shaft. This is given by

$$\dot{\omega} = \frac{1}{J}\left(\tau_d - \tau_l\right) \tag{2.4}$$

where ω is the impeller speed, J is the moment of inertia of rotating parts, τ_d is the torque applied to the impeller by the driving unit and τ_l is the

load torque due to fluid flow in impeller and friction of rotating mechanical parts. The load torque resulting from fluid flow in impeller is approximated by the Euler pump equation and the friction is modeled as a linear term of impeller speed

$$\tau_l(w_c, \omega) = \tau_c(w_c, \omega) + \tau_f(\omega) \quad (2.5)$$

$$\tau_c(w_c, \omega) = k_c |w_c| \omega \quad (2.6)$$

$$\tau_f(\omega) = k_f \omega \quad (2.7)$$

where $k_c = \sigma r_i^2$ and k_f is a friction constant. The slip factor, σ, is a parameter between zero and one, commonly taken as a value close to one, describing to which extent the fluid leaves the impeller in the same angle as the impeller blade. The impeller radius, r_i, is the radius of the impeller wheel. The term (2.7) represents the simplest form of viscous friction. More sophisticated models are $\tau_f(\omega) = k_f |\omega|^{\delta_f} sgn(\omega)$ or the Stribeck effect, [15].

2.2.4 Comments to model

For the plenum it is assumed that the thermodynamic properties are uniform over the volume. There will be regions of the inlet and outlet for which the fluid velocities are decelerating and accelerating due to the inn and out flows. Hence, the plenum should be large enough such that these regions can be ignored. Moreover, the plenum should be of much larger diameter than the ducts so that fluid velocity is converted to pressure. Furthermore, isentropic process is assumed for the plenum which in essence means no heat losses. Hence, the heat loss should be low relative to the overall energy related to the plenum.

Flows in the ducts are assumed one dimensional and incompressible. For the incompressible assumption to hold, velocities in ducts should be relatively small. A commonly accepted parameter for this is a sufficiently small Mach number, $Ma \leq 0.3$. Furthermore, flows in ducts are not necessarily one dimensional. This is especially the case for the duct containing the compressor, where the very nature of the machine imposes rotational velocity to the fluid. However, this condition can be considered valid if the connecting systems experience the duct flow to be one dimensional. One way of satisfying this is to introduce sufficient duct length upstream and downstream compressor and throttle, such that the flows at system boundaries are nearly one dimensional. Alternatively one can introduce flow straighteners.

The fraction $\frac{A}{L}$ appearing in duct mass flow equations is related to the actual flow path and not necessarily the physical length and cross section of the duct. Recall that these parameters where introduced to the model by assuming one dimensional flow in a constant area duct which especially for the duct containing the compressor is not the case. Hence, the fraction should be chosen so that the model complies with observed transient data, rather than the actual measures of length and cross section of ducts.

For the remaining of this thesis, a system where the throttling device is placed immediately downstream the plenum without any considerable ducting related to it is considered. By recasting (2.3) into

$$\frac{L_t}{A_t}\frac{dw_t}{dt} = (p_p - p_a - F_t)$$

and using $L_t \approx 0$, it can be seen that $F_t \approx p_p - p_a$. In essence, this states that dynamics of the throttle duct is so fast relative to other system dynamics so that throttle mass flow can be considered as a static mapping in terms of other system states. A model for the throttle mass flow will be taken as

$$w_t\left(p_p\right) = k_t sgn\left(p_p - p_a\right)\sqrt{|p_p - p_a|} \tag{2.8}$$

where the sign and absolute value have been introduced for simulation purposes of the model $w_t\left(p_p\right) = k_t\sqrt{p_p - p_a}$, when surge can result in $p_p < p_a$. To this end the throttle mass flow is assumed symmetric in terms of positive and negative flow as a function of pressure difference across the devise. Throttle through flow area is reflected through the constant k_t. In the case of a variable area throttling devise, e.g. control valve, this constant then becomes a function of the through flow area and can be modeled as

$$k_t = k_t\left(A_{t\%}\right), \tag{2.9}$$

where $A_{t\%}$ represents the percentage opening.

2.3 Compressor map

The forcing term, F_c, was introduced as resultant forces acting on the fluid by the compressor. The assumption of one dimensional and incompressible flow in this duct does not hold locally in the compressor where both density and

fluid velocity will vary along the flow path, but should rather be the behavior experienced by connecting systems. Locally in the compressor the fluid first experiences acceleration, both linear as well as rotational, when traversing the impeller. Then the fluid experiences a deceleration in the diffuser and/or volute. Motivated by Newton's second law of motion, the acceleration of fluid in impeller can be considered as a result of body forces set up by the impeller speed. The fluid also experiences friction/surface forces when traversing the compressor stage. Body forces acts on fluid density whereas friction forces are related to fluid velocity and surface area. All this suggests that the forcing term should be a function of density, fluid velocity and impeller speed, $F_c(\rho_c, v_c, \omega)$, expressed in terms of volume and surface integrals for time varying and nonuniform density and velocity. However, the overall model assumes incompressible flow which makes ρ_c constant and v_c uniform. Therefore the model is assumed to be a function of compressor mass flow and impeller speed,

$$F_c = F_c(w_c, \omega), \tag{2.10}$$

with compressor mass flow reflecting both fluid velocity and mass.

The forcing term is usually found experimentally as a nonlinear mapping of compressor mass flow and impeller speed, based on steady state data. From (2.2) it can be recognized that this steady state relation is given in terms of pressures, $F_c(w_c, \omega) = p_p - p_a$. Dynamic behavior has also been suggested in the form $\tau \dot{F}_c = (F_{c,ss}(w_c, \omega) - F_c)$, e.g. [11] and [13], with varying motivation. In the following, it is assumed that the forcing term can be represented as a pure static mapping of mass flow and impeller speed. This assumption requires that potential dynamic effects related to the forcing term, e.g. mass conservation for compressor stage, are fast relative to the duct mass flow and impeller speed dynamics.

Compressor performance is commonly described with a compressor characteristic, ψ_c. This characteristic relates the steady state compressor pressure ratio as a function of compressor mass flow and impeller speed. The compressor characteristic for the current model is then defined by $\psi_c = \frac{p_p}{p_a}$, and can be related to the forcing term by

$$\psi_c = 1 + \frac{F_c(w_c, \omega)}{p_a}. \tag{2.11}$$

Compressor characteristic is typically visualized with a compressor map, such as shown in Figure 2.2. This map consists of a collection of constant

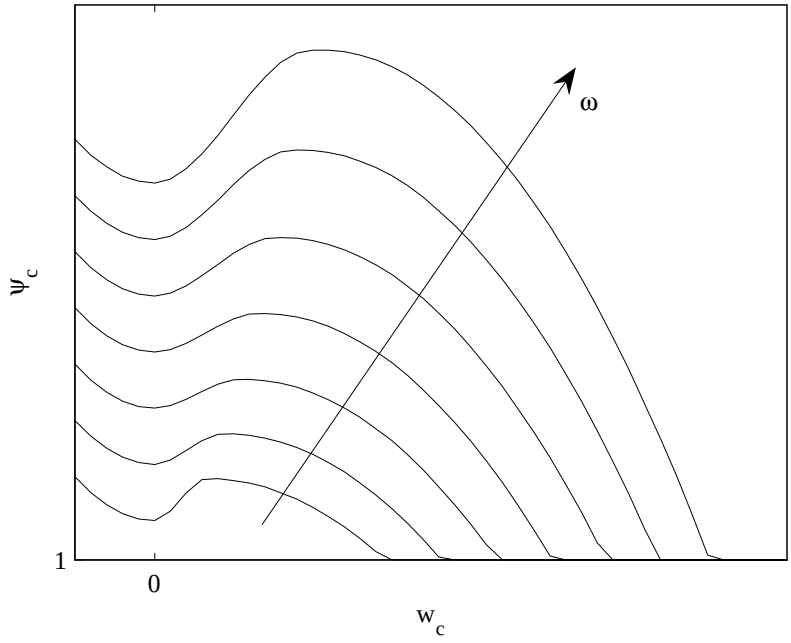

Figure 2.2: Compressor map

speed lines for which the pressure ratio is shown as a function of mass flow.

In order for simulation and possibly implementation, when a compressor characteristic is required for a control algorithm, one needs a mathematical model. In the case of variable speed applications this needs to be a function of mass flow as well as impeller speed. One way of retrieving such a characteristic is to use polynomial fit on experimental data. The polynomial

$$\psi_c(w_c, \omega) = c_3(\omega) w_c^3 + c_2(\omega) w_c^2 + c_0(\omega), \; w_c > 0 \tag{2.12}$$

$$c_i(\omega) = c_{i2}\omega^2 + c_{i1}\omega + c_{i0} \tag{2.13}$$

was used in [16] for variable speed applications, inspired by the polynomial for the constant speed case suggested in [6]. Theoretical approaches for expressing the compressor characteristics are also reported [17]. Identification by experimental data can be problematic for the region of the characteristic for which instabilities occur, when this requires control to retrieve steady state data. However, by reducing the duct length between compressor and

plenum in the identifying process one can extend the region for which steady experimental data can be retrieved, [14]. For identification of negative mass flow, a device that can enforce this flow on the compressor is needed. In [13] this approach was taken and it was shown that the steady state characteristics for constant speed negative mass flow could be approximated by $\psi_c(w_c,\omega)|_{\omega \text{ constant}} = c_4 w_c^2 + c_5$. Following the approach taken by [16] for the open loop stable region, the coefficients can be made functions of impeller speed

$$\psi_c(w_c,\omega) = c_4(\omega)\, w_c^2 + c_5(\omega), \;\; w_c < 0 \tag{2.14}$$

in which case $c_5(\omega)$ will represent the compressor characteristics at zero mass flow for a given speed. Note that combining (2.12)-(2.13) and (2.14) requires $c_0(\omega) = c_5(\omega)$ in order for the characteristics to be continuous at zero mass flow.

2.4 Pressure measurements in duct

There might be a relatively high uncertainty involved with a model of the compressor characteristic, especially in the region of the map for which it is open loop unstable. Combining this with the general desire for more system information in form of measurements to form a richer feedback basis for control motivates the introduction of a pressure measurement that can replace compressor characteristic model when required for implementation.

2.4.1 Upstream compressor

Consider the configuration shown in Figure 2.3, where a pressure measurement now divides the upstream plenum duct in two control volumes. It is still assumed that flow in the entire duct is one dimensional, incompressible and constant area. It is also assumed that the flow in the duct upstream the compressor is inviscid, implying that no forces other than boundary pressures are acting on this flow. Following the previous derivation of duct mass flow (2.2) then gives

$$\dot{w}_{cu} = \frac{A_c}{L_{cu}}(p_a - p_{cu}) \tag{2.15}$$

$$\dot{w}_c = \frac{A_c}{L_c}(p_{cu} - p_p + F_c(w,\omega)) \tag{2.16}$$

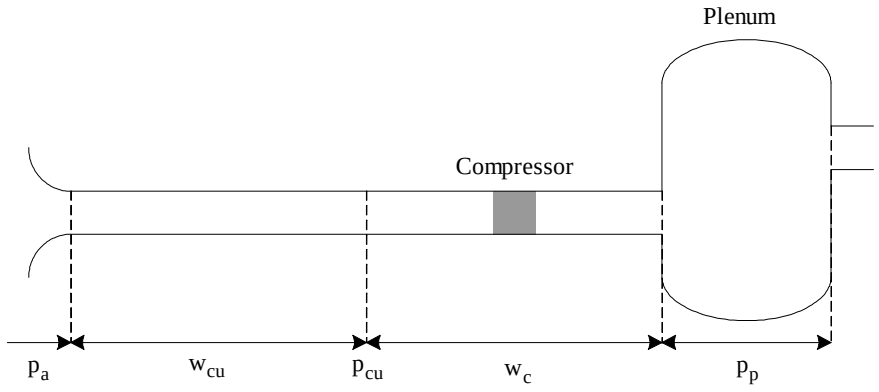

Figure 2.3: Pressure measurement upstream compressor

where the subscript cu refers to upstream compressor duct. Furthermore, the mass flows are related by $w_c = w_{cu}$ due to the flow assumptions. By now comparing $\dot{w}_c = \dot{w}_{cu}$ it is possible to derive an explicit expression

$$F_c(w,\omega) = \frac{L_c}{L_{cu}} p_a + p_p - \frac{L_c + L_{cu}}{L_{cu}} p_{cu} \tag{2.17}$$

relating $F_c(w,\omega)$ and well defined measurable signals. Note that this relation holds for transients as well as steady state.

The forcing term and pressures in steady state are related by $p_{cu} = p_a$ and $F_c(w_c,\omega) = p_p - p_{cu}$, which gives $F_c(w_c,\omega) = p_p - p_a$. The compressor characteristic is in this configuration defined by $\psi_c = \frac{p_p}{p_{cu}}$, which in steady state gives $\psi_c = 1 + \frac{F_c(w,\omega)}{p_a}$. This is identical to the characteristic found in (2.11).

By using (2.17) in (2.16) to substitute for p_{cu} it can be shown that

$$\dot{w}_c = \frac{A_c}{L_c + L_{cu}} \left(\underbrace{F_c(w_c,\omega) + p_a}_{p_c(w_c,\omega)} - p_p \right) \tag{2.18}$$

and by using (2.17) in (2.16) to substitute for $F_c(w,\omega)$ it can be shown that

$$\dot{w}_c = \frac{A_c}{L_c + L_{cu}} \left(\underbrace{\left(1 + \frac{L_c}{L_{cu}}\right)(p_a - p_{cu}) + p_p}_{p_c(t)} - p_p \right). \tag{2.19}$$

Hence, the dynamics describing mass flow in the upstream ducting of the plenum takes on the structure $\dot{w}_c = k_{cu1}(p_c - p_p)$ where p_c is either a measurement

$$p_c(t) = k_{cu2}(p_a - p_{cu}(t)) - p_p(t)$$

of known and well defined signals or a function of mass flow and impeller speed

$$p_c(w_c,\omega) = F_c(w_c,\omega) + p_a.$$

The structure of the dynamics is identical to that of the original Greitzer model when using $p_c(w_c,\omega)$, but the signal $p_c(t) = p_c(w_c,\omega)$ is now also available as a measurement.

2.4.2 Downstream compressor

Following the previous approach, equations for the case when a pressure measurement is installed downstream the compressor is derived. Consider the configuration shown in Figure 2.4, where a pressure measurement divides the upstream plenum duct in two control volumes of which the unforced part, not containing the compressor, now is downstream the compressor. It is still assumed that flow in the entire duct is one dimensional, incompressible and constant area. It is also assumed that the flow in the duct downstream the compressor is inviscid, implying that no forces other than boundary pressures are acting on this flow. Following the previous derivation of duct mass flow then gives

$$\dot{w}_c = \frac{A_c}{L_c}(p_a - p_{cd} + F_c(w,\omega)) \tag{2.20}$$

$$\dot{w}_{cd} = \frac{A_c}{L_{cd}}(p_{cd} - p_p) \tag{2.21}$$

where the subscript cd refers to downstream compressor duct. Furthermore, the mass flows are related by $w_c = w_{cd}$ due to the flow assumptions. By now

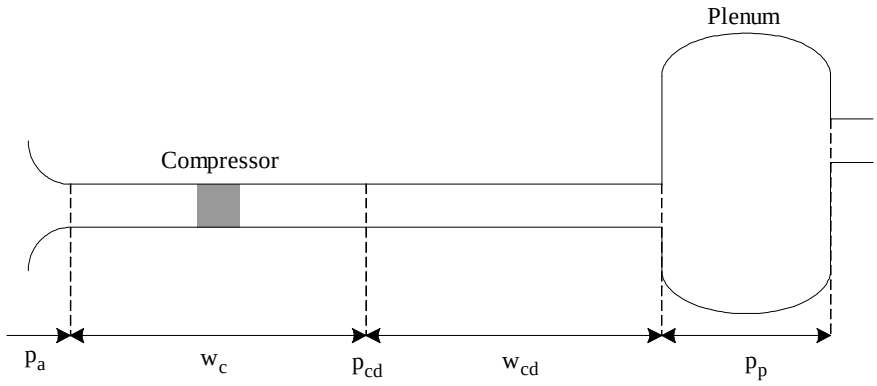

Figure 2.4: Pressure measurement downstream compressor

comparing $\dot{w}_c = \dot{w}_{cd}$ it is possible to derive an explicit expression

$$F_c(w,\omega) = \frac{L_c}{L_{cd}}(p_{cd} - p_p) + p_{cd} - p_a \tag{2.22}$$

relating $F_c(w,\omega)$ and well defined measurable signals. Note that this relation holds for transients as well as steady state.

The pressures and forcing term in steady state are related by $p_{cd} = p_p$ and $F_c(w_c,\omega) = p_{cd} - p_a$, which gives $F_c(w_c,\omega) = p_p - p_a$. The compressor characteristic is in this configuration defined by $\psi_c = \frac{p_{cd}}{p_a}$, which in steady state gives $\psi_c = 1 + \frac{F_c(w,\omega)}{p_a}$. This is identical to that found in (2.11).

By inserting (2.22) in (2.20) to substitute for p_{cd} it can be shown that

$$\dot{w}_c = \frac{A_c}{L_c + L_{cd}}\left(\underbrace{p_a + F_c(w,\omega)}_{p_c(w_c,\omega)} - p_p\right) \tag{2.23}$$

and by using (2.22) in (2.20) to substitute for $F_c(w,\omega)$ it can be shown that

$$\dot{w}_c = \frac{A_c}{L_c + L_{cd}}\left(\underbrace{\left(1 + \frac{L_c}{L_{cd}}\right)p_{cd} - \frac{L_c}{L_{cd}}p_p}_{p_c(t)} - p_p\right). \tag{2.24}$$

Hence, the dynamics describing mass flow in the upstream ducting of the plenum takes on the structure $\dot{w}_c = k_{cd1}(p_c - p_p)$ where p_c is either a measurement

$$p_c(t) = (1 + k_{cd2})\, p_{cd}(t) - k_{cd2} p_p(t)$$

of known and well defined signals or a function of mass flow and impeller speed

$$p_c(w_c, \omega) = F_c(w_c, \omega) + p_a.$$

The structure of the dynamics is identical to that of the Greitzer model when using $p_c(w_c, \omega)$, but the signal $p_c(t) = p_c(w_c, \omega)$ is now also available as a measurement.

2.4.3 Comments

The dynamic dimension of the overall compression system model is not increased by defining the new control volumes, these new volumes simply introduce measurements at well defined locations for an already present dynamic equation. Note that in order to simulate the compression system, one need to use a model of the compressor characteristic to generate w_c. However, in control or observer design and implementation the signal p_c is also available as a measurement.

From (2.2), (2.18) and (2.23) it can be seen that the structure

$$\dot{w}_c = \frac{A_c}{L_c'}(p_c(w_c, \omega) - p_p) \tag{2.25}$$

is preserved for the various divisions of the duct, where L_c' varies among the divisions. Furthermore, for all three configurations the relation (2.11) is preserved. This gives an opportunity to formulate p_c in terms of the compressor characteristic

$$p_c(w_c, \omega) = p_a + F_c(w, \omega) = \psi_c(w_c, \omega)\, p_a, \tag{2.26}$$

which might be convenient when compressors are often described in terms of the characteristic from a supplier.

When splitting up the control volumes, the boundaries should be chosen such that the assumptions of the individual systems hold. This implies that measurements first and foremost should be placed at locations where the flow is fairly one dimensional, which involves having sufficient length of duct

upstream and/or downstream the compressor. Furthermore, flow in ducts divisions should appear incompressible both to each other and to plenum.

The discussed division of the compressor ducts can alternatively appear in a combination, both upstream and downstream. The various relations are then given by combining the equations already derived for the individual cases. The throttle duct can be approached in the same manner as was done for the compressor duct. Deriving the various equations will then consist of the exact same exercise as was done for the compressor duct.

2.5 Model properties

The following chapters will use the model described by (2.1), (2.4), (2.5), (2.8) and (2.25) in derivation of control laws and observers. When applying Lyapunov methods for this purpose it is required that system dynamics is locally Lipschitz, that is $f(x)$ of $\dot{x} = f(x)$ being locally Lipschitz, in order to guarantee existence and uniqueness of a solution $x(t)$ for a given initial condition $x(t_0)$. A sufficient condition for this is for $f(x)$ to be continuous differentiable, [18]. The models for throttle mass flow (2.8) and load torque (2.5) involves absolute values and sign functions, which are not continuously differentiable. However, by using the approximation $sign(a) \approx \tanh(\zeta a)$ and $|a| = sign(a)\, a \approx a \tanh(\zeta a)$, these functions also becomes continuously differentiable. The error made by these approximations becomes smaller when ζ increases, as can be seen from $\lim_{\zeta\to\infty} \tanh(\zeta a) \to sign(a)$. Note that these approximations are active when the mass flows are close to zero, both for compressor and throttle mass flow. Models for compressor torque and throttle mass flow are expected to be somewhat inaccurate for relatively small mass flows. Hence, the errors introduced by these approximations are considered to be more of a mathematical detail than a source for model error. For mathematical completeness it is also assumed that the compressor characteristic is continuously differentiable.

The compressor characteristic is strictly increasing with increasing impeller speed, shown theoretically in [19]. Combining this with (2.5)-(2.8)

and (2.26) it can be seen that

$$\begin{aligned}(a-b)\left(w_t(a)-w_t(b)\right) &> 0 && (2.27)\\ (a-b)\left(p_c(c,a)-p_c(c,b)\right) &> 0 && (2.28)\\ (a-b)\left(\tau_l(c,a)-\tau_l(c,b)\right) &> 0 && (2.29)\\ (a-b)\left(\tau_c(c,a)-\tau_c(c,b)\right) &> 0 && (2.30)\\ (a-b)\left(\tau_f(a)-\tau_f(b)\right) &> 0 && (2.31)\end{aligned}$$

where a, b, and c are some arbitrary parameters, which in view of the discussion on continuously differentiable system dynamic implies that $\frac{\partial w_t(a)}{\partial a} > 0$, $\frac{\partial p_c(c,a)}{\partial a} > 0$, $\frac{\partial \tau_l(c,a)}{\partial a} > 0$ and $\frac{\partial \tau_f(a)}{\partial a} > 0$. These are so called sector properties that will be utilized in the control and observer design of subsequent chapters. Furthermore, it is known from (2.26) that

$$p_c(w_c,\omega) \geq p_a \tag{2.32}$$

since $\psi_c(w_c,\omega) \geq 0$. This latter inequality follows from the fact that pressure downstream the compressor always will be larger than or equal to pressure upstream the compressor. Another way of viewing this is that the forcing term, $F_c(w_c,\omega)$, always will be positive, at least as long as the impeller is rotating in its design direction. In other words, the resultant force imposed by the impeller on the fluid is acting along the positive fluid flow direction.

2.6 System equilibrium and open loop stability

Let the equilibrium values for system states and input be denoted by $(\cdot)^e$. From (2.25) the relation

$$p_p^e = p_c(w_c^e,\omega^e) \tag{2.33}$$

can be recognized for system equilibrium, which in view of (2.32) implies that

$$p_p^e \geq p_a. \tag{2.34}$$

From (2.1) and (2.8) the relation $w_c^e = k_t sgn\left(p_p^e - p_a\right)\sqrt{\left|p_p^e - p_a\right|}$ is found, which in combination with (2.34) implies that

$$w_c^e \geq 0 \tag{2.35}$$

and gives the relation

$$w_c^e = k_t\sqrt{p_p^e - p_a}. \tag{2.36}$$

Using (2.3) and (2.5)-(2.7) gives the relation $\tau_d^e = k_c \left|w_c^e\right| \omega^e + k_f \omega^e$, and

$$\tau_d^e = k_c w_c^e \omega^e + k_f \omega^e \tag{2.37}$$

follows from (2.35).

For dimensional simplicity, open loop stability is evaluated by considering the system (2.1) and (2.25) for a constant speed ω^e, the so called constant/fixed speed compression system. Deviation from equilibrium is defined by $x = \left[p_p - p_p^e,\ w_c - w_c^e\right]^T$, resulting in the dynamic equation $\dot{x} = f(x)$ where

$$f(x) = \begin{bmatrix} \frac{c_p^2}{V_p}\left(x_2 - w_t\left(x_1 + p_p^e\right) + w_c^e\right) \\ \frac{A_c}{L_c'}\left(p_c\left(x_2 + w_c^e, \omega^e\right) - x_1 - p_p^e\right) \end{bmatrix}. \tag{2.38}$$

The Jacobian of (2.38) evaluated at equilibrium is then given by

$$\begin{aligned} A &= \left[\begin{matrix} -\frac{c_p^2}{V_p}\frac{\partial w_t\left(x_1+p_p^e\right)}{\partial x_1} & \frac{c_p^2}{V_p} \\ -\frac{A_c}{L_c'} & \frac{A_c}{L_c'}\frac{\partial p_c\left(x_2+w_c^e,\omega^e\right)}{\partial x_2} \end{matrix}\right]\Bigg|_{x=0} \\ &= \left[\begin{matrix} -\frac{c_p^2}{V_p}\frac{\partial w_t(p_p)}{\partial p_p} & \frac{c_p^2}{V_p} \\ -\frac{A_c}{L_c'} & \frac{A_c}{L_c'}\frac{\partial p_c\left(w_c,\omega^e\right)}{\partial w_c} \end{matrix}\right]\Bigg|_{\substack{p_p=p_p^e \\ w_c=w_c^e}}, \end{aligned} \tag{2.39}$$

which can be shown to have eigenvalues

$$\lambda_{1,2}(A) = \frac{1}{2}\Lambda\left(p_p^e, w_c^e\right) \pm \sqrt{-\frac{c_p^2}{V_p}\frac{A_c}{L_c'}\Lambda^2\left(p_p^e, w_c^e\right)} \tag{2.40}$$

$$\Lambda\left(p_p^e, w_c^e\right) = \frac{A_c}{L_c'}\left.\frac{\partial p_c\left(w_c, \omega^e\right)}{\partial w_c}\right|_{w_c=w_c^e} - \frac{c_p^2}{V_p}\left.\frac{\partial w_t\left(p_p\right)}{\partial p_p}\right|_{p_p=p_p^e}. \tag{2.41}$$

From (2.40) it can be seen that the square root results in complex conjugated values or zero, since all the constants involved are positive and Λ is squared. This implies that $\mathrm{Re}\left(\lambda(A)\right) = \frac{1}{2}\Lambda\left(p_p^e, w_c^e\right)$. From (2.41) and (2.26) it can then be recognized that $\mathrm{Re}\left(\lambda(A)\right) < 0$ when

$$\left.\frac{\partial \psi_c\left(w_c, \omega^e\right)}{\partial w_c}\right|_{w_c=w_c^e} < \frac{L_c' c_p^2}{p_a A_c V_p}\left.\frac{\partial w_t\left(p_p\right)}{\partial p_p}\right|_{p_p=p_p^e} \tag{2.42}$$

holds and $\mathrm{Re}\left(\lambda(A)\right) > 0$ when (2.42) with the inequality changed holds.

Lemma 2.1 *An equilibrium for the system (2.1), (2.8) and (2.25) is asymptotically stable if (2.42) is satisfied. The equilibrium point is unstable if (2.42) is satisfied with the inequality changed.*

Proof. The proof follows from (2.38)-(2.42) and Theorem 4.7 of [18]. ■

Remark 2.1 *From (2.27) it is known that* $\left.\frac{\partial w_t(p_p)}{\partial p_p}\right|_{p_p=p_p^e} > 0$. *Hence, every equilibrium for which the compressor characteristic has a negative gradient with respect to mass flow is a stable equilibrium.*

The relation (2.42) forms a boundary in the compressor map, called the surge line. This is shown in Figure 2.5, among other things, as the line passing through peaks of constant speed lines. Operating points to the right and left of the surge line constitutes open loop stable and unstable respectively. This can be verified by evaluating the mass flow gradient of the compressor characteristic in these regions. Negative gradient can be recognized for relatively high mass flows as well as for negative mass flow. However, it has been shown there is no negative mass flow equilibrium for this system, and stability of such points are of no practical interest.

By using (2.26), (2.33) and (2.36) it can be shown that

$$\psi_c\left(w_c^e, \omega^e\right) = \frac{w_c^e}{k_t^2 p_a} + 1, \tag{2.43}$$

which expresses possible equilibrium points in the compressor map in terms of the throttle model. Figure 2.5 shows this relation for two different values of the throttle gain k_t. As can be seen from the figure, these two throttle gains correspond to two fundamentally different sets of equilibrium points. One is confined to the left and the other to the right of the surge line, constituting open loop unstable and stable equilibria respectively. Hence, the throttle gain determines to a large extent whether the equilibrium point is open loop stable or unstable. In the case of a variable area throttle, reducing the opening will move the throttle characteristic towards the left in the compressor map and visa versa.

For a constant speed compression system, the equilibrium will be given by the intersection of the throttle characteristic and the speed line corresponding to ω^e. In the variable speed case (2.37) is used to rewrite

$$\psi_c\left(w_c^e, \omega^e\right) = \psi_c\left(w_c^e, \frac{\tau_d^e}{k_c w_c^e + k_f}\right) = \psi_c\left(\left(\frac{\tau_d^e}{\omega^e} - k_f\right)\frac{1}{k_c}, \omega^e\right), \tag{2.44}$$

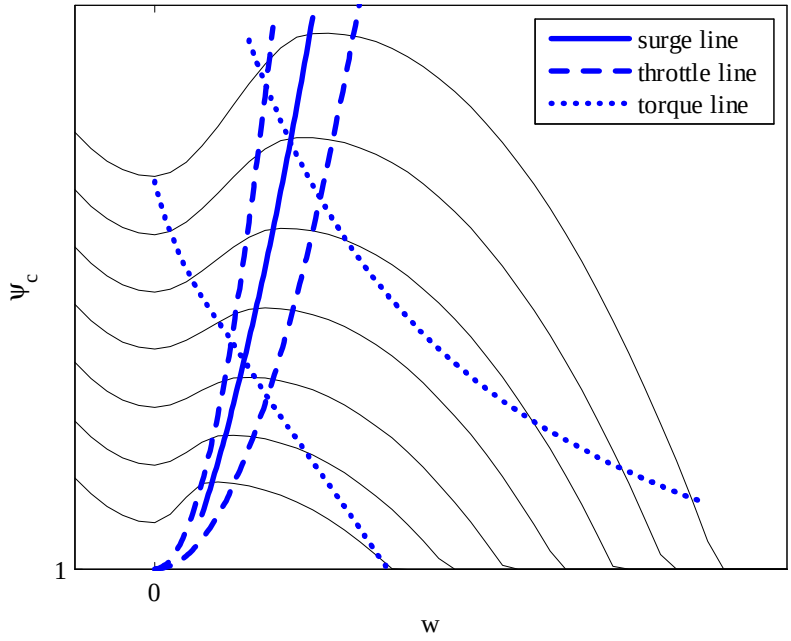

Figure 2.5: Equilibrium and surge line in compressor map

relating compressor torque to the compressor map. In contrast to (2.43) this requires a model of the compressor characteristic. If this is not available, (2.37) can be combined with (2.43) to substitute for w_c^e,

$$\psi_c\left(w_c^e, \omega^e\right) = \left(\frac{\tau_d^e}{\omega^e} - k_f\right) \frac{1}{k_t^2 k_c p_a} + 1. \tag{2.45}$$

The difference of (2.44) and (2.45) is that (2.44) is based purely on the torque equilibrium relations, whereas (2.45) combines torque and throttle mass flow equilibrium. Figure 2.5 illustrates the relation (2.44) for two different constant torque inputs τ_d^e, where the highest value of τ_d^e corresponds to the upper line. An equilibrium point for the variable speed compression system is then given by the intersection of the throttle and torque characteristic.

Consider now a situation in which a control law has been developed for drive torque, able of stabilizing any desirable operating point. Furthermore, this control law requires information of the desired equilibrium values, sys-

tem states and inputs, in order for implementation. In view of the previous discussion it follows that both k_t and τ_d^e must be chosen in order to reach any point in the compressor map. However, in practice one generally wishes to specify the operating point in terms of system states and derive system input on the basis of this choice. At least two system states are needed to uniquely describe a desired equilibrium. Consider first the case when p_p^e and w_c^e are specified. This gives the opportunity to determine k_t from (2.36) and ω^e from (2.33) by evaluating the inverse function of $p_c\left(w_c^e, \omega^e\right)$. The input τ_d^e can now be found by (2.37). This procedure involves evaluating the inverse of $p_c\left(w_c, \omega\right)$, requiring an analytical function of this mapping. Note that a unique ω^e should result from evaluation of the inverse function since the mapping $p_c\left(w_c, \omega\right)$ is strictly positive in ω. It can also be recognized from the compressor map that for some given p_p^e and w_c^e, a unique ω^e is related. Consider next the case when p_p^e and ω^e are specified. The parameter w_c^e must now be determined before k_t and τ_d^e can be evaluated. This must be determined from (2.33) by evaluating the inverse function of $p_c\left(w_c^e, \omega^e\right)$. However, a solution of this inverse function can result in as many as three solutions for w_c^e (negative, in open loop unstable region or in open loop stable region). This can also be recognized by inspection of the compressor map. Hence, the mass flow must also be chosen. Finally, consider the case when w_c^e and ω^e are specified. This gives the opportunity to determine p_p^e from (2.33) and τ_d^e from (2.37). The parameter k_t can now be found by (2.36). This procedure also involves the use of a compressor map. However, the inverse function is not needed. This is an advantage since models of compressor maps can be composed of several functions, where each function describes some region of the compressor characteristic. The related algorithm for evaluating the compressor characteristic for some given inputs, e.g. mass flow and impeller speed, uses some clever lookup to decide which function/region to be evaluated. Hence, the calculation of an inverse function in such situations can be troublesome.

Chapter 3

Control laws

3.1 Introduction

Active surge control was first introduced in [20]. Since then a vast amount of results have been published on the topic, and for a comprehensive description of different approaches the reader is referred to [2], [3], [4] and [5]. Much of the literature is devoted to using the throttle downstream plenum for actuation. A more resent result for this approach is given in [21] and [22]. Theoretical and experimental studies are carried out by using pressure upstream the compressor as feedback to a variable area throttle. Other examples of actuators involve a closed coupled valve (CCV), recirculation valve, blow off or bleed valves and impeller speed or torque. A detailed study of actuator and sensing for surge control is offered in [23] and [24].

Results on using the drive unit for surge control are, however, limited. In [25] a control law using CCV and impeller torque as actuators was reported. In this scheme the CCV actuation can be considered to achieve active surge control, whereas the torque actuation gives the desired speed. In [26] a control law using throttle downstream plenum and torque as actuators was presented. Also here the torque control was used to achieve desired speed, whereas the throttle was used for active surge control. Similar results regarding CCV and throttle actuation can be found in [27], where the drive torque is used to compensate for model uncertainty.

Active surge control using only the compressor drive unit was first introduced in [19]. A control law for impeller speed was presented, which could stabilize any point in the compressor map. Furthermore, a control law for

drive torque was presented. This control ensured convergence to some region enclosing the desired operating point, but could not guarantee convergence to the operating point itself.

In this chapter control laws for stabilization of any desired equilibrium point of the model presented in Chapter 2, using either impeller speed or torque as control input to the system, are derived. Throughout this chapter a variables deviation from a desired equilibrium point is defined as $\bar{(\cdot)} = (\cdot) - (\cdot)^e$, with $(\cdot)^e$ denoting the desired equilibrium.

This chapter starts by presenting a surge control law for impeller speed in Section 3.2. This is an extensions of the proportional feedback from mass flow presented [19], introducing integral effect and a nonlinear gain.

Section 3.3 presents novel active surge control laws for drive torque. Some basic control structures are derived in Section 3.3.1 and Section 3.3.2. Section 3.3.3 shows that these basic control laws can be extended with a passive part. Adaptive versions of basic control laws, alternatively also including the passive part, are presented in Section 3.3.4. The adaptive laws addresses model parameters appearing in the control law, making it completely independent of these constants. Section 3.3.5 shows how the basic control laws, possibly also including passive part, can be extended with nonlinear damping to reduce effects of model structural uncertainties. Finally, some comments are offered in Section 3.4.

This chapter is more or less a summary of results presented in [28], [29] and [30]. These articles, however, also contains some simulations. Furthermore, alternative variants/formulation of adaptive control laws and nonlinear damping can be found in these.

3.2 Impeller speed as control input

When considering the impeller speed as control input for the compression system, the dynamic model is given by (2.1), (2.8) and (2.25). Impeller speed, entering the system through p_c, is now the control input to be designed. This means that dynamics related to the impeller speed, (2.4), should be fast. More specifically, the impeller speed dynamics should be fast relative to duct mass flow and plenum pressure dynamics, in the sense that it appears to take on a desired value instantaneously.

Proposition 3.1 *The control law*

$$\begin{aligned}\omega &= -\bar{w}_c\alpha\left(\bar{w}_c,\bar{p}_p,w_i\right)+sat\left(w_i\right)+\omega^e\\ \dot{w}_i &= -c_i\bar{w}_c\end{aligned}$$

where $\alpha\left(\cdot\right)$ *is some function satisfying*

$$\frac{\partial\left(\bar{w}_c\alpha\left(\bar{w}_c,\bar{p}_p,w_i\right)\right)}{\partial\bar{w}_c}\geq\frac{\frac{\partial p_c\left(w_c^e,\omega^e\right)}{\partial w_c^e}+\delta}{\frac{\partial p_c\left(w_c^e,\omega^e\right)}{\partial\omega^e}},$$

sat $\left(w_i\right)$ *has arbitrary limits,* $c_i\geq 0$ *and* $\delta>0$*, leaves the desired equilibrium asymptotically stable.*

Proof. Deviation from desired equilibrium is defined as

$$x=\begin{bmatrix}p_p-p_p^e & w_c-w_c^e & c_i\int\left(w_c-w_c^e\right)dt\end{bmatrix}^T,\ u=\omega-\omega^e \tag{3.1}$$

for notational convenience. The dynamic model (2.1), (2.25) and $\dot{w}_i$ of Proposition 3.1 can be rewritten in terms of error variables

$$\begin{aligned}\dot{x}_1 &= k_1\left(x_2-f_1\left(x_1\right)\right) &(3.2)\\ \dot{x}_2 &= k_2\left(f_2\left(x_2,u\right)-x_1\right) &(3.3)\\ \dot{x}_3 &= -c_ix_2 &(3.4)\end{aligned}$$

using (3.1), where $k_1=\frac{c_p^2}{V_p}$, $k_2=\frac{A_c}{L_c'}$ and the functions

$$\begin{aligned}f_1\left(x_1\right) &= w_t\left(x_1+p_p^e\right)-w_t\left(p_p^e\right) &(3.5)\\ f_2\left(x_2,u\right) &= p_c\left(x_2+w^e,u+\omega^e\right)-p_c\left(w^e,\omega^e\right) &(3.6)\end{aligned}$$

is found by using (2.33) and (2.36). These functions satisfies $f_1\left(0\right)=f_2\left(0,0\right)=0$. Furthermore, from (3.5), (3.6) and (2.27)-(2.28) it can be recognized that

$$\begin{aligned}\left(a-b\right)\left(f_1\left(a\right)-f_1\left(b\right)\right) &> 0 &(3.7)\\ \left(a-b\right)\left(f_2\left(c,a\right)-f_2\left(c,a\right)\right) &> 0. &(3.8)\end{aligned}$$

Consider now the function

$$V\left(x\right)=\frac{1}{2k_1}x_1^2+\frac{1}{2k_2}x_2^2+\frac{1}{c_i}\int_0^{x_3}f_2\left(0,sat\left(\sigma\right)\right)d\sigma \tag{3.9}$$

which is positive definite and radially unbounded in x due to (3.8). The time derivative along the solutions of (3.2)-(3.4) is found as

$$\dot{V}(x) = -\underbrace{\left(x_1 f_1(x_1) + \delta x_2^2\right)}_{W(x)} + x_2 \underbrace{\left(f_2(x_2, u(x)) + \delta x_2 - f_2(0, sat(x_3))\right)}_{f(x)} \tag{3.10}$$

for some $\delta > 0$, where $W(x)$ is positive semi definite in x and the control input has been defined explicitly as a function of system states.

Following [19], the objective is now to design $u(x)$ such that $f(x)|_{x_2=0} = 0$ and $\frac{\partial f(x)}{\partial x_2} \leq 0$. This will place $f(x)$ in a sector such that $x_2 f(x) \leq 0$. Defining

$$u(x) = -x_2 \alpha(x) + sat(x_3) \tag{3.11}$$

guarantees $f(x)|_{x_2=0} = 0$. Furthermore, this definition leaves $\alpha(x)$ to be chosen such that the gradient requirement

$$\begin{aligned} 0 &\geq \frac{\partial f(x)}{\partial x_2} = \frac{\partial f_2(x_2, u(x))}{\partial x_2} + \frac{\partial f_2(x_2, u(x))}{\partial u(x)} \frac{\partial u(x)}{\partial x_2} \\ &\Updownarrow \\ \frac{\partial (x_2 \alpha(x))}{\partial x_2} &\geq \left(\frac{\partial f_2(x_2, u(x))}{\partial u(x)}\right)^{-1} \left(\frac{\partial f_2(x_2, u(x))}{\partial x_2} + \delta\right) \end{aligned} \tag{3.12}$$

is satisfied, where it has been used that (3.8) ensures $\frac{\partial f_2(x_2, u(x))}{\partial u(x)} > 0$. An upper bound on (3.10) is now found as

$$\dot{V}(x) \leq -W(x) \ \ \forall x \in D \tag{3.13}$$

where D describes the domain for which (3.12) holds, and Proposition 3.1 guarantees that D contains the origin. This implies that $x = 0$ is stable, [18]. Furthermore, by defining the set

$$S = \left\{ x \in D \middle| \, \dot{V}(x) = 0 \right\} = \{ x \in D | \, x_1 = x_2 = 0 \} \tag{3.14}$$

it can be seen that no solution can stay identical in (3.14) other than $x = 0$,

$$\left.\begin{array}{l} x_1 \equiv 0 \\ x_2 \equiv 0 \end{array}\right\} \Rightarrow f_2(0, sat(x_3)) \equiv 0 \Rightarrow x_3 \equiv 0, \tag{3.15}$$

where the last implication follows from (3.8). This implies that the origin of (3.2)-(3.4) is asymptotically stable, [18]. ■

Corollary 3.1 *By choosing* $\alpha(\bar{w}_c, \bar{p}_p, w_i) = c_s$ *and setting the saturation limits for* w_i *to zero, the control law becomes identical to that reported in [19].*

Proof. With $\alpha(\bar{w}_c, \bar{p}_p, w_i) = c_s$ it follows that

$$\frac{\partial(\bar{w}_c \alpha(\bar{w}_c, \bar{p}_p, w_i))}{\partial \bar{w}_c} = c_s$$

where $c_s \geq (\frac{\partial p_c(w_c^e, \omega^e)}{\partial w_c^e} + \delta)/(\frac{\partial p_c(w_c^e, \omega^e)}{\partial \omega^e})$ is required in order to satisfy the requirements of Proposition 3.1. Furthermore, setting saturation limits to zero results in the control law

$$\begin{aligned} \omega &= -\bar{w}_c \alpha(\bar{w}_c, \bar{p}_p, w_i) + sat(w_i) + \omega^e \\ &= -c_s \bar{w}_c + \omega^e. \end{aligned}$$

■

Proposition 3.1 can be considered a PI type control law, where $\bar{w}_c \alpha(\bar{w}_c, \bar{p}_p, w_i)$ represents a nonlinear gain, $sat(w_i)$ represents the integral effect on mass flow deviation and ω^e is a reference feed forward term. As discussed in Chapter 2, it might be challenging to find the corresponding equilibrium values for all system states. The errors made when choosing inconsistent equilibrium point might now be corrected by the introduced integrating effect, eventually taking the system towards the mass flow equilibrium. This is especially expected to be the case when α is chosen as a function of mass flow only, in which case the only uncertainty related to equilibrium values is in the constant feed forward term ω^e.

The region of attraction for this control law is limited by some domain D, for which both the model is valid and

$$\frac{\partial(\bar{w}_c \alpha(\bar{w}_c, \bar{p}_p, w_i))}{\partial \bar{w}_c} \geq \frac{\frac{\partial p_c(\bar{w}_c + w_c^e, \bar{\omega} + \omega^e)}{\partial(\bar{w}_c + w_c^e)} + \delta}{\frac{\partial p_c(\bar{w}_c + w_c^e, \bar{\omega} + \omega^e)}{\partial(\bar{\omega} + \omega^e)}} \tag{3.16}$$

holds. The model is for one thing confined to positive impeller speeds, which will restrict the magnitude of the control action from below. From (3.16) it can be seen that requirements for the nonlinear control gain, $\bar{w}_c \alpha(\bar{w}_c, \bar{p}_p, w_i)$, is dictated by the compressor map gradients. In this sense, the success of this control law depends largely on the specifics of the compressor. Section

3.3.1 discusses the domain D and its implication on the region of attraction in more detail.

The saturated integrator was introduced to the system on the basis of passivity of the integrator itself and (2.28). This can be seen from the proof, in the way this control part was introduced to the Lyapunov function. A similar approach can possibly be used for other passive control parts. To illustrate this, consider a low pass filtered and saturated gain. Following the notation of the proof, a passive first order filter can be formulated by $a\dot{x}_4 = -x_4 + cz$ and $y = sat(x_4)$. Here z is filter input, y is filter output, $a > 0$ is filter time constant and $c > 0$ is filter gain. By considering $V(x_4) = \frac{a}{c}\int_0^{x_4} f_2(0, sat(\sigma))\, d\sigma$, the time derivative is found as $\dot{V}(x_4) = -\frac{1}{c}x_4 f_2(0, sat(x_4)) + z f_2(0, sat(x_4))$. Due to (3.8) the term $x_4 f_2(0, sat(x_4))$ is positive definite in x_4. Furthermore, by defining the filter input, $z = -x_2$, the term $x_2 f_2(0, sat(x_4))$ can be handled in the same manner as the saturated integrator (including it in $f(x)$ of (3.10)). This would rewrite the control input of Proposition 3.1 as $u(x) = -x_2\alpha(x) + sat(x_3) + sat(x_4)$. Note that this extension does not influence the requirement (3.16) explicitly, but will influence the magnitude of ω. However, this effect can be limited by the saturation.

3.3 Drive torque as control input

In this section backstepping is applied to design an input τ_d to asymptotically stabilize a desired equilibrium of (2.1), (2.4)-(2.8) and (2.25). To this end it is assumed that dynamics related to the driving unit for generating a desired torque is fast relative to plenum pressure, duct mass flow and impeller speed dynamics.

By closer inspection of the model it is clear that it is in a pure-feedback form [31]. The only reason for it not to be in a strict-feedback form can be found in the mass flow dynamics, where ω does not appear affine, but through a nonlinear mapping $p_c(w, \omega)$. The practical implication of this is that stepping back on ω becomes somewhat more complicated, especially since only qualitative properties of this function is assumed known.

Using backstepping to stabilize the compression system was also done in [32], where flow through the throttle was used to manipulate system dynamics of a model capturing the phenomenons of both surge and rotating stall.

Since then, a number of publications reports control laws for compression systems based on backstepping design.

3.3.1 Basic control law

Proposition 3.2 *Either of the control laws*

$$\begin{aligned}\tau_d &= -c_1\left(\bar{\omega}+c_2\bar{w}_c\right)-c_2\frac{JA_c}{L_c'}\left(p_c\left(w,\omega\right)-p_p\right)+\tau_l\left(w_c,\omega\right)\\ \tau_d &= -c_1\left(\bar{\omega}+c_2\bar{w}_c\right)-c_2\frac{JA_c}{L_c'}\left(p_c\left(w,\omega\right)-p_p\right)-c_2k_c\left|w_c\right|\bar{w}_c-c_2k_f\bar{w}_c+\tau_d^e\end{aligned}$$

where

$$c_2 \geq \frac{\frac{\partial p_c(w_c^e,\omega^e)}{\partial w_c^e}+\delta}{\frac{\partial p_c(w_c^e,\omega^e)}{\partial \omega^e}},$$

$c_1 > 0$ *and* $\delta > 0$*, will make the desired equilibrium asymptotically stable.*

Proof. For notational convenience the notations

$$x = \begin{bmatrix}p_p-p_p^e & w_c-w_c^e & \omega-\omega^e\end{bmatrix}^T,\ u=\tau_d-\tau_d^e \tag{3.17}$$

are introduced. Using these definitions rewrites the system (2.1), (2.4)-(2.8) and (2.25) can be rewritten in terms of error variables as

$$\begin{aligned}\dot{x}_1 &= k_1\left(x_2-f_1\left(x_1\right)\right) &(3.18)\\ \dot{x}_2 &= k_2\left(f_2\left(x_2,x_3\right)-x_1\right) &(3.19)\\ \dot{x}_3 &= k_3\left(u-f_3\left(x_2,x_3\right)\right) &(3.20)\end{aligned}$$

where $k_1=\frac{c_p^2}{V_p}$, $k_2=\frac{A_c}{L_c'}$, $k_3=\frac{1}{J}$ and the functions

$$\begin{aligned}f_1\left(x_1\right) &= w_t\left(x_1+p_p^e\right)-w_t\left(p_p^e\right) &(3.21)\\ f_2\left(x_2,x_3\right) &= p_c\left(x_2+w^e,x_3+\omega^e\right)-p_c\left(w_c^e,\omega^e\right) &(3.22)\\ f_3\left(x_2,x_3\right) &= \tau_l\left(x_2+w^e,x_3+\omega^e\right)-\tau_l\left(w^e,\omega^e\right). &(3.23)\end{aligned}$$

is found by using (2.33), (2.36) and (2.37). From (3.21)-(3.23) it can be seen that $f_1\left(0\right)=f_2\left(0,0\right)=f_3\left(0,0\right)=0$. Furthermore, from (3.21)-(3.23) and (2.27)-(2.29) it follows that

$$\begin{aligned}\left(a-b\right)\left(f_1\left(a\right)-f_1\left(b\right)\right) &> 0 &(3.24)\\ \left(a-b\right)\left(f_2\left(c,a\right)-f_2\left(c,b\right)\right) &> 0 &(3.25)\\ \left(a-b\right)\left(f_3\left(c,a\right)-f_3\left(c,b\right)\right) &> 0. &(3.26)\end{aligned}$$

The backstepping design is started by defining

$$z_1 = x_1 \tag{3.27}$$

as the first backstepping variable. In the z_1 dynamics, x_2 is considered as virtual control. This introduces the second backstepping variable

$$z_2 = x_2 - \alpha_2 (z_1) \tag{3.28}$$

where α_2 is the related stabilizing function. Considering the function $V_1 (z_1) = \frac{1}{2} d_1 z_1^2$ for some constant $d_1 > 0$, it can be seen from (3.18), (3.27) and (3.28) that $\dot{V}_1 (z_1) = d_1 k_1 z_1 f_1 (z_1) + d_1 k_1 z_1 z_2 + d_1 k_1 z_1 \alpha_2 (z_1)$. The term $z_1 f_1 (z_1)$ is negative definite in z_1 due to (3.24). This implies that α_2 is not absolutely needed to render $\dot{V}_1$ negative definite in z_1. Even if a choice different from

$$\alpha_2 (z_1) = 0 \tag{3.29}$$

could give freedom later in the design, it is preferred to keep the structural complexity of the controller low.

From (3.28) and (3.29) it follows that $z_2 = x_2$. In the related dynamics, x_3 is considered as virtual control. This introduces the third backstepping variable

$$z_3 = x_3 - \alpha_3 (z_1, z_2) \tag{3.30}$$

where α_3 is the related stabilizing function. Considering the function

$$V_2 (z_1, z_2) = \frac{1}{2} d_1 z_1^2 + \frac{1}{2} d_2 z_2^2 \tag{3.31}$$

for some constant $d_2 > 0$ it can be seen from (3.18), (3.19) and (3.27)-(3.30) that

$$\begin{aligned} \dot{V}_2 (z_1, z_2) \;=\; & -d_1 k_1 z_1 f_1 (z_1) - \delta d_2 k_2 z_2^2 - d_2 \left(k_2 - \frac{k_1 d_1}{d_2} \right) z_1 z_2 \\ & + d_2 k_2 z_2 \left(f_2 (z_2, \alpha_3 (z_1, z_2)) + \delta z_2 \right) \\ & + d_2 k_2 z_2 \underbrace{\left(f_2 (z_2, z_3 + \alpha_3 (z_1, z_2)) - f_2 (z_2, \alpha_3 (z_1, z_2)) \right)}_{f_2' (z_1, z_2, z_3)} \end{aligned} \tag{3.32}$$

for some constant $\delta > 0$. The cross term in $z_1 z_2$ can be cancelled by an appropriate choice of d_1. Furthermore, the term $z_2 \left(f_2 (z_2, \alpha_3 (z_1, z_2)) + \delta z_2 \right)$

is handled in the same manner as in [19]

$$\begin{aligned} \alpha_3(z_1, z_2) &= -c_2 z_2 && (3.33) \\ c_2 &\geq \frac{\frac{\partial f_2(z_2,\alpha_3)}{\partial z_2} + \delta}{\frac{\partial f_2(z_2,\alpha_3)}{\partial \alpha_3}} && (3.34) \end{aligned}$$

resulting in $z_2\left(f_2\left(z_2, \alpha_3\left(z_1, z_2\right)\right) + \delta z_2\right) \leq 0$. Using (3.33)-(3.34) and choosing $d_1 = \frac{k_2 d_2}{k_1}$ bounds (3.32) from above according to

$$\dot{V}_2(z_1, z_2) \leq -k_2 d_2 z_1 f_1(z_1) - d_2 k_2 \delta z_2^2 + d_2 k_2 z_2 f_2'(z_1, z_2, z_3) \tag{3.35}$$

on a domain for which (3.34) is satisfied.

From (3.30) and (3.33) it follows that $z_3 = x_3 + c_2 z_2$. Considering the function

$$V_3(z_1, z_2, z_3) = V_2(z_1, z_2) + \frac{1}{2} d_3 z_3^2 \tag{3.36}$$

for some constant $d_3 > 0$, an upper bound

$$\begin{aligned} \dot{V}_3(z_1, z_2, z_3) \leq\ & d_2 k_2 z_1 f_1(z_1) - d_2 k_2 \delta z_2^2 \\ & + d_2 k_2 z_2 f_2'(z_1, z_2, z_3) \\ & + d_3 k_3 z_3 (\tau_d - f_3(z_2, z_3 + \alpha_3(z_2)) \\ & + c_2 \frac{k_2}{k_3} \left(f_2\left(z_2, z_3 + \alpha_3(z_2)\right) - z_1\right) - \tau_d^e) \end{aligned} \tag{3.37}$$

is found by using (3.17), (3.19), (3.20), (3.28)-(3.30), (3.33) and (3.35). Note that the control input τ_d is now available in (3.37). Before choosing this, the sign indefinite term $z_2 f_2'(z_1, z_2, z_3)$ needs attention. Applying the mean value theorem it can be recognized that

$$\begin{aligned} z_2 f_2'(z_1, z_2, z_3) &= z_2\left(f_2\left(z_2, z_3 + \alpha_3(z_1, z_2)\right) - f_2\left(z_2, \alpha_3(z_1, z_2)\right)\right) \\ &= \left.\frac{\partial f_2(r_1, r_2)}{\partial r_2}\right|_{L_{1,2}} z_2 z_3, \end{aligned} \tag{3.38}$$

where r_1 and r_2 are found as

$${L_{1,2}}^1\left(\begin{bmatrix} z_2 \\ \alpha_3 \end{bmatrix}, \begin{bmatrix} z_2 \\ z_3 + \alpha_3 \end{bmatrix}\right) = \left\{ \begin{array}{l} r_1 \,|\, r_1 = z_2 \\ r_2 \,|\, r_2 = -c_2 z_2 + (1-\theta) z_3,\ 0 < \theta < 1 \end{array} \right\} \tag{3.39}$$

by using (3.33). The resulting cross term $z_2 z_3$ is now dominated by using the already present quadratic term $-d_2 k_2 \delta z_2^2$ in (3.37) and a quadratic term z_3^2 resulting from the choice

$$\tau_d = \underbrace{-c_1 z_3}_{\tau_{d1}} + \tau_{d2}. \tag{3.40}$$

Redefining the constants $\delta = \delta_1 + \delta_2$ and $c_1 = c_{11} + c_{12}$ for notational convenience, (3.37) is now rewritten using (3.38) and (3.40)

$$\begin{aligned} \dot{V}_3(z) \leq & -\underbrace{\left(d_2 k_1 z_2 f_1(z_1) + d_2 k_2 \delta_1 z_2^2 + d_3 k_3 c_{11} z_3^2\right)}_{W(z)} - d_3 k_3 z_{2,3}^T Q(t) z_{2,3} \\ & + d_3 k_3 z_3 (\tau_{d2} - f_3(z_2, z_3 + \alpha_3) \\ & + c_2 \frac{k_2}{k_3} \left(f_2(z_2, z_3 + \alpha_3) - z_1\right) - \tau_d^e) \end{aligned} \tag{3.41}$$

where

$$Q(t) = \begin{bmatrix} \frac{d_2 k_2}{d_3 k_3} \delta_2 & -\frac{1}{2} \frac{d_2 k_2}{d_3 k_3} \frac{\partial f_2(r_1, r_2)}{\partial r_2} \\ -\frac{1}{2} \frac{d_2 k_2}{d_3 k_3} \frac{\partial f_2(r_1, r_2)}{\partial r_2} & c_{12} \end{bmatrix}, \tag{3.42}$$

$z = \begin{bmatrix} z_1 & z_2 & z_3 \end{bmatrix}^T$ and $z_{2,3} = \begin{bmatrix} z_2 & z_3 \end{bmatrix}^T$. Note that the matrix (3.42) is considered as a function of time due to the term $\frac{\partial f_2(r_1, r_2)}{\partial r_2}$, where $r_1 = z_2$ and r_2 is some point on a line segment.

The upper left determinants of (3.42) are calculated as

$$\left\{ \begin{array}{l} \frac{d_2 k_2}{d_3 k_3} \delta_2, \\ \frac{d_2 k_2}{d_3 k_3} \delta_2 c_{12} - \frac{1}{4} \frac{d_2 k_2}{d_3 k_3} \left(\frac{\partial f_2(r_1, r_2)}{\partial r_2} \right)^2 \end{array} \right\}, \tag{3.43}$$

showing that the matrix is positive definite in t if the fraction $\frac{d_2}{d_3}$ is chosen sufficiently small as to suppress the effect of $\frac{\partial f_2(r_1, r_2)}{\partial r_2}$ for all t. From (3.39) it is seen that r_1 and r_2 is defined by a linear combinations of z_2 and z_3. As discussed in Chapter 2, $\frac{\partial f_2(r_1, r_2)}{\partial r_2}$ (defined in terms of $\frac{\partial p_c(a,b)}{\partial b}$) is continuous in its arguments. Hence, $\frac{\partial f_2(r_1, r_2)}{\partial r_2}$ is bounded for bounded $z_{2,3}$ and (3.42) is made positive definite in $z_{2,3}$ semi globally by choosing $\frac{d_2}{d_3}$ sufficiently small.

Various control laws can now de derived, depending on how the terms in the same bracket as τ_{d2} of (3.41) are handled. One approach is to cancel all

terms, as is done with the first control law of Proposition 3.2. This rewrites (3.41) as

$$\dot{V}_3(z) \leq -W(z) \ \ \forall z \in D \tag{3.44}$$

where it follows from (3.41) that $W(z)$ is positive definite in z. The domain D is described by the region for which the model is valid, (3.34) holds and (3.42) is positive definite. Since (3.42) is positive definite in $z_{2,3}$ semi globally, the domain D is in essence described by model validity and (3.34). The domain is guaranteed to contain $z = 0$ by the requirement for c_2 made in Proposition 3.2. It then follows from (3.36) and (3.44) that V_3 is positive definite and radially unbounded on D and $\dot{V}_3$ is negative definite on D. Hence, $z = 0$ is asymptotically stable.

The expression for compressor torque in (3.41) can be rewritten using (2.5)-(2.7) and (3.23)

$$f_3(z_2, z_3 + \alpha_3) = f_3(z_2, z_3) + \underbrace{k_c |z_2 + w^e| \alpha_3 + k_f \alpha_3}_{f_3(z_2, z_3+\alpha_3) - f_3(z_2, z_3)}. \tag{3.45}$$

From (3.23) and (3.26) it is known that

$$z_3 f_3(z_2, z_3) = (z_3 - 0)(f_3(z_2, z_3) - f_3(z_2, 0)) > 0. \tag{3.46}$$

Control law two of Proposition 3.2 is now given by letting τ_{d2} in (3.41) only cancel the $k_c |z_2 + w^e| \alpha_3 + k_f \alpha_3$ of (3.45), rewriting the upper bound (3.41)

$$\dot{V}_3(z) \leq -W(z) - d_3 k_3 z_3 f_3(z_2, z_3) \ \ \forall z \in D \tag{3.47}$$

where D is as discussed for (3.44). Note that even though $z_3 f_3(z_2, z_3)$ is positive definite and radially unbounded in z_3, $c_1 > 0$ is still needed to guarantee (3.42) positive definite on D. ■

It follows from the control synthesis that the region of attraction for these control laws is limited to some region within a domain D for which $|\bar{w}_c| < \infty$, $|\bar{\omega} + c_2 \bar{w}_c| < \infty$ and

$$c_2 \geq \left. \frac{\frac{\partial p_c(a,b)}{\partial a}}{\frac{\partial p_c(a,b)}{\partial b}} \right|_{\substack{a = \bar{w}_c + w_c^e \\ b = -c_2 \bar{w}_c + \omega^e}}. \tag{3.48}$$

From (2.28) it is known that p_c is strictly increasing in impeller speed, which suggests that there exists some positive constant g_ω such that $\frac{\partial p_c(a,b)}{\partial b} \geq$

$g_\omega \forall (a,b)$. From Figure 2.2 it can be seen that the mass flow gradient is positive between zero mass flow and the surge line, and negative for other ranges. One imitate consequence of this is that the gain c_2 must be positive in order to stabilize equilibrium points in the open loop unstable regime. It is reasonable to assume that $\frac{\partial p_c(a,b)}{\partial b}$ is continuous in this region, which suggests that there exists some positive constant g_w such that $\frac{\partial p_c(a,b)}{\partial b} \leq g_w \ \forall (a,b)$ (since $\frac{\partial p_c(a,b)}{\partial b} < 0$ outside this region). Combining these bounds on gradients, the region of attraction can be chosen arbitrary large by choosing $c_2 \geq \frac{g_w}{g_\omega}$. However, as discussed in Chapter 2 the model is only valid for positive impeller speed. Hence, the term $c_2\bar{w}_c$ is restricted to $b = \omega^e - c_2\bar{w}_c$ being positive. Furthermore, in practical applications this control gain will be upper bounded due to measurement noise and actuator saturation. The domain for which the stability analysis holds,

$$D = \left\{ (\bar{p}_p, \bar{w}_c, \bar{\omega}) \in R^3 \middle| \, \bar{p}_p \geq -p_p^e, \ -\infty < c_2\bar{w}_c \leq \omega^e, \ -\omega^e \leq \bar{\omega} < \infty \right\}, \tag{3.49}$$

is defined for mathematical rigor. In addition to the discussed criteria, a condition guaranteeing $p_p > 0$ has been included in D. Note that D is not the region of attraction, but a domain for which the region of attraction must be a subset of. For a more detailed discussion of estimating a region of attraction, the interested reader can consult [18].

Control laws of Proposition 3.2 involves direct cancellations of system models in the control synthesis. Both the forcing term p_c and compressor load torque τ_l can be found in the expressions for τ_d. The differences of the control laws are found in the way compressor torque is handled. The first law directly cancels the model for compressor torque, whereas the second cancels parts of it. Control law two has an additional stabilizing term, $z_3 f_3(z_2, z_3)$, in the derivative of the Lyapunov function used for analysis, compared with control law one. Comparing one and two is seems like the cancellation done in two is more robust since it leaves an additional stabilizing term. This claim has no rigorous justification in mathematics, but is based the observation that the time derivative of the Lyapunov function becomes "more negative" for control law two than for one.

3.3.2 Avoiding cancellations

The basic control laws presented in Section 3.3.1 can be divided into two parts, $\tau_d = \tau_{d1} + \tau_{d2}$. These are $\tau_{d1} = -c_1(\bar{\omega} + c_2\bar{w}_c)$ and τ_{d2} is different for the two control laws. The first part of the control laws can be thought of as dealing with the effect of using impeller speed as virtual control in the backstepping procedure, it is introduced to handle a "residue function" resulting from this step, whereas the second term contains the cancellations done in the final step. These cancellations involve models of compressor torque and possibly compressor characteristic, if not measurement is used.

In the following propositions it is investigated whether one can avoid compensating for impeller torque, compressor characteristics or both. The motivation for this is to make the control law independent of models for which uncertainty can be related. It turns out that this can be done if the gain c_1 is chosen sufficiently large. Moreover, from the control laws point of view, the region of attraction can be chosen arbitrary large by choosing c_1 sufficiently large. However, as already discussed the region of attraction will be limited and must be contained in a domain for which the model is valid.

Avoiding compressor torque in the control law

Proposition 3.3 *The control law*

$$\tau_d = -c_1(\bar{\omega} + c_2\bar{w}_c) - c_2\frac{JA_c}{L_c'}(p_c(w,\omega) - p_p) + \tau_d^e$$

where

$$c_2 \geq \frac{\frac{\partial p_c(w_c^e,\omega^e)}{\partial w_c^e} + \delta}{\frac{\partial p_c(w_c^e,\omega^e)}{\partial \omega^e}},$$

$c_1 > 0$ *sufficiently large and* $\delta > 0$*, will make the desired equilibrium asymptotically stable.*

Proof. Using the control law from Proposition 3.3 in (3.37) and the derivation leading to (3.47) gives an upper bound

$$\begin{aligned}\dot{V}_3(z) &\leq -W(z) - d_3k_3z_3f_3(z_2,z_3) \\ &\quad + d_3k_3(c_2k_c|z_2 + w^e| + c_2k_f)z_2z_3 - d_3k_3z_{2,3}^TQ(t)z_{2,3} \quad (3.50)\\ &\leq -W(z) - d_3k_3z_{2,3}^TQ'(t,z_2)z_{2,3} \quad (3.51)\end{aligned}$$

where

$$Q'(t,z_2) = \begin{bmatrix} \frac{d_2k_2}{d_3k_3}\delta_2 & q'_{12} \\ q'_{21} & c_{12} \end{bmatrix} \tag{3.52}$$

$$q'_{12} = q'_{21} = -\frac{1}{2}\left(\frac{d_2k_2}{d_3k_3}\frac{\partial f_2(r_1,r_2)}{\partial r_2} + c_2k_c\left|z_2+w^e\right| + c_2k_f\right) \tag{3.53}$$

The upper left determinants of (3.52) are

$$\left\{ \begin{array}{l} \frac{d_2k_2}{d_3k_3}\delta_2, \\ \frac{d_2k_2}{d_3k_3}\left(\delta_2c_{12} - \frac{1}{4}\left(\sqrt{\frac{d_2k_2}{d_3k_3}}\frac{\partial f_2(r_1,r_2)}{\partial r_2} + \sqrt{\frac{d_3k_3}{d_2k_2}}\left(k_c\left|z_2+w^e\right|+k_f\right)c_2\right)^2\right) \end{array} \right\} \tag{3.54}$$

which results in competing arguments in trying to suppress the effect of both $\frac{\partial f_2(r_1,r_2)}{\partial r_2}$ and $c_2\left(k_c\left|z_2+w^e\right|+k_f\right)$ using $\frac{d_2}{d_3}$. This implies that c_{12} also must be used to suppress the sign indefinite terms. ■

Avoiding compressor characteristic in the control law

Proposition 3.4 *Either of the control laws*

$$\tau_d = -c_1\left(\bar{\omega}+c_2\bar{w}_c\right) + c_2\frac{JA_c}{L'_c}\bar{p}_p + \tau_l\left(w_c,\omega\right)$$

$$\tau_d = -c_1\left(\bar{\omega}+c_2\bar{w}_c\right) + c_2\frac{JA_c}{L'_c}\bar{p}_p - c_2k_c\left|w_c\right|\bar{w}_c - c_2k_f\bar{w}_c + \tau_d^e$$

where

$$c_2 \geq \frac{\frac{\partial p_c(w_c^e,\omega^e)}{\partial w_c^e}+\delta}{\frac{\partial p_c(w_c^e,\omega^e)}{\partial \omega^e}},$$

$c_1 > 0$ *sufficiently large and* $\delta > 0$*, will make the desired equilibrium asymptotically stable.*

Proof. Using either control law one or two from Proposition 3.4 in (3.37) and following the derivation leading to (3.44) or (3.47) respectively, gives an upper bound

$$\dot{V}_3(z) \leq -W(z) - d_3k_3z_{2,3}^TQ(t)z_{2,3} + d_3k_3z_3c_2\frac{k_2}{k_3}f_2\left(z_2,z_3+\alpha_3\right) \tag{3.55}$$

leaving a cross term $z_3 f_2(z_2, z_3+\alpha_3)$. This term can be reformulated

$$\begin{aligned} z_3 f_2(z_2, z_3+\alpha_3) &= (z_3-0)(f_2(z_2, z_3+\alpha_3) - f_2(0,0)) \\ &= \left(\left.\frac{\partial f_2(r_3,r_4)}{\partial r_3}\right|_{L_{3,4}} - c_2 \left.\frac{\partial f_2(r_3,r_4)}{\partial r_4}\right|_{L_{3,4}} \right) z_2 z_3 \\ &\quad + \left.\frac{\partial f_2(r_3,r_4)}{\partial r_4}\right|_{L_{3,4}} z_3^2 \end{aligned} \tag{3.56}$$

using the mean value theorem, where $\begin{bmatrix} r_3 & r_4 \end{bmatrix}^T$ is some point on the line segment

$$L_{3,4}\left(\begin{bmatrix} 0 & 0 \end{bmatrix}^T, \begin{bmatrix} z_2 & z_3+\alpha_3 \end{bmatrix}^T\right). \tag{3.57}$$

The upper bound (3.55) is now rewritten using (3.56)

$$\dot{V}_3(z) \leq -W(z) - d_3 k_3 z_{2,3}^T Q'(t) z_{2,3} \tag{3.58}$$

where

$$Q'(t) = \begin{bmatrix} \frac{d_2 k_2}{d_3 k_3}\delta_2 & q'_{12} \\ q'_{21} & c_{12} - c_2 \frac{k_2}{k_3}\frac{\partial f_2(r_3,r_4)}{\partial r_4} \end{bmatrix} \tag{3.59}$$

$$\begin{aligned} q'_{12} &= q'_{21} \\ &= -\frac{1}{2}\left(\frac{d_2 k_2}{d_3 k_3}\frac{\partial f_2(r_1,r_2)}{\partial r_2} \right. \\ &\quad \left. -c_2\frac{k_2}{k_3}\left(\frac{\partial f_2(r_3,r_4)}{\partial r_3} - c_2\frac{\partial f_2(r_3,r_4)}{\partial r_4}\right)\right) \end{aligned} \tag{3.60}$$

The upper left determinants of (3.59) are

$$\left\{ \begin{array}{l} \frac{d_2 k_2}{d_3 k_3}\delta_2, \\ \frac{d_2 k_2}{d_3 k_3}\left(\delta_2\left(c_{12} - c_2\frac{k_2}{k_3}\frac{\partial f_2(r_3,r_4)}{\partial r_4}\right)\right. \\ \qquad \left. -\frac{1}{4}\left(\sqrt{\frac{d_2 k_2}{d_3 k_3}}\left(\frac{\partial f_2(r_1,r_2)}{\partial r_2} - \frac{d_3}{d_2}c_2\frac{\partial f_2(r_3,r_4)}{\partial r_3} + \frac{d_3}{d_2}c_2\frac{\partial f_2(r_3,r_4)}{\partial r_4}\right)\right)^2\right) \end{array} \right\} \tag{3.61}$$

where it can be recognized that c_2 must be chosen sufficiently large in order to guarantee $Q'(t)$ positive definite. ■

Compressor torque and pressure downstream the compressor

Proposition 3.5 *The control law*

$$\tau_d = -c_1\left(\bar{\omega} + c_2\bar{w}_c\right) + c_2\frac{JA_c}{L_c'}p_p + \tau_d^e$$

where

$$c_2 \geq \frac{\frac{\partial p_c(w_c^e,\omega^e)}{\partial w_c^e} + \delta}{\frac{\partial p_c(w_c^e,\omega^e)}{\partial \omega^e}},$$

$c_1 > 0$ *sufficiently large and* $\delta > 0$*, will make the desired equilibrium asymptotically stable.*

Proof. The proof follows by combining the proof of Proposition 3.4 and Proposition 3.5. ■

3.3.3 Passive extension

In the following it is shown that the control laws from Section 3.3.1 and Section 3.3.2 can be extended with a passive control part. Before the passive control part is introduced, some preliminary passive properties are derived for the closed loop system with previously proposed control laws.

Lemma 3.1 *Let*

$$\tau_d = \tau_s + \tau_p$$

where τ_s *is any of the control inputs from Proposition 3.2 - Proposition 3.5, then the system is strictly passive* $\tau_p \rightarrow (\bar{\omega} + c_2\bar{w}_c)$*.*

Proof. Define the storage function

$$V_s(z) = \frac{1}{d_3k_3}V_3(z) \tag{3.62}$$

where $V_3(z)$ is equal to that of (3.36). It then follows from the proofs of the propositions that

$$\dot{V}_s(z) \leq -\underbrace{\frac{1}{d_3k_3}W(z)}_{W_s(z)} - z_{2,3}^T Q'(t)\, z_{2,3} + z_3\tau_p \tag{3.63}$$

with $W(z)$ as in (3.41) and $Q'(t)$ varying for the various propositions. As shown in proofs of these propositions, this matrix is made positive definite semi globally (by increasing the gain c_1 in the case of not cancelling terms). Hence,

$$z_3\tau_p \geq \dot{V}_s(z) + W_s(z) \ \ \forall z \in D \tag{3.64}$$

where W_s is positive definite and D is given by (3.49). It follows that $z_3\tau_p$ is a strictly passive pair, [18]. ■

Lemma 3.2 *Let*

$$\tau_d = \tau_s + \tau_p$$

where τ_s is any of the control inputs from Proposition 3.2 - Proposition 3.5, then the system is output strictly passive and finite gain $\mathcal{L}_2$ stable $\tau_p \rightarrow (\bar{\omega} + c_2\bar{w}_c)$. Moreover, the $\mathcal{L}_2$ gain decreases when c_1 increases beyond what is required from the proposition in question.

Proof. The lower bound (3.64) is rewritten

$$z_3\tau_p \geq \dot{V}_s(z) + c_{11}z_3^2 \ \forall z \in D \tag{3.65}$$

extracting $c_{11}z_3^2$ from W_s. Since the system is output strictly passive of the given form, it is also finite gain $\mathcal{L}_2$ stable with $\mathcal{L}_2$ gain less than or equal $\frac{1}{c_{11}}$, [18]. ■

The input τ_p is at disposal and can be chosen freely. This motivates the investigation of extending the existing control laws by a passive part. It is known from the general theory of passivity that a strictly passive system in feedback interconnection with a strictly passive or a output strictly passive and zero state observable system gives asymptotic stability of the overall system. Let $\Sigma_s : \tau_p \rightarrow (\bar{\omega} + c_2\bar{w}_c)$ denote the closed loop system from previous propositions, where the subscript s refers to the use of τ_s for this system (the "stabilizing" control law). The task now is to chose some passive system $\Sigma_p : (\bar{\omega} + c_2\bar{w}_c) \rightarrow -\tau_p$, where this definition of input and output will result in the standard feedback interconnection of passive system for Σ_s and Σ_p. Notice that Σ_p input is a linear combination of equilibrium error variables for compressor mass flow and impeller speed, and system output is our "free to choose" control input τ_p. Hence, the system Σ_p can be chosen under restriction of a given input and output pair, meaning that dynamics of the system can be chosen freely. Choosing it to comply with the properties of

strictly passive or output strictly passive and zero state observable will guarantee asymptotic stability for overall feedback interconnection, [18]. Such a dynamic system can for instance be a PID type control law, [33]. Other examples involves saturated integrator and saturated low pass filtered gain, [18]. Furthermore, the passive system need not be dynamic. It can also be a static feedback, a so called passive memoryless function. Moreover, the overall τ_p can be composed of several of these alternatives in parallel, sum of passive systems, when passive systems in parallel preserves their passive properties, [18].

It is believed that best results for the overall control law is obtained by choosing c_1 and c_2 of the basic control law as small as possible so that stability is achieved, and then tune the passive part of the controller for performance. The motivation for this is found in measurement noise and actuator saturation, since a passive controller can offer low pass filtering and saturation in addition to gain. Furthermore, a dynamic control law can also offer integrating effect on its error variable to improve possible steady state error.

For Proposition 3.2, where c_1 can be chosen arbitrary small, the term $-c_1(\bar{\omega} + c_2\bar{w}_c)$ can be replaced by a saturated version. Let Σ_p contain the passive relation $y_p = sat(c_1' u_p)$, which rewrites in terms of error variables as $-\tau_p = sat(c_1'(\bar{\omega} + c_2\bar{w}_c))$. By now choosing c_1 vanishingly small in the sense that the effect of $-c_1(\bar{\omega} + c_2\bar{w}_c)$ on τ_d can be ignored, replaces this term with the saturated version offered by τ_p.

Proposition 3.6 *Let*

$$\tau_d = \tau_s + \tau_p$$

where τ_s is any of the control inputs from Proposition 3.2 - Proposition 3.5 and τ_p is generated by some passive system $\Sigma_p : (\bar{\omega} + c_2\bar{w}_c) \rightarrow -\tau_p$ for which a positive definite and radially unbounded storage function is related. Then the desired equilibrium will be stable. Furthermore, p_p, w_c and ω will converge to the desired equilibrium when initial values are sufficiently close.

Proof. Consider the function

$$V(z, z_p) = V_s(z) + V_p(z_p) \tag{3.66}$$

where z_p represent states of the passive system, V_s is as in (3.62) and V_p is a storage function for the passive dynamics. It follows from the assumption for

V_p and (3.62) that V is positive definite and radially unbounded in (z, z_p). Furthermore, the upper bound

$$-\tau_p z_3 \geq \dot{V}_p(z_p) \tag{3.67}$$

follows from the passive properties of Σ_p. Combing this with the upper bound (3.64) of Lemma 3.1 gives

$$\begin{aligned} \dot{V}(z, z_p) &= \dot{V}_s(z) + \dot{V}_p(z_p) \\ &\leq -W_s(z) \ \forall (z, z_p) \in D' \end{aligned} \tag{3.68}$$

where $D' = \{(z, z_p) \in R^n | \, z \in D\}$, $n = 3 + \dim(z_p)$ and D is identical to (3.49) and W_s as in (3.64). Since W_s is positive semi definite in (z, z_p), it follows that $(z, z_p) = (0, 0)$ is stable.

Let Ω_c be a compact positively invariant set defined by

$$\Omega_c = \{(z, z_p) \in R^n | \, V(z, z_p) \leq c\} \subset D' \tag{3.69}$$

for some constant c. The existence of such a set follows from V being positive definite and radially unbounded, [18]. By defining

$$E = \left\{ (z, z_p) \in \Omega_c | \, \dot{V} = 0 \right\} = \{(z, z_p) \in \Omega_c | \, z = 0\}, \tag{3.70}$$

it follows by invariance arguments that every solution starting in Ω_c approaches $z = 0$ as $t \to \infty$, [18]. ■

The region of attraction for this control law will not only depend on the gains of τ_s, but also on specifics of the passive system such as storage function and saturation of states. Whether or not states of the passive system converges to some equilibrium point depends in large on type of passivity. As already mentioned, convergence for these states can be guaranteed if Σ_p satisfies the property of strictly passive or output strictly passive and zero state observable. On the other hand, if Σ_p only satisfy the somewhat less restrictive property of passive one can only guarantee that these system states are bounded.

3.3.4 Adaptive extension

The state feedback backstepping procedure in Section 3.3.1 and Section 3.3.2 resulted in some basic control laws, where their differences lies in how they

compensate for compressor torque and the compressor characteristic. It has also been shown in Section 3.3.3 that these basic control laws can be extended with a passive part (static or dynamic) $\tau_d = \tau_s + \tau_p$, where τ_s is one of the basic control laws that must be present to ensure stability and τ_p is the passive component. Furthermore, the stabilizing part can be divided in two, $\tau_s = \tau_{s1} + \tau_{s2}$, where $\tau_{s1} = -c_1(\bar{\omega} + c_2\bar{w}_c)$ and τ_{s2} varies among the different implementation.

Uncertainties involved in cancelling terms are sought improved by parameter estimation. More specifically, constant parameters appearing affine in the cancelling terms will be addressed. This turns out to be rather straight forward since all cancellations comply with the so called matching condition, meaning that the cancelled terms are in the span of the control variable. More specifically, all cancellations are done in finial step of procedure by τ_{s2}.

Three different constants (treating $\frac{JA_c}{L_c'}$ as one constant only) appears affine in the control laws of Proposition 3.2 - Proposition 3.5. The parameter $\frac{JA_c}{L_c'}$ appears in all implementations, whereas k_c and k_f appears in some of them. Parameter estimators are derived by certainty equivalence. This involves replacing constants in the control law by their parameter estimates, and then do design to derive the dynamic part of estimators. Estimates will generally be denoted by θ, with subscript 1 referring to $\frac{JA_c}{L_c'}$, subscript 2 referring to k_c and subscript 3 referring to k_f. To cover the most general case, the adaptive version of Proposition 3.2 is derived for the case when a passive control law of Proposition 3.6 is included. Deriving the adaptive version of Proposition 3.3-Proposition 3.5 will consist of the exact same exercise, and is therefore omitted.

Proposition 3.7 *Let*

$$\tau_d = \tau_s + \tau_p,\ \tau_s = \tau_{s1} + \tau_{s2},\ \tau_{s1} = -c_1(\bar{\omega} + c_2\bar{w}_c)$$

then both

$$\begin{aligned}
\tau_{s2} &= \theta_2 |w_c| \omega + \theta_3\omega - c_2\theta_1 (p_c(w_c, \omega) - p_p) \\
\dot{\theta}_1 &= c_{\theta 1}c_2(\bar{\omega} + c_2\bar{w}_c)(p_c(w_c, \omega) - p_p) \\
\dot{\theta}_2 &= -c_{\theta 2}(\bar{\omega} + c_2\bar{w}_c)|w_c|\omega \\
\dot{\theta}_3 &= -c_{\theta 3}(\bar{\omega} + c_2\bar{w}_c)\omega
\end{aligned}$$

and

$$\begin{aligned}
\tau_{s2} &= -c_2\theta_2 \left|w_c\right| \bar{w}_c + c_2\theta_3\bar{w}_c - c_2\theta_1 \left(p_c\left(w_c,\omega\right) - p_p\right) + \tau_d^e \\
\dot{\theta}_1 &= c_{\theta 1}c_2 \left(\bar{\omega} + c_2\bar{w}_c\right)\left(p_c\left(w_c,\omega\right) - p_p\right) \\
\dot{\theta}_2 &= c_2c_{\theta 2}\left(\bar{\omega} + c_2\bar{w}_c\right)\left|w_c\right|\bar{w}_c \\
\dot{\theta}_3 &= -c_2c_{\theta 3}\left(\bar{\omega} + c_2\bar{w}_c\right)\bar{w}_c
\end{aligned}$$

ensures a stable desired equilibrium. Furthermore, p_p, w_c and ω will converge to the desired equilibrium when starting sufficiently close.

Proof. Deviation of parameter estimates from their actual value is denoted $z_{\theta i} = k_{\theta i} - \theta_i$, with $k_{\theta i}$ referring to the actual and unknown constant. Consider the function

$$V_\theta\left(z, z_p, z_\theta\right) = V_s\left(z\right) + V_p\left(z_p\right) + \frac{1}{2c_{\theta 1}}z_{\theta 1}^2 + \frac{1}{2c_{\theta 2}}z_{\theta 2}^2 + \frac{1}{2c_{\theta 3}}z_{\theta 3}^2 \tag{3.71}$$

where V_s is given in (3.62) and V_p is as in Proposition 3.6. The time derivative of this function is found as

$$\begin{aligned}
\dot{V}_\theta\left(z, z_p, z_\theta\right) \leq\ & -W_s\left(z\right) + z_3(\tau_{s2} - f_3\left(z_2, z_3 + \alpha_3\right) \\
& + c_2\frac{k_2}{k_3}\left(f_2\left(z_2, z_3 + \alpha_3\right) - z_1\right) - \tau_d^e) \\
& + \frac{1}{c_{\theta 1}}\dot{z}_{\theta 1}z_{\theta 1} + \frac{1}{c_{\theta 2}}\dot{z}_{\theta 2}z_{\theta 2} + \frac{1}{c_{\theta 3}}\dot{z}_{\theta 3}z_{\theta 3}
\end{aligned} \tag{3.72}$$

using τ_d of Proposition 3.7, analysis leading to (3.41), the definition of W_s in (3.63) and $-\tau_p z_3 \geq \dot{V}_p\left(z_p\right)$. This upper bound is rewritten

$$\begin{aligned}
\dot{V}_\theta\left(z, z_p, z_\theta\right) \leq\ & -W_s\left(z\right) \\
& + z_3(\tau_{s2} - \theta_2\left|z_2 + w^e\right|\left(z_3 + \alpha_3 + \omega^e\right) - \theta_3\left(z_3 + \alpha_3 + \omega^e\right) \\
& + \theta_1 c_2\left(f_2\left(z_2, z_3 + \alpha_3\right) - z_1\right)) \\
& + z_{\theta 1}\left(\frac{1}{c_{\theta 1}}\dot{z}_{\theta 1} + c_2 z_3\left(f_2\left(z_2, z_3 + \alpha_3\right) - z_1\right)\right) \\
& + z_{\theta 2}\left(\frac{1}{c_{\theta 2}}\dot{z}_{\theta 2} - z_3\left|z_2 + w^e\right|\left(z_3 + \alpha_3 + \omega^e\right)\right) \\
& + z_{\theta 3}\left(\frac{1}{c_{\theta 3}}\dot{z}_{\theta 3} - z_3\left(z_3 + \alpha_3 + \omega^e\right)\right)
\end{aligned} \tag{3.73}$$

using (2.5)-(2.7), (3.23) and the definition for z_θ. The first control law of Proposition 3.7 is now given by using τ_{s2}, $\dot{z}_{\theta 1}$, $\dot{z}_{\theta 2}$, and $\dot{z}_{\theta 3}$ to cancel the content of their brackets in (3.73), resulting in the upper bound

$$\dot{V}_\theta(z, z_p, z_\theta) \leq -W_s(z) \,\forall\, (z, z_p, z_\theta) \in D' \tag{3.74}$$

where $D' = \{(z, z_p, z_\theta) \in R^n | \, z \in D\}$, $n = 6 + \dim(z_p)$ and D is identical to (3.49). Since W_s is positive semi definite in (z, z_p, z_θ) it follows that $(z, z_p, z_\theta) = (0, 0, 0)$ is stable.

Let Ω_c be a compact positively invariant set defined by

$$\Omega_c = \{(z, z_p, z_\theta) \in R^n | \, V_\theta((z, z_p, z_\theta)) \leq c\} \subset D' \tag{3.75}$$

for some constant c. The existence of such a set follows from V_θ being positive definite and radially unbounded, [18]. By defining

$$E = \left\{ (z, z_p, z_\theta) \in \Omega_c | \, \dot{V} = 0 \right\} = \{(z, z_p, z_\theta) \in \Omega_c | \, z = 0\}, \tag{3.76}$$

it follows by invariance arguments that every solution starting in Ω_c approaches $z = 0$ as $t \to \infty$, [18].

Using (3.45) the upper bound (3.72) is rewritten

$$\begin{aligned} \dot{V}_\theta(z, z_p, z_\theta) \;\leq\; & -W_s(z) - z_3 f_3(z_2, z_3) \\ & + z_3(\tau_{s2} - k_c |z_2 + w^e| \alpha_3 + k_f \alpha_3 \\ & + c_2 \frac{k_2}{k_3} (f_2(z_2, z_3 + \alpha_3) - z_1) - \tau_d^e) \\ & + \frac{1}{c_{\theta 1}} \dot{z}_{\theta 1} z_{\theta 1} + \frac{1}{c_{\theta 2}} \dot{z}_{\theta 2} z_{\theta 2} + \frac{1}{c_{\theta 3}} \dot{z}_{\theta 3} z_{\theta 3} \end{aligned} \tag{3.77}$$

which in terms of z_θ and θ is

$$\begin{aligned} \dot{V}_\theta(z, z_p, z_\theta) \;\leq\; & -W_s(z) - z_3 f_3(z_2, z_3) \\ & + z_3(\tau_{s2} - \theta_2 |z_2 + w^e| \alpha_3 + \theta_3 \alpha_3 \\ & + \theta_1 c_2 (f_2(z_2, z_3 + \alpha_3) - z_1) - \tau_d^e) \\ & + z_{\theta 1} \left(\frac{1}{c_{\theta 1}} \dot{z}_{\theta 1} + z_3 c_2 (f_2(z_2, z_3 + \alpha_3) - z_1) \right) \\ & + z_{\theta 2} \left(\frac{1}{c_{\theta 2}} \dot{z}_{\theta 2} - z_3 |z_2 + w^e| \alpha_3 \right) \\ & + z_{\theta 3} \left(\frac{1}{c_{\theta 3}} \dot{z}_{\theta 3} + z_3 \alpha_3 \right). \end{aligned} \tag{3.78}$$

The second control law of Proposition 3.7 is now given by using τ_{s2}, $\dot{z}_{\theta 1}$, $\dot{z}_{\theta 2}$, and $\dot{z}_{\theta 3}$ to cancel the content of their brackets in (3.78), resulting in the upper bound

$$\dot{V}_\theta(z, z_p, z_\theta) \leq -\frac{1}{d_3 k_3} W(z) \in D' \tag{3.79}$$

where $D' = \{(z, z_p, z_\theta) \in R^n | \, z \in D\}$, $n = 6 + \dim(z_p)$ and D is identical to (3.49). Following the same arguments as for (3.74), it is concluded that $(z, z_p, z_\theta) = (0, 0, 0)$ is stable and every solution starting in Ω_c approaches $z = 0$ as $t \to \infty$ ■

The constant τ_d^e is used by the second control law of Proposition 3.7. From (2.37) it is known that this constant can be expressed as $\tau_d^e = k_c w_c^e \omega^e + k_f \omega^e$, where the uncertain parameters k_c and k_f appears. It is a simple exercise to also include these in the parameter estimate, which will rewrite $\tau_d^e = \theta_2 |w_c^e| \, \omega^e + \theta_3 \omega^e$ and add some term to the dynamics of θ_2 and θ_3. Alternatively τ_d^e can be considered as an unknown constant altogether.

Proposition 3.7 is an adaptive extension of Proposition 3.2, but the control laws of Proposition 3.3 - Proposition 3.5 can also relatively simply be extended with adaptive gains in the same manner. In the case of not compensating for compressor torque, the update law for θ_1 will remain exactly the same as presented here. The estimates θ_2 and θ_3 are not needed in this case, unless one wishes to replace k_c and k_f of τ_d^e. In the case of not compensating for pressure downstream the compressor, the estimates θ_2 and θ_3 will remain exactly the same as presented, while the update law for θ_1 will change slightly ($\dot{\theta}_1 = -c_{\theta 1} c_2 (\bar{\omega} + c_2 \bar{w}_c) \bar{p}_p$). In the case of not compensating for compressor torque nor pressure downstream the compressor, the update laws will be as in the individual aforementioned cases.

It is considered a design choice whether c_2 is included as part of the uncertain parameter $k_{\theta 1}$ or not. This control gain can be defined as being part of the unknown parameter, in which case it will completely disappear from τ_{s2}. An alternative formulation to the one presented can be made by splitting up the brackets enclosing p_c and p_p, and then treat the constant appearing affine in these variables as two different constants. Treating them as different constants has no root in physics, but might have an influence on overall system dynamics.

As was discussed for the passive extension for the control law, the region of attraction will now depend on the overall system dynamics.

3.3.5 Nonlinear damping

An alternative approach to adaptive control in order to reduce the effect of model uncertainties is to introduce nonlinear damping. This will give the opportunity to reduce the effect of structural as well as parameter errors introduced by the model, in contrast to the adaptive part that addressed parameters appearing affine in cancelled terms only, [31]. As discussed in Section 3.3.4, these cancellations can be found in τ_{s2} and are done in the final step of the design procedure. Since the terms implemented in τ_{s2} are only models, these cancellation will involve some uncertainty with respect to the actual value.

A relationship between model and actual value will generally be modeled as

$$f_\Delta = f\Delta_f(t) \tag{3.80}$$
$$\Delta_f(t) = 1 + \Delta(t) \tag{3.81}$$

for each cancellation, where f_Δ represents the actual value of the phenomena modeled by f and $\Delta(t)$ is bounded. From this it can be recognized that $\Delta(t)$ represents the models deviation from its real value, with $\Delta(t) = 0$ implying perfect match of model and actual value. Model error increases as $\Delta(t)$ deviates away from zero.

In order to limit the effect of errors introduced by uncertainty in cancelling model terms, the control law is extended with a nonlinear damping part τ_Δ. This is not introduced to achieve asymptotic stability in the presence of uncertainty, but rather limit the effect of these and to guarantee bounded of solutions in presence of uncertainty. Furthermore, it is assumed that the uncertainties related to the various models do not corrupt the properties stated by (2.27)-(2.31).

Proposition 3.8 *Let*

$$\begin{aligned}
\tau_d &= \tau_s + \tau_p + \tau_\Delta \\
\tau_s &= \tau_{s1} + \tau_{s2},\ \tau_{s1} = -c_1(\bar{\omega} + c_2\bar{w}_c) \\
\tau_\Delta &= \tau_{\Delta 1} + \tau_{\Delta 2},\ \tau_{\Delta 1} = -c_{\Delta 1}c_2^2(\bar{\omega} + c_2\bar{w}_c)\left(\frac{JA_c}{L_c'}(p_c(w,\omega) - p_p)\right)^2
\end{aligned}$$

where τ_p is generated by a strictly passive system for which a positive definite and radially unbounded storage function is related. Then either of the control

laws

$$\begin{aligned}\tau_{s2} &= -c_2\frac{JA_c}{L_c'}\left(p_c\left(w,\omega\right)-p_p\right)+\tau_l\left(w_c,\omega\right)\\ \tau_{\Delta 2} &= -c_{\Delta 2}\left(\bar{\omega}+c_2\bar{w}_c\right)\left(\tau_l\left(w_c,\omega\right)\right)^2\end{aligned}$$

or

$$\begin{aligned}\tau_{s2} &= -c_2\frac{JA_c}{L_c'}\left(p_c\left(w,\omega\right)-p_p\right)-c_2k_c\left|w_c\right|\bar{w}_c-c_2k_f\bar{w}_c+\tau_d^e\\ \tau_{\Delta 2} &= -c_{\Delta 2}\left(\bar{\omega}+c_2\bar{w}_c\right)\left(\tau_d^e-c_2k_c\left|w_c\right|\bar{w}_c-c_2k_f\bar{w}_c\right)^2\end{aligned}$$

will guarantee convergence to a set containing the desired equilibrium in presence of model uncertainty related to $\frac{JA_c}{L_c'}\left(p_c\left(w,\omega\right)-p_p\right)$ *and* $\tau_l\left(w_c,\omega\right)$.

Proof. Consider the function

$$V_\Delta\left(z,z_p\right)=V_s\left(z\right)+V_p\left(z_p\right) \tag{3.82}$$

where V_s is given by (3.62) and V_p is as in Proposition 3.8. The time derivative of this function is upper bounded by $\dot{V}_\Delta\left(z,z_p\right)=\frac{1}{d_3k_3}\dot{V}_3\left(z\right)+\dot{V}_p\left(z_p\right)\leq \frac{1}{d_3k_3}\dot{V}_3\left(z\right)-W_p\left(z_p\right)-\tau_pz_3$, using the assumptions related to the passive part. Substituting τ_d of Proposition 3.8 for τ_d of Proposition 3.2 in the derivation leading to (3.41) results in

$$\begin{aligned}\dot{V}_\Delta\left(z,z_p\right) \leq\ & -\underbrace{\left(\frac{1}{d_3k_3}W\left(z\right)+W_p\left(z_p\right)\right)}_{W_\Delta(z,z_p)}\\ & +z_3(\tau_{s2}+\tau_\Delta-f_{3\Delta}\left(z_2,z_3+\alpha_3\right)\\ & +c_2\frac{k_{2\Delta}}{k_{3\Delta}}\left(f_{2\Delta}\left(z_2,z_3+\alpha_3\right)-z_1\right)-\tau_{d\Delta}^e)\end{aligned} \tag{3.83}$$

where it has been used that $Q\left(t\right)$ is positive definite semi globally. In this relation $f_{3\Delta}\left(z_2,z_3+\alpha_3\right)$, $\frac{k_{2\Delta}}{k_{3\Delta}}\left(f_{2\Delta}\left(z_2,z_3+\alpha_3\right)-z_1\right)$ and $\tau_{d\Delta}^e$ are actual values, previously cancelled by τ_{s2} under assumption of accurate models. Recalling that

$$f_{3\Delta}\left(z_2,z_3+\alpha_3\right)=\tau_{l\Delta}\left(z_2+w^e,z_3+\alpha_3+\omega^e\right)-\tau_{l\Delta}\left(w^e,\omega^e\right) \tag{3.84}$$

and $\tau_{l\Delta}\left(w^e,\omega^e\right)=\tau^e_{d\Delta}$, leaves $\tau_{l\Delta}\left(z_2+w^e,z_3+\alpha_3+\omega^e\right)$ as a resultant for $f_{3\Delta}$ and $\tau^e_{d\Delta}$ in (3.83). By now using (3.80), (3.81), and the first τ_{s2} of Proposition 3.8 rewrites (3.83)

$$\begin{aligned}\dot{V}_\Delta\left(z,z_p\right) &\leq -W_\Delta\left(z,z_p\right)\\ &\quad +z_3(\tau_\Delta-\underbrace{\tau_l\left(z_2+w^e,z_3+\alpha_3+\omega^e\right)}_{f'_2}\Delta_2\left(t\right)\\ &\quad +c_2\underbrace{\frac{k_2}{k_3}\left(f_2\left(z_2,z_3+\alpha_3\right)-z_1\right)}_{f'_1}\Delta_1\left(t\right)).\end{aligned}\tag{3.85}$$

where $W_\Delta\left(z,z_p\right)$ is positive definite and the f''s are models. Inserting $\tau_\Delta=\tau_{\Delta1}+\tau_{\Delta2}=-c_{\Delta1}c_2^2z_3f_1'^2-c_{\Delta2}z_3f_2'^2$ and the first $\tau_{\Delta2}$ of Proposition 3.8, this inequality can now be upper bounded as

$$\begin{aligned}\dot{V}_\Delta\left(z,z_p\right) &\leq -W_\Delta\left(z,z_p\right)\\ &\quad -c_{\Delta1}c_2^2\left(z_3f'_1-\frac{1}{2c_2c_{\Delta1}}\Delta_1\left(t\right)\right)^2+\frac{\Delta_1^2\left(t\right)}{4c_{\Delta1}}\\ &\quad -c_{\Delta2}\left(z_3f'_2+\frac{1}{2c_{\Delta2}}\Delta_2\left(t\right)\right)^2+\frac{\Delta_2^2\left(t\right)}{4c_{\Delta2}}\\ &\leq -W_\Delta\left(z,z_p\right)+\frac{\Delta_1^2\left(t\right)}{4c_{\Delta1}}+\frac{\Delta_2^2\left(t\right)}{4c_{\Delta2}}.\end{aligned}\tag{3.86}$$

This inequality is the basis of discussion related to the first control law of Proposition 3.8, which is shortly detailed.

Proceeding now to the second control law of Proposition 3.8, the term $f_{3\Delta}\left(z_2,z_3+\alpha_3\right)$ in (3.83) is expressed as in (3.45)

$$f_{3\Delta}\left(z_2,z_3+\alpha_3\right)=f_{3\Delta}\left(z_2,z_3\right)+\underbrace{f_{3\Delta}\left(z_2,z_3+\alpha_3\right)-f_{3\Delta}\left(z_2,z_3\right)}_{f'_{3\Delta}}\tag{3.87}$$

which rewrites (3.83)

$$\begin{aligned}\dot{V}_\Delta\left(z,z_p\right) &\leq -W_\Delta\left(z,z_p\right)+z_3(\tau_{s2}+\tau_\Delta-\underbrace{\left(f'_{3\Delta}\left(z_2,z_3\right)+\tau^e_{d\Delta}\right)}_{f''_{3\Delta}}\\ &\quad +c_2\frac{k_{2\Delta}}{k_{3\Delta}}\left(f_{2\Delta}\left(z_2,z_3+\alpha_3\right)-z_1\right))\end{aligned}\tag{3.88}$$

where it has been used that $z_3 f_{3\Delta}(z_2, z_3) > 0$. By now using (3.80), (3.81), and the second τ_{s2} of Proposition 3.8 gives the upper bound

$$\begin{aligned}\dot{V}_\Delta(z, z_p) \leq & -W_\Delta(z, z_p) \\ & + z_3(\tau_\Delta - \underbrace{(f_3(z_2, z_3 + \alpha_3) - f_3(z_2, z_3) + \tau_d^e)}_{f_2'} \Delta_2(t) \\ & + c_2 \underbrace{\frac{k_2}{k_3}(f_2(z_2, z_3 + \alpha_3) - z_1)}_{f_1'} \Delta_1(t))\end{aligned} \tag{3.89}$$

for (3.88), where f_2' has changed relative to (3.85). By now choosing $\tau_\Delta = \tau_{\Delta 1} + \tau_{\Delta 2} = -c_{\Delta 1} c_2^2 z_3 f_1'^2 - c_{\Delta 2} z_3 f_2'^2$ and the second $\tau_{\Delta 2}$ of Proposition 3.8 then results in an identical upper bound as (3.86).

Common for both control laws is that they use $V_\Delta(z, z_p) = V_s(z) + V_p(z_p)$ which is positive definite and radially unbounded in (z, z_p). An upper bound on the time derivative of this is found as $\dot{V}_\Delta(z, z_p) \leq -W_\Delta(z, z_p) + \Delta(t)$, where $W_\Delta(z, z_p)$ is positive definite and radially unbounded and

$$\Delta(t) = \frac{\Delta_1^2(t)}{4c_{\Delta 1}} + \frac{\Delta_2^2(t)}{4c_{\Delta 2}} \tag{3.90}$$

is bounded and decreases with increasing control gains. As discussed previously, the upper bound (3.86) is valid on $D' = \{(z, z_p) \in R^n | \, z \in D\}$, $n = 3 + \dim(z_p)$, where D is identical to (3.49) due to validity of the model. Since $V_\Delta(z, z_p)$ and $W_\Delta(z, z_p)$ are positive definite and radially unbounded, there exists class $\mathcal{K}_\infty$ functions γ_1, γ_1 and γ_3 such that $\gamma_1(\|(z, z_p)\|) \leq V_\Delta(z, z_p) \leq \gamma_2(\|(z, z_p)\|)$ and $\gamma_3(\|(z, z_p)\|) \leq W_\Delta(z, z_p)$. This implies that

$$\begin{aligned}\dot{V}_\Delta(z, z_p) &\leq -W_\Delta(z, z_p) + \Delta(t) \\ &\leq -(1 - \eta) W_\Delta(z, z_p) - \eta \gamma_3(\|(z, z_p)\|) + \Delta(t) \\ &\leq -(1 - \eta) W_\Delta(z, z_p) \;\; \forall \|(z, z_p)\| \geq \gamma_3^{-1}\left(\frac{\Delta(t)}{\eta}\right)\end{aligned} \tag{3.91}$$

$\forall t \geq 0$ and $\forall (z, z_p) \in D'$, where γ_3^{-1} is the inverse function of γ_3 and η some scalar $0 < \eta < 1$. Let $B_r = \{(z, z_p) \in R^n | \, \|z, z_p\| \leq r\} \subset D'$. For sufficiently small Δ_i's or equivalently sufficiently large $c_{\Delta i}$'s, the inequality

$$\gamma_3^{-1}\left(\frac{\Delta(t)}{\eta}\right) < \gamma_2^{-1}(\gamma_1(r)) \tag{3.92}$$

holds. Hence, the overall system is uniformly ultimately bounded (for sufficiently small Δ_i's or equivalently sufficiently large $c_{\Delta i}$'s), [18]. ■

The control parts $\tau_{\Delta 1}$ and $\tau_{\Delta 2}$ acts on uncertainties related to mass flow dynamic equation and compressor torque respectively. The collected effect of uncertainties can be formulated $\Delta(t) = \frac{\Delta_1^2(t)}{4c_{\Delta 1}} + \frac{\Delta_2^2(t)}{4c_{\Delta 2}}$, where subscript 1 and 2 refers to mass flow dynamic and compressor torque models respectively. Alternative formulations can be made by splitting up the terms/functions. For the mass flow dynamics one could e.g. consider $\frac{A_c}{L_c'} p_c(w_c, \omega)$ and $-\frac{A_c}{L_c'} p_p$ as separate functions, rather than one function, $\frac{A_c}{L_c'}(p_c(w_c, \omega) - p_p)$, as was done in the derivation of this control law. For the compressor torque one could e.g. consider $\tau_c(w_c, \omega)$ and $\tau_f(\omega)$ as separate functions, rather than one function $\tau_l(w_c, \omega)$.

As already mentioned, these results hold whether or not the passive control part is used. The practical difference lies in the estimates of the global bound, since the function used to analyze the system will be different for the two cases. However, $\Delta(t)$ will be the same whether or not the passive part is included. Furthermore, these results also give a estimate on bounds of solutions, including effect of initial conditions. This can be used to estimate a less restrictive (smaller) bound on gains, by restricting the region of attraction to some subset of the possible operating regime.

Nonlinear damping was introduced to guarantee bounded solutions in presence of uncertainty in cancelled dynamics. The results show that solutions are bounded by the collected effect of uncertainty $\Delta(t)$. Using the definition of $\Delta(t)$, it can be recognized that this is a positive valued function. Moreover, it can be seen that increasing the gains $c_{\Delta i}$ will reduce the magnitude of $\Delta(t)$. Furthermore, it can be seen from the proof that $\Delta(t) = 0$ results in an asymptotically stable equilibrium. Tuning of control gains will be depend both on system parameters and the passive part of the controller, since these factors influence region of attraction and the ultimate bound.

3.4 Comments

None of the derived control laws, neither speed nor torque, are based on an explicit analytical expression for the compressor characteristic, but rather on an overall property related to mass flow and impeller speed gradients.

More specifically, the relation

$$\frac{\frac{\partial p_c(w_c,\omega)}{\partial w_c}}{\frac{\partial p_c(w_c,\omega)}{\partial \omega}} \tag{3.93}$$

appears in all of the control laws, where some control gain is required larger than the magnitude of this fraction in the region of interest. For implementation, on the other hand, the compressor characteristic is required for some of the control laws. As discussed in Chapter 2 this can be implemented by either a model, or a measurement in the case of sufficient length of upstream and/or downstream ducts for the compressor.

A model for throttle mass flow does not appear in any of the control laws. Furthermore, an explicit expression for throttle mass flow is not used in analysis leading to the control laws. The analysis only rely on the strictly passive property stated in (2.27). Hence, the control laws will be valid for any throttling devise satisfying this property.

All stability results are derived using a quadratic Lyapunov function from which asymptotic convergence to a desired equilibrium, or a set containing desired equilibrium in the case of nonlinear damping, is guaranteed by initial conditions sufficiently close to this equilibrium. Recalling the proofs it can be seen that exponential convergence can be concluded if $-\bar{p}_p \left(w_t\left(\bar{p}_p + p_p^e\right) - w_p\left(p_p^e\right)\right) \leq -\delta_p \bar{p}_p^2$. This is equivalent with $\frac{\partial w_t(p_p)}{\partial p_p} \geq \delta_p p_p$, which can be seen to be the case for (2.8), semi globally in p_p. Since none of the control laws presented concludes with global or semi global stability, due to model limitations, this introduces no restriction on the domain for which convergence will be exponential.

When evaluating how system parameters influences the control laws, it can be recognized that the fraction (3.93) appears in both speed and torque control algorithms. For the speed control it gives a lower bound for the mass flow gradient of the nonlinear gain, $\bar{w}_c \alpha\left(\bar{w}_c, \bar{p}_p, w_i\right)$, whereas it gives a lower bound for the gain c_2 in the case of torque control. In general it is desirable with this bound low, that is (3.93) small, giving grater freedom for tuning. This parameter is associated with the compressor stage only, or more precisely the forcing term of the compressor stage, and the upstream ambient pressure (where it is reasonable to assume that p_a of (2.26) has no effect on the relation (3.93)). An illustration of this fraction is shown in Figure 3.1 for the same compressor map as shown in Figure 2.2, based on

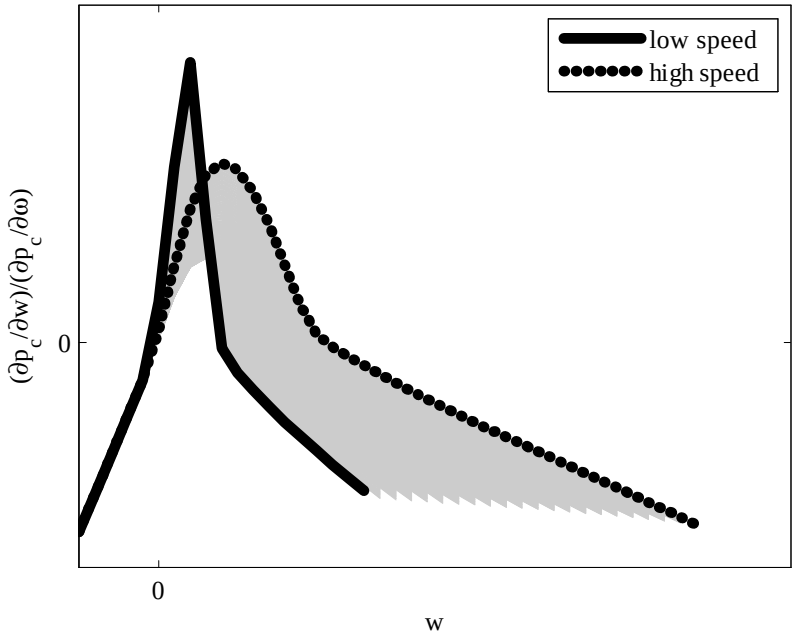

Figure 3.1: Fraction of compressor map gradients

data from a real compressor. Furthermore, the parameters A_c, L_c' and J can be recognized for the torque control laws in the configuration $\frac{JA_c}{L_c'}$. This parameter is multiplied by c_2 and pressure equilibrium deviation. Hence, if the system is designed such that $\frac{JA_c}{L_c'}$ is relatively small, this will reduce the magnitudes required by τ_d in transients.

All the control laws presented in this chapter uses mass flow in feedback. Measurement of mass flow is, however, not available for transient behavior. This implies that the control laws must be integrated with a mass flow estimate before implementation is possible.

Chapter 4

Observers for mass flow

4.1 Introduction

As was pointed out in the discussion of control laws in Chapter 3, there is a need for feedback from mass flow. However, this measurement is not easily obtained. To overcome this problem, observers for mass flow are derived based on the dynamic model of the compression system. This gives a module based design, by which it is meant that control laws are derived assuming access to mass flow and observers are derived without taking the specific control law into account. For implementation one then follows the so-called certainty of equivalence, and replaces the assumed measured mass flow in the control law by its estimate. For linear system the separation principal ensures that this interconnected system, of control and observer, preserves the stability results achieved for the individual cases. For nonlinear system, on the other hand, this principle does not generally hold.

Compared with the vast amount of literature on control and the repeatedly appearing mass flow as feedback, relatively little is found on observers for this variable. Some early results are reported in [34], based on the pressure mass flow dynamics of the compression system. However, this result does not investigate the stability of the observer itself, but presents an integrated observer control design for the system. This integrated design starts with defining an observer for the system, which is used as the basis for control synthesis (fundamentally different approach compared with the module based). Reduced order observer design for the somewhat more complicated compression system model of Moore and Greitzer, [6] and [7], is evaluated

as a case study in [35] for integrated design. Some references to other high-gain observers for this system are also given. A more recent reduced order observer for this system can be found in [36].

This chapter starts by introducing a general observer from the literature in Section 4.2, used by later sections to derive observers for the compression system presented Chapter 2. In Section 4.3 two reduced order observers for mass flow are derived. Their differences lie in whether the compressor map is implemented as a model or measurement. In Section 4.4 two observers for mass flow and pressure are derived, based on the observer in Section 4.2, where their differences lies in whether the compressor map is implemented as a model or measurement. In Section 4.5 two observers for mass flow, pressure and impeller speed are derived, based on the observer in Section 4.2, where their differences lies in whether the compressor map is implemented as a model or measurement. Section 4.6 gives some comments to the derived observers.

The reduced order observes from Section 4.3 can also be found in [37] and [38], accompanied by simulations. In addition to simulations, [37] also offers a detailed analysis on how measurement noise influences the observer. Furthermore, a separation principle is discussed for the situation in which a mass flow estimate is used in control laws of the compression system. One of the full order observers in Section 4.5 and an accompanying reduced order observer for mass flow is presented in [39], where simulations are offered.

4.2 Theoretical background

The general observer proposed by Murat Arcak and coauthors will be the basis for this chapter and is now briefly presented for completeness. A comprehensive description of the observer can be found in [40], [35], [41], [42] and references therein. The model used for observer design is given by

$$\dot{x} = Ax + G\gamma(\underbrace{Hx}_{v}) + \varrho\,(u, y) \tag{4.1}$$

$$y = \begin{bmatrix} y_1 & y_2 \end{bmatrix}^T = \begin{bmatrix} Cx & h\,(u, x) \end{bmatrix}^T \tag{4.2}$$

where $x \in R^n$, $u \in R^m$, $y_1 \in R^{r_1}$, $y_2 \in R^{r_2}$ and $\gamma : R^p \to R^p$. In this structure the unmeasured states enters the dynamics through the linear mapping

Ax and the nonlinear mapping $\gamma(Hx)$. Furthermore, the mapping γ is assumed to satisfy the sector property

$$(v-w)^T(\gamma(v)-\gamma(w)) \geq 0 \forall v, w \in R^p \tag{4.3}$$

or some decoupled version of it[1]. Notice that (4.3) is equivalent to

$$\frac{\partial \gamma(a)}{a} + \left(\frac{\partial \gamma(a)}{a}\right)^T \geq 0 \forall a \in R^p \tag{4.4}$$

when γ is differentiable. The observer

$$\dot{\hat{x}} = A\hat{x} + G\gamma(\underbrace{H\hat{x} + K_2(C\hat{x}-y_1)}_{w}) + \varrho(u,y) + K_1(C\hat{x}-y_1) \tag{4.5}$$

is proposed the system (4.1)-(4.2). By defining $e = x - \hat{x}$ and considering the Lyapunov function

$$V(e) = e^T P e \tag{4.6}$$

where $P = P^T$ is positive definite, it can be shown that

$$\dot{V}(t,e) \leq -2e^T Q_1 e - 2(v-w)^T Q_2(\gamma(v)-\gamma(w)) \tag{4.7}$$

if the linear matrix inequality (LMI)

$$\begin{bmatrix} (A+K_1C)^T P + P(A+K_1C) + Q_1 & PG + (H+K_2C)^T Q_2 \\ G^T P + Q_2(H+K_2C) & 0 \end{bmatrix} \leq 0 \tag{4.8}$$

is satisfied[2]. Note that this is an LMI in P, Q_1, Q_2, PK_1 and Q_2K_2. The stability properties are now given by the matrixes Q_1 and Q_2. By requiring Q_1 positive definite and choosing Q_2 as the identity matrix, it follows from (4.6), (4.7) and (4.4) or (4.5) that $e = 0$ is exponentially stable. In this case the observer gain K_2 follows directly from the solution of the LMI, and K_1 can be calculated using P^{-1} (which exists since $P > 0$). The structure of Q_2 can vary with the structure of γ. Let $\gamma(v) = \begin{bmatrix}\gamma_{[1]}^T(v_{[1]}) & \cdots & \gamma_{[l]}^T(v_{[l]})\end{bmatrix}^T$ and $Q_2 = diag\{q_{21}I_{[1]}, \ldots, q_{2l}I_{[l]}\}$. Here $\gamma_{[i]}$ are vectors, q_{2i} are positive scalars and $I_{[i]}$ is an identity matrix of same dimension as $\gamma_{[i]}$. The last term of (4.7) can then be expressed $-2\sum_i q_{2i}(v_{[i]}-w_{[i]})^T(\gamma_{[i]}(v_{[i]})-\gamma_{[i]}(w_{[i]}))$, which is negative if the individual $\gamma_{[i]}(v_{[i]})$'s satisfies (4.3) or (4.4). The resulting Q_2 will relax the LMI relative to $Q_2 = I$.

[1] The variable w is used to keep with the notation of referred publications, and should not be confused with mass flow.

[2] See Appendix B.1

4.3 Reduced order observer for mass flow

In this section reduced order observers for mass flow in the compression system presented in Chapter 2 are derived. From (2.1), (2.4)-(2.8) and (2.25) it can be recognized that mass flow appears linearly in the pressure dynamics, through p_c in the mass flow dynamics and through τ_c in the impeller speed dynamics. Note that more information of system mass flow is reflected through the pressure dynamics than impeller speed dynamics, since the impeller speed dynamics does not reflect the sign of the mass flow. Based on these simple considerations, a reduced order observer based on mass flow and plenum pressure dynamics is investigated. Furthermore, it is reasonable to assume that plenum pressure and impeller speed measurements are available. Whether or not a measurement of compressor characteristic can be used, depends on sufficient upstream and/or downstream compressor ducting as discussed in Chapter 2.

4.3.1 Measurement of compressor pressure

Proposition 4.1 *The observer*

$$\begin{aligned}\dot{\hat{\chi}} &= c_o\frac{c_p^2}{V_p}\hat{\chi} + \frac{A_c}{L_c'}p_c(t) - \left(\frac{A_c}{L_c'} + \frac{c_p^2}{V_p}c_o^2\right)p_p(t) - c_o\frac{c_p^2}{V_p}w_t(p_p(t))\\ \hat{w}_c &= \hat{\chi} - c_o p_p\end{aligned}$$

where $c_o < 0$ is exponentially stable.

Proof. The measurements $y = \{p_p,\ \omega,\ p_c\}$ are assumed available. Define

$$\chi = w_c + c_o p_p \tag{4.9}$$

which by using (2.1), (2.8), (4.9) and (2.25) results in the dynamic equation

$$\begin{aligned}\dot{\chi} &= c_o\frac{c_p^2}{V_p}\chi + \frac{A_c}{L_c'}p_c(\chi - c_o p_p(t), \omega(t))\\ &\quad + \underbrace{\left(-\frac{A_c}{L_c'} - \frac{c_p^2}{V_p}c_o^2\right)p_p(t) - c_o\frac{c_p^2}{V_p}w_t(p_p(t))}_{\varrho(t)}\end{aligned} \tag{4.10}$$

where measured signals are indicated by being explicit dependent on time. An observer for this dynamic equation can be taken as

$$\dot{\hat{\chi}} = c_o \frac{c_p^2}{V_p} \hat{\chi} + \varrho(t) + g(\hat{\chi}, y) \tag{4.11}$$

where g is a function of available signals. By defining

$$e_\chi = \chi - \hat{\chi}, \tag{4.12}$$

it follows from (4.10) and (4.11) that

$$\dot{e}_\chi = c_o \frac{c_p^2}{V_p} e_\chi + \frac{A_c}{L_c'} p_c(\chi - c_o p_p(t), \omega(t)) - g(\hat{\chi}, y). \tag{4.13}$$

Notice that $p_c(\chi - c_o p_p(t), \omega(t)) = p_c(w_c, \omega(t)) = p_c(t)$. Hence, by choosing

$$g(\hat{\chi}, y) = \frac{A_c}{L_c'} p_c(t) \tag{4.14}$$

(4.13) can be rewritten as $\dot{e}_\chi = c_o \frac{c_p^2}{V_p} e_\chi$. It follows that $e_\chi = 0$ is exponentially stable if $c_o < 0$. Defining the mass flow estimate $\hat{w}_c$ as in Proposition 4.1 and using (4.9) it can be recognized that

$$e_{w_c} = w_c - \hat{w}_c = \chi - c_o p_p - \hat{\chi} + c_o p_p = e_\chi \tag{4.15}$$

from which it is concluded that $e_{w_c} = 0$ is exponentially stable if $c_o < 0$. ■

4.3.2 Model of compressor pressure

Proposition 4.2 *The observer*

$$\begin{aligned} \dot{\hat{\chi}} &= c_o \frac{c_p^2}{V_p} \hat{\chi} + \frac{A_c}{L_c'} p_c(\hat{\chi} - c_o p_p(t), \omega(t)) \\ &\quad - \left(\frac{A_c}{L_c'} + \frac{c_p^2}{V_p} c_o^2 \right) p_p(t) - c_o \frac{c_p^2}{V_p} w_t(p_p(t)) \\ \hat{w}_c &= \hat{\chi} - c_o p_p \end{aligned}$$

where $c_o < 0$ is sufficiently negative, is exponentially stable.

Proof. The measurements $y = \{p_p,\ \omega\}$ are assumed available. Follow the proof of Proposition 4.1 leading to (4.13). In contrast to the previous proposition, the measurement p_c is not available. Consider now

$$g\left(\hat{\chi}, y\right) = \frac{A_c}{L_c'} p_c\left(\hat{\chi} - c_o p_p\left(t\right), \omega\left(t\right)\right) \tag{4.16}$$

which by using (4.12) rewrites (4.13)

$$\dot{e}_\chi = c_o \frac{c_p^2}{V_p} e_\chi + \frac{A_c}{L_c'}\left(p_c\left(\chi - c_o p_p\left(t\right), \omega\left(t\right)\right) - p_c\left(\chi - e_\chi - c_o p_p\left(t\right), \omega\left(t\right)\right)\right). \tag{4.17}$$

The time derivative of

$$V\left(e_\chi\right) = \frac{1}{2} e_\chi^2 \tag{4.18}$$

along the solution of (4.17) is found as

$$\begin{aligned} \dot{V}\left(t, e_\chi\right) &= -\delta e_\chi^2 + \frac{A_c}{L_c'} e_\chi \left(\left(\delta + c_o \frac{L_c' c_p^2}{A_c V_p}\right) e_\chi \right. \\ &\quad \left. + \underbrace{\left(p_c\left(\chi - c_o p_p\left(t\right), \omega\left(t\right)\right) - p_c\left(\chi - e_\chi - c_o p_p\left(t\right), \omega\left(t\right)\right)\right)}_{\alpha(t, e_\chi)}\right) \end{aligned} \tag{4.19}$$

for some $\delta > 0$. Applying the mean value theorem on α of (4.19) results in

$$p_c\left(\chi - c_o p_p\left(t\right), \omega\left(t\right)\right) - p_c\left(\chi - e_\chi - c_o p_p\left(t\right), \omega\left(t\right)\right) = \left.\frac{\partial p_c\left(a, \omega\left(t\right)\right)}{\partial a}\right|_L e_\chi \tag{4.20}$$

where a is some point on the line segment joining $\chi - c_o p_p\left(t\right)$ and $\chi - e_\chi - c_o p_p\left(t\right)$. Notice that this is equivalent with the line segment joining w_c and $\hat{w}_c$. Inserting (4.20) in (4.19) gives

$$\dot{V}\left(t, e_\chi\right) = -\delta e_\chi^2 + \frac{A_c}{L_c'} e_\chi^2 \left(\left(\delta + c_o \frac{L_c' c_p^2}{A_c V_p}\right) + \left.\frac{\partial p_c\left(a, \omega\left(t\right)\right)}{\partial a}\right|_L\right) \tag{4.21}$$

which shows that $\dot{V}\left(t, e_\chi\right) \leq -\delta e_\chi^2$ by choosing c_o sufficiently negative. Stability of $e_{w_c} = w_c - \hat{w}_c = 0$ follows from the same arguments as in the proof of Proposition 4.1. ■

4.4 Observer for pressure and mass flow

The reduced order observer is highly dependent on plenum pressure dynamic model. In an attempt to make the observer more robust, an observer for both plenum pressure and duct mass flow is investigated. In doing so, the observer will contain more model information in the sense that both pressure as well as mass flow dynamics is explicitly incorporated. This configuration allows for feedback to compensate for model uncertainties in both of these equations. Note also that this dynamic system is highly coupled.

4.4.1 Measurement of compressor pressure

Proposition 4.3 *The observer*

$$\begin{aligned} A &= \begin{bmatrix} 0 & \frac{c_p^2}{V_p} \\ -\frac{A_c}{L_c'} & -c_2 \end{bmatrix}, \; G = \begin{bmatrix} -1 & 0 \\ 0 & 1 \end{bmatrix}, \; H = \begin{bmatrix} 1 & 0 \\ 0 & 1 \end{bmatrix}, \; C = \begin{bmatrix} 1 & 0 \end{bmatrix}, \\ \gamma &= \begin{bmatrix} \frac{c_p^2}{V_p} w_t\left(w_1\right) \\ c_2 w_2 \end{bmatrix}, \; \varrho = \begin{bmatrix} 0 \\ \frac{A_c}{L_c'} p_c\left(t\right) \end{bmatrix} \end{aligned}$$

where $c_2 \geq 0$, is exponentially stable if the LMI is solvable with $Q_2 = diag\left\{q_{21}, q_{22}\right\} > 0$.

Proof. The pressure mass flow dynamic model is given by (2.1), (2.8) and (2.25). The definitions

$$x_1 = p_p, \; x_2 = w_c, \; x_3 = \omega, \; u = \tau_d \tag{4.22}$$

$$k_1 = \tfrac{c_p^2}{V_p}, \; k_2 = \tfrac{A_c}{L_c'}, \; k_3 = \tfrac{1}{J}, \; k_4 = k_t, \; k_5 = p_a, \; k_6 = k_c, \; k_7 = k_f \tag{4.23}$$

$$f_1\left(x_1\right) = sgn\left(x_1 - k_5\right)\sqrt{\left|x_1 - k_5\right|} \tag{4.24}$$

$$f_2\left(x_2, x_3\right) = p_c\left(x_2, x_3\right) \tag{4.25}$$

$$f_3\left(x_2, x_3\right) = \left|x_2\right| x_3 \tag{4.26}$$

are introduced for notational convenience. Variables, constants and functions related to impeller speed dynamics (2.4) are included for later use. The available measurements are $y = \left\{x_1, x_3, \; f_2\right\}$. Using (4.22)-(4.25), the

dynamic model (2.1), (2.8) and (2.25) is expressed

$$\begin{aligned}\begin{bmatrix}\dot{x}_1\\ \dot{x}_2\end{bmatrix}&=\begin{bmatrix}0 & k_1\\ -k_2 & 0\end{bmatrix}\begin{bmatrix}x_1\\ x_2\end{bmatrix}+\begin{bmatrix}-k_1k_4f_1(x_1)\\ 0\end{bmatrix}+\begin{bmatrix}0\\ k_2f_2(x_2,x_3)\end{bmatrix}\\ &=\begin{bmatrix}0 & k_1\\ -k_2 & -c_2\end{bmatrix}\begin{bmatrix}x_1\\ x_2\end{bmatrix}+\begin{bmatrix}-k_1k_4f_1(x_1)\\ c_2x_2\end{bmatrix}+\begin{bmatrix}0\\ k_2f_2(x_2,x_3)\end{bmatrix}\\ &=\underbrace{\begin{bmatrix}0 & k_1\\ -k_2 & -c_2\end{bmatrix}}_{A}\begin{bmatrix}x_1\\ x_2\end{bmatrix}+\underbrace{\begin{bmatrix}-1 & 0\\ 0 & 1\end{bmatrix}}_{G}\underbrace{\begin{bmatrix}k_1k_4f_1(x_1)\\ c_2x_2\end{bmatrix}}_{\gamma}+\underbrace{\begin{bmatrix}0\\ k_2f_2(x_2,x_3)\end{bmatrix}}_{\varrho}\end{aligned}\tag{4.27}$$

$$y_1 = \underbrace{\begin{bmatrix}1 & 0\end{bmatrix}}_{C}\begin{bmatrix}x_1\\ x_2\end{bmatrix}\tag{4.28}$$

where $c_2 \geq 0$ is a design constant to be chosen, $\gamma(v_1, v_2) = \begin{bmatrix}\gamma_1(v_1) & \gamma_2(v_2)\end{bmatrix}^T$ and $v = \begin{bmatrix}x_1 & x_2\end{bmatrix}^T$. From (4.24) and (2.27) it can be recognized that (4.3) holds for $\gamma_1(v_1)$, and since $c_2 \geq 0$ it follows that (4.3) holds for $\gamma_2(v_2)$. This allows for $Q_2 = diag\{q_{21}, q_{22}\}$ due to the decomposition of γ. ■

Remark 4.1 *The observer*

$$\begin{aligned}A &= \begin{bmatrix}0 & \frac{c_p^2}{V_p}\\ -\frac{A_c}{L_c'} & 0\end{bmatrix},\ G=\begin{bmatrix}-1\\ 0\end{bmatrix},\ H=\begin{bmatrix}1 & 0\end{bmatrix},\ C=\begin{bmatrix}1 & 0\end{bmatrix},\\ \gamma &= \frac{c_p^2}{V_p}w_t(w_1),\ \varrho=\begin{bmatrix}0\\ \frac{A_c}{L_c'}p_c(t)\end{bmatrix}\end{aligned}$$

is exponentially stable if the LMI is solvable with the scalar $Q_2 > 0$.

Proof. For $c_2 = 0$ the system (4.27) can be expressed

$$\begin{aligned}\begin{bmatrix}\dot{x}_1\\ \dot{x}_2\end{bmatrix} &= \begin{bmatrix}0 & k_1\\ -k_2 & 0\end{bmatrix}\begin{bmatrix}x_1\\ x_2\end{bmatrix}+\begin{bmatrix}-k_1k_4f_1(x_1)\\ 0\end{bmatrix}+\begin{bmatrix}0\\ k_2f_2(x_2,x_3)\end{bmatrix}\\ &= \underbrace{\begin{bmatrix}0 & k_1\\ -k_2 & 0\end{bmatrix}}_{A}\begin{bmatrix}x_1\\ x_2\end{bmatrix}+\underbrace{\begin{bmatrix}-1\\ 0\end{bmatrix}}_{G}\underbrace{k_1k_4f_1(x_1)}_{\gamma}+\underbrace{\begin{bmatrix}0\\ k_2f_2(x_2,x_3)\end{bmatrix}}_{\varrho}.\end{aligned}\tag{4.29}$$

From (4.24) and (2.27) it can be recognized that (4.3) holds for $\gamma(v)$. Furthermore, since γ is scalar it follows that Q_2 is scalar. ■

4.4.2 Model of compressor pressure

Proposition 4.4 *The observer*

$$\begin{aligned} A &= \begin{bmatrix} 0 & \frac{c_p^2}{V_p} \\ -\frac{A_c}{L_c'} & -c_2 \end{bmatrix}, \; G = \begin{bmatrix} -1 & 0 \\ 0 & 1 \end{bmatrix}, \; H = \begin{bmatrix} 1 & 0 \\ 0 & 1 \end{bmatrix}, \; C = \begin{bmatrix} 1 & 0 \end{bmatrix}, \\ \gamma &= \begin{bmatrix} \frac{c_p^2}{V_p} w_t\left(w_1\right) \\ \frac{A_c}{L_c'} p_c\left(w_2, \omega\right) + c_2 w_2 \end{bmatrix}, \; \varrho = \begin{bmatrix} 0 \\ 0 \end{bmatrix} \end{aligned}$$

where $c_2 > 0$ is sufficiently large, is exponentially stable if the LMI is solvable with $Q_2 = diag\left\{q_{21}, q_{22}\right\} > 0$.

Proof. The available measurements are $y = \{x_1, x_3\}$. Using (4.22)-(4.25), the dynamic model (2.1), (2.8) and (2.25) is expressed

$$\begin{aligned} \begin{bmatrix} \dot{x}_1 \\ \dot{x}_2 \end{bmatrix} &= \begin{bmatrix} 0 & k_1 \\ -k_2 & 0 \end{bmatrix} \begin{bmatrix} x_1 \\ x_2 \end{bmatrix} + \begin{bmatrix} -k_1 k_4 f_1\left(x_1\right) \\ k_2 f_2\left(x_2, x_3\right) \end{bmatrix} + \begin{bmatrix} 0 \\ 0 \end{bmatrix} \\ &= \begin{bmatrix} 0 & k_1 \\ -k_2 & -c_2 \end{bmatrix} \begin{bmatrix} x_1 \\ x_2 \end{bmatrix} + \begin{bmatrix} -k_1 k_4 f_1\left(x_1\right) \\ k_2 f_2\left(x_2, x_3\right) + c_2 x_2 \end{bmatrix} + \begin{bmatrix} 0 \\ 0 \end{bmatrix} \\ &= \underbrace{\begin{bmatrix} 0 & k_1 \\ -k_2 & -c_2 \end{bmatrix}}_{A} \begin{bmatrix} x_1 \\ x_2 \end{bmatrix} + \underbrace{\begin{bmatrix} -1 & 0 \\ 0 & 1 \end{bmatrix}}_{G} \underbrace{\begin{bmatrix} k_1 k_4 f_1\left(x_1\right) \\ k_2 f_2\left(x_2, x_3\right) + c_2 x_2 \end{bmatrix}}_{\gamma} + \underbrace{\begin{bmatrix} 0 \\ 0 \end{bmatrix}}_{\varrho} \quad (4.30) \\ y_1 &= \underbrace{\begin{bmatrix} 1 & 0 \end{bmatrix}}_{C} \begin{bmatrix} x_1 \\ x_2 \end{bmatrix} \quad (4.31) \end{aligned}$$

where c_2 is a design constant to be chosen, $\gamma\left(t, v_1, v_2\right) = \begin{bmatrix} \gamma_1\left(v_1\right) & \gamma_2\left(t, v_2\right) \end{bmatrix}^T$ and $v = \begin{bmatrix} x_1 & x_2 \end{bmatrix}^T$. The function γ is different from that discussed for (4.1) in the sense that it is now also a function of time. This comes from the appearance of x_3 (impeller speed), which is not a system state in this model configuration. However, this signal is assumed available as a measurement and can be related to the model (4.1)-(4.2) by considering x_3 as a system input. From (4.24) and (2.27) it can be recognized that (4.3) holds for

$\gamma_1(v_1)$. It follows from the mean value theorem that

$$\begin{aligned}
&(v_2 - w_2)(\gamma_2(t, v_2) - \gamma_2(t, w_2)) \\
&= (v_2 - w_2)(k_2 f_2(v_2, x_3) + c_2 v_2 - k_2 f_2(w_2, x_3) - c_2 w_2) \\
&= (v_2 - w_2)(k_2(f_2(v_2, x_3) - f_2(w_2, x_3)) + c_2(v_2 - w_2)) \\
&= (v_2 - w_2)\left(k_2 \left.\frac{\partial f_2(a, x_3)}{\partial a}\right|_L (v_2 - w_2) + c_2(v_2 - w_2)\right) \\
&= (v_2 - w_2)^2 \left(k_2 \left.\frac{\partial f_2(a, x_3)}{\partial a}\right|_L + c_2\right) \qquad (4.32)
\end{aligned}$$

where a is evaluated at some point on the line segment L joining v_2 and w_2. Hence, for (4.32) to be positive semi definite it is required that

$$k_2 \left.\frac{\partial f_2(a, x_3)}{\partial a}\right|_L + c_2 \geq 0 \Rightarrow \left.\frac{\partial f_2(a, x_3)}{\partial a}\right|_L \geq -\frac{c_2}{k_2} \qquad (4.33)$$

which is guaranteed for c_2 sufficiently large. This allows for $Q_2 = diag\{q_{21}, q_{22}\}$ due to the decomposition of γ. ■

4.5 Full order observer

In the same spirit as the previous section, more model information is included by also using impeller speed dynamics in the observer. The introduction of impeller speed does not add any new relations for plenum pressure. In fact, plenum pressure and impeller mass flow are completely decoupled dynamic equations. However, compressor mass flow and impeller speed are coupled equations.

4.5.1 Measurement of compressor pressure

Proposition 4.5 *The observer*

$$A = \begin{bmatrix} 0 & \frac{c_p^2}{V_p} & 0 \\ -\frac{A_c}{L_c'} & -c_2 & 0 \\ 0 & -c_3 & -\frac{k_f}{J} \end{bmatrix},\ G = \begin{bmatrix} -1 & 0 & 0 \\ 0 & 1 & 0 \\ 0 & 0 & -1 \end{bmatrix},\ H = \begin{bmatrix} 1 & 0 & 0 \\ 0 & 1 & 0 \\ 0 & 0 & 1 \end{bmatrix},$$

$$C = \begin{bmatrix} 1 & 0 & 0 \\ 0 & 0 & 1 \end{bmatrix},\ \varrho = \begin{bmatrix} 0 \\ \frac{A_c}{L_c'} p_c(t) - c_3\omega \\ \frac{1}{J}u + c_4\omega^3 \end{bmatrix},\ \gamma = \begin{bmatrix} \frac{c_p^2}{V_p} w_t(w_1) \\ c_2 w_2 + c_3 w_3 \\ \frac{1}{J}\tau_c(w_2, w_3) - c_3 w_2 + c_4 w_3^3 \end{bmatrix}$$

where $c_2 > 0$, $c_3 \in R$, $c_2 c_4 > \frac{k_c^2}{J^2 12}$, *is exponentially stable if the LMI is solvable with* $Q_2 = diag\left\{q_{21}, q_{22}, q_{22}\right\} > 0$.

Proof. Using the notation (4.22)-(4.26), available measurements are $y = \{x_1,\ x_3,\ f_2\}$. The dynamic model (2.1), (2.4)-(2.8) and (2.25) is expressed

$$\begin{aligned}
\begin{bmatrix} \dot{x}_1 \\ \dot{x}_2 \\ \dot{x}_3 \end{bmatrix} &= \begin{bmatrix} 0 & k_1 & 0 \\ -k_2 & 0 & 0 \\ 0 & 0 & -k_3 k_7 \end{bmatrix} \begin{bmatrix} x_1 \\ x_2 \\ x_3 \end{bmatrix} + \begin{bmatrix} -k_1 k_4 f_1(x_1) \\ 0 \\ -k_3 k_6 f_3(x_2, x_3) \end{bmatrix} + \begin{bmatrix} 0 \\ k_2 f_2(x_2, x_3) \\ k_3 u \end{bmatrix} \\
&= \begin{bmatrix} 0 & k_1 & 0 \\ -k_2 & -c_2 & 0 \\ 0 & -c_3 & -k_3 k_7 \end{bmatrix} \begin{bmatrix} x_1 \\ x_2 \\ x_3 \end{bmatrix} + \begin{bmatrix} -k_1 k_4 f_1(x_1) \\ c_2 x_2 + \alpha_2(y) \\ -k_3 k_6 f_3(x_2, x_3) + c_3 x_2 + \alpha_3(y) \end{bmatrix} \\
&\quad + \begin{bmatrix} 0 \\ k_2 f_2(x_2, x_3) - \alpha_2(y) \\ k_3 u - \alpha_3(y) \end{bmatrix} \\
&= \underbrace{\begin{bmatrix} 0 & k_1 & 0 \\ -k_2 & -c_2 & 0 \\ 0 & -c_3 & -k_3 k_7 \end{bmatrix}}_{A} \begin{bmatrix} x_1 \\ x_2 \\ x_3 \end{bmatrix} + \underbrace{\begin{bmatrix} 0 \\ k_2 f_2(x_2, x_3) - \alpha_2(y) \\ k_3 u - \alpha_3(y) \end{bmatrix}}_{\varrho} \\
&\quad + \underbrace{\begin{bmatrix} -1 & 0 & 0 \\ 0 & 1 & 0 \\ 0 & 0 & -1 \end{bmatrix}}_{G} \underbrace{\begin{bmatrix} k_1 k_4 f_1(x_1) \\ c_2 x_2 + \alpha_2(y) \\ k_3 k_6 f_3(x_2, x_3) - c_3 x_2 - \alpha_3(y) \end{bmatrix}}_{\gamma}
\end{aligned} \tag{4.34}$$

$$y_1 = \underbrace{\begin{bmatrix} 1 & 0 & 0 \\ 0 & 0 & 1 \end{bmatrix}}_{C} \begin{bmatrix} x_1 \\ x_2 \\ x_3 \end{bmatrix} \tag{4.35}$$

where $c_2 x_2$, $c_3 x_2$, $\alpha_2(y)$ and $\alpha_3(y)$ has been added and subtracted for design freedom. The term $(v-w)^T(\gamma(v) - \gamma(w))$ can be expressed

$$\begin{aligned}
(v-w)^T(\gamma(v) - \gamma(w)) &= (v_1 - w_1)(\gamma_1(v_1) - \gamma_1(w_1)) \\
&\quad + (v' - w')^T(\gamma'(v') - \gamma'(w'))
\end{aligned} \tag{4.36}$$

where $v = (x_1, x_2, x_3)$,

$$\gamma_1(v_1) = k_1 k_4 f_1(v_1) \tag{4.37}$$

$$\gamma'(v') = \begin{bmatrix} c_2 v_2 + \alpha_2(v_3) \\ k_3 k_6 f_3(v_2, v_3) - c_3 v_2 - \alpha_3(v_3) \end{bmatrix} \tag{4.38}$$

which defines $v' = \begin{bmatrix} v_2 & v_3 \end{bmatrix}^T$ and the α's has been chosen as functions of v_3. From the (4.24) and (2.27) it follows that (4.3) holds for (4.37). The multivariable sector property (4.4) is evaluated for (4.38)

$$\begin{aligned} &\frac{\partial \gamma'(v')}{\partial v'} + \left(\frac{\partial \gamma'(v')}{\partial v'}\right)^T \\ &= \begin{bmatrix} 2c_2 & k_3 k_6 \frac{\partial f_3(v_2,v_3)}{\partial v_2} + \frac{\partial \alpha_2(v_3)}{\partial v_3} - c_3 \\ k_3 k_6 \frac{\partial f_3(v_2,v_3)}{\partial v_2} + \frac{\partial \alpha_2(v_3)}{\partial v_3} - c_3 & 2\left(k_3 k_6 \frac{\partial f_3(v_2,v_3)}{\partial v_3} - \frac{\partial \alpha_3(v_3)}{\partial v_3}\right) \end{bmatrix} \end{aligned} \quad (4.39)$$

Recalling the discussion of compressor torque model in Chapter 2, the function (4.26) is approximated by

$$f_3(x_2, x_3) \approx \tanh(\zeta x_2)\, x_2 x_3 \quad (4.40)$$

when evaluating $\frac{\partial f_3(v_2,v_3)}{\partial v_2}$ for (4.39). From (4.40) it follows that

$$\frac{\partial f_3(x_2, x_3)}{x_2} = x_3 \underbrace{\left(\zeta x_2 \left(1 - \tanh^2(\zeta x_2)\right) + \tanh(\zeta x_2)\right)}_{k_8(t)} \quad (4.41)$$

where $k_8(t)$ is in the range of -1 to 1, resulting in $\frac{\partial f_3(v_2,v_3)}{\partial v_2} = k_8(t)\, v_3$ and $\frac{\partial f_3(v_2,v_3)}{\partial v_3} = |v_2|$, where $\frac{\partial f_3(v_2,v_3)}{\partial v_3}$ is derived without the approximation. This rewrites (4.39)

$$\begin{aligned} &\frac{\partial \gamma'(v')}{\partial v'} + \left(\frac{\partial \gamma'(v')}{\partial v'}\right)^T \\ &= \begin{bmatrix} 2c_2 & k_3 k_6 k_8(t)\, v_3 + \frac{\partial \alpha_2(v_3)}{\partial v_3} - c_3 \\ k_3 k_6 k_8(t)\, v_3 + \frac{\partial \alpha_2(v_3)}{\partial v_3} - c_3 & 2\left(k_3 k_6 |v_2| - \frac{\partial \alpha_3(v_3)}{\partial v_3}\right) \end{bmatrix} \end{aligned} \quad (4.42)$$

which is positive definite by requiring

$$0 < 2c_2 \quad (4.43)$$

$$0 < 4c_2 \left(k_3 k_6 |v_2| - \frac{\partial \alpha_3(v_3)}{\partial v_3}\right) - \left(\frac{\partial \alpha_2(v_3)}{\partial v_3} + k_3 k_6 k_8(t)\, v_3 - c_3\right)^2 \quad (4.44)$$

for the upper left determinants. From the (4.43) it is clear that

$$c_2 > 0 \quad (4.45)$$

is required. Furthermore, by choosing

$$\alpha_2(v_3) = c_3 v_3 \tag{4.46}$$
$$\alpha_3(v_3) = -c_4 v_3^3 \tag{4.47}$$

the inequality (4.44) is rewritten $4c_2k_3k_6|v_2| + (12c_2c_4 - k_3^2k_6^2k_8^2(t))v_3^2 > 0$. Since $k_8(t)$ is in the range of -1 to 1 this inequality is formulated as

$$c_2c_4 > \frac{k_3^2k_6^2}{12} \tag{4.48}$$

where it follows from (4.45) that $c_4 > 0$. Furthermore, this observer introduces a optional constant c_3 in the linear part of the system which can be chosen positive, negative or even zero. Note that choosing $c_3 = 0$ results in $\alpha_2 = 0$. Finally, the decomposition of γ allows for $Q_2 = \{q_{21}, q_{22}, q_{22}\}$. ■

4.5.2 Model of compressor pressure

Two observers will now be derived for the case of which a measurement of the compressor map is unavailable. Even though the two observers estimate the same system states, their dynamics differs.

Proposition 4.6 *The observer*

$$A = \begin{bmatrix} 0 & \frac{c_p^2}{V_p} & 0 \\ -\frac{A_c}{L_c'} & -c_2 & 0 \\ 0 & -c_3 & -\frac{k_f}{J} \end{bmatrix},\ G = \begin{bmatrix} -1 & 0 & 0 & 0 \\ 0 & 1 & 1 & 0 \\ 0 & 0 & 0 & -1 \end{bmatrix},\ H = \begin{bmatrix} 1 & 0 & 0 \\ 0 & 1 & 0 \\ 0 & 1 & 0 \\ 0 & 0 & 1 \end{bmatrix},$$

$$C = \begin{bmatrix} 1 & 0 & 0 \\ 0 & 0 & 1 \end{bmatrix},\ \varrho = \begin{bmatrix} 0 \\ -c_3\omega \\ \frac{1}{J}u + c_4\omega^3 \end{bmatrix},\ \gamma = \begin{bmatrix} \frac{c_p^2}{V_p} w_t(w_1) \\ \frac{A_c}{L_c'} p_c(w_2, \omega) + c_{21} w_2 \\ c_{22} w_3 + c_3 w_4 \\ \frac{1}{J}\tau_c(w_3, w_4) - c_3 w_3 + c_4 w_4^3 \end{bmatrix},$$

$$c_2 = c_{21} + c_{22},\ c_{22}c_4 > \frac{k_c^2}{J^2 12},$$

and c_{21} sufficiently large, is exponentially stable if the LMI is solvable with $Q_2 = diag\{q_{21}, q_{22}, q_{22}, q_{23}\} > 0$.

Proof. Using the notation (4.22)-(4.26), available measurements are $y = \{x_1,\ x_3,\ f_2\}$. The dynamic model (2.1), (2.4)-(2.8) and (2.25) is now expressed

$$\begin{aligned}
\begin{bmatrix}\dot{x}_1\\ \dot{x}_2\\ \dot{x}_3\end{bmatrix} &= \begin{bmatrix}0 & k_1 & 0\\ -k_2 & 0 & 0\\ 0 & 0 & -k_3k_7\end{bmatrix}\begin{bmatrix}x_1\\ x_2\\ x_3\end{bmatrix} + \begin{bmatrix}-k_1k_4f_1(x_1)\\ k_2f_2(x_2,x_3)\\ -k_3k_6f_3(x_2,x_3)\end{bmatrix} + \begin{bmatrix}0\\ 0\\ k_3u\end{bmatrix}\\
&= \begin{bmatrix}0 & k_1 & 0\\ -k_2 & -c_2 & 0\\ 0 & -c_3 & -k_3k_7\end{bmatrix}\begin{bmatrix}x_1\\ x_2\\ x_3\end{bmatrix} + \begin{bmatrix}-k_1k_4f_1(x_1)\\ k_2f_2(x_2,x_3)+c_2x_2+\alpha_2(y)\\ -k_3k_6f_3(x_2,x_3)+c_3x_2+\alpha_3(y)\end{bmatrix}\\
&\quad + \begin{bmatrix}0\\ -\alpha_2(y)\\ k_3u-\alpha_3(y)\end{bmatrix}\\
&= \underbrace{\begin{bmatrix}0 & k_1 & 0\\ -k_2 & -c_2 & 0\\ 0 & -c_3 & -k_3k_7\end{bmatrix}}_{A}\begin{bmatrix}x_1\\ x_2\\ x_3\end{bmatrix} + \underbrace{\begin{bmatrix}0\\ -\alpha_2(y)\\ k_3u-\alpha_3(y)\end{bmatrix}}_{\varrho}\\
&\quad + \underbrace{\begin{bmatrix}-1 & 0 & 0 & 0\\ 0 & 1 & 1 & 0\\ 0 & 0 & 0 & -1\end{bmatrix}}_{G}\underbrace{\begin{bmatrix}k_1k_4f_1(x_1)\\ k_2f_2(x_2,x_3)+c_{21}x_2\\ c_{22}x_2+\alpha_2(y)\\ k_3k_6f_3(x_2,x_3)-c_3x_2-\alpha_3(y)\end{bmatrix}}_{\gamma}
\end{aligned} \tag{4.49}$$

$$y_1 = \underbrace{\begin{bmatrix}1 & 0 & 0\\ 0 & 0 & 1\end{bmatrix}}_{C}\begin{bmatrix}x_1\\ x_2\\ x_3\end{bmatrix} \tag{4.50}$$

where c_2x_2, c_3x_2, $\alpha_2(y)$ and $\alpha_3(y)$ has been added and subtracted for design freedom and $c_2 = c_{21} + c_{22}$. The term $(v-w)^T(\gamma(v)-\gamma(w))$ can be expressed

$$\begin{aligned}
(v-w)^T(\gamma(v)-\gamma(w)) &= (v_1-w_1)(\gamma_1(v_1)-\gamma_1(w_1))\\
&\quad + (v'-w')^T(\gamma'(v')-\gamma'(w'))\\
&\quad + (v''-w'')^T(\gamma''(v'')-\gamma''(w''))
\end{aligned} \tag{4.51}$$

where

$$\begin{aligned}
\gamma_1(v_1) &= k_1 k_4 f_1(x_1), && (4.52)\\
\gamma'(t, v') &= k_2 f_2(x_2, x_3) + c_{21} x_2, && (4.53)\\
\gamma''(v'') &= \begin{bmatrix} c_{22} x_2 + \alpha_2(y) \\ k_3 k_6 f_3(x_2, x_3) - c_3 x_2 - \alpha_3(y) \end{bmatrix}, && (4.54)
\end{aligned}$$

$v_1 = x_1$, $v' = x_2$, $v'' = \begin{bmatrix} x_2 & x_3 \end{bmatrix}^T$. This results in

$$v = \begin{bmatrix} v_1 & v'^T & v''^T \end{bmatrix}^T = \begin{bmatrix} v_1 & v_2 & v_3 & v_4 \end{bmatrix}^T = \begin{bmatrix} x_1 & x_2 & x_2 & x_3 \end{bmatrix} \quad (4.55)$$

which defines H. As in the proof of Proposition 4.4, the function γ' has a time argument. From the (4.24) and (2.27) it follows that (4.3) holds for (4.52). The term (4.53) is identical to that analyzed for Proposition 4.4, and it follows from (4.33) that

$$c_{21} > 0 \quad (4.56)$$

sufficiently large guarantees (4.4) for (4.53). Furthermore, the term (4.54) is identical to (4.39) analyzed for Proposition 4.5, and it follows from (4.45)-(4.48) that

$$\begin{aligned}
c_{22} &> 0 && (4.57)\\
\alpha_2(y) &= c_3 x_3 && (4.58)\\
\alpha_3(y) &= -c_4 x_3^3 && (4.59)\\
c_{22} c_4 &> \frac{k_3^2 k_6^2}{12} && (4.60)
\end{aligned}$$

guarantees (4.4) for (4.54). Finally, the decomposition of γ allows for $Q_2 = \{q_{21}, q_{22}, q_{23}, q_{23}\}$. ■

Proposition 4.7 *The observer*

$$A = \begin{bmatrix} 0 & \frac{c_p^2}{V_p} & 0 \\ -\frac{A_c}{L_c'} & -c_2 & 0 \\ 0 & -c_3 & -\frac{k_f}{J} \end{bmatrix},\ G = \begin{bmatrix} -1 & 0 & 0 & 0 & 0 \\ 0 & 1 & 0 & 1 & 0 \\ 0 & 0 & 1 & 0 & -1 \end{bmatrix},\ H = \begin{bmatrix} 1 & 0 & 0 \\ 0 & 0 & 1 \\ 0 & 1 & 0 \\ 0 & 1 & 0 \\ 0 & 0 & 1 \end{bmatrix},$$

$$C = \begin{bmatrix} 1 & 0 & 0 \\ 0 & 0 & 1 \end{bmatrix},\ \varrho = \begin{bmatrix} 0 \\ -\alpha_2(\omega) \\ \frac{1}{J}u - \alpha_3(\omega) \end{bmatrix},\ \gamma = \begin{bmatrix} \frac{c_p^2}{V_p} w_t(w_1) \\ \frac{A_c}{L_c'} p_c(w_3, w_2) + c_{21} w_3 + \alpha_{21}(w_2) \\ c_{31} w_3 + \alpha_{31}(w_2) \\ c_{22} w_4 + \alpha_{22}(w_5) \\ \frac{1}{J}\tau_c(w_4, w_5) - c_{32} w_4 - \alpha_{32}(w_5) \end{bmatrix},$$

$$\alpha_2(z) = \alpha_{21}(z) + \alpha_{22}(z),\ \alpha_3(z) = \alpha_{31}(z) + \alpha_{32}(z),$$
$$\alpha_{21}(z) = c_5 z,\ \alpha_{22}(z) = c_{32} z,\ \alpha_{31}(z) = -c_{21} z,\ \alpha_{32}(z) = -c_4 z^3,$$
$$c_2 = c_{21} + c_{22},\ c_3 = c_{31} + c_{32},$$
$$c_{31} > 0,\ c_{22} > 0,\ c_{22} c_4 > \frac{k_c^2}{J^2 12},\ c_{32} \in R$$

and $c_5 c_{31}$ sufficiently large, is exponentially stable if the LMI is solvable with $Q_2 = diag\{q_{21}, q_{22}, q_{22}, q_{23}, q_{23}\} > 0$.

Proof. Using the notation (4.22)-(4.26), available measurements are $y = \{x_1,\ x_3,\ f_2\}$. The dynamic model (2.1), (2.4)-(2.8) and (2.25) is now expressed

$$\begin{aligned}
\begin{bmatrix}\dot{x}_1\\ \dot{x}_2\\ \dot{x}_3\end{bmatrix} &= \begin{bmatrix}0 & k_1 & 0\\ -k_2 & 0 & 0\\ 0 & 0 & -k_3k_7\end{bmatrix}\begin{bmatrix}x_1\\ x_2\\ x_3\end{bmatrix} + \begin{bmatrix}-k_1k_4f_1(x_1)\\ k_2f_2(x_2,x_3)\\ -k_3k_6f_3(x_2,x_3)\end{bmatrix} + \begin{bmatrix}0\\ 0\\ k_3u\end{bmatrix}\\
&= \begin{bmatrix}0 & k_1 & 0\\ -k_2 & -c_2 & 0\\ 0 & -c_3 & -k_3k_7\end{bmatrix}\begin{bmatrix}x_1\\ x_2\\ x_3\end{bmatrix} + \begin{bmatrix}-k_1k_4f_1(x_1)\\ k_2f_2(x_2,x_3)+c_2x_2+\alpha_2(y)\\ -k_3k_6f_3(x_2,x_3)+c_2x_2+\alpha_3(y)\end{bmatrix}\\
&\quad + \begin{bmatrix}0\\ -\alpha_2(y)\\ k_3u-\alpha_3(y)\end{bmatrix}\\
&= \underbrace{\begin{bmatrix}0 & k_1 & 0\\ -k_2 & -c_2 & 0\\ 0 & -c_3 & -k_3k_7\end{bmatrix}}_{A}\begin{bmatrix}x_1\\ x_2\\ x_3\end{bmatrix} + \underbrace{\begin{bmatrix}0\\ -\alpha_2(y)\\ k_3u-\alpha_3(y)\end{bmatrix}}_{\varrho}\\
&\quad + \underbrace{\begin{bmatrix}-1 & 0 & 0 & 0 & 0\\ 0 & 1 & 0 & 1 & 0\\ 0 & 0 & 1 & 0 & -1\end{bmatrix}}_{G}\underbrace{\begin{bmatrix}k_1k_4f_1(x_1)\\ k_2f_2(x_2,x_3)+c_{21}x_2+\alpha_{21}(y)\\ c_{31}x_2+\alpha_{31}(y)\\ c_{22}x_2+\alpha_{22}(y)\\ k_3k_6f_3(x_2,x_3)-c_{32}x_2-\alpha_{32}(y)\end{bmatrix}}_{\gamma} \qquad (4.61)\\
y_1 &= \underbrace{\begin{bmatrix}1 & 0 & 0\\ 0 & 0 & 1\end{bmatrix}}_{C}\begin{bmatrix}x_1\\ x_2\\ x_3\end{bmatrix} \qquad (4.62)
\end{aligned}$$

where c_2x_2, c_3x_2, $\alpha_2(y)$ and $\alpha_3(y)$ has been added and subtracted for design freedom, and

$$\begin{aligned}
c_2 &= c_{21}+c_{22} && (4.63)\\
c_3 &= c_{31}+c_{32} && (4.64)\\
\alpha_2(y) &= \alpha_{21}(y)+\alpha_{22}(y) && (4.65)\\
\alpha_3(y) &= \alpha_{31}(y)+\alpha_{32}(y)\,. && (4.66)
\end{aligned}$$

The term $(v-w)^T(\gamma(v)-\gamma(w))$ can be expressed

$$\begin{aligned}(v-w)^T(\gamma(v)-\gamma(w)) &= (v_1-w_1)(\gamma_1(v_1)-\gamma_1(w_1)) && (4.67)\\ &\quad +(v'-w')^T(\gamma'(v')-\gamma'(w')) && (4.68)\\ &\quad +(v''-w'')^T(\gamma''(v'')-\gamma''(w'')) && (4.69)\end{aligned}$$

where

$$\begin{aligned}\gamma_1(v_1) &= k_4 f_1(x_1), && (4.70)\\ \gamma'(v') &= \begin{bmatrix} k_2 f_2(x_2,x_3)+c_{21}x_2+\alpha_{21}(y)\\ c_{31}x_2+\alpha_{31}(y)\end{bmatrix}, && (4.71)\\ \gamma''(v'') &= \begin{bmatrix} c_{22}x_2+\alpha_{22}(y)\\ k_3k_6f_3(x_2,x_3)-c_{32}x_2-\alpha_{32}(y)\end{bmatrix}, && (4.72)\end{aligned}$$

$v_1=x_1$, $v'=\begin{bmatrix}x_3 & x_2\end{bmatrix}^T$, $v''=\begin{bmatrix}x_2 & x_3\end{bmatrix}^T$. This results in

$$v=\begin{bmatrix}v_1 & v'^T & v''^T\end{bmatrix}^T=\begin{bmatrix}v_1 & v_2 & v_3 & v_4 & v_5\end{bmatrix}^T=\begin{bmatrix}x_1 & x_3 & x_2 & x_2 & x_3\end{bmatrix}^T \quad (4.73)$$

which defines H. From the (4.24) and (2.27) it follows that (4.3) holds for (4.70). The term (4.72) is identical to (4.39) analyzed in proof of Proposition 4.5, and it follows from (4.45)-(4.48) that

$$\begin{aligned}\alpha_{22}(y) &= c_{32}v_5 = c_{32}x_3 && (4.74)\\ \alpha_{32}(y) &= -c_4v_5^3 = -c_4x_3^3 && (4.75)\\ c_{22} &> 0,\ c_{22}c_4 > \frac{k_3^2k_6^2}{12},\ c_{32}\in R && (4.76)\end{aligned}$$

guarantees (4.4) for (4.72). Considering α_{21} and α_{31} as functions of x_3, the condition (4.4) is evaluated for (4.71)

$$\begin{aligned}&\frac{\partial\gamma'(v')}{\partial v'}+\left(\frac{\partial\gamma'(v')}{\partial v'}\right)^T\\ &=\begin{bmatrix} 2\left(k_2\frac{\partial f_2(v_3,v_2)}{\partial v_2}+\frac{\partial\alpha_{21}(v_2)}{\partial v_2}\right) & k_2\frac{\partial f_2(v_3,v_2)}{\partial v_3}+c_{21}+\frac{\partial\alpha_{31}(v_2)}{\partial v_2}\\ k_2\frac{\partial f_2(v_3,v_2)}{\partial v_3}+c_{21}+\frac{\partial\alpha_{31}(v_2)}{\partial v_2} & 2c_{31}\end{bmatrix} \quad (4.77)\end{aligned}$$

where by requiring

$$0 < 2\left(k_2\frac{\partial f_2(v_3,v_2)}{\partial v_2}+\frac{\partial \alpha_{21}(v_2)}{\partial v_2}\right) \tag{4.78}$$

$$0 < 4\left(k_2\frac{\partial f_2(v_3,v_2)}{\partial v_2}+\frac{\partial \alpha_{21}(v_2)}{\partial v_2}\right)c_{31} - \left(k_2\frac{\partial f_2(v_3,v_2)}{\partial v_3}+c_{21}+\frac{\partial \alpha_{31}(v_2)}{\partial v_2}\right)^2 \tag{4.79}$$

for the upper left determinants will guarantee (4.4) for (4.77). For (4.78) it is sufficient to require

$$\frac{\partial \alpha_{21}(v_2)}{\partial v_2} \geq 0 \tag{4.80}$$

since $\frac{\partial f_2(v_3,v_2)}{\partial v_2} > 0$ by (4.25) and (2.28). Using this same property in (4.79) along with

$$\begin{aligned} \alpha_{21}(v_2) &= c_5 v_2 = c_5 x_3 \\ \alpha_{31}(v_2) &= -c_{21} v_2 = -c_{21} x_3 \\ c_{31} &> 0, \end{aligned}$$

rewrites this inequality as

$$4c_5c_{31} - \left(k_2\frac{\partial f_2(v_3,v_2)}{\partial v_3}\right)^2 > 0 \Rightarrow c_5c_{31} > \frac{k_2^2}{4}\left(\frac{\partial f_2(v_3,v_2)}{\partial v_3}\right)^2.$$

It follows that (4.4) hold for (4.77) by choosing $c_5c_{31} > 0$ sufficiently large. ■

4.6 Comments

As already commented on in Chapter 2 and Chapter 3, the model is only valid in a limited domain of the state space. More specifically, the impeller speed and plenum pressure is limited to being positive. This implies that the region of attraction for the observer will be limited. Whether or not this has any practical implication will, among other things, depend on control gains. For some of the proposed observers the function $\gamma\left(H\hat{x}+K_2\left(C\hat{x}-y_1\right)\right)$ contains the compressor map taking on arguments of estimated speed. A relatively high gain compared to magnitudes expected from $\hat{y}_1 - y$ could cause

the estimated speed to be negative, being an undefined situation for the compressor map model. The same can be argued for the throttle model and plenum pressure estimate. Especially in transients, e.g. if the observer is initiated with initial values relatively far from the actual values, this might cause problems.

Several observers have been derived. Their differences can be divided in how they compensate for compressor pressure, measurement or model, and which dynamic equations it is derived on behalf of. When using a model of the compressor characteristic it is required that some observer gain is sufficiently large, as opposed to the case when the compressor map is implemented by a measurement. Three different dynamic models can be identified for the derivation of the observers. The first is the reduced order observer. In this case a dynamic relation is derived on the basis of plenum pressure and duct mass flow dynamics to generate an estimate of duct mass flow only. These observers are highly dependent on the accuracy of the plenum pressure and compressor mass flow dynamics, when no feedback is available to explicitly correct potential inaccuracy for these models. The second dynamic system for which observers are derived is composed by plenum pressure and duct mass flow. In this configuration, more model information is given to the observer and estimates of both pressure and mass flow are generated. Inaccuracy in the individual dynamic models can now be compensated by feedback. This is also the case for the third configuration, which extends the second configuration by including the impeller speed dynamics. It is believed that the best configuration for observers it that of which corresponds best with experimental data. This argument follows from the fact that the derived observers are model based. Furthermore, if it is possible to use a measurement to represent the compressor characteristic, this relaxes the conditions for the observers when it is not necessary to chose parameters sufficiently large.

All observers derived on the basis of that presented in Section 4.2 exploits (2.27) for $w_t(p_p)$. Moreover, this mapping is modeled as $w_t(p_p) = k_t w_t'(p_p)$ and it is used that $k_t \geq 0$ and $w_t'(p_p)$ is passive. Hence, the throttle device for which the derived observers are valid is not restricted to (2.8), but any device that satisfies the mentioned conditions. As commented upon in Chapter 2, the throttle might be a variable area device. In this case the variable area is considered as a system input and throttle mass flow is modeled as

$w_t(p_p) = k_t(A_{t,\%})\, w_t'(p_p)$. It follows from

$$\begin{aligned}(v-w)(w_t(v)-w_t(w)) &= (v-w)(k_t(A_{t,\%})\, w_t'(v) - k_t(A_{t,\%})\, w_t'(w)) \\ &= k_t(A_{t,\%})(v-w)(w_t'(v)-w_t'(w)) \geq 0\end{aligned}$$

that the observers are also valid for variable area throttles by changing the implementation from $w_t(p_p) = k_t w_t'(p_p)$ to $w_t(p_p) = k_t(A_{t,\%})\, w_t'(p_p)$.

The inequality (4.8) is an LMI in P, Q_1, Q_2 $R_1 = PK_1$ and $R_2 = Q_2K_2$, where R_1 and R_2 are defined to solve (4.8) as an LMI. Hence, the control gains are calculated by $K_1 = P^{-1}R_1$ and $K_2 = Q_2^{-1}R_2$ after solving the LMI, and no explicit criteria can be posted for these gains when the LMI is solved.[3]

Tuning of the observer gains was therefore done in several steps. The gain K_1 was derived by pole placement for $A + K_1C$. The gain K_2 was derived by a matrix structure multiplied by a scalar, where the structure was chosen such that the components of $K_{2,structure}y_1^e$ would be in the same order of magnitude as Hx^e (where the superscript e refers to system equilibrium). The resulting K_1 and K_2 were then checked with (4.8) to see if they where possible solutions. Note that choosing $K_2 = 0$ will reduce the observer to be a copy of the model, in terms of estimated states, with a linear injection term added. However, it is shown in [35] that (4.18) might be unsolvable for $K = 0$ whereas being solvable for $K \neq 0$.

Reduced order observers for mass flow can be derived based on the higher order observers for (4.1). It is shown in [35] that a solution for the reduced order observer exists if and only if a solution for the full order observer exists. Hence, any of the observers in Proposition 4.3 through Proposition 4.7 can be used to generate a reduced order observer for mass flow only if the LMI is solvable for the higher order observers.

[3]Note that requiring $Q_2 > 0$ rather than $Q_2 \geq 0$ in the proposed observers is done in order to guarantee the existence of Q_2^{-1} rather than being a necessity for stability.

Part II

Experiments

Chapter 5

Laboratory

To evaluate theoretical results, a compression system laboratory was planned and built. Inspired by that of reported in [43] and [14], the main components of this laboratory can be considered as compressor, plenum volume, duct connecting compressor and plenum, a valve downstream plenum, driving system for compressor (electric motor, drive and gear) and controller board. In addition to these components the setup consists of several sensors, a computer to develop and compile applications to the controller board and signal converters to interface signals between controller board and process. A sketch of the setup is shown in Figure 5, where signals enclosed by a circle are measured signals whereas signals enclosed by a square represents reference signals to the unit. These signals are summarized in Table 5. Furthermore, the figure indicates dimensions of ducting and plenum[1] in millimeters. A picture of the setup is shown in Figure 5.1.

The drive is an ABB $11kW$ ACS800. More specifically ACS800-01-0016-2+D150+L500+L503. This drive gives the opportunity to control the motor by either speed or torque. That is, the drive accepts either speed or torque as reference inputs. Furthermore, both motor speed and torque are available as measurements from this unit. These are estimated values generated from knowledge of voltages, currents and temperatures of the drive in addition to the knowledge of the electric motor connected to the drive. The inputs to this unit (A/D converter) operates on an $6ms$ update cycle, whereas the the output (D/A converter) operates on an $24ms$ cycle.

The electric motor is an ABB $11kW$ M3A squirrel cage induction ma-

[1] Circular vessel where 380 refers to the diameter.

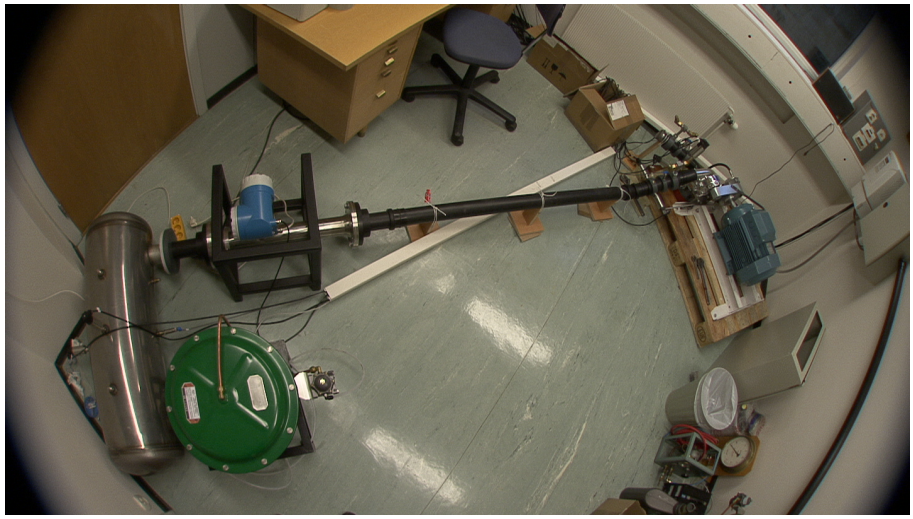

Figure 5.1: Overview of laboratory

chine. More specifically, M3AA 160MA 3GAA 161 101-ASC 445. The nominal speed for this machine is approximately $3000rpm$, with maximum recommended speed limited to $4500rpm$. The nominal torque is $36Nm$, with maximal torque of approximately 2.5 times the nominal torque. For the laboratory setup, ranges of $0 - 4500rpm$ and $0 - 36Nm$ were chosen as the ranges for motor speed and torque. Simultaneous values for these variables will be limited by a maximum of $11kW$.

The gear between motor and impeller shaft can de divided in two. The first is a gear manufactured by the in house workshop and the second is a gear contained in the compressor unit. The in house produced gear has a ratio of $\frac{60}{24}$ whereas the internal gear of the compressor has a ratio of 3.45, resulting in a total gear ratio of 8.625 between motor and impeller shaft. In view of motor speed and torque ranges, this implies that the impeller can take on speeds in the range $0 - 38800rpm$ and torques in the range $0 - 4.2Nm$. As for the motor, simultaneous values for these variables will be limited by a maximum of $11kW$ (minus the energy dissipated by the drive system).

The compressor is a Vortech V-1 S-Trim Race M. This is a supercharger, single stage centrifugal compressor, intended for the automobile industry.

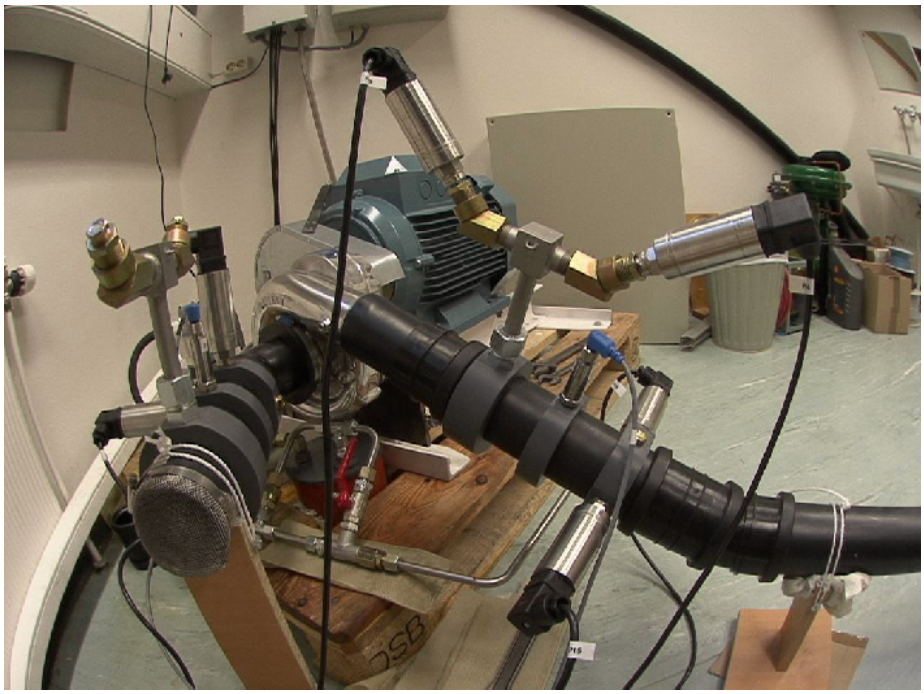

Figure 5.2: Compressor and related connections

The unit accepts speeds in the range $0 - 50000rpm$, giving the possibility to produce mass flow in the range $0 - 0.6kg/s$ and pressure ratios in the range $0 - 2.4$. However, due to power and speed limitation of the driving system as well as efficiency for the compressor itself, this unit will only be run in the lower speed regions. Upstream connection external diameter is $89mm$, upstream connection inner diameter is $79mm$ (same as inducer) downstream connection external diameter is $70mm$ and downstream connection inner diameter is $60mm$. A picture of the compressor and connecting ducts is shown in Figure 5.2. The electric motor and external gear can also be seen in this picture.

The compressor was fitted with an oil loop for lubrication and cooling of rotating parts. This loop consists of a small oil reservoir, an oil pump, a manual valve and piping, where the valve is used to control oil pressure over the compressor. This system was manufactured by the in house workshop, using a oil cooling pump from Mocal intended for automobile applications.

Parts of the oil lubrication loop can be seen below the compressor in Figure 5.2.

The control valve is a Ficher Design GX Control Valve. More specifically, 3 inch GX Valve & Actuator; Type DVC2000 67CFR; DVC2000 FIELDVUE. Process connection port size is $70mm$. The control unit of this valve accepts a reference input as well as providing a measurement of the actual valve opening. Furthermore, the valve was set up with equal percentage characteristic.

The plenum volume was manufactured at the in house workshop. The volume of this cylindrical vessel is approximately $0.1m^3$. Pressure and temperature measurements were fitted with the plenum. These where all mounted mid way along the length of the vessel, with pressure measurements 180° relative to each other.

Polypropylene (PP) piping was chosen to connect various components involving fluid flow. This material was chosen since it allows for easy and fast re-configuration of the setup, as well as being easily available with a vast specter of accessories such as bends, branches, sockets, t-pieces and so on. The dimensions of these pipes are $75mm$ and $70mm$ for external and inner diameter respectively.

The controller board is a DS1103 PPC from dSPACE. The CPU on this board is a PowerPC750GX running at $1GHz$ with $32MB$ application memory. This board has 32 bit-I/O channels, 20 A/D channels and 8 D/A channels. The A/D channels are built up of 16 multiplexed channels using 4 sample and hold A/D converters and 4 parallel channels, each of which uses a dedicated sample and hold. Conversion times for these converters are $1\mu s$ and $800ns$ for the multiplexed and parallel channels respectively. Settling time for the D/A channels are $5\mu s$. Both A/D and D/A converters have a resolution of 16-bit and accepts signals in the range $\pm 10V$. However, these converters where set up with 16-bit resolution for the range $0 - 10V$. This was done to reduce noise for signals in mid range, when this would correspond to $0V$. The board has the possibility to use 50 bit-I/O and 36 A/D channels by utilizing the slave DSP, but this was not necessary for the current setup.

The computer is a standard Dell desktop computer. This is used to develop and compile programs to be run at the controller board, as well as an interface to the controller board when this is running some application. This can e.g. be setting some reference, readout of some measurement or

changing some control parameter.

All analogous signals in the process, the various measurements and reference signals, communicates on the $4-20mA$ protocol. Hence, signal converters are needed to interface process analogous signals with the $0-10V$ controller board analogous signals. The Nokeval signal converter 641 was chosen for this purpose. These converters are relatively versatile with respect to conversion ranges and configuration as well as giving possibility to chose between several time constants for a low pass filer embedded in the unit (anti aliasing filter). The lowest possible time constant for the 1. order low pass filter is $50\mu s$, which is the setting chosen for the setup. Furthermore, these converters are claimed to respond well for frequencies up to $5000Hz$. Digital communication with the drive is necessary in order to start and stop the motor, as well as choosing between speed and torque reference. The controller board operates with voltages at TTL levels for digital communication, whereas the drive communicates with $0V$ and $24V$ as low and high bit. An optocoupler form Phenix Contact was used to interface these signals. More specifically, the unit EMG 17-OV-TTL/ 60DC/3 was used. Figure 5.3 shows a picture of analog interface connections between process and controller board, as well as the controller board and its signal interface.

The pressure transmitters are Druck PTX 610 units. These are high performance pressure transmitters intended for research and critical industrial applications, and offer a bandwidth of better than $1kHz$. The range for these transmitters is $0.9-1.6$ $bara$. This range was chosen to get a good resolution for the measured values, since the setup is limited to relatively low pressures due to limitation in speed and power. The output of these transmitters will not deviate from the straight line connecting zero and full scale by more than 0.15% of full scale.

Temperature transmitters are Endress+Hauser Easytemp TMR31. More specifically, TMR31-A1XBBAAB1AAA. These are Pt100 elements with a measurement range of $-50-150$ $^{\circ}C$. The range of these devises can be configured, and was set to $0-100^{\circ}C$ to give relatively good resolution for temperatures encountered in the laboratory. Measurement error of these transmitters is less than $0.27^{\circ}C$ for the chosen range, and response times are given as $t_{50} \leq 2s$ and $t_{90} \leq 4s$.

The mass flow transmitter is a Endress+Hauser t-mass 65F80. More specifically, 65F80-AE2AG1AAAAAA. This is a thermal mass flow meter, where the transmitter itself is mounted approximately midway along a duct

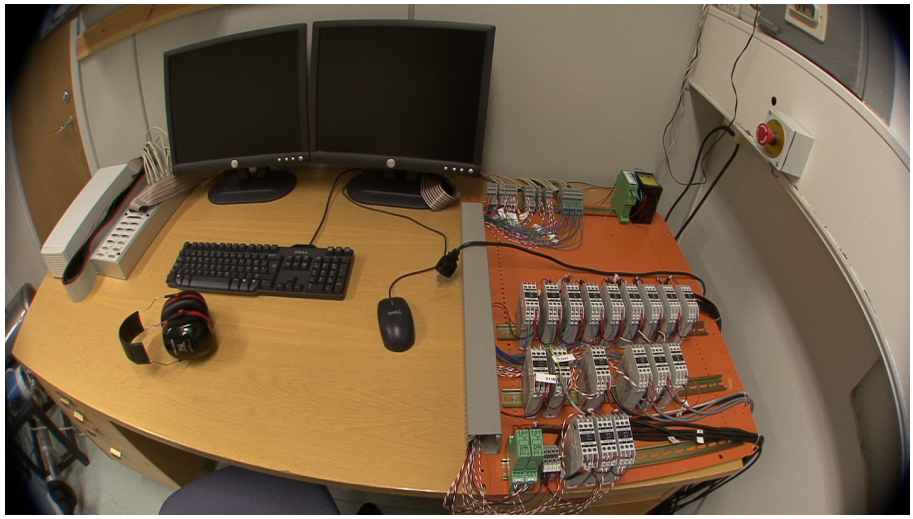

Figure 5.3: Signal interface. Signal interface between process and controller board to rthe right, and the controller board and its signal interface to the left.

of diameter $80mm$ and length $630mm$, as illustrated in Figure 5 with the shaded length of duct upstream and downstream Ft. This transmitter is able to measure mass flows in the range $0.003 - 0.56kg/s$. The range can be configured by the device, and a range of $0 - 0.26kg/s$ was chosen on the background of mass flows encountered in the setup. The measurement error of this transmitter is less than 2% of measured value, and response time is typically $t_{63} \leq 2s$.

The Pitot tubes is a Endress+Hauser deltaset DPP 50. More specifically, DPP50-A1F2A11Y. This is a devise originally intended for mass flow measurements, when fitted with a tailored differential pressure transmitter. However, its purpose for the current setup will be to measure total as well as static pressure. The Pitot tube offers pressure taps for both upstream and downstream pressure, for which pressure transmitters are mounted in order to measure total and static pressure respectively.

The mass flow transmitter and temperature transmitters are not used in implementation of control laws and observers. The mass flow transmitter was installed for system identification and evaluation of observers for steady

state. Temperature measurements are installed so that a complete picture of thermodynamic properties can be established at these points.

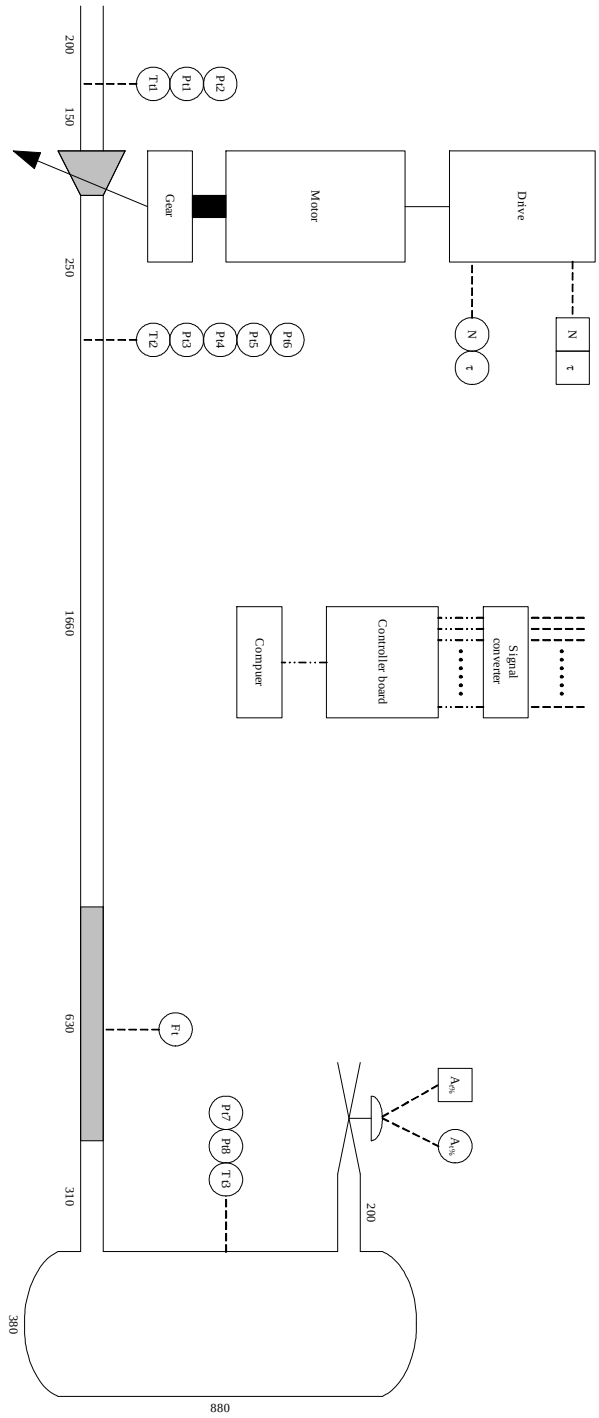

Figure 5.4: Sketch of compression laboratory

Unit	Description	Specification	Range (in lab)
$Pt1$	Compressor upstream pressure	PTX 610	$0.9 - 1.6$ $bara$
$Pt2$	Compressor upstream pressure	PTX 610	$0.9 - 1.6$ $bara$
$Pt3$	Compressor downstream pressure	PTX 610	$0.9 - 1.6$ $bara$
$Pt4$	Compressor downstream pressure	PTX 610	$0.9 - 1.6$ $bara$
$Pt5$	Pitot tube upstream pressure	PTX 610	$0.9 - 1.6$ $bara$
$Pt6$	Pitot tube downstream pressure	PTX 610	$0.9 - 1.6$ $bara$
$Pt7$	Plenum pressure	PTX 610	$0.9 - 1.6$ $bara$
$Pt8$	Plenum pressure	PTX 610	$0.9 - 1.6$ $bara$
$Tt1$	Compressor upstream temperature	TMR31	$0 - 100$ $°C$
$Tt2$	Compressor downstream temperature	TMR31	$0 - 100$ $°C$
$Tt3$	Plenum temperature	TMR31	$0 - 100$ $°C$
Ft	Mass flow	t-mass 65F80	$0 - 0.26$ kg/s
$A_{t\%}$	Throttle opening (measurement and reference)	DVC2000	$0 - 100$ %
N	Motor speed (measurement and reference)	ACS800	$0 - 4500rpm$
τ	Motor torque (measurement and reference)	ACS800	$0 - 36Nm$

Table 5.1: Transmitters in compression laboratory

Chapter 6

Model validation

6.1 Introduction

This chapter aims at identifying a model for the laboratory setup described in Chapter 5. To this end, both static and dynamic identification is performed. In order to apply the controllers and observers presented in Chapter 3 and Chapter 4, the identification process is constantly compared with the model of Chapter 2 to evaluate whether the performance of the setup can be formulated in this structure. Also important is whether the compressor map can be formulated as a measurement or not.

Control validation of transient response involves plots of both measured and simulated data. For all plots of this type, measured data are represented by black lines whereas simulations are represented by lighter lines.

6.2 Steady sate model identification

6.2.1 Measurement data

Data used for steady state analysis represent 10 different valve openings for 7 different constant speeds, in addition to a measurement when the valve is completely removed. Therefore, for each of the seven speeds there are 11 data points. A 30 seconds recording was conducted for each point and filtered with MATLAB's `filtfilt`. Data corresponding to highest speed and valve removed was not carried out due to limitation of motor power. Furthermore, data corresponding to lowest speed and throttle opening was corrupted.

Symbol	Impeller speed
◯	$10300[rpm]$
$\times$	$12800[rpm]$
$+$	$15300[rpm]$
$*$	$17900[rpm]$
□	$20400[rpm]$
◊	$22900[rpm]$
▽	$25400[rpm]$

Table 6.1: Constant speeds and corresponding symbols used in figures throughout this chapter

While conducting experiments the ambient pressure was $p_a = 1.011 - 1.012$ bar, according to Trondheim weather station. Temperature in the laboratory varied noticeable during experiments. The reason for this is due to the relatively small facility of the laboratory compared to the amount of heated air discharged from the compression system.

Table 6.1 shows symbols used in figures throughout this chapter for various impeller speeds. These figures generally show some property, such as pressure, plotted as a function of valve opening. The eleven data points related to each constant speed does not necessarily correspond in terms of valve opening. Increasing valve opening is therefore represented in terms of indexes reaching from one to eleven in plots. However, index ten and eleven corresponds to 100% open and valve completely removed for all speeds. Furthermore, all variables are in SI units unless otherwise is specified.

Pressure measurements

Pressure upstream the compressor, p_{cu}, was measured with two sensors mounted 90 degrees relative to each other in the piping wall. A plot of their readings is shown in Figure C.1. From this figure it can be seen that steady state pressures decreases with increasing impeller speed and increasing valve opening, which implies the clear tendency of pressure decrease with increasing mass flow.

Analogous to the pressure sensors upstream the compressor, two sensors where mounted downstream the compressor 180 degrees relative to each other in the piping wall. A plot of their reading is shown in Figure C.2.

From this figure it can be seen that pressure downstream the compressor, p_{cd}, generally increases with increasing impeller speed and decreases with increasing valve opening. This is as expected from the characteristics for a turbo compressor. When the valve is removed, a dramatic change in pressures can be observed. This is not surprising, since removing the valve can be considered a dramatic change in valve opening, and the absence of a restriction at system termination prevents pressure build up. Furthermore, it can be seen that deviation of the two sensors increases with increasing pressure. This implies that the sensor scaling parameter was slightly off.

A Pitot tube was mounted downstream of the compressor, with pressure taps for both flow directions. A plot of their reading is shown in Figure C.3. From this plot it can be seen that the deviation of total and static pressure increases with increasing valve opening. This is as expected from Bernoulli's equation for incompressible flow

$$p_t = p_s + \frac{1}{2}\rho v^2 \tag{6.1}$$

since higher valve opening implies higher mass flow and therefore higher fluid velocity when considering incompressible flow. Readouts of pressure when the valve is removed shows same tendency for p_s as for p_{cd}, clustering at relatively low pressure, and $p_t - p_s$ increases with increasing impeller speed which implies that fluid velocity increases with impeller speed. However, some inconsistency can be recognized when comparing p_s and p_{cd} in the sense that p_s clusters with a smaller distribution than p_{cd}.

Plenum pressure was also measured using two sensors, mounted 90 degrees relative to each other midway along the circular vessel. A plot of their reading is shown in Figure C.4. Same comments hold for these readings as for the pressure sensors downstream the compressor, except that the two sensors shows identical readouts.

Temperature measurements

Temperatures where measured upstream, T_{cu}, and downstream, T_{cd}, the compressor, as well as in plenum, T_p. In general, the measurements where conducted before temperatures where completely settled. However, temperature downstream the compressor changed rather quickly when a new operating point was selected, in contrast to temperature in plenum.

A plot of temperatures upstream the compressor is shown in Figure C.5. This plot shows little, if any, tendency. If any conclusion can be drawn, it seems like temperature increases with increasing impeller speed. The inconsistency is probably caused by varying temperature in the facility, as temperature in the laboratory varied considerably with various operating points.

A plot of the temperatures downstream the compressor is shown in Figure C.6. This plot shows the tendency of increasing temperature with increasing impeller speed and decreasing temperature with increasing valve opening. This observation is consistent with pressure observations downstream the compressor, Figure C.2, when evaluating the ideal gas low for incompressible flow

$$p = \rho RT, \tag{6.2}$$

showing that temperature decreases with decreasing pressure.

A plot of the temperatures in plenum is shown in Figure C.7. The same comments hold for this plot as for the plot of downstream compressor temperatures.

From the plots of temperature downstream the compressor and plenum, which are the plots showing some consistency, it can be seen that data for the case when the valve was removed is not consistent with the other data in the plots. This is probably due to turning the system off and back on after a while, in order to remove the valve. However, it can be seen that data becomes more consistent when reducing the impeller speed. This is probably due to starting measurements at the highest speed, and then stepping down. This results in the system being heated back up when reaching the lower speeds.

Mass flow measurements

A mass flow measurement was mounted upstream the plenum, w_{cd}, to measure steady sate mass flow in ducts. A plot of its reading is shown in Figure C.8. From the plot it can be seen that mass flow increases with increasing impeller speed and valve opening. Furthermore, it can be seen that mass flow increases considerably when removing the valve. This is as expected when considering a standard compressor map.

Mass flow can also be estimated using the Pitot pressure measurements,

total and static, downstream the compressor. The total pressure is given by

$$p_t = p_s + p_v \tag{6.3}$$

where p_s is the static pressure and p_v is pressure component due to fluid velocity. These pressures give first and foremost an estimate of the fluid velocity. However, this velocity can be used together with density and duct area to estimate the mass flow. For incompressible flow, the velocity pressure component is given by $p_v = \frac{1}{2}\rho v^2$, and fluid velocity can then be expressed by

$$v = \sqrt{\frac{2\left(p_t - p_s\right)}{\rho}}. \tag{6.4}$$

This relation gives an estimate of fluid velocity, from which duct volume and mass flow can be expressed

$$q = vA \tag{6.5}$$
$$w = \rho q = \rho A v \tag{6.6}$$

in the case of one dimensional flow. For incompressible flow, the density is constant and approximated by that of ambient conditions, $\rho \approx 1.2\frac{kg}{m^3}$. It follows from (6.4) and (6.6) that

$$w = A\sqrt{2\rho\left(p_t - p_s\right)}. \tag{6.7}$$

The relation in (6.7) results in relatively large errors for the data at hand. However, by introducing a scaling factor to this equation, $w_{est} = \alpha A\sqrt{2\rho}\sqrt{p_t - p_s}$, the estimate is significantly improved. Note that this scaling factor has no root in physics, but was introduced and tuned to better fit w_{est} with measured data. Estimated mass flows for A calculated from a circular duct diameter of $70 \cdot 10^{-3}m$ and $\alpha = 0.63$ are shown in Figure 6.1. These estimates are represented by deviation relative to measured value divided by measured value. From the figure it can be seen that this estimate for the most part is confined to a region of 10% accuracy relative to actual mass flow measurement. The inaccuracies can probably be explained by assumptions of incompressible and one dimensional flow. Even though these assumptions appear to hold relative to connecting systems, this is not necessity the case locally in the flow. Whether or not the compressibility effect can be ignored when calculating the estimated mass flow depends,

among other things, on how sensitive (6.7) is to variations in ρ. Another source of error might be that the Pitot tube is mounted relatively close to the compressor exit, which might result in the flow pattern effects different from one dimensional. For compressible flow the relation

$$v = \sqrt{2\left(\frac{\kappa}{\kappa-1}\right)\left(\frac{p_s}{\rho_s}\right)\left(\left(1+\frac{(p_t-p_s)}{p_s}\right)^{\left(\frac{\kappa-1}{\kappa}\right)}-1\right)} \tag{6.8}$$

is suggested [44], where ρ_s is the static density and κ is the ratio of specific heats. By now assuming ideal gas, (6.2), the density can be calculated using measurement of temperature and pressure. Furthermore, assumption of ideal gas makes the ratio of specific heats, κ, a function of temperature only. Moreover, this parameter can be taken as a constant for relatively low variations in temperature (typically $\kappa = 1.4$ for ambient conditions). Estimating mass flow using the relations (6.6) and (6.8) gave better results than (6.7), but not so significantly that the somewhat more complicated (6.8) is discussed further.

6.2.2 Reynolds and Mach number for duct

The Reynolds number for flow in a circular pipe is given by

$$\mathrm{Re}_D = \frac{\rho v D}{\mu} \tag{6.9}$$

where D is the diameter of the pipe and μ is the dynamic viscosity of the fluid. The relation (6.6) can be used to rewrite (6.9) as

$$\mathrm{Re}_D = \frac{4w}{\mu\pi D} \tag{6.10}$$

for a circular pipe. Furthermore, the dynamic viscosity is approximated by the Power law

$$\mu = \mu_0\left(\frac{T}{T_0}\right)^{0.7} \tag{6.11}$$

where $\mu_0 = 1.71 \cdot 10^{-5} kg/(m \cdot s)$ and $T_0 = 273K$ [45].

Mach number for pipe flow is given by

$$Ma = \frac{v}{c} \tag{6.12}$$

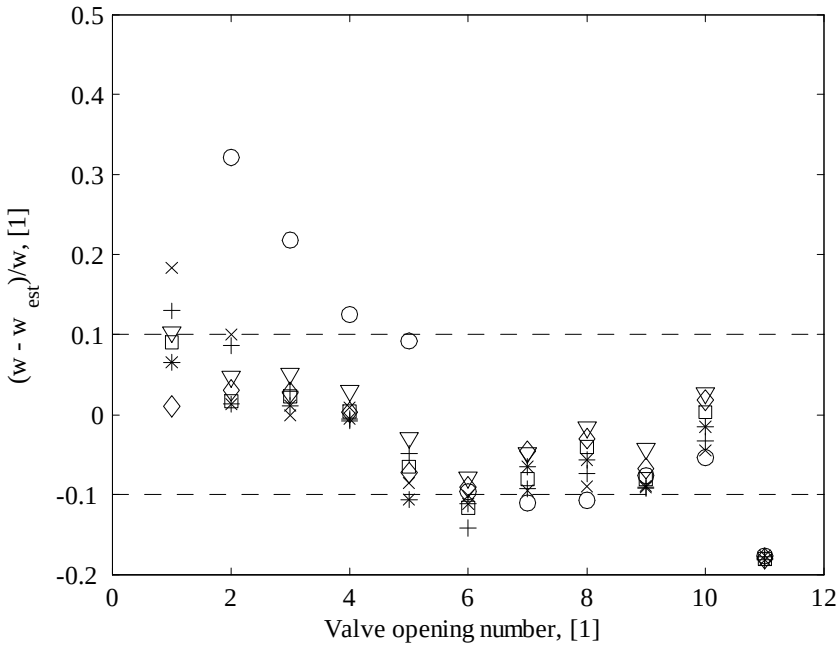

Figure 6.1: Aproximated mass flow from Pitot tube

where v is fluid velocity and c is speed of sound. Speed of sound for an ideal gas is given by

$$c = \sqrt{\kappa RT}. \tag{6.13}$$

Using (6.2), (6.6) and (6.13), (6.12) can be rewritten as

$$Ma = \frac{w}{pA}\sqrt{\frac{RT}{\kappa}} \tag{6.14}$$

and the Mach number can now be calculated from measurements of pressure, temperature and mass flow.

The entrance length for turbulent flow is approximated as

$$L_e = 4.4 \cdot \mathrm{Re}_D^{\frac{1}{6}} \cdot D \tag{6.15}$$

and describes the distance needed for developing a constant velocity profile when fluid enters a duct, [45].

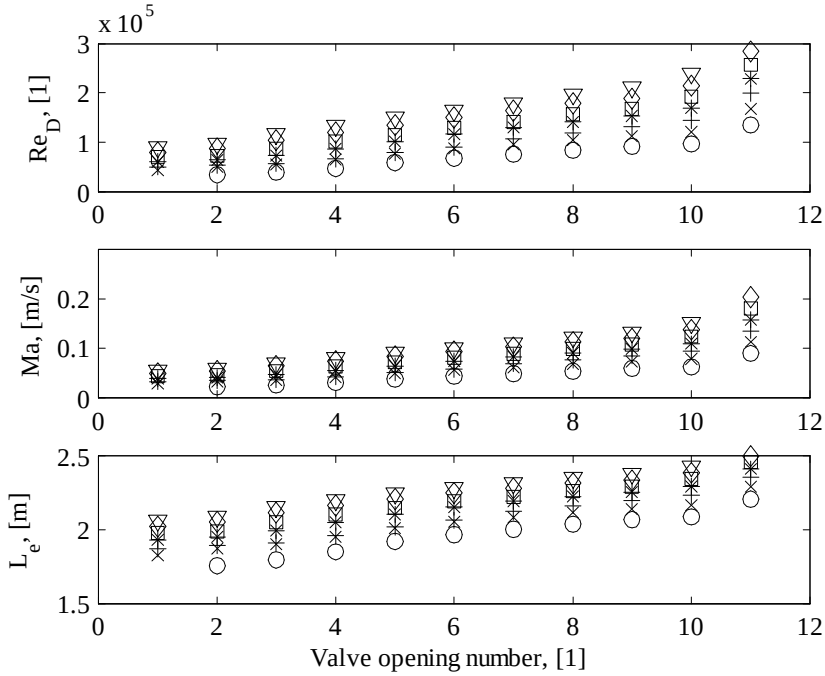

Figure 6.2: Characteristic values for flow

Figure 6.2 shows plots of the Reynolds numbers, Mach numbers and entrance lengths. All these properties increases with increasing impeller speed and mass flow. From the plot of Reynolds numbers it can be seen that these are well above 2300. This indicates that flow in ducts is turbulent, since the accepted value for separating laminar and turbulent flow is 2300, [45]. From the plot of Mach numbers it can be seen that these are below 0.3. This implies that flow in ducts can be considered incompressible, since the accepted boundary for this approximately 0.3, [45]. The entrance length is between 2 and 2.5 meters. This is well above the length related to upstream compressor duct, implying that the flow profile in this duct will never be fully developed. Hence, effects of flow entering a duct and developing towards a flow profile will be dominant, [45].

6.2.3 Duct flow considerations

By temporarily violating the notation of Chapter 2, consider the one dimensional momentum equations for incompressible flow

$$\dot{w}_{cu} = \frac{A}{L_{cu}}(p_a + F_{cu} - p_{cu}) \tag{6.16}$$

$$\dot{w}_{c} = \frac{A}{L_{c}}(p_{cu} + F_{c} - p_{cd}) \tag{6.17}$$

$$\dot{w}_{cd} = \frac{A}{L_{cd}}(p_{cd} + F_{cd} - p_{p}) \tag{6.18}$$

describing mass flow dynamics for duct upstream compressor, duct containing the compressor and duct downstream the compressor respectively. These equations take on a general form of pressure difference across the duct and some forcing term (e.g. compressor, friction, flow profile), where the forcing terms are used to capture un-modeled dynamics. In contrast to the equations presented in Chapter 2, these include forcing terms in the compressor upstream and downstream ducts. Note that the sign convention is such that a positive force works along the positive flow direction, where positive direction is defined from ambient to plenum. In steady state these forcing terms are given by

$$F_{cu} = p_{cu} - p_a \tag{6.19}$$

$$F_{c} = p_{cd} - p_{cu} \tag{6.20}$$

$$F_{cd} = p_{p} - p_{cd}. \tag{6.21}$$

Figure 6.3 shows plots of the various forcing terms as a functions of mass flow and impeller speed for the steady state data. In addition to the terms (6.19)-(6.21), this figure also shows the difference of plenum and ambient pressure. Pressure difference in upstream compressor duct, F_{cu}, is completely described by duct mass flow since all impeller speeds collapses into one line. Pressure difference in the duct containing the compressor, F_c, is seen to be a function of both mass flow and impeller speed. Pressure difference in downstream compressor duct, F_{cd}, has the same qualitative behavior as compressor stage pressure difference (not shown by this plot), but the overall values are vanishingly small relative to that of the compressor duct. Moreover, F_{cd} is vanishingly small relative to any of the other pressure

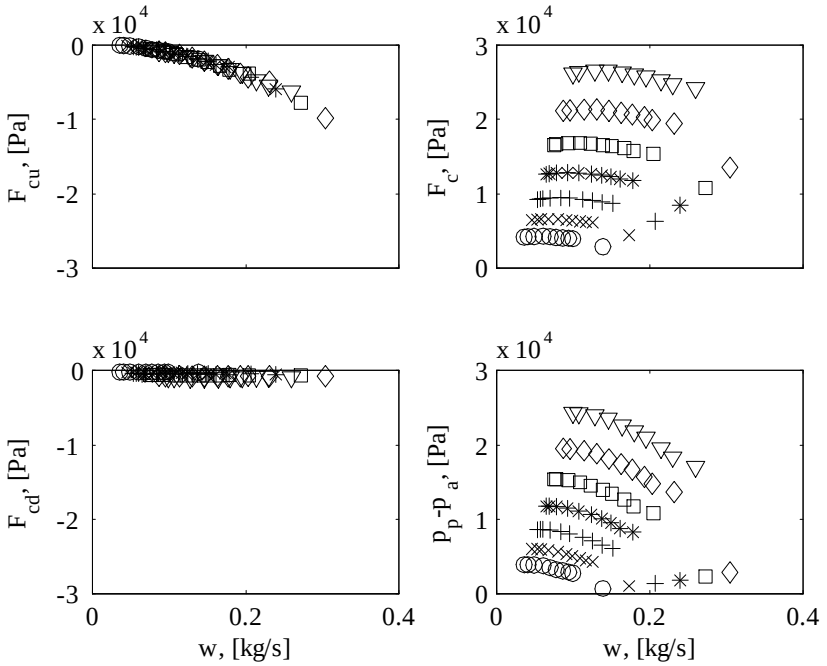

Figure 6.3: Forcing terms in steady state

differences. The pressure differences of plenum and ambient shows the same qualitative behavior as F_c.

From these consideration the approximations

$$F_{cu} \approx F_{cu}(w) \tag{6.22}$$

$$F_{cd} \approx 0 \tag{6.23}$$

seems reasonable, which indicates that flow in duct upstream the compressor is not explicitly dependent on the compressor and that flow in duct downstream of compressor is inviscid. Furthermore, from (6.19)-(6.23) it follows that

$$p_p - p_a \approx F_c - F_{cu}. \tag{6.24}$$

6.2.4 Valve characteristic

Following (2.8)-(2.9) the characteristic is assumed to be of the form

$$w_t\left(A_{t\%}, p_p\right) = k_t\left(A_{t\%}\right)\sqrt{p_p - p_a} \tag{6.25}$$

for positive flow, where $A_{t\%} = 0$ and $A_{t\%} = 100$ for completely closed and fully open valve respectively. Since steady state data are available for w_t, $A_{t\%}$, p_p and p_a, the unknown function k_t of (6.25) is determined from

$$\frac{w_t\left(A_{t\%}, p_p\right)}{\sqrt{p_p - p_a}} = k_t\left(A_{t\%}\right). \tag{6.26}$$

The plots of Figure 6.4 shows the steady state data for this equation, where $\frac{w_t(A_{t\%},p)}{\sqrt{p_p-p_a}} = k_t\left(A_{t\%}\right)$ is plotted as a function of $A_{t\%}$. From the figure it can be seen that data for various speeds and valve openings collapses to one line, making the given structure of (6.25) a reasonable model. Note that when the actual fitting is carried out, points are added to represent the origin of the figure. This is done to incorporate zero mass flow through the valve when it is completely closed.

Inspired by the structure of data in Figure 6.4, a 2. order polynomial

$$k_t\left(A_{t\%}\right) = k_1 A_{t\%}^2 + k_2 A_{t\%} + k_3 \tag{6.27}$$

was fitted using MATLAB's `polyfit`. This resulted in

$$k_1 = 0.0203 \cdot 10^{-5} \tag{6.28}$$
$$k_2 = -0.0691 \cdot 10^{-5} \tag{6.29}$$
$$k_3 = -0.1718 \cdot 10^{-5} \tag{6.30}$$

for the various coefficients. The approximation (6.27)-(6.30) is shown in the upper plot of Figure 6.5.

In order to see if a simpler structure for $k_t\left(A_{t\%}\right)$ could describe the data sufficiently,

$$k_t\left(A_{t\%}\right) = kA_{t\%}^2 \tag{6.31}$$

was investigated. Least squares method was used for the fit, resulting in

$$k = 1.9259 \cdot 10^{-7}. \tag{6.32}$$

The approximations (6.31) and(6.32) is shown in the lower plot of Figure 6.5. Little difference can be seen by comparing the two approximations. Hence, the somewhat simpler function (6.31) is used hereafter.

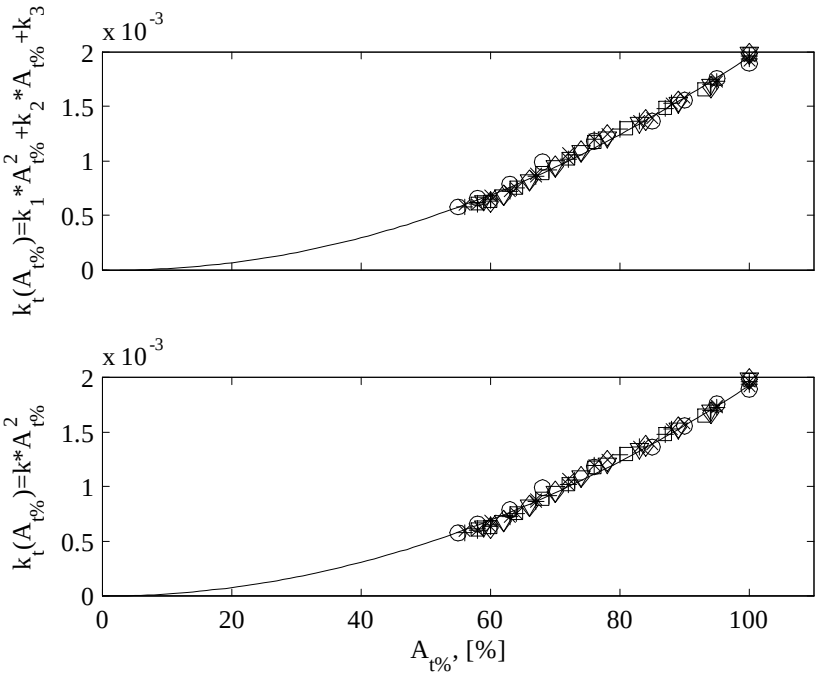

Figure 6.4: Valve characteristic

6.2.5 Compressor characteristic

The compressor characteristic for this system is first and foremost described by the steady state pressure, mass flow and impeller speed relations of F_c, when this is the forcing term for the duct containing the compressor. The discussion in Section 6.2.3 showed that also F_{cu} had an considerable effect, whereas F_{cd} had relatively small amplitudes. In addition to identify F_{cu} and F_c, it is interesting to evaluate

$$F_c' = p_p - p_a \tag{6.33}$$

which represents a forcing term in a momentum equation from ambient to plenum, entire duct upstream plenum. Note that in view of (6.23), $p_{cd} \approx p_p$, this term can also be though of as representing the forcing for a momentum equation reaching from ambient to compressor downstream pressure. From (6.23) it follows that

$$F_c' \approx F_{cu} + F_c. \tag{6.34}$$

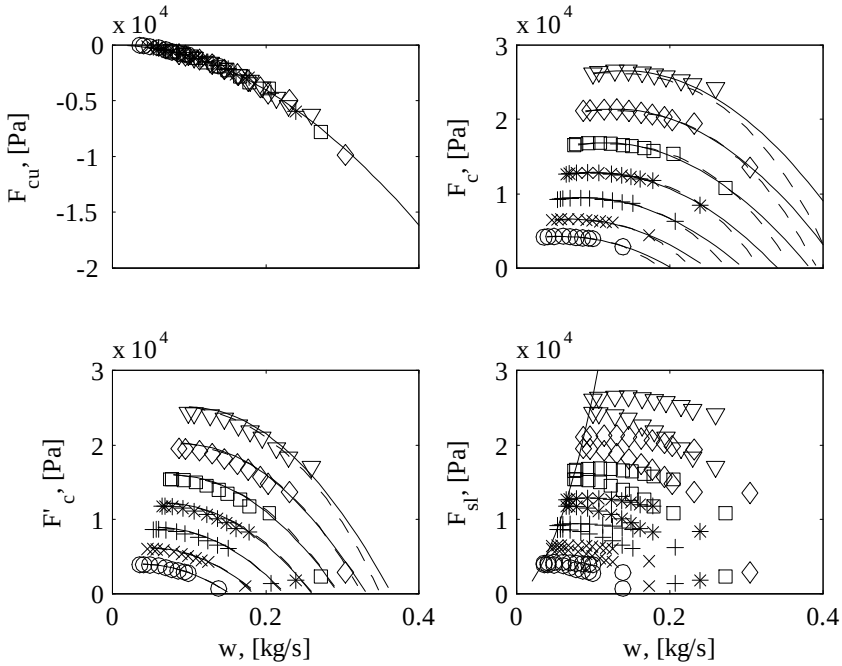

Figure 6.5: Compressor characteristic for open loop stable region. Solid and dashed lines correspond to 2. order polynomial and Moore-Greitzer polynomial respectively.

Based on the upper left plot of Figure 6.3, a model for the upstream forcing term is taken as

$$F_{cu} = -k_{cu} w^2. \tag{6.35}$$

where the gain

$$k_{cu} = 1.0109 \cdot 10^5 \tag{6.36}$$

was found when fitting the data using least squares method. The approximation (6.35)-(6.36) is shown in the upper left plot of Figure 6.5.

From the upper right plot of Figure 6.3 it can be seen that F_c is a function of both mass flow and impeller speed. Fitting this characteristic for the open loop stable region was therefore done in several steps, following the approach described in [16]. First each individual speed line was fitted

with a polynomial of mass flow. Two polynomials

$$F_c = k_{c1}w^2 + k_{c2}w + k_{c3} \quad (6.37)$$

$$F_c = k_{c1}w^3 + k_{c2}w^2 + k_{c3} \quad (6.38)$$

were investigated for the fit. These represent a standard 2. order polynomial and a so called Moore-Greitzer polynomial respectively. The resulting coefficients of these polynomials where made functions of impeller speed. This was done by fitting each of the coefficients with a second order polynomial in speed, making the various coefficients of (6.37) and (6.38) functions of impeller speed. The resulting compressor characteristic is therefore continuous in both mass flow and impeller speed. The upper right plot of Figure 6.5 shows the resulting approximation. From this plot it can be seen that the Moore-Greitzer polynomial has a steeper mass flow gradient for higher mass flows than the 2. order polynomial. Furthermore, a closer inspection shows that the Moore and Greitzer polynomial has negative mass flow gradients at the surge line, while the 2. order polynomial has positive or zero gradients.

Based on (6.34), a model for F_c' is simply taken as the sum of (6.35) and (6.37) or (6.38). This approximation is shown in the lower left plot of Figure 6.5.

Based on Figure 6.3, the surge line was modeled as

$$F_{sl} = k_{sl1}w^2 + k_{sl2}w + k_{sl3}. \quad (6.39)$$

The coefficients of this polynomial was evaluated with MATLAB's `polyfit` based on data for each speed lines lowest throttle opening, and resulted in

$$k_{sl1} = 21.89 \cdot 10^5 \quad (6.40)$$

$$k_{sl2} = 52.18 \cdot 10^3 \quad (6.41)$$

$$k_{sl3} = -17.56 \cdot 10. \quad (6.42)$$

The approximation (6.39)-(6.42) is shown in the lower right plot of Figure 6.5 with steady data for both F_c and F_c'. As can be seen from this plot, the surge line holds for both of these forcing terms, even though it is derived from data for F_c.

6.2.6 Torque characteristic

As discussed in Chapter 2, the Euler pump equation gives the structure $\tau_c(w, \omega) = k_1 |w| \omega$ for torque on impeller due to fluid flow. Furthermore,

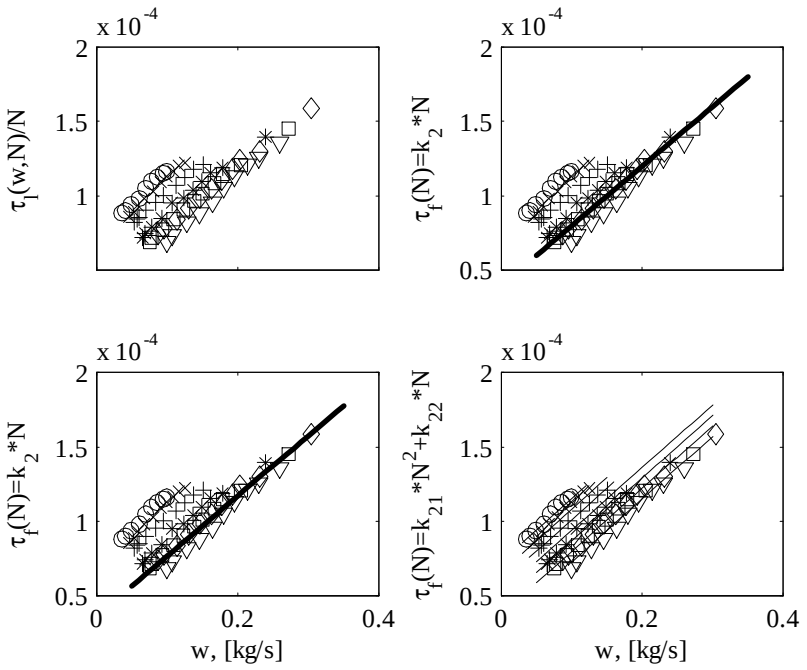

Figure 6.6: Torque characeristic

due to friction of rotating parts (motor drive shaft and gears) it is reasonable to expect a torque characteristic of the form $\tau_l(w,\omega) = k_1|w|\,\omega + \tau_f(\omega)$, where $\tau_f(\omega)$ represents a friction term. Since steady state data is available for τ_l, w and ω, the unknown parameter k_1 and function τ_f is determined from

$$\frac{\tau_l(w,N)}{N} = k_1|w| + \frac{\tau_f(N)}{N}, \tag{6.43}$$

now expressed in terms of $N[rpm]$ rather than $\omega[rad/s]$ to be consistent with variables used in plots. The upper left plot of Figure 6.6 shows steady state data for this equation, where (6.43) is plotted for the individual speeds as a function of w. From this plot it can be seen that data for individual speeds are nearly straight lines, making the given structure of $k_1|w|$ a reasonable model. Furthermore, it can be seen that $\frac{\tau_f(N)}{N}$ decreases with increasing speed. However, it is seen that the highest speeds form a cluster where speed differences are not that significant.

Based on this last observation, one possible approximation is

$$\tau_f(N) = k_2 N \tag{6.44}$$

which gives $\tau_l(w, N) = k_1 |w| N + k_2 N$. Note that this structure is identical to that given by (2.5)-(2.7). This is most valid for the higher speeds, since these forms more or less a cluster. The constants where calculated as

$$k_1 = 4.0046 \cdot 10^{-4} \tag{6.45}$$
$$k_2 = 3.9662 \cdot 10^{-5} \tag{6.46}$$

using the four highest speeds, and

$$k_1 = 4.0325 \cdot 10^{-4} \tag{6.47}$$
$$k_2 = 3.6494 \cdot 10^{-5} \tag{6.48}$$

using the three highest speeds. These calculations where done in two steps. First k_1 and k_2 where calculated from (6.43) for each speed using MATLAB's `polyfit`. Then these constants where averaged for the speeds in question. The result is shown in the upper right and lower left plot of Figure 6.6 for the four and three highest speeds respectively.

From the plot of (6.43) it seems like the various speed curves have approximately the same slope, but that the offset varies with speed. The parameter k_2 is therefore modeled as a linear function of speed, $k_{2,\ modified} = k_{21}N + k_{22}$, resulting in

$$\tau_f(N) = k_{21}N^2 + k_{22}N. \tag{6.49}$$

Various constants where found in the same manner as for (6.44), except that 1. order polynomial fit of k_2's from the individual speed lines was performed rather than averaging. This procedure resulted in

$$k_1 = 4.2170 \cdot 10^{-4} \tag{6.50}$$
$$k_{21} = -2.8340 \cdot 10^{-9} \tag{6.51}$$
$$k_{22} = 1.0145 \cdot 10^{-4} \tag{6.52}$$

and the approximation (6.43) and (6.49)-(6.52) is shown in the lower right plot of Figure 6.6.

When working in the laboratory it was noticed that load torque readings where unreliable and inconsistent for lower speeds whereas more consistent and repeatable for higher speeds. An explanation for this might be that the drive system requires a minimum speed to heat up the various parts and lubrication system to a point where speed variations have little effect.

Step	Description
1	$\tau_d = 1.420$ to $\tau_d = 1.475$ for $A_{t\%} = 90$ (N=12600-13000)
2	$\tau_d = 1.475$ to $\tau_d = 1.420$ for $A_{t\%} = 90$ (N=13000-12600)
3	$\tau_d = 2.025$ to $\tau_d = 2.080$ for $A_{t\%} = 66$ (N=23700-24100)
4	$\tau_d = 2.080$ to $\tau_d = 2.025$ for $A_{t\%} = 66$ (N=24100-23700)

Table 6.2: Torque step data

6.2.7 Comments

Steady state analysis indicated that duct downstream the compressor can be used to implement a measurement of p_c, according to the model discussed in Chapter 2. This is not the case for duct upstream of the compressor.

Steady state analysis showed that the 2. order polynomial had positive or zero mass flow gradients at the surge line, while the related to the Moore - Greitzer polynomial was negative. It is widely accepted that surge occurs for positive sloped operating points, indicating that the second order polynomial is a better fit in this respect. However, the Moore-Greitzer polynomial had a steeper mass flow gradient for higher mass flows than the second order polynomial. This agrees better with the stone wall, or choking, phenomena.

6.3 Transient model identification

Transient analysis considers both steps in torque as well as surge data. Step data is described in Table 6.2. Each of the step responses were gathered ten times with same initial conditions. These time series where den averaged for the individual steps. Surge data for constant impeller speed was gathered for each of the speeds of Table 6.1 by throttling into the open loop unstable region.

6.3.1 Pressures for constant speed surge

Figure 6.7 shows all pressures during a surge cycle for $N = 22891rpm$, which corresponds to the second highest impeller speed for surge data. Surge frequency is approximately $4.55Hz$. Pressure downstream compressor is available from both duct wall and a Pitot tube. This gives the possibility

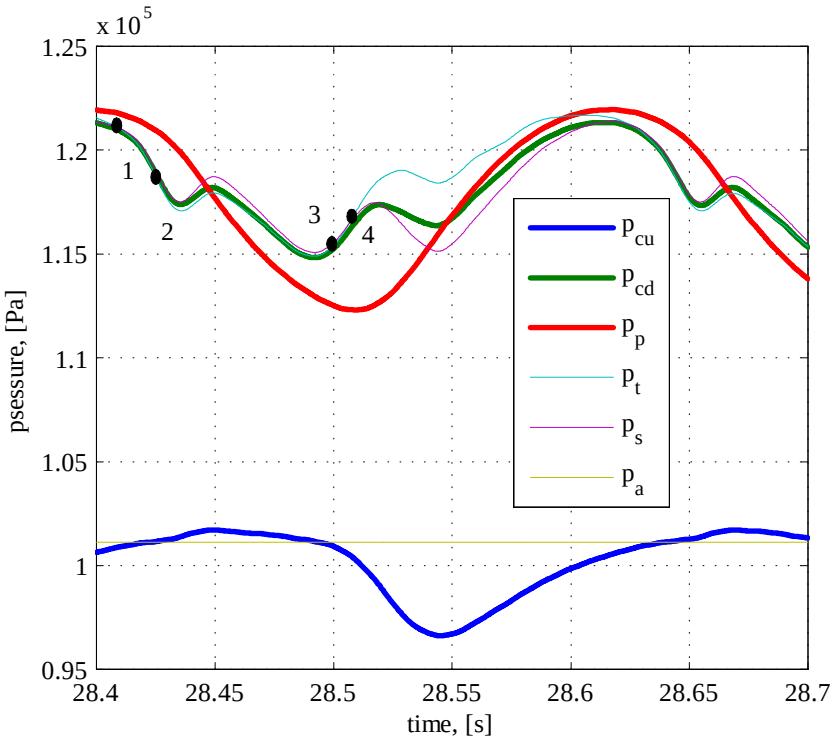

Figure 6.7: Pressures for constant speed surge, $N = 22891rpm$.

to evaluate the flow in some more detail at this point. The flow behavior of these data can be divided in four regions:

- The region between point 1 and 2 corresponds to zero mass flow, going into negative mass flow. This can be seen by evaluating the Pitot tube pressures, since downstream pressure goes from being smaller to larger than upstream pressure in this region (the velocity component is switching side). Downstream compressor pressure and both Pitot tube pressures are approximately equal in this region, since all these represent the static pressure due to the absence of a velocity component. Furthermore, it can be seen that compressor upstream pressure goes from being smaller to larger than ambient pressure in this region. This agrees with entering negative mass flow, since upstream pressure

must be larger than ambient pressure to set up negative mass flow in this force free upstream duct.

- The region between point 2 and 3 corresponds to negative mass flow. Also this is seen by evaluating Pitot tube pressures, where the upstream pressure is smaller than the downstream pressure in this region (the velocity component acts on the downstream side). This suggests that Pitot tube upstream pressure should be equal to compressor downstream pressure, which is practically the case, since both these represent the static pressure. Furthermore, it can be seen that upstream compressor pressure is larger than ambient pressure in this region, resulting in a pressure gradient along the negative flow direction for the upstream duct.

- The region between point 3 and 4 corresponds to zero mass flow, going into positive mass flow. This can be seen by evaluating the Pitot tube pressures, since upstream pressure goes from being smaller to larger than downstream pressure in this region (due to the velocity component changing side). Downstream compressor pressure and Pitot tube pressures are approximately equal in this region since they all represent static pressure. Furthermore, it can be seen that upstream compressor pressure has become slightly smaller than ambient, setting up a positive pressure gradient with respect to flow.

- The region between point 4 and 1 corresponds to positive mass flow. Again, this is seen from Pitot tube pressures since upstream is larger than downstream pressure. It was expect that downstream Pitot tube pressure and downstream compressor pressure to be equal in this region, which only is the case in the beginning and towards the end of the region. This inconsistency can have several reasons such as calibration inaccuracy, internal flow phenomena, Pitot tube related properties or a combination of these. The local flow in combination with Pitot tube properties is believed to be the most likely reason, since the calibration seems to be relatively good for the other regions.

It is also worth noticing that intermediate pressure peeks in compressor downstream pressure follows a change in flow direction. Furthermore, change in flow direction downstream compressor occurs approximately at the same time as upstream and ambient pressures intersect.

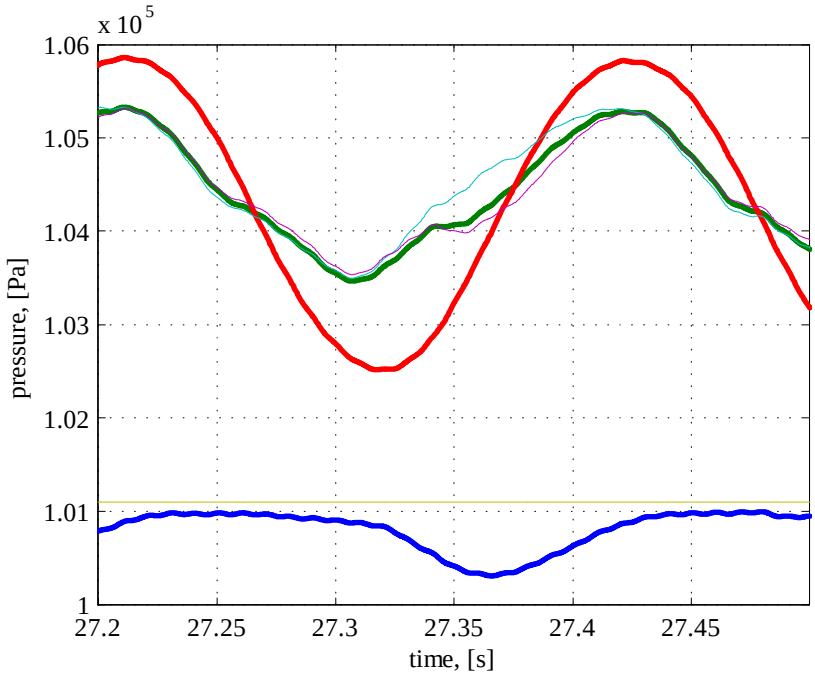

Figure 6.8: Pressures for constant speed surge, $N = 10283rpm$.

Figure 6.8 shows a surge cycle for the lowest speed line. From this figure it can be seen that the intermediate pressure peeks are almost completely removed. Furthermore, from upstream compressor and ambient pressure it seems like this surge cycle do not posses negative mass flow. However, by evaluating the Pitot pressure, analogous the previous discussion, one comes to the conclusion that also this constitutes a deep surge cycle. By further investigation, it can be seen that a small offset change of Pitot pressures gives conclusion of only positive mass flow, and a small offset change of upstream compressor and ambient pressures gives the possibility of negative mass flow. Yet another explanation might be that we have negative mass flow locally downstream of the compressor, which never reaches the upstream duct.

A mass flow estimate for surge data is generated using (6.7) with a scaling of 0.63. This is done in order to get an indication of the relation of pressure differences and mass flow, analogous to that of the steady state analysis. Figure 6.9 shows pressure differences versus estimated mass flow

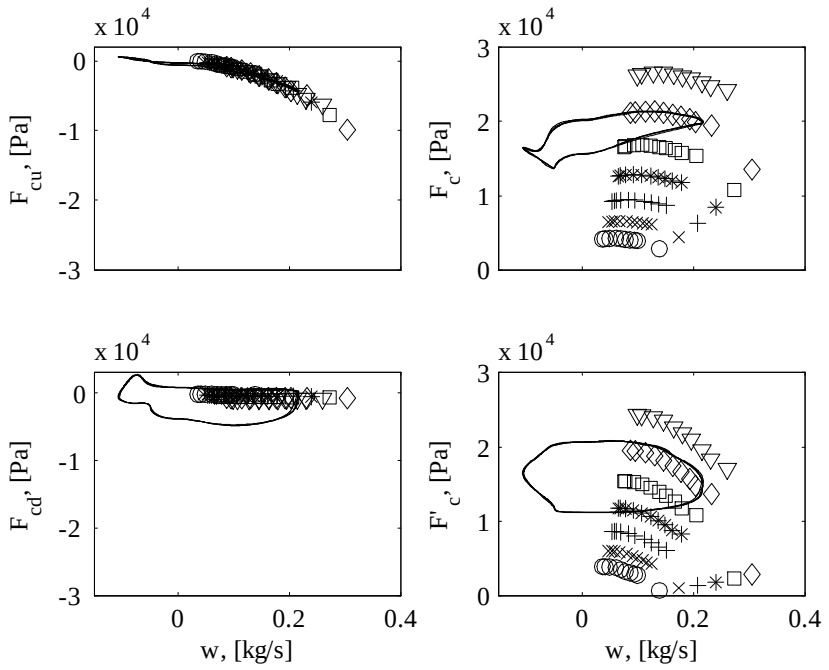

Figure 6.9: Pressure diferences for constant speed surge, $N = 22891rpm$.

in surge for the second highest impeller speed. Investigating the difference of compressor upstream and ambient pressures shows that this lies strictly on the characteristic derived for the steady state (for positive flow), which is not the case for the other pressure differences. This indicates that dynamics related to the upstream duct mass flow can be neglected, in which case (6.16) reduces to

$$p_{cu} = p_a + F_{cu}\left(w_{cu}\right) \forall t. \tag{6.53}$$

This is not surprising, since the upstream duct is relatively short with respect to the other ducts (duct containing compressor is almost twice as long and downstream compressor duct is almost twelve times longer).

Combining this, no dynamics in upstream duct, with the findings of upstream and ambient pressures crossing each other approximately the same instance as flow downstream compressor changes sign, indicates that upstream compressor duct and compressor duct has the instantaneously same

mass flow value. All this rewrites the dynamic equations (6.16)-(6.18) as

$$\dot{w}_c = \frac{A}{L_c}\left(p_a + \underbrace{F_{cu}(w_c) + F_c(w_c, \omega)}_{F_c'} - p_{cd}\right) \tag{6.54}$$

$$\dot{w}_{cd} = \frac{A}{L_{cd}}(p_{cd} - p_p) \tag{6.55}$$

where (6.16) now is incorporated in (6.54). From evaluation of the Mach number in Section 6.2.2 it is known that flow in ducts are incompressible, indicating that $w_c = w_{cd}$. This implies that (6.54)-(6.55) comply with the structure and assumptions of (2.20)-(2.21), leading to the relation (2.23) and (2.24) for duct mass flow.

6.3.2 Mass flow and pressure dynamics

Downstream compressor duct

In Chapter 2 the pressure and mass flow dynamics is derived as

$$\dot{p}_p = \frac{c_p^2}{V_p}(w_{cd} - w_t(A_{t\%}(t), p_p)) \tag{6.56}$$

$$\dot{w}_{cd} = \frac{A_c}{L_{cd}}(p_{cd}(t) - p_p) \tag{6.57}$$

where explicit time notation indicates that these signals are now considered system inputs available as measurements. The valve characteristic (2.8)-(2.9) and (6.31)-(6.32) will be used for (6.56). Furthermore, the speed of sound is evaluated by $c_p = \sqrt{\kappa_p R T_p}$. Various constants are taken as

$$\kappa_p = 1.4\ [1] \tag{6.58}$$

$$R = \frac{8.314 \cdot 10^3}{28.97}\ [\frac{J}{kg \cdot K}] \tag{6.59}$$

$$V_p = 0.1\ [m^3] \tag{6.60}$$

$$A_c = \pi * (0.5 \cdot 70 \cdot 10^{-3})^2\ [m^2] \tag{6.61}$$

$$L_{cd} = 280 \cdot 10^{-2}\ [m] \tag{6.62}$$

and T_p as the average of the measurement time series in question. Since the compressor is not included in this system, these parameters are from physical

length, area and volume. Recall that when the compressor is included, this involves a model for which L (or similarly A/L) represents some equivalent length.

The second order system (6.56)-(6.57) is simulated with $A_{t\%}(t)$ and $p_{cd}(t)$ as input time series from the torque step data in Table 6.2. The result of the simulation is shown in Figure C.9 through Figure C.12. These figures show a comparison of measured and simulated plenum pressure and duct mass flow. For transient evaluation, only the pressure is interesting due to the poor dynamic capabilities of the mass flow measurements. However, they will still be used to evaluate steady state values. Each figure shows two plots of the same data. Left column presents the actual response, whereas the simulated response is shifted in the right column to better compare the dynamic performance. The steady state differences are due to inaccuracies in the static mapping w_t, which gives a slightly different equilibrium. Furthermore, the simulated responses can be seen to have a transient response in the very beginning (settling after approximately one to three seconds). This is caused by the initial conditions of the simulations, when these are taken identical to those of the measured values. From the figures it can be seen that the dynamic response of the simulated pressure is in good accordance with the measured pressure. Furthermore, the steady state responses are within reasonable accuracy. Plenum temperature varies between 314 and 337, which implies a variation of approximately $\pm 3.5\%$ relative to 326.

The second order system (6.56)-(6.57) is simulated with $A_{t\%}(t)$ and $p_{cd}(t)$ as inputs when undergoing surge in constant speed. The results are shown in Figure C.13 through Figure C.19 for seven different speeds, equal to those in Table 6.1. The figures show good agreement for measured and simulated plenum pressure, with respect to both frequency and amplitude. Unfortunately, no measurements are available to evaluate transient mass flow. Simulated mass flow is therefore compared with the somewhat uncertain and inaccurate estimate (6.7) using a scaling of 0.63. However, since the dynamic equations are highly correlated (since $A_{t\%}(t)$ is practically constant one can consider p_{cd} as only input), the simulated mass flow is assumed to be in good agreement with the actual when pressures shows good results.

Compressor characteristic

From (2.23)-(2.24) and (6.17)-(6.18), (6.23), (6.53) and (6.33) it follows that

$$F_c'(w_c,\omega) = \left(1+\frac{L_c}{L_{cd}}\right)p_{cd}(t) - \frac{L_c}{L_{cd}}p_p(t) - p_a \tag{6.63}$$

where $p_{cd}(t)$, $p_p(t)$ and p_a are available and L_{cd} has been established as (6.62) by simulations. Hence, the only unknown parameter in (6.63) is L_c. This is considered a tuning parameter for the model, and will be chosen such (6.63) holds.[1] Furthermore, the steady part of $F_c'(w_c,\omega)$ has been established in Section 6.2.5. The open loop unstable and negative mass flow region for this characteristic will in large be determined from its zero mass flow value as well as a qualified guess of the negative mass flow quadratic characteristic gain, both of which is determined from the right hand side of (6.63) for surge data.

When tuning L_c for the right hand side of (6.63) there is a couple of criteria that should be satisfied. First of all, when representing (6.63) with corresponding mass flow in a compressor map, this plot should coincide with steady state data. Second, the value of $F_c'(w_c,\omega)$ should be the same for a given w_c throughout the surge cycle (independent on whether the mass flow is increasing or decreasing).

Tuning of L_c was done in several steps. First the two dimensional model (6.56)-(6.57) is simulated to generate $w_c(t)$ for the surge cycle in question. Then the right hand side of (6.63) is plotted with $w_c(t)$ in the compressor map for evaluation. The parameter

$$L_c = 180\cdot 10^{-2} \tag{6.64}$$

was chosen such that $w_c(t) = 0$ gave the same value $F_c'(w_c,\omega)$ for both decreasing and increasing w_c. The plots used for evaluation are shown in Figure C.20 through Figure C.26.

Based on responses shown in Figure C.20 through Figure C.26, estimates on forcing term value for zero mass flow was retrieved. A first order polynomial fit was evaluated for these data using MATLAB's `polyfit` in order to

[1] As commented upon in Chapter 2.2, A_c/L_c should be regarded as a tuning parameter for the model. The parameter A_c is often chosen as some "reference/characteristic" area corresponding to inducer or connecting duct diameter, leaving L_c for tuning. A more comprehensive description and an alternative approach to finding this tuning parameter is given in [46].

arrive at an expression being continuous in ω. The approximation resulted in

$$F'_{c,w=0} = 1.0236N - 8.4541 \cdot 10^3 \tag{6.65}$$

where F'_c is expressed in terms of N rather than ω.

From Figure C.20 through Figure C.26 it can be seen that the mass flow gradient at zero mass flow is approximately zero. This is as expected from theory, since the compressor represents a restriction for negative mass flow. The region between zero mass flow and open loop stable region (zero mass flow and surge line) is now fitted using a cubic polynomial of given boundary conditions. For zero mass flow it is required that the mass flow gradient of this polynomial is zero. At the surge line it is required that the mass flow gradient is equal to that of the connecting open loop stable speed line. Note that these restrictions on boundary gradients make the characteristic continuously differentiable.

Based on Figure C.20 through Figure C.26 the coefficient for negative mass flow is determined. This is assumed the same for each speed line, resulting in

$$F'_{c,w<0} = F'_{c,w=0} + 0.8 \cdot 10^6 w_c^2 \tag{6.66}$$

for negative mass flow, where $F'_{c,w=0}$ is included to incorporate the speed line.

For simulation, the evaluation of the compressor characteristic will now be an algorithm consisting of essentially two steps. First the region for evaluation is decided (negative mass flow, positive mass flow and open loop unstable or positive mass flow and open loop unstable). Then the appropriate F'_c is evaluated and combined with p_a to generate $p_c(w_c, \omega)$. The resulting compressor characteristic, represented in terms of the forcing term $F'_c(w_c, \omega)$, is shown in Figure 6.10 for (2.37) along with steady state data and zero mass flow points.

Simulations of (6.56) and (6.57) are shown in Figure C.27 through Figure C.33 for all constant speed surge data using a model $p_c(w_c, \omega)$. In this case the system inputs are given by $A_{t\%}$ and ω, being constant for each simulation. Recall from Chapter 2 that this implementation yields a duct length $L' = L_c + L_{cd}$. The simulations shows reasonably good fit to experimental data in terms of frequency and amplitude. The phase deviation of simulated and measured response observed in plots is due to inaccuracy of frequency for the simulated response.

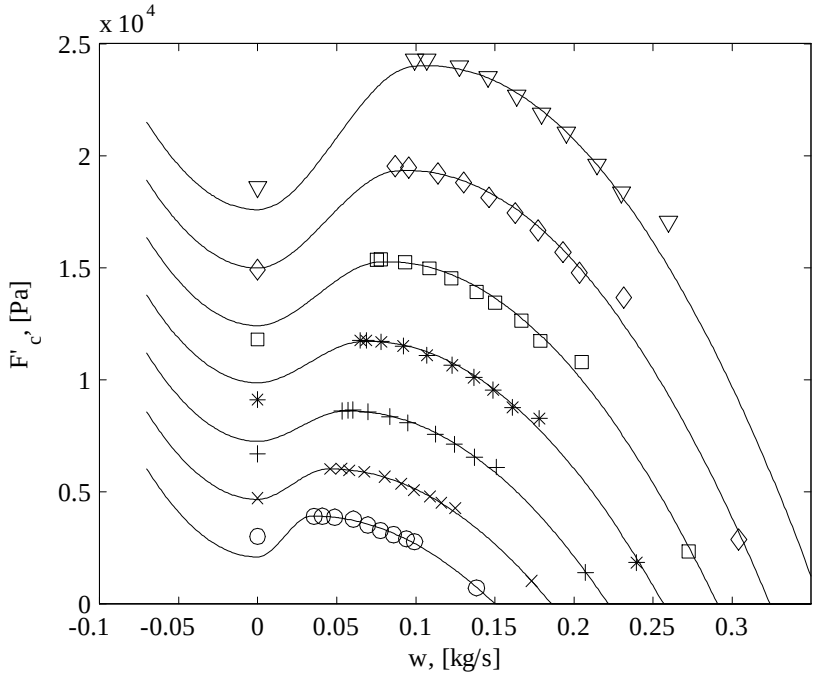

Figure 6.10: Compressor characteristic, F_c' for laboratory.

6.3.3 Impeller speed

The speed dynamics is on the form $\dot{\omega} = \frac{1}{J}\left(\tau_d - \tau_l\left(w, \omega\right)\right)$, where the compressor load torque characteristic is discussed in Section 6.2.6. This discussion presented two structures for the characteristic, one for higher speed and one that aimed at fitting the characteristic for all speeds. It was also commented upon that torque data for lower speeds was somewhat hampered with uncertainty.

Step data described in Table 6.2 will be used to identify the time constant of the impeller dynamics. Data 1 and 2 corresponds to impeller speeds in the lower range, whereas data 3 and 4 corresponds to impeller speeds in the higher range. Hence, for torque steps in 1 and 2 the model (6.49)-(6.52) will be used, whereas (6.44) and (6.47)-(6.48) is used for steps 3 and 4. In order to identify the parameter k, that is, the inertia J of rotating parts,

$$\dot{N} = k\left(\tau_d - \tau_l\left(w, N\right)\right) \tag{6.67}$$

was simulated using τ_d and w as system input. The simulation was an iterative process of tuning k until the simulated N was reasonable close to the measured response for N. The following discussion considers

$$k = 10^4 \tag{6.68}$$

for various methods of generating w. All the figures presented shows the actual response in the upper plot, whereas the simulated response is shifted in the lover plot to better compare the responses. The deviation shown in the upper plot comes from model uncertainty of τ_l resulting in slightly different steady state values.

First the simulation was carried out using the measurement of mass flow. As already pointed out, this measurement yields poor dynamic performance. The result is shown in Figure C.34 through Figure C.37. All of these figures involve overshoot for simulated response. This can be explained by the slow response of mass flow measurement, when a deviation of measured and actual mass flow results in an incorrect value for τ_l in simulation. This is also supported by the observation that the overshoot settles at the same time as mass flow measurement converged to steady state value. Furthermore, for the lower speed responses it can be seen that measurement and simulation generates approximately the same change in speed whereas more or less the exact same change in speed is observed from the higher speed response. This is as expected since the model for τ_l is better for high speeds than for low speeds, as discussed in Section 6.2.6. Due to the overshoot it is difficult to evaluate the dynamic performance for these simulations.

The step response poses a relatively small change in mass flow. Therefore a simulation was carried out for constant mass flow input, where the mass flow was derived by averaging over the time series in question. The result is shown in Figure C.38 through Figure C.41. Common for all these responses is that speed change observed by measurement differs from those found by simulation. This comes from using averaged mass flow since this results in an incorrect value for τ_l in steady state. The dynamic response seems to be within reasonable accuracy.

Finally the system was simulated with mass flow estimated from Pitot tube pressures, (2.7) using a correction factor of 0.63. The results are shown in Figure C.42 through Figure C.45. These figures show no overshoot and produce more or less the same speed change as that observed by the measurements, especially for higher speeds. The deviations can be explained from

the inaccuracy of this estimate, as discussed in Section 6.2.1. Furthermore, the dynamic response is within reasonable accuracy.

Chapter 7

Observer validation

7.1 Introduction

Some of the observers from Chapter 4 will now be evaluated for data from the setup described in Chapter 5 and Chapter 6. More specifically, the observers from Proposition 4.1 through Proposition 4.4 are investigated. These yield observers based on the dynamic model of plenum pressure and duct mass flow. Chapter 6 showed that this model was in reasonably good agreement with experimental data. For the impeller speed dynamics, on the other hand, there was some model uncertainty/inaccuracy for the lower speed regime. Hence, to provide the model based observer with as accurate model as possible, the model is restricted to pressure and mass flow. Keep in mind that the main purpose of these observers is to generate a mass flow estimate needed as feedback to the control laws.

The observers from Proposition 4.1 through Proposition 4.4 represents two reduced order observers for mass flow and two observers estimating both pressure and mass flow. As pointed out in Chapter 4, the differences lies in whether the compressor characteristic p_c of (2.25) is implemented as a model or a measurement. Furthermore, as discussed in Chapter 2 the implementation as measurement is only possible if there is a sufficient length of duct upstream or downstream the compressor. It was concluded in Chapter 6 that the current setup had sufficient length downstream duct to introduce this measurement. This chapter also gave indications that $w_c \approx w_{cd}$, which completes the assumptions made to arrive at (2.25). Recall that $L_c' = L_c + L_{cd}$ and that $p_c(t) = \left(1 + \frac{L_c}{L_{cd}}\right) p_{cd} + \frac{L_c}{L_{cd}} p_p$ in case of measurement, where L_c is

Observer	Description
1	Proposition 4.1
1b	Proposition 4.1 using L_{cd} and p_{cd}
2	Proposition 4.2
3	Proposition 4.3
3b	Proposition 4.3 using L_{cd} and p_{cd}
4	Proposition 4.4

Table 7.1: Observers to be tested with experimentally data

a parameter tuned to best fit the experimental data whereas L_{cd} is a physical parameter. These considerations rise the question of whether (2.21) is a better model of mass flow than (2.25) for the observer, in the case when a measurement of p_c is used. Therefore, observers involving implementations of p_c as a measurement were also implemented using (2.21). It can easily be verified from Chapter 4 that this involves replacing L_c' by L_{cd} and $p_c(t)$ by $p_{cd}(t)$ for the propositions in question. For convenience of later reference, the various observers to be tested are now summarized in Table 7.1.

The observer gain

$$c_o = -10^{-5} \tag{7.1}$$

was chosen for the reduced order observers. This gain was motivated by the equation $\hat{w}_c = \hat{\chi} - c_o p_p$, to limit the effect of measurement noise from p_p on $\hat{w}_c$, since p_p is in the order of $10^5 - 10^6$ larger than w_c. The observers for pressure and mass flow was implemented with

$$K_1 = \begin{bmatrix} -50 \\ -1.25 \cdot 10^{-3} \end{bmatrix}, \; K_2 = \begin{bmatrix} 0 \\ 0 \end{bmatrix}. \tag{7.2}$$

Investigating the LMI (4.8) with MATLAB's `feasp` resulted in the conclusion that the LMI might be feasible, but not strictly feasible (recall that the LMI need only be feasible, and can not be strict feasible due to the zeros in lower right block of matrix). Note that this choice of K_2 implies that c_2 vanishes from the implementation, since in this case one has that $w_2 = \hat{w}_c$ and $w_1 = \hat{p}_p$. Hence, these observers represent a copy of the model in terms of estimated states and measured signals with a linear injection term comparing estimated and measured plenum pressure.

Initial conditions for estimated states, $\hat{\chi}$ or $\hat{p}_p$ and $\hat{w}_c$, are set to zero.

Step	Description
1	$N = 12500$ to $N = 22500$ at $A_{t\%} = 100$
2	$A_{t\%} = 100$ to $A_{t\%} = 60$ at $N = 22500$
3	$N = 22500$ to $N = 12500$ at $A_{t\%} = 60$
4	$A_{t\%} = 60$ to $A_{t\%} = 100$ at $N = 12500$

Table 7.2: Step data for observer validation

7.2 Data

The aforementioned observers were tested for several sets of data. These data can be divided in two:

- step in speed and valve references for the open loop stable regime
- surge data for constant speed, that is, surge data when the drive is feed with a constant speed reference

Step data was conducted first and foremost to evaluate the steady state performance of the mass flow estimate, since measurement of mass flow only is available for steady state. However, the transient performance of pressure estimate can also be evaluated from these data. The surge experiments were conducted to evaluate the transient performance of the observers. Due to the absence of a reliable transient mass flow measurement, the estimated mass flows were compared with the approximated mass flow calculated from Pitot tube pressures, as described in Chapter 2. Due to the inaccuracy of this approximation, evaluation of transient mass flow estimates will only give qualitative results.

Step data aimed at covering the entire range of the open loop stable region. To this end, operating points for low speed near surge line, low speed for fully open throttle, high speed for fully open throttle and high speed near surge line were evaluated. The step data is summarized for convenience of later reference in Table 7.2.

Constant impeller speed surge data for seven different speeds, similar to those in Table 6.1, were investigated. These form a relatively good resolution with respect to available speeds in the setup. Surge data is summarized for convenience of later reference in Table 7.3.

Surge	Description
1	$N = 10000$ and $A_{t\%} = 48$
2	$N = 12500$ and $A_{t\%} = 50$
3	$N = 15000$ and $A_{t\%} = 51$
4	$N = 17500$ and $A_{t\%} = 52$
5	$N = 20000$ and $A_{t\%} = 53$
6	$N = 22500$ and $A_{t\%} = 53$
7	$N = 25000$ and $A_{t\%} = 54$

Table 7.3: Surge data for observer validation

Step data was sampled at 1000Hz whereas surge data was sampled at 5000Hz. This implies that the surge data are hampered with somewhat more noise than the step data. Furthermore, during step 3 the system encountered surge in transition from one operating point to the other.

7.3 Result

Observer validation involves plots of both measured and simulated data. For all plots of this type, measured data are represented by black lines whereas estimated states are represented by lighter lines.

7.3.1 Step data

The result of step data is presented Figure D.1 through Figure D.4 in Appendix D, corresponding to data of Table 7.2 respectively. These figures consists of six rows and two columns, where the rows correspond to the observers described in Table 7.1 respectively. The fist column shows mass flow estimate and measured mass flow, whereas the second column shows the observer error relative to measured mass flow.

Common for all plots of measured and estimated mass flow is that the measured mass flow converges much slower to the new operating point. This is due to the poor dynamic performance of the measurement. From Figure D.2 it can be seen that the mass flow estimate for observer 2 does not follow the actual mass flow. This agrees with theoretical findings in the sense that c_o must be chosen sufficiently small in order to guarantee convergence for this

observer. By reducing the gain to $c_o = -2.3 \cdot 10^{-5}$, also this observer converge for step data 2. However, this magnitude of the observer gain increases the noise of the estimate to a level of which it it completely useless. Observer 1 and 1b shows no noticeable difference for the data sets. The same holds for 3 and 3b. Comparing the reduced order observers and observers for both mass flow and pressure, it can be seen that the observers 3 through 4 yields slightly better accuracy and noise levels. Furthermore, it seems like observer 4 on average gives slightly better accuracy and lower noise levels than observer 3 and 3b. It should be noted that the noise levels represented by the relative error plots are in the range of the noise level related to the mass flow estimate.

Performance of pressure estimates are not represented by these figures, but will be visualized when discussing the surge data. However, these estimates showed good performance for the step data. Their relative error was in the range of $\pm 1\%$ (mostly within $\pm 0.5\%$) of measured value, both in steady state and transient. Furthermore, the noise level of the estimates where reduced by a factor of 0.001 relative to noise on measured signals.

7.3.2 Surge data

The result of surge experiments shown in Figure D.5 through Figure D.11, corresponding to data of Table 7.3 respectively. Analogous to the step data, these figures consists of six rows corresponding to the observers in Table 7.1 respectively. Furthermore, the three columns represent mass flow pressure and pressure relative error. The mass flow estimate is compared with the mass flow approximation from Pitot tube pressures. Since this approximation involves uncertainty, it makes no sense to evaluate the mass flow relative error in this case.

First it can be noted that observer 2 performs poorer than other observers for lower impeller speeds. This is probably due to insufficient magnitude of the observer gain, which is required for this observer. It can also be noted that the reduced order observers are subject to some noise which is not present in the smoother mass flow estimates generated from observer 3 through 4. This is not easily seen by the presented figures, but was established when investigating the figures in MATLAB. For observer 3 through 4 it can be seen that relative pressure error is confined to $\pm 1\%$ of the measured value. Investigating pressure estimate and measured value in detail

reveals that the estimated value is smooth, whereas the measured value is hampered with noise in the same order of magnitude as the relative error. It follows that the noise seen in the plots of relative error is due to the measurement and not the estimate. Removing the noise from these plots, consider a smooth line in the center of the noise, it can be recognized that the pressure estimates oscillate about the actual value with relatively small amplitude. Furthermore, it is noted that these oscillations in general are larger for observer 4 than for 3 and 3b. Finally it is noted that the mass flow estimate generated by observer 1, 1b, 3 through 4 are consistent with respect to amplitude and frequency, and qualitatively in agreement with the approximated mass flow.

Comments regarding pressure estimate and noise levels is illustrated by Figure 7.1, showing a plots of measured and estimated pressure. The left plot shows convergence of the pressure estimate, whereas the right plot shows a surge cycle corresponding to the box in the left plot. It is seen that the estimate poses a much smoother, and nose free, signal than that of the measured.

7.4 Comments

From both step and surge data it can be concluded that observer 2 performs poorly for the gain (7.1). This is especially the case for lower speeds. Step and surge data show consistency with respect to disturbance rejection, in the sense that mass flow estimate generated with observers for both plenum pressure and duct mass flow yields better disturbance rejection than the reduced order observers. Furthermore, pressure estimates are quite good for both disturbance rejection and accuracy. Moreover, observers 3 and 3b seem to perform slightly better than observer 4 when evaluating the estimated pressure.

It is difficult to evaluate the performance of the mass flow estimate in transients. The various observers show consistency in both frequency and amplitude for the estimated mass flow. Also, these estimates show relatively good qualitative agreement with the Pitot tube pressures approximated mass flow. Combining these observations with the accuracy of the pressure estimate and the highly correlated dynamic model for pressure and mass flow, it is believed that the transient performance for mass flow estimates of ob-

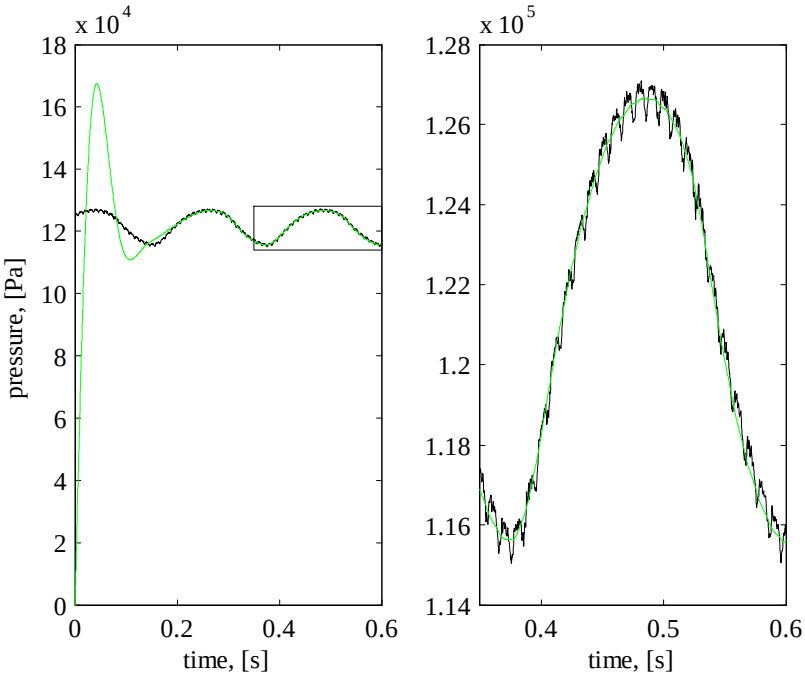

Figure 7.1: Pressures for observer 3b of Table 7.1 applied on surge data 7 of Table 7.3

server 3 and 3b perform reasonably good. However, the step data indicates that mass flow estimate can deviate from the measured with as much as 10%.

Chapter 8

Control validation

8.1 Introduction

This chapter evaluates two of the control laws presented in Chapter 3 on the setup described in Chapter 5 and 6. As pointed out in Chapter 3, an observer for mass flow is needed in order to implement these control laws. Based on the results from Chapter 7, the observer from Proposition 4.3 will be used for this purpose. This observer is implemented with the same gains as used for observer 3b of Table 7.1, from which it is more similar to that of Remark 4.1 than Proposition 4.3. Even though this observer offers estimates of both mass flow and plenum pressure, offering considerable noise rejection for plenum pressure, only the mass flow estimate will be used in the control law.

Figures used for evaluating control laws are found in Appendix E. These figures show various system states, estimated mass flow, actual control input and commanded control input. System states and actual control inputs are shown as solid black lines, whereas commanded control inputs are shown by lighter solid lines.

All plots of torque and speed contain a noise burst appearing with a frequency of approximately 10 seconds. This phenomenon only appears for measurements coming from the drive. Hence, it is believed that this component itself causes these noise burst.

Implementation of the control presented in [19] is reported in [47].

8.2 Speed control

The control law of Proposition 3.3 was implemented with $\alpha\left(\bar{w}_c, \bar{p}_p, w_i\right) = c_s$, resulting in

$$\omega = -c_s \bar{w}_c + sat\left(w_i\right) + \omega^e \tag{8.1}$$

$$\dot{w}_i = -c_i \bar{w}_c \tag{8.2}$$

It follows from (2.16) and the related discussion that choosing the positive constant c_a sufficiently large ensures asymptotic stability of the desired equilibrium. Based on relative orders of magnitude for ω and ω_c, the stabilizing control gain was chosen as $c_s = -4 \cdot 10^4$. Furthermore, the integrator gain was chosen as $c_i = 5 \cdot 10^4$ and a saturation of ± 4000 for the integrator term was set. Note that the stabilizing gain has opposite sign of that derived in theory. During experiments it turned out that a positive valued stabilizing gain resulted in instability. This was the case for some regions of the open loop stable as well as for the open loop unstable region. For the open loop stable region, equilibrium points became unstable when approaching the surge line. Furthermore, a higher gain resulted in an earlier encounter with instability when approaching surge line. For the open loop unstable regime, any positive valued c_s resulted in instability.

The first experiment, presented in Figure E.1, aims at illustrating the effect of integral control. To this end, the controller is provided with incorrect equilibrium information. More specifically, $w_c^e = 0.09$ and $N^e = 12000$ is used for $A_{t\%} = 70$. This can be regarded as an incorrect feed forward value, since the given value of mass flow equilibrium corresponds to $N^e = 20000$ for the throttle opening in question. Figure E.1 shows a scenario for which the integrator term in (8.1) is initially turned off. Then the integrator is turned on after approximately 10 seconds, before being turned back off after approximately 25 seconds. Equilibrium values to the controller are shown by dash dotted lines. Steady state error can be recognized from the figure when the integrator is turned off, whereas mass flow converges to the desired equilibrium in presence of the integrator.

The remaining of this section will evaluate active surge control for operating points on $N = 15000$. It is therefore interesting to establish for which throttle opening the system enters surge on this speed line. Figure E.2 shows that valve openings of $A_{t\%} = 56$ and below corresponds to open loop unstable operating points for which surge will occur. This point was found by

throttling down at constant speed until reaching audible surge. The capture shown in Figure E.2 was started when the valve opening had settled at the given throttle value, and no audible surge was identified until some time into the recording. However, from the figure it can be seen that surge is present throughout the entire time series. It starts out with relatively low amplitudes, going into amplitudes of negative mass flow. The audible surge experienced in the laboratory is therefore probably deep surge.

Figure E.3 to Figure E.6 show active surge control for a selection of throttle openings. As discussed in Chapter 2 it is a challenge to find corresponding equilibrium points for this region of the compressor map. This was solved for the experiments in question by setting $N^e = 15000$ for (8.1), and then tune w^e until N was approximately 15000 (or equivalently $w_i \approx 0$). Figure E.3 shows active surge control for $A_{t\%} = 52$. The amplitudes for the uncontrolled case are in the range of that in Figure E.2. Active surge control reduces the amplitude of oscillations for this operating point, but is unable to completely remove surge cycles. The same comments can be made for operating points $A_{t\%} = 53$ and $A_{t\%} = 54$, shown in Figure E.4 and Figure E.5 respectively. However, it should be noted that amplitudes decreases considerably with increasing valve opening. Figure E.6 shows that surge is stabilized for $A_{t\%} = 56$, being the throttle opening for which deep surge was first encountered at this speed line.

Figure E.7 shows that the controller is able to take the system out of surge. This figure shows a scenario in which the stem is initially operated at constant speed for $A_{t\%} = 56$. The control law is activated after approximately 11 seconds, resulting in system stated converging to the desired value. Figure E.8 shows a same type scenario for $A_{t\%} = 54$, where the control law is turned on and off. Initially the control is on. Then it is turned off after approximately 10 seconds, before being turned back on after approximately 18 seconds. It can be recognized that the control reduces amplitudes of the surge cycle considerably. The controlled case results in mild surge, whereas the uncontrolled case constitutes deep surge. Note that amplitudes for the controlled case in Figure E.8 is larger than that presented in Figure E.5, even though the throttle opening is the same. This can be explained from the way in which these operating points are reached. Data represented in Figure E.3 through Figure E.5 are results of throttling in step wise from $A_{t\%} = 56$ with the control law active, and no deep surge cycles are encountered during the transition into the throttle opening in question. Data presented in Figure

E.8, on the other hand, is a result of turning on and off the controller (also prior to the time series presented). Hence, the control tries to recover from deep surge in this case rather than stable operation or mild surge.

8.3 Torque control

The control law

$$\tau_d = -c_1 \left(\bar{\omega} + c_2 \bar{w}_c\right) - c_2 \frac{JA_c}{L_c'} \left(p_c\left(t\right) - p_p\right) + \tau_d^e \tag{8.3}$$

of Proposition 3.3 was implemented to evaluate torque control, where the time argument indicates that a measurement was used rather than a model. This was chosen, among many possibilities offered by Chapter 3.3, due to its simplicity. Furthermore, simulations indicate that this implementation works just as well as control laws of Proposition 3.2. In fact, it was shown in [29] that the control law of Proposition 3.3 performs better than control laws of Proposition 3.2 in terms of convergence, even for relatively small values of c_1.

Several of the experimental data for torque control is carried out for impeller speeds in the vicinity of $N = 20000$, which is a considerably higher speed than that associated with speed control. It follows from Figure 3.1 that this higher speed is more challenging to stabilize in terms of the requirements related to (3.93), when mass flows as low as the intersection of low and high speeds in this figure will not be reached.

Figure E.9 through Figure E.12 presents experimental data for $c_1 = 10^{-6}$ and c_2 in the order of 10^3, which practically means that

$$\begin{aligned} \tau_d &= -c_1 \left(\bar{\omega} + c_2 \bar{w}_c\right) - c_2 \frac{JA_c}{L_c'} \left(p_c\left(t\right) - p_p\right) + \tau_d^e \\ &\approx -c_2 \frac{JA_c}{L_c'} \left(p_c\left(t\right) - p_p\right) + \tau_d^e. \end{aligned} \tag{8.4}$$

This allows for a convenient way of reaching the desired speed or mass flow for a given throttle opening, even when equilibrium values are uncertain. Increasing τ_d^e will increase impeller speed as well as mass flow, and reducing τ_d^e will reduce speed and mass flow. This can be seen from Figure 2.5 and the related discussion.

In contrast to speed control, saturation of the control action had to be implemented for torque control. This was needed in order to keep torque and power within allowable ranges for the drive system, especially for situation in which the controller tried to recover from surge. The explanation for this can be found in the term $c_2 \frac{JA_c}{L_c'} (p_c(t) - p_p)$ of (8.4). In surge, $p_c(t) - p_p \neq 0$, the large order of magnitudes for pressures resulted in large amplitudes for this term relative to reasonable/available control inputs τ_d. Pressures are in order of 10^5 and available torques are in order of 10^0. Furthermore, the constant $c_2 \frac{JA_c}{L_c'}$ was not small enough as to reduce the amplitude of pressures to those of torques in this application.

Audible surge was first encountered at $A_{t\%} = 57$ for $N = 20000$. Figure E.9 shows active surge control of this operating point, where the system is initially operating at constant speed. After approximately 3 second the control is turned on, resulting in stabilization of the desired equilibrium. The control is turned off again after approximately 7 seconds, and the system enters surge. Finally the control is turned back on after approximately 15 seconds, and the desired equilibrium is again stabilized. Actuator saturation was set at $\tau_{d,\max} = 3\ Nm$ and the stabilizing gain was chosen as $c_2 = 10^3$ for this experiment. Close inspection reveals that the control saturates once or twice in taking the system out of surge. Figure E.10 and Figure E.11 shows a similar scenario for $A_{t\%} = 55$ and $A_{t\%} = 53$ respectively. The stabilizing gain used for these experiments was chosen as $c_2 = 3 \cdot 10^3$, and the saturation was set to $\tau_{d,\max} = 3\ Nm$ and $\tau_{d,\max} = 4\ Nm$ respectively. From Figure E.10 it can be recognized that this control saturates during the entire stabilization period, whereas the control in Figure E.11 only saturates once or twice when taking the system out of surge.

The experiment shown in Figure E.12 differs from previous in the way the equilibrium was reached. In this scenario the control was activated at $N = 10000$ and $A_{t\%} = 50$, with a stabilizing gain of $c_2 = 2 \cdot 10^3$. Then τ_d^e was increased step wise to investigate which speeds that could be reached before going into surge. Impeller speed of approximately $N = 18000$ was reached before audible surge occurred. Plots shown in Figure E.12 does not report this result, but shows stable operation at $N = 15000$ for the valve opening in question. Control was turned off after approximately 16 seconds, and it is seen that the constant speed resulted in surge. Furthermore, the controller was unable to take the system out of surge when turning it back on after at approximately 18 seconds. It can be recognized that commanded

control more or less bounces between its saturations of zero and $\tau_{d,\max} = 2$.

Figure E.13 and Figure E.14 uses (8.1) for the same operating points as in experiments of Figure E.10 and Figure E.11 respectively, with $c_1 = 2 \cdot 10^{-3}$ and c_2 as previously. The term $-c_1 (\bar{\omega} + c_2 \bar{w}_c)$ is now a considerable contributor for the control. Furthermore, equilibrium values for w_c^e, ω^e and τ_d^e are taken equal to those of the corresponding previously stabilized equilibriums. Figure E.13 shows that this control is able of taking the system in and out of surge. However, steady state errors can be recognized for the controlled part of the time series. From Figure E.14 it can be seen the equilibrium can be stabilized. However, the controller is not able to recover from surge at constant speed.

Figure 8.1 shows the last 10 seconds of the same data as Figure E.11 in a compressor map. These are experimental data for $A_{t\%} = 53$ and $N = 20000$, where the controller takes the system out of surge. Experimental data are plotted using plenum pressure measurement and estimated mass flow. As can be seen from the figure, experimental data does not settle at the theoretically expected equilibrium, being the intersection of throttle and constant speed line. Furthermore, there is a difference between data equilibrium and the actual equilibrium reached. This can be explained by inaccuracy of mass flow estimate, when the actual equilibrium is found using mass flow measurement for steady state and data equilibrium uses the mass flow estimate. As can be seen from the figure, pressures are equal whereas mass flow differs for these equilibria. This is in accordance to discussions of Chapter 7, showing steady state deviation of measured and estimated mass flow. The deviation of actual and theoretical equilibrium can be explained by model inaccuracy.

8.4 Comments

Experiments of speed control required a stabilizing control gain of opposite sign compared to that expected from theory. Recall that speed control assumed the internal speed control loop of drive and electric motor was so fast as it appear to take on the reference speed instantaneously, relative to dynamics of mass flow and pressure. Violation of this assumption is believed to be the most likely explanation for inconsistency with theory. Comparing experiment of Figure E.12 with those of Figure E.1 through Figure E.8

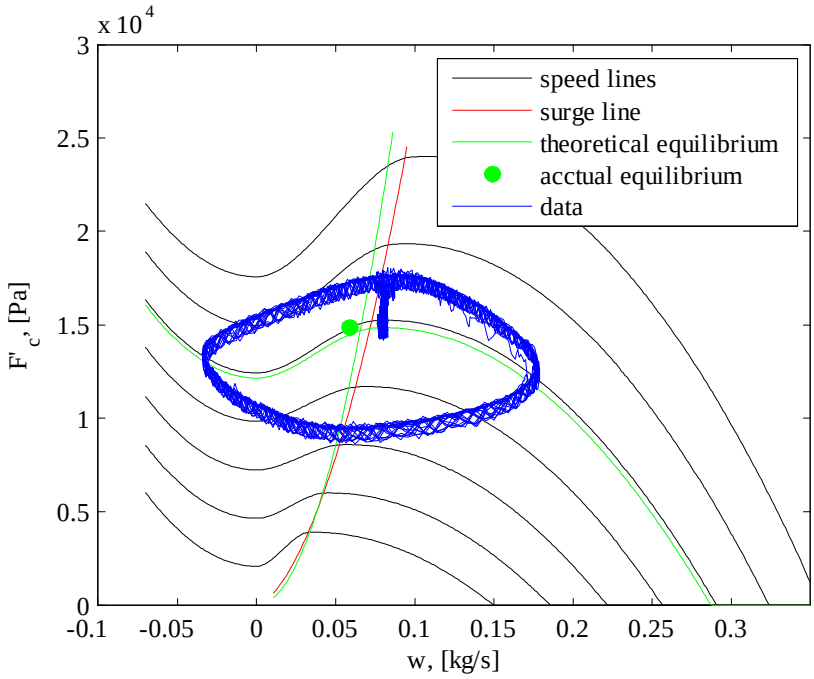

Figure 8.1: Stabilization of surge presented in a compressor map

suggests that torque control works better than speed control. Furthermore, torque control agrees better with theory than speed control.

As pointed out several times throughout the thesis, finding corresponding equilibrium points for this system is challenging. The effect of this can be seen when comparing the experiments of Figure E.10 and Figure E.11 with those of Figure E.13 and Figure E.14. The first two experiments, not using equilibrium values, were able to stabilize the desired equilibrium as well as taking it in and out of surge. When implementing with equilibrium values, on the other hand, experiments showed steady state error and for the first case and not being able to take system out of surge in the second case.

When implementing (8.4) it was noted that τ_d^e had to be chosen considerably higher than that of measured torque, but still within the same order of magnitude. Furthermore, a higher τ_d^e was required when increasing c_2. This indicates that the term $c_2 \frac{JA_c}{L_c'} \left(p_c\left(t\right) - p_p\right)$ takes on a positive value, or

in other words

$$p_c > p_p \tag{8.5}$$

in steady state. This can be explained by related to (6.18), (6.21) and (6.23), concluding that the downstream compressor forcing term, F_{cd}, could be ignored. However, from the lower left plot of Figure 6.3 it can be recognized that this terms takes on negative values (relatively small compared with other forcing terms). The steady state relation $p_c = p_p - F_{cd}$ of (6.18) then explains (8.5).

It is common in compressor literature to evaluate the active surge controllers by the reduction in mass flow that can be achieved for a constant speed line, relative the mass flow for which surge occurs. For this purpose, the measured mass flow at steady state is used. Two impeller speeds, $N = 15000$ and $N = 20000$, has been investigated for active surge control. For $N = 15000$ the throttle opening $A_{t\%} = 56$ resulted in surge after having operating in mild surge for some time. For the controlled case, the mass flow for this operating point was found as $w = 0.053\ kg/s$. Speed control was not able to significantly decrease this mass flow. For torque control, however, the throttle could be reduced to $A_{t\%} = 50$. Mass flow for this operating point was $0.042\ kg/s$. This implies that a relative reduction of more than 20 percent, since surge is encountered at a higher valve opening than $A_{t\%} = 56$. For $N = 20000$ deep surge was encountered at $A_{t\%} = 57$, implying that surge occurs for a somewhat higher valve opening. Mass flow for the controlled case of $A_{t\%} = 57$ was $w = 0.07\ kg/s$. Torque control was able to stabilize $A_{t\%} = 53$ at $N = 20000$, for which the mass flow was $w = 0.059\ kg/s$. This implies that a relative reduction of more than 15 percent was achieved for this speed line.

Chapter 9

Further work

It was shown in Chapter 7 that the mass flow estimates are subject to some steady state error. One approach to improve on this error might be to tune observers differently. One could e.g. investigate if using the gain K_2 of (4.5) would improve the mass flow estimate of Proposition 4.3 and/or Proposition 4.4. Alternatively one could investigate if the use of full order observers, including also impeller speed, could improve the steady state deviation.

An other approach to improve observers is to use the measurement $p_c(t)$ more actively. The observers of Chapter 4 use this measurement to cancel or copy dynamics only. One could consider this signal used to compare correctness of estimated states, e.g. as linear injection terms $k\left(p_c\left(\hat{w}_c, \omega\right) - p_c\left(t\right)\right)$ or $k\left(p_c\left(\hat{w}_c, \hat{\omega}\right) - p_c\left(t\right)\right)$, in order to improve observer performance. This approach is, however, not easily implemented using the system structure and properties of the observer in Chapter 4.2. An Extended Kalman Filter (EKF), on the other hand, gives the opportunity and framework to follow this approach. However, some preliminary studies indicated that the EKF did not significantly improve steady state performance of the mass flow estimate. Furthermore, this approach is dependent on an accurate model for p_c to guarantee that $\hat{w}_c = w_c$ implies $p_c\left(\hat{w}_c, \omega\right) - p_c\left(t\right) = 0$.

Yet another approach to improve mass flow estimate, which is believed to be the most promising, is to model the mass flow sensor with a dynamic equation. One could e.g. consider

$$\begin{aligned} \dot{x}_{w_{c,m}} &= f_{w_c}\left(t, x_{w_{c,m}}\right) \\ w_{c,m} &= h_{w_c}\left(t, x_{w_{c,m}}\right) \end{aligned}$$

where $w_{c,m}$ represents the actual measurement of some sensor, and incorporate this dynamic relation in the observer. This will give a framework in which the mass flow estimate can be compared with the actual mass flow.

It was shown in Chapter 8 that speed control, for the current setup, works in the open loop stable region and at the surge line. The control law (8.1) offers convergence to a desired mass flow equilibrium, also in presence of an incorrect value for the impeller speed equilibrium. In view of discussions for mass flow estimate steady state deviation and the use of this state in feedback, the system converges to a state for which the estimated mass flow equals the desired equilibrium. Hence, the actual mass flow for which the system converges to can deviate somewhat from that of the desired mass flow. Speed control results are based on experimental results rather than theory. The reason for this is that the stabilizing gain for this controller had to be implemented with opposite sign of what was expected from theory. Torque control, on the other hand, works as expected from theory and was able to extend the operating range of the machine considerably. It is believed that torque control works better than speed control since the internal loop drive and electric motor is much faster for torque than for speed. This fact is supported by the manufacturer of the drive. When deriving control laws, the drive system loop was ignored and it was assumed that this acted instantaneously to a reference signal. Hence, a relatively slow drive system loop violates this assumption.

To improve speed control one can consider extending the model by

$$\begin{aligned} \dot{x}_\omega &= f_\omega\left(t, x_\omega, \omega_r\right) \\ \omega &= h_\omega\left(t, x_\omega, \omega_r\right), \end{aligned}$$

where ω is impeller speed and ω_r is a reference signal fed to the drive, in order to capture dynamics of drive and motor loop. This will alter the dynamic dimension and structure for the dynamic model used to derive speed control, and new analysis and control synthesis must be performed. However, this approach will eliminate the assumption and requirement of a fast actuator dynamic. The same approach can be used to model dynamic effects of the actuator torque control loop, in an attempt to improve results for this scheme.

Only the very simplest structure of the torque control scheme was experimentally validated. Further work on this scheme should therefore start with experimental testing of more complex structures for control algorithms,

such as using the passive part for integral effect, models for compressor load torque, nonlinear damping and adaptive schemes. Adaptive schemes are especially interesting when implementing models for load torque, since Chapter 6 revealed that there is some uncertainty related to the friction parameter k_f of (2.7). Furthermore, the effect discussed for (8.5) indicates that the controller should be implemented with integral effect. However, before implementing more sophisticated schemes it is believed that especially one issue needs some further attention. This is, as commented upon several times throughout the thesis, the problem of corresponding equilibriums. The most critical variable in this respect is believed to be $\bar{\omega} - c_2\bar{w}_c$, since this is used as input to the passive control part as well as appearing repeatedly in nonlinear damping and adaptive control schemes.

The performance of speed and torque measurements provided by the drive turned out to be rather poor during transients. This was noticed during active surge control, when audible speed and torque changes were not reflected by measurements. Speed measurement is required by torque control and observers implementing $p_c\left(\hat{w}_c, \omega\left(t\right)\right)$. Furthermore, observers incorporating speed dynamics assume access to both speed and torque measurements. The assumption of instantaneous torque control for the drive system loop indicates that observers can be implemented with torque commanded by the control algorithm, but this is an ideal case and the observer should preferably be implemented with a measurement of drive toque. Since speed measurements are cheap and easy to install, it is highly recommended to install such a transmitter in the laboratory setup.

An un-modeled effect not taken into account in theory is that of backlash and flexibility of the gear stage. The supercharger internal gear consists of cog wheels, whereas the external gear uses driving belt. It is believed that the effect of these was observed when trying to stabilize surge for very low mass flow, far below that of reported in Chapter 8. In some of these experiments an audible high frequency component, much higher than that of the surge frequency, was observed for the drive system. Since these effect where encountered for relatively small throttle opening compared to those of which surge could be stabilized, it is considered a more important task to widen the stable operating range of the system before these effects are further pursued.

Appendix A

Physics

A.1 Conservation Laws

The material presented here is taken from [15] and [45], adopting the notation used in [15].

A.1.1 Integral form

Consider a control volume $V_c(t)$ with a surface $\partial V_c(t)$. Let $\vec{v}_c(t)$ be the velocity of the surface at some specified point, with $\vec{n}$ being normal vector of dA pointing outwards at this location. The integral balance laws are then given by

$$\begin{aligned}
\frac{d}{dt}\int_{V_c(t)} \rho dV &= -\int_{\partial V_c(t)} \rho\left((\vec{v}-\vec{v}_c)\cdot\vec{n}\right) dA \\
\frac{d}{dt}\int_{V_c(t)} \rho\vec{v} dV &= \sum \vec{F} - \int_{\partial V_c(t)} \rho\vec{v}\left((\vec{v}-\vec{v}_c)\cdot\vec{n}\right) dA \\
\frac{d}{dt}\int_{V_c(t)} \rho\left(\vec{r}\times\vec{v}\right) dV &= \sum \vec{N}_0 - \int_{\partial V_c(t)} \rho\left(\vec{r}\times\vec{v}\right)\left((\vec{v}-\vec{v}_c)\cdot\vec{n}\right) dA \\
\frac{d}{dt}\int_{V_c(t)} e\rho dV &= \dot{Q} + \dot{W}_s + \dot{W}_p + \dot{W}_\nu - \int_{\partial V_c(t)} e\rho\left((\vec{v}-\vec{v}_c)\cdot\vec{n}\right) dA
\end{aligned}$$

where $\vec{v}$ is the fluid velocity, ρ is the fluid density, $\vec{F}$ is the a force acting on the system, $\vec{r}$ is a distance, M_0 a moment about a point 0, e is the specific energy (per unit mass), $\dot{Q}$ is heat into the volume, $\dot{W}_s$ is shaft work, $\dot{W}_p$ is

pressure work, $\dot{W}_\nu$ is viscous stress work (in interaction with control surface), specific internal energy. Furthermore, the relations

$$\begin{aligned}
\vec{F}_{pressure} &= \int_{\partial V_c(t)} -p\vec{n}dA \\
\vec{F}_{body} &= \int_{V_c(t)} \rho\vec{f}dV \\
\vec{N}_0 &= \left(\vec{r}\times\vec{F}\right)_0 \\
\dot{Q} &= -\int_{\partial V_c(t)} \vec{j}_Q\cdot\vec{n}dA \\
\dot{W}_p &= -\int_{\partial V_c(t)} p\left(\vec{v}\cdot\vec{n}\right)dA \\
\dot{W}_\nu &= \int_{\partial V_c(t)} \vec{v}\cdot\left(\vec{n}\cdot\vec{\tau}\right)dA
\end{aligned}$$

For a fixed control volume, the derivative can be moved inside the volume integral $\frac{d}{dt}\left(\int_{V_c(t)}\phi dV\right) = \int_{V_c}\frac{\partial\phi}{\partial t}dV$.

A.1.2 Differential form

In local form the balance equations are given by

$$\begin{aligned}
\frac{D\rho}{Dt} &= -\rho\vec{\nabla}\cdot\vec{v} \\
\rho\frac{D\vec{v}}{Dt} &= -\vec{\nabla}p+\rho\vec{f}+\vec{\nabla}\cdot\vec{\tau} \\
\rho\frac{Du}{Dt} &= -p\vec{\nabla}\cdot\vec{v}+\vec{\tau}:\vec{\nabla}\vec{v}-\vec{\nabla}\cdot\vec{j}_Q
\end{aligned}$$

where $\frac{D(\cdot)}{Dt} = \frac{\partial(\cdot)}{\partial t}+\vec{v}\cdot\vec{\nabla}(\cdot)$, $\vec{\tau}$ is the viscous stress tensor, $\vec{j}_Q$ is the heat flux into the volume and $\vec{\tau}:\vec{\nabla}\vec{v} = \vec{\nabla}\cdot(\vec{\tau}\cdot\vec{v})-\vec{v}\cdot\vec{\nabla}\cdot\vec{\tau}$. From Fourier's law we have that $\vec{j}_Q = -\alpha\vec{\nabla}(\rho c_p T)$, where α is the thermal diffusivity. For a Newtonian fluid the viscous stress tensor is given by

$$\vec{\tau} = \lambda\left(\vec{\nabla}\cdot\vec{v}\right)\vec{I}+2\mu\vec{E}$$

where λ and μ are the Lame coefficients, and $\vec{E}$ is the rate of strain tensor.

A.1.3 Local form

In local form the balance equations are given by

$$\begin{aligned} \frac{D\rho}{Dt} &= -\rho\vec{\nabla}\cdot\vec{v} \\ \rho\frac{D\vec{v}}{Dt} &= -\vec{\nabla}p + \rho\vec{f} + \vec{\nabla}\cdot\vec{\tau} \\ \rho\frac{Du}{Dt} &= -p\vec{\nabla}\cdot\vec{v} + \vec{\tau} : \vec{\nabla}\vec{v} - \vec{\nabla}\cdot\vec{j}_Q \end{aligned}$$

where $\frac{D(\cdot)}{Dt} = \frac{\partial(\cdot)}{\partial t} + \vec{v}\cdot\vec{\nabla}(\cdot)$, $\vec{\tau}$ is the viscous stress tensor, $\vec{j}_Q$ is the heat flux into the volume and $\vec{\tau} : \vec{\nabla}\vec{v} = \vec{\nabla}\cdot(\vec{\tau}\cdot\vec{v}) - \vec{v}\cdot\vec{\nabla}\cdot\vec{\tau}$. From Fourier's law we have that $\vec{j}_Q = -\alpha\vec{\nabla}(\rho c_p T)$, where α is the thermal diffusivity. For a Newtonian fluid the viscous stress tensor is given by

$$\vec{\tau} = \lambda\left(\vec{\nabla}\cdot\vec{v}\right)\vec{I} + 2\mu\vec{E}$$

where λ and μ are the Lame coefficients, and $\vec{E}$ is the rate of strain tensor.

A.2 Type of flow

A.2.1 Incompressible flow

The flow is said to be incompressible if density is constant in time and space,

$$\frac{D\rho}{Dt} = 0.$$

From the local form of the mass conservation it can be seen that this implies

$$\vec{\nabla}\cdot\vec{v} = 0.$$

A commonly accepted criterion for this summation is relatively low fluid speed, $Ma \leq 0.3$.

A.2.2 Inviscid flow

The flow is said to be inviscid if it is frictionless. This implies that the stress tensor is zero,

$$\vec{\tau} = 0.$$

A.2.3 One dimensional

One dimensional flow can be defined as fluid with only one velocity component flowing along some path of given cross-section. Moreover, the intensive properties are assumed to be uniform over the cross section at any point along the path. This implies that three dimensional volume integrals collapses to scalars with $dV = A(\xi)\, d\xi$, where ξ parameterize the path.

A.3 Thermodynamics

The material here is taken from [48] and [15].

A.3.1 Thermodynamic property data

Properties are macroscopic characteristics of a system such as mass, volume, energy, pressure and temperature, to which numerical values can be assigned at a given time without knowledge of the history of the system. Enthalpy is defined on mass basis as

$$h = u + p\rho^{-1}$$

where u is specific internal energy, p is pressure and ρ is density. The SI unit for h and u is $[J/kgK]$

The specific heats c_v and c_p for pure simple compressible substances are intensive properties defined by

$$\begin{aligned} c_v &= \left.\frac{\partial u(T,\rho)}{\partial T}\right|_{\rho} \\ c_p &= \left.\frac{\partial h(T,p)}{\partial T}\right|_{p} \end{aligned}$$

where the subscripts denotes which parameter that are hold fixed during differentiation. For the specific heats we have $c_p > c_v$. The SI units for c_v and c_p are $[J/kgK]$ for mass basis. The specific heat ratio is defined as

$$k = \frac{c_p}{c_v}$$

and is simply a dimensionless number.

A.3.2 p-v-T relation for gases

The universal gas constant is defined as $\bar{R} = 8.314\,[kJ/kmol \cdot K]$, whereas the gas constant for a specific gas is defined by

$$R = \frac{\bar{R}}{M}$$

where M is the molecular weight. For air $M = 28.99\,[kg/kmol]$. The compressibility factor is defined as

$$Z = \frac{p}{\rho RT}$$

A.3.3 Ideal gas model

The ideal gas low is when the compressibility factor is assumed unity, which gives $pV = mRTorp = \rho RT$. Any gas that satisfying the equation $p = \rho RT$, has specific internal energy function which is only variable in temperature, T. This gives the following for internal energy and enthalpy for an ideal gas $u(T, v) = u(T)$ and $h(u, p, v) = h(T) = u(T) + RT$. The preceding properties are summarized as the ideal gas model

$$\begin{aligned} pv &= \rho RT \\ u(T, \rho) &= u(T) \\ h(u, p, \rho) &= h(T) = u(T) + RT \end{aligned}$$

From the definition of specific heats and the fact that u and h are functions of temperature only for an ideal gas, we have the relationships $du(T) = c_v(T)\,dT$ and $dh(T) = c_p(T)\,dT$. This leads to the equations

$$\begin{aligned} u(T_2) - u(T_1) &= \int_{T_1}^{T_2} c_v(T)\,dT \\ h(T_2) - h(T_1) &= \int_{T_1}^{T_2} c_p(T)\,dT \end{aligned}$$

giving the relation of two different system states. Furthermore, we have

$$\begin{aligned} c_p(T) &= c_v(T) + R \\ c_p(T) &= \frac{k(T)}{k(T) - 1} R \\ c_v(T) &= \frac{1}{k(T) - 1} R \end{aligned}$$

where $k > 1$ since $c_p > c_v$. The foregoing expressions require the specific heats as function of temperature. These relations are available as graphs, tables and equations.

Appendix B

Calculations

B.1 Circle criterion observer

B.1.1 Error dynamics

Let

$$\begin{aligned} e &= x - \hat{x} \\ v &= Hx \\ w &= H\hat{x} + K_2 (C\hat{x} - y) \\ z &= v - w \\ \psi(t, z) &= \gamma(v) - \gamma(w) = \gamma(v(t)) - \gamma(v(t) - z) \end{aligned}$$

where time dependence is expressed explicitly to indicate which signals are regarded as time signals. The error dynamics is found as

$$\begin{aligned} \dot{e} &= (A + K_1 C) e + G\psi(t, z) \\ z &= (H + K_2 C) e \end{aligned}$$

which can be reformulated

$$\begin{aligned} \dot{e} &= A_e e + B_e \psi(t, z) \\ z &= C_e e \end{aligned}$$

by defining $A_e = (A + K_1 C)$, $B_e = G$ and $C_e = (H + K_2 C)$.

B.1.2 Lyapunov analysis

Consider the function

$$V(e) = e^T P e$$

where $P = P^T > 0$. The time derivative of V along the solution of the error system is given by

$$\begin{aligned}
\dot{V}(t,e) &= 2e^T P A_e e + 2e^T P B_e \psi(t,z) \\
&= 2e^T P A_e e + 2e^T P B_e \psi(t,z) + e^T Q_1 e + 2z^T Q_2 \psi(t,z) \\
&\quad -e^T Q_1 e - 2z^T Q_2 \psi(t,z) \\
&= 2e^T P A_e e + e^T Q_1 e + 2e^T \left(P B_e + C_e^T Q_2\right) \psi(t,z) \\
&\quad -e^T Q_1 e - 2z^T Q_2 \psi(t,z) \\
&= e^T \left(A_e^T P + P A_e + Q_1\right) e + 2e^T \left(P B_e + C_e^T Q_2\right) \psi(t,z) \\
&\quad -e^T Q_1 e - 2z^T Q_2 \psi(t,z) \\
&= \begin{bmatrix} e \\ \psi(t,z) \end{bmatrix}^T \begin{bmatrix} A_e^T P + P A_e + Q_1 & P B_e + C_e^T Q_2 \\ B_e^T P + Q_2 C_e & 0 \end{bmatrix} \begin{bmatrix} e \\ \psi(t,z) \end{bmatrix} \\
&\quad -2e^T Q_1 e - 2z^T Q_2 \psi(t,z)
\end{aligned}$$

where $Q_1 = Q_1^T$ and $Q_2 = Q_2^T$. By requiring

$$\begin{bmatrix} A_e^T P + P A_e + Q_1 & P B_e + C_e^T Q_2 \\ B_e^T P + Q_2 C_e & 0 \end{bmatrix} \leq 0$$

the time derivative of V is upper bounded by

$$\dot{V}(t,e) \leq -2e^T Q_1 e - 2z^T Q_2 \psi(t,z).$$

Appendix C

Figures for model validation

C.1 Steady state data

C.1.1 Pressures

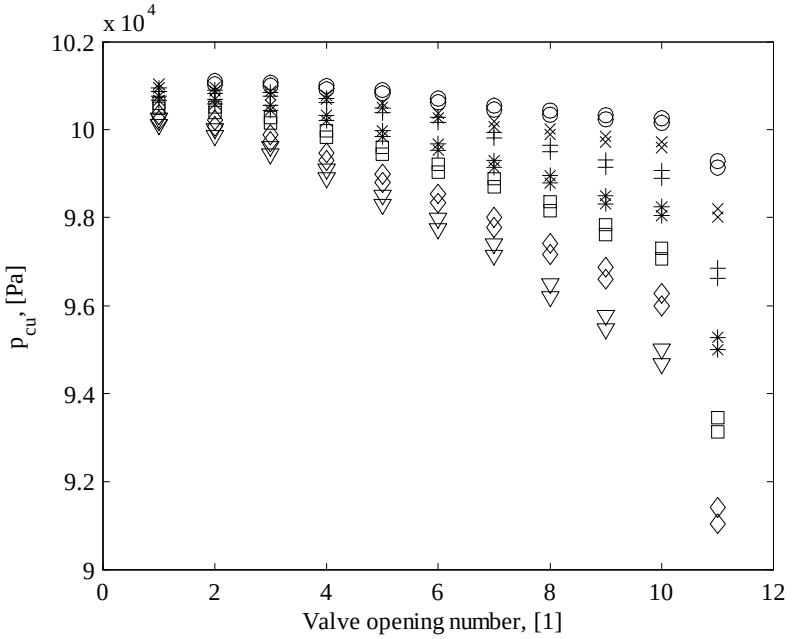

Figure C.1: Compressor upstream pressure

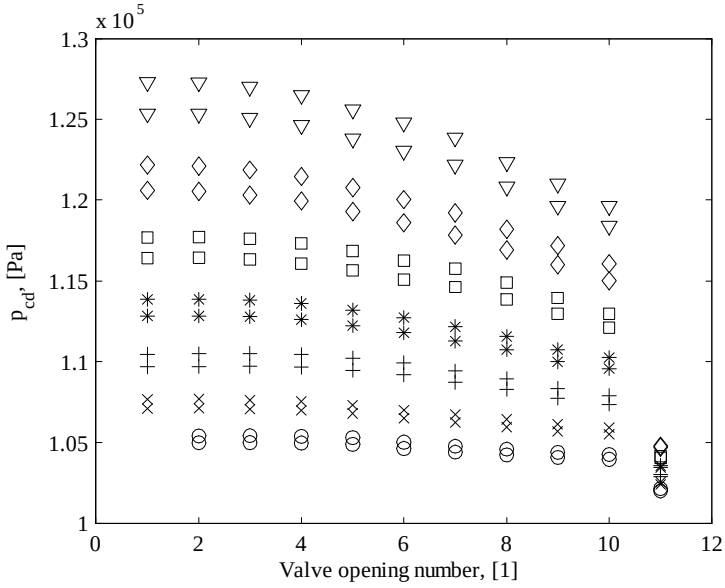

Figure C.2: Compressor downstream pressure

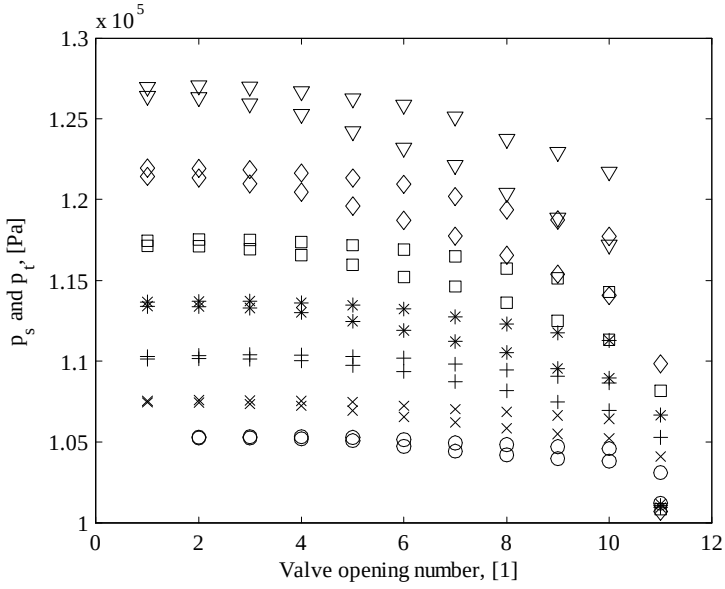

Figure C.3: Pitot tube pressures

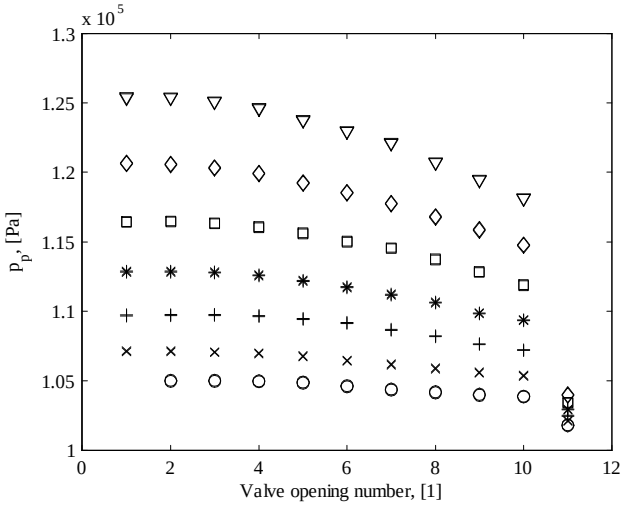

Figure C.4: Plenum pressure

C.1.2 Temperatures

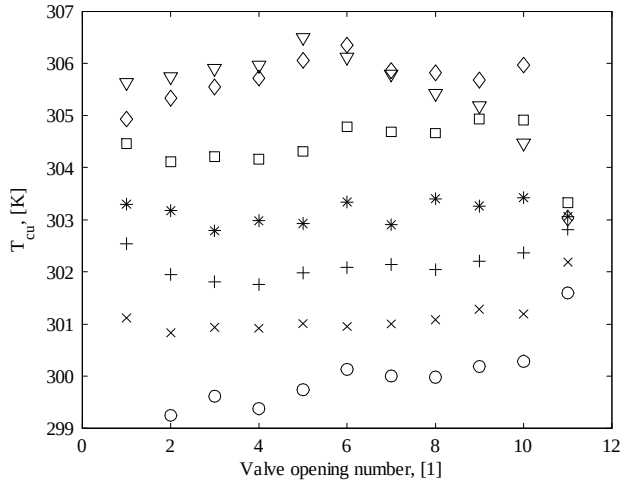

Figure C.5: Compressor upstream temperature

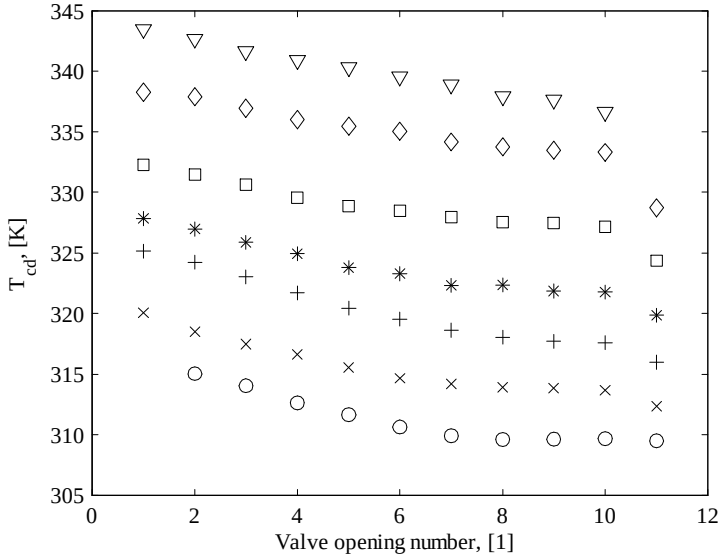

Figure C.6: Compressor downstream temperature

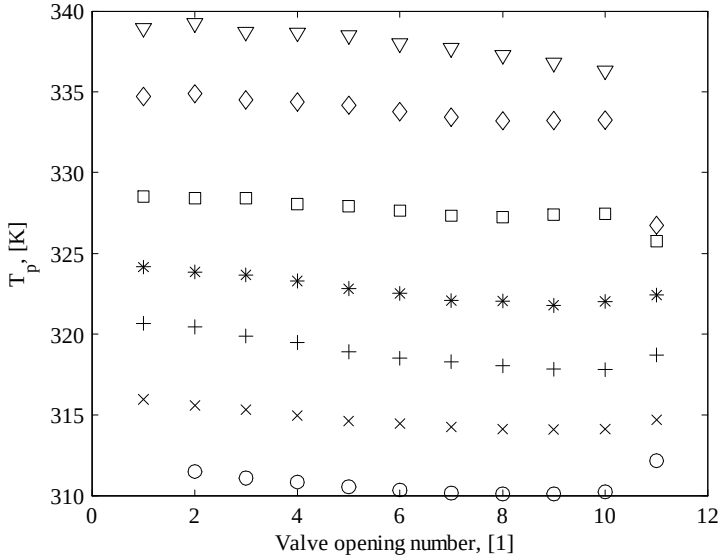

Figure C.7: Plenum temperature

C.1.3 Mass flow

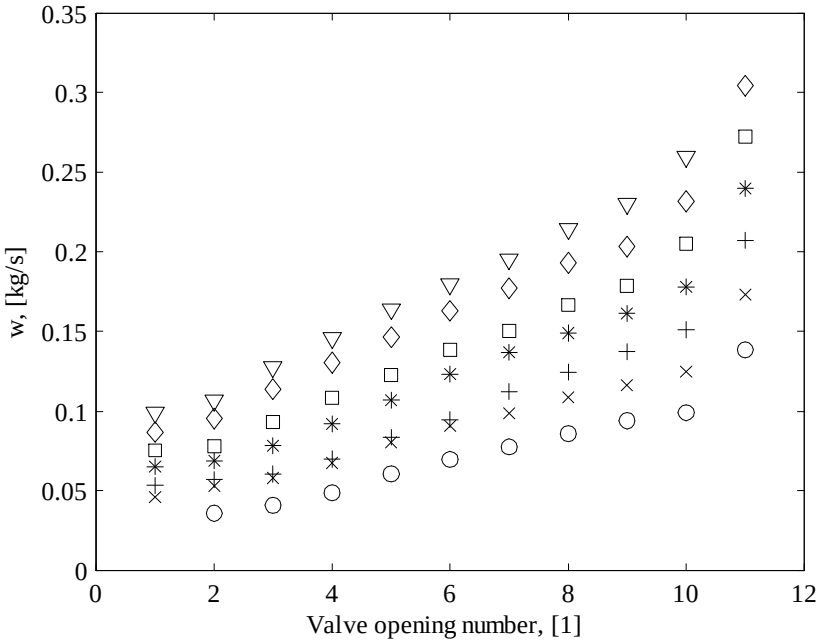

Figure C.8: Compressor downstream mass flow

C.2 Transient data

C.2.1 Pressure and mass flow from step in torque

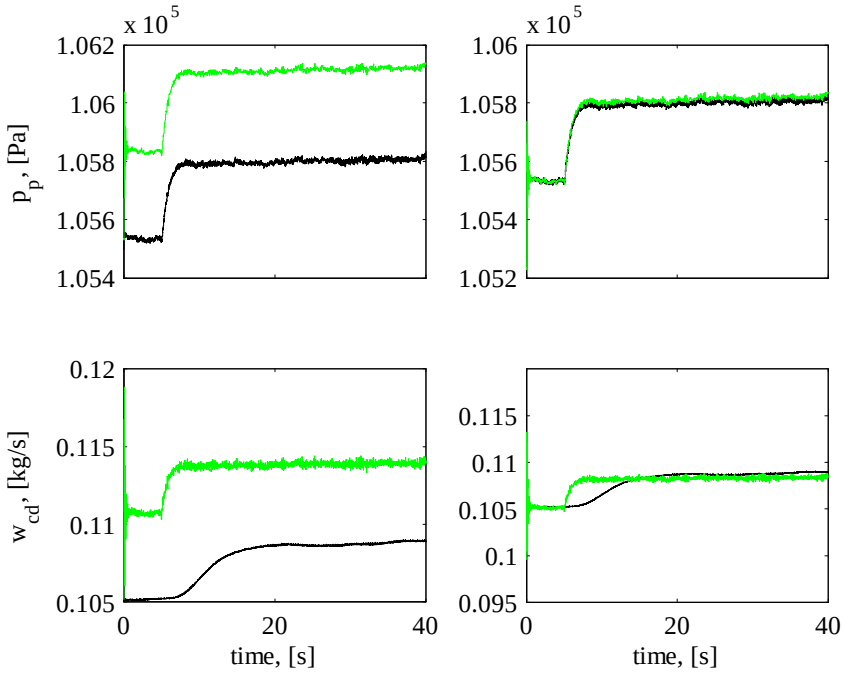

Figure C.9: Step 1 of Table 6.2

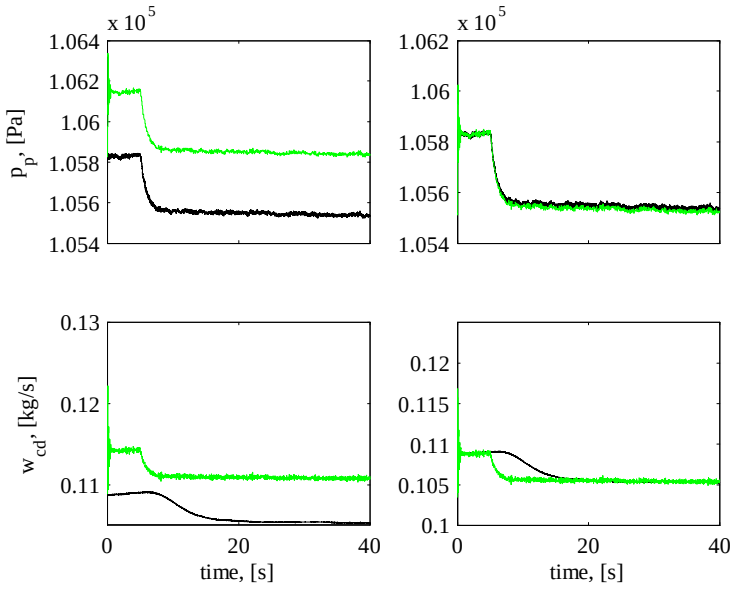

Figure C.10: Step 2 of Table 6.2

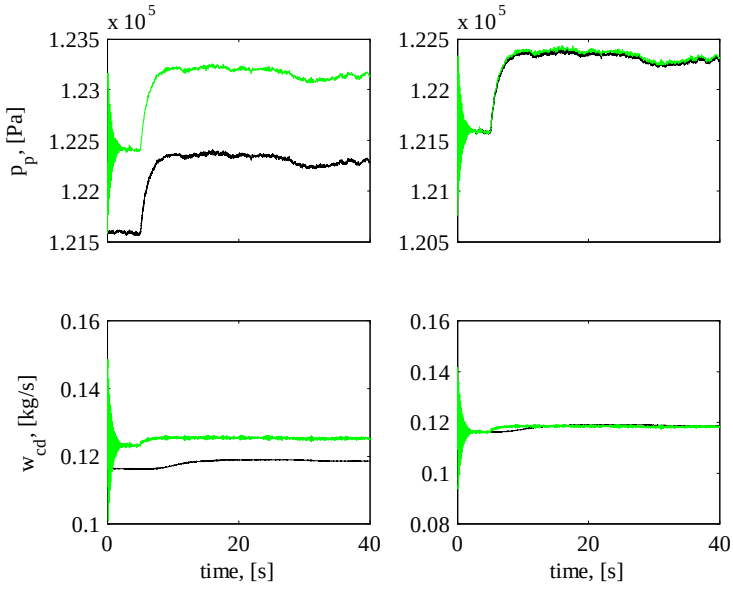

Figure C.11: Step 3 of Table 6.2

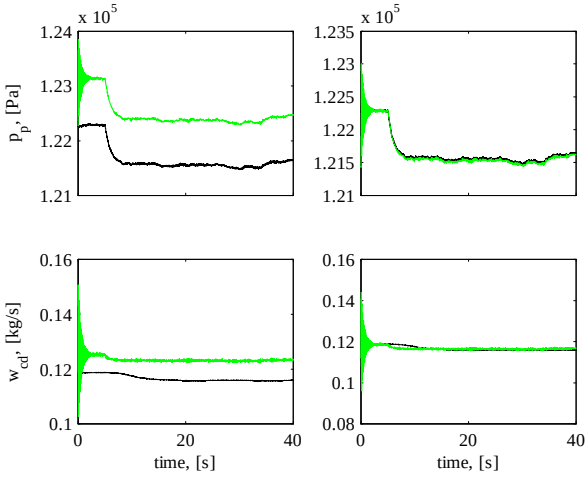

Figure C.12: Step 4 of Table 6.2

C.2.2 Pressure and mass flow from constant speed surge

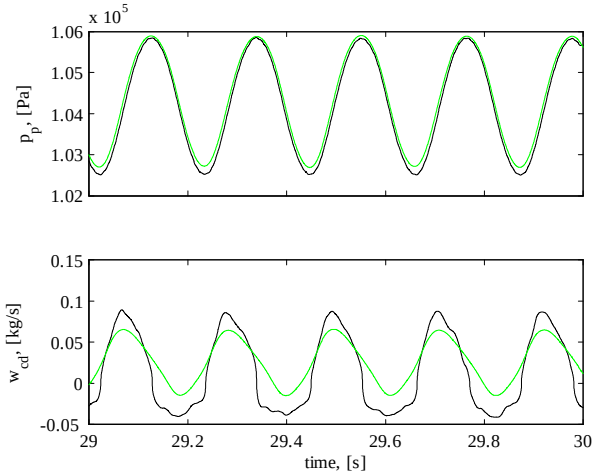

Figure C.13: $N = 10300[rpm]$

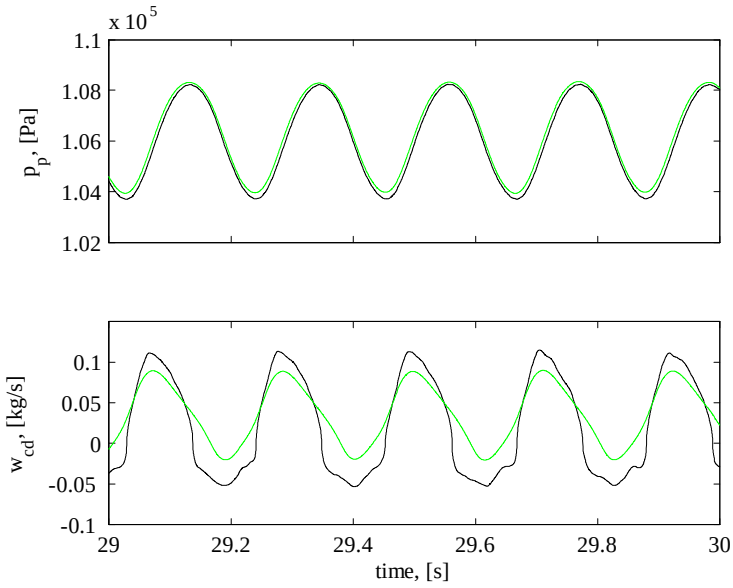

Figure C.14: $N = 12800[rpm]$

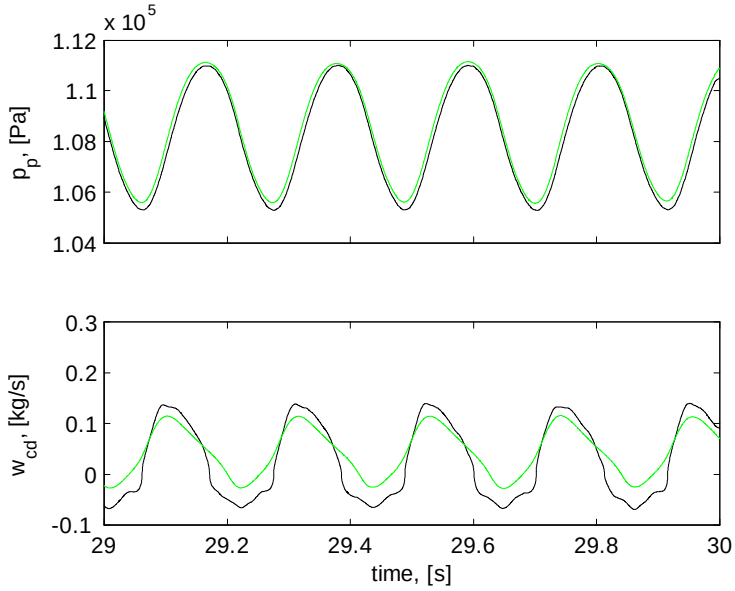

Figure C.15: $N = 15300[rpm]$

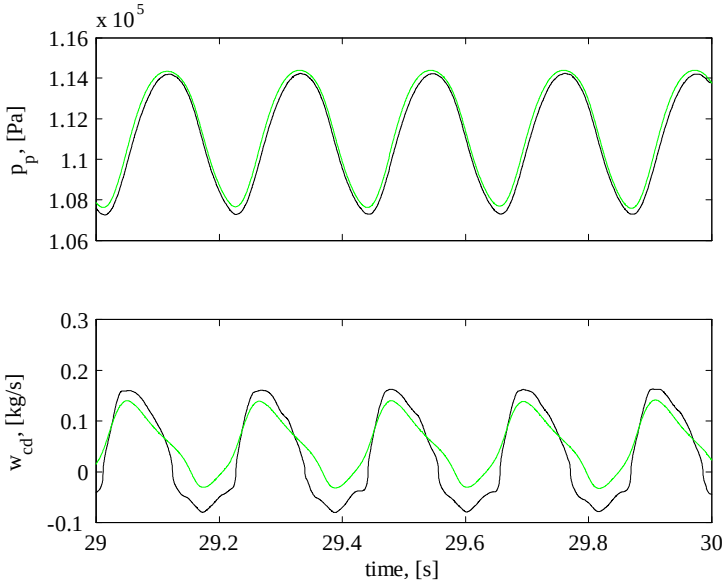

Figure C.16: $N = 17900[rpm]$

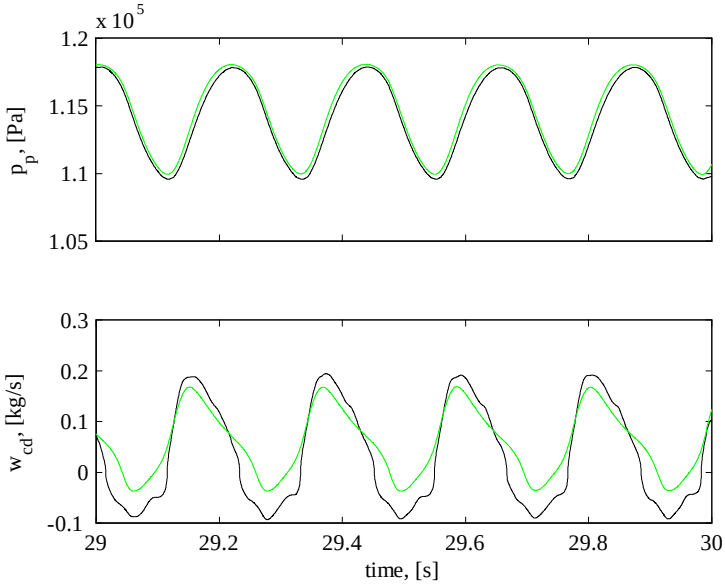

Figure C.17: $N = 20400[rpm]$

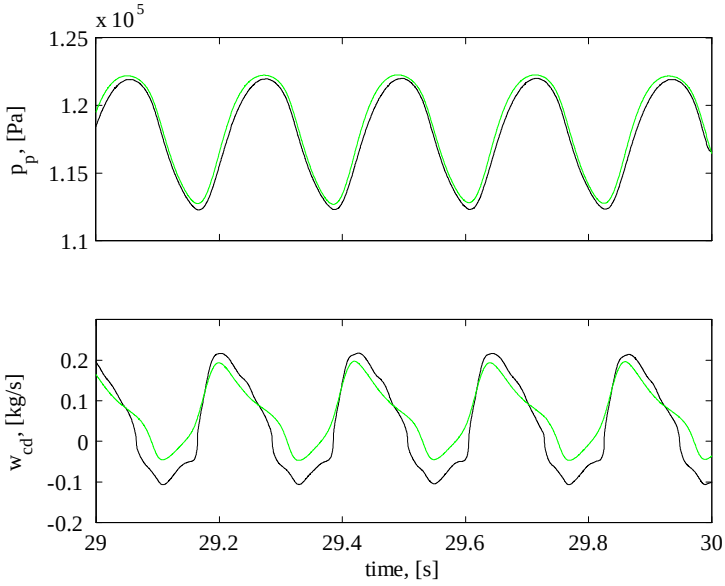

Figure C.18: $N = 22900[rpm]$

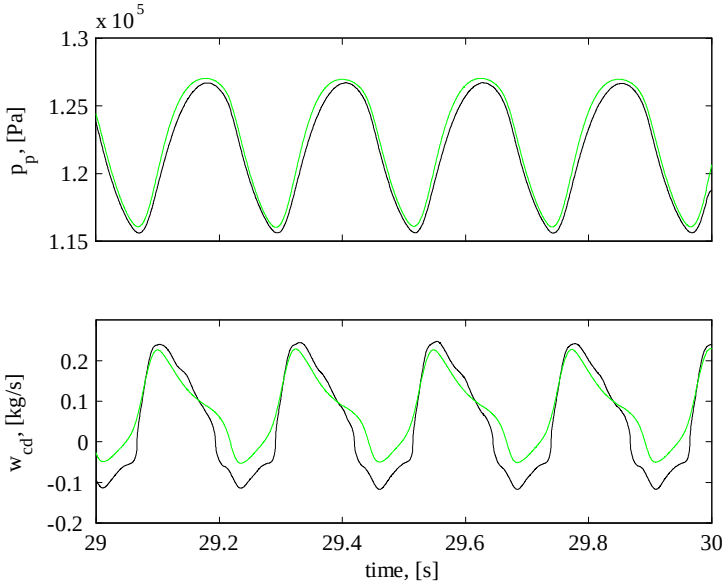

Figure C.19: $N = 25400[rpm]$

C.2.3 Compressor characteristic from constant speed surge

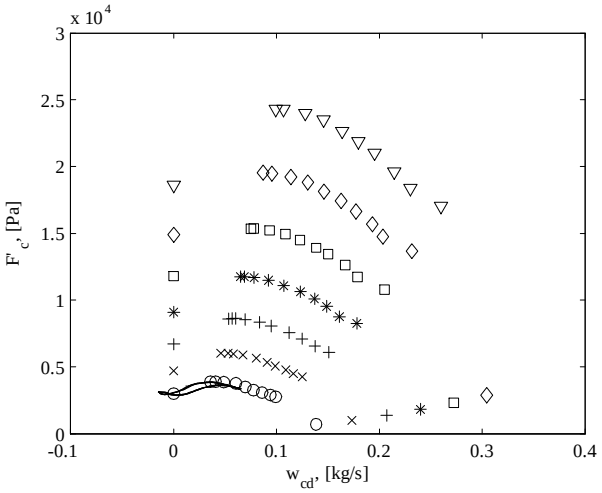

Figure C.20: $N = 10300[rpm]$

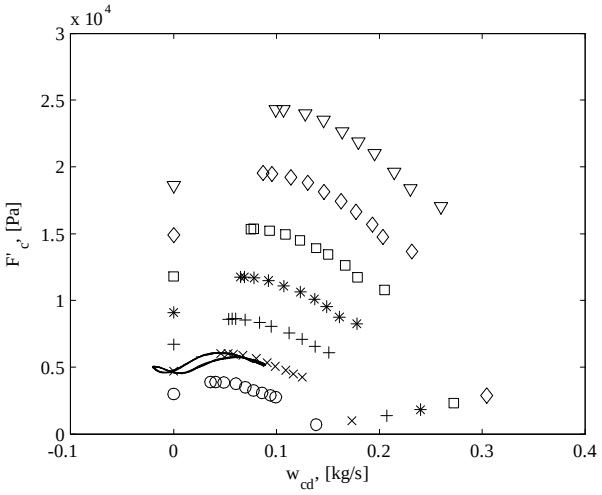

Figure C.21: $N = 12800[rpm]$

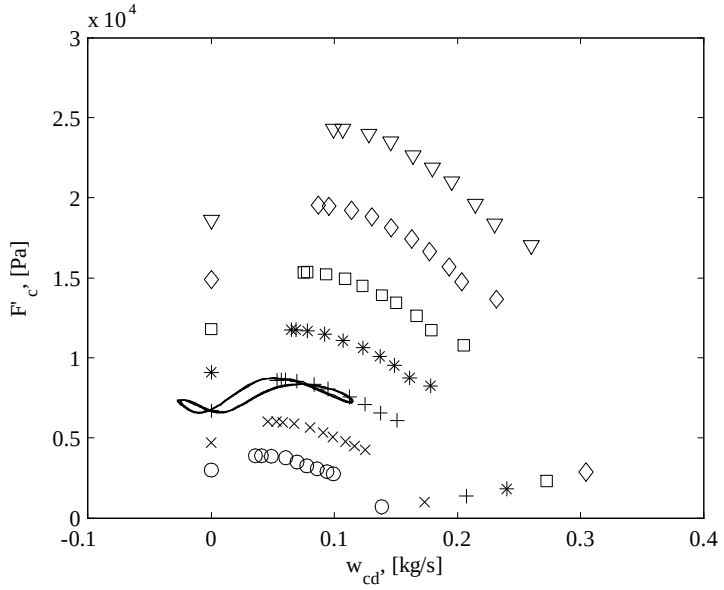

Figure C.22: $N = 15300[rpm]$

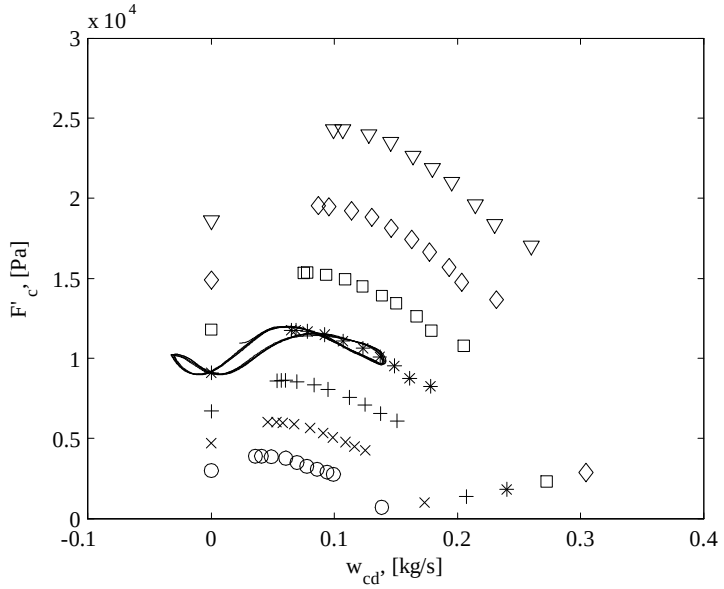

Figure C.23: $N = 17900[rpm]$

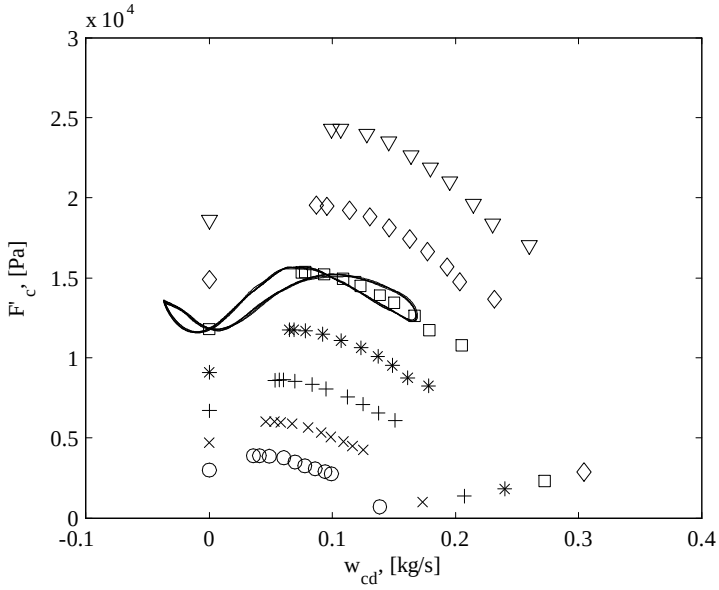

Figure C.24: $N = 20400[rpm]$

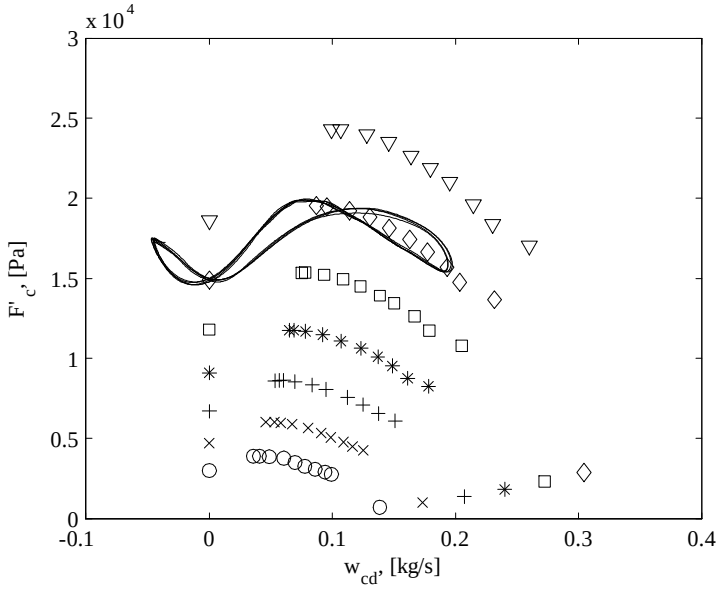

Figure C.25: $N = 22900[rpm]$

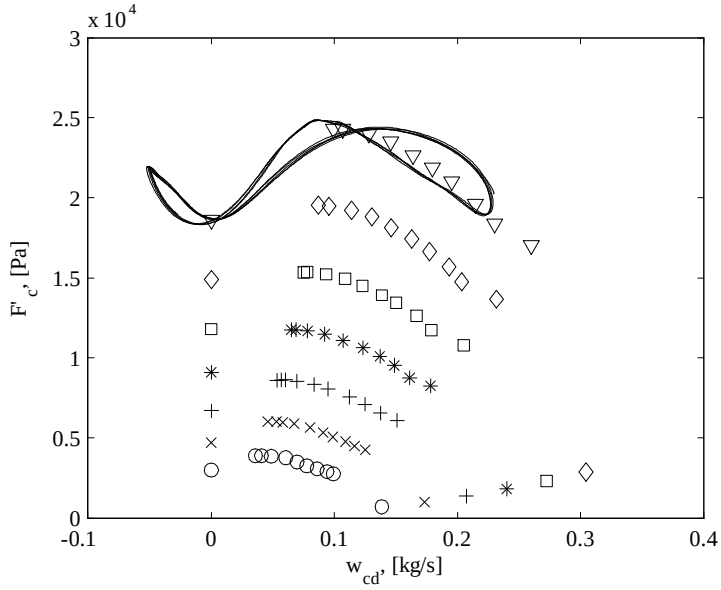

Figure C.26: $N = 25400[rpm]$

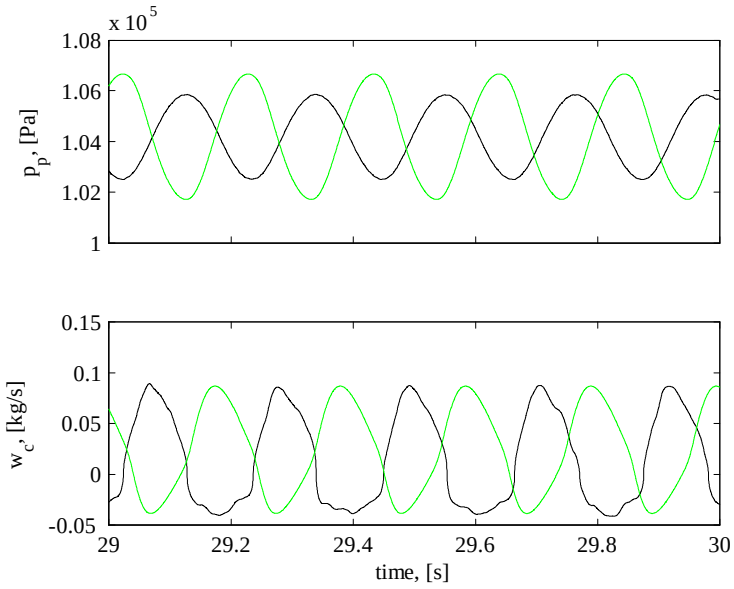

Figure C.27: $N = 10300[rpm]$

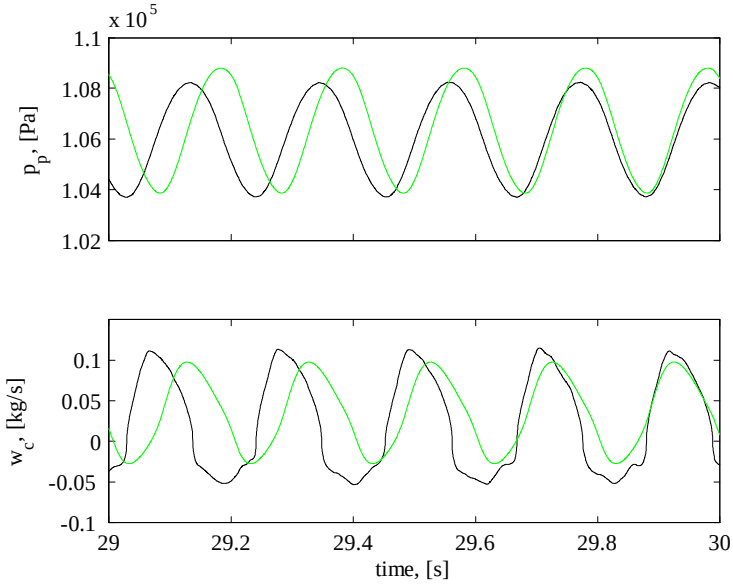

Figure C.28: $N = 12800[rpm]$

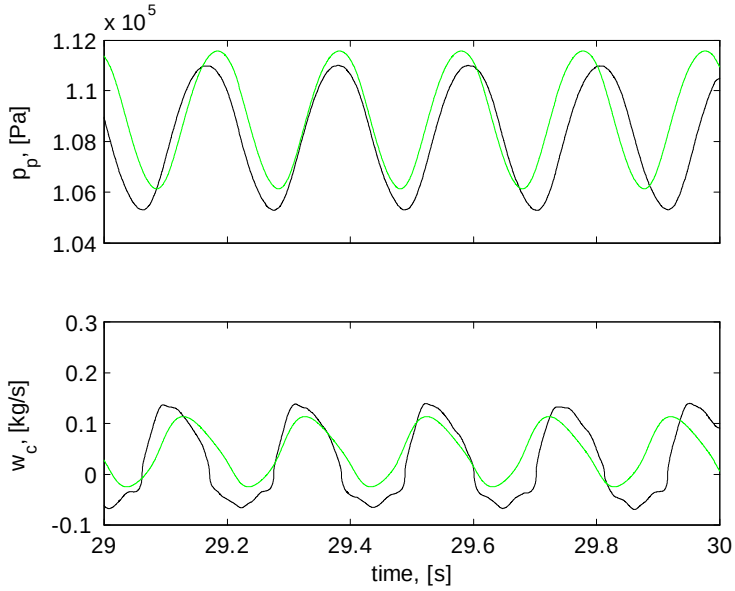

Figure C.29: $N = 15300[rpm]$

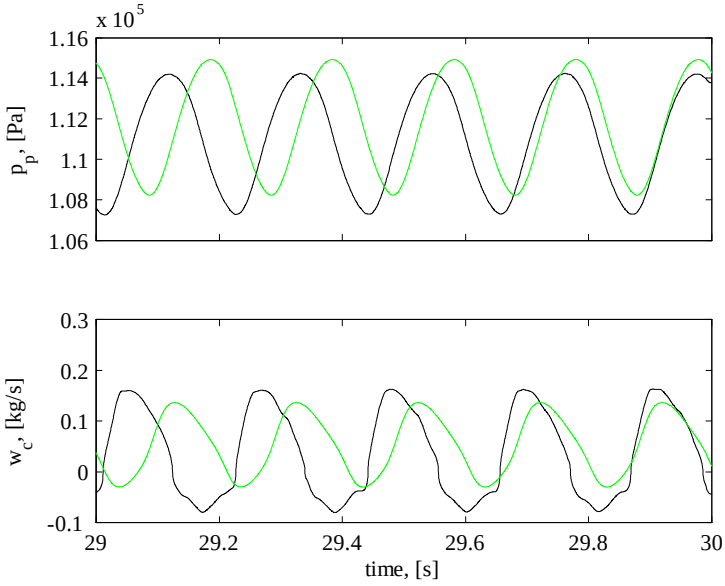

Figure C.30: $N = 17900[rpm]$

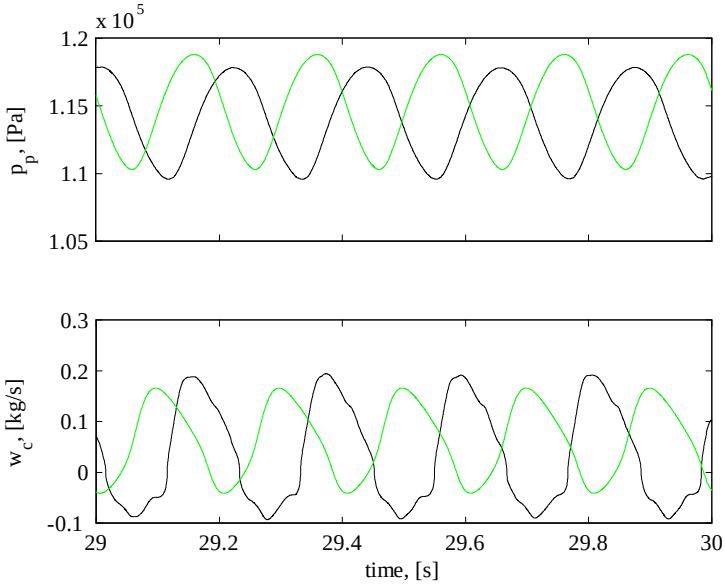

Figure C.31: $N = 20400[rpm]$

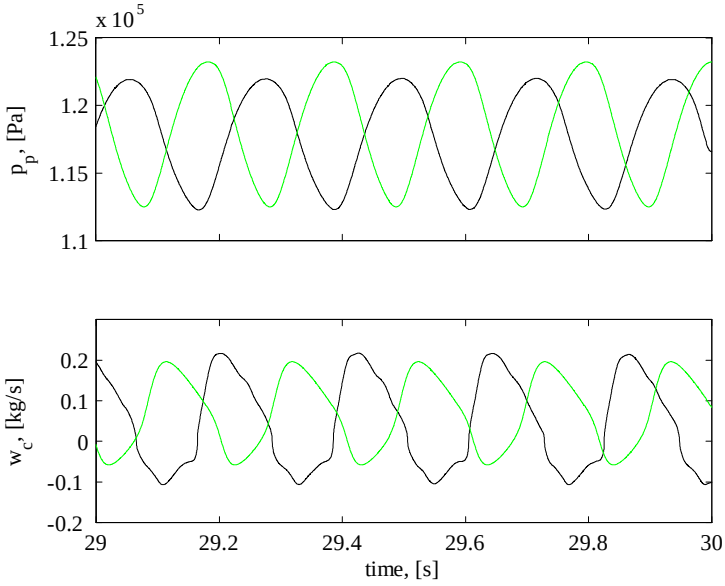

Figure C.32: $N = 22900[rpm]$

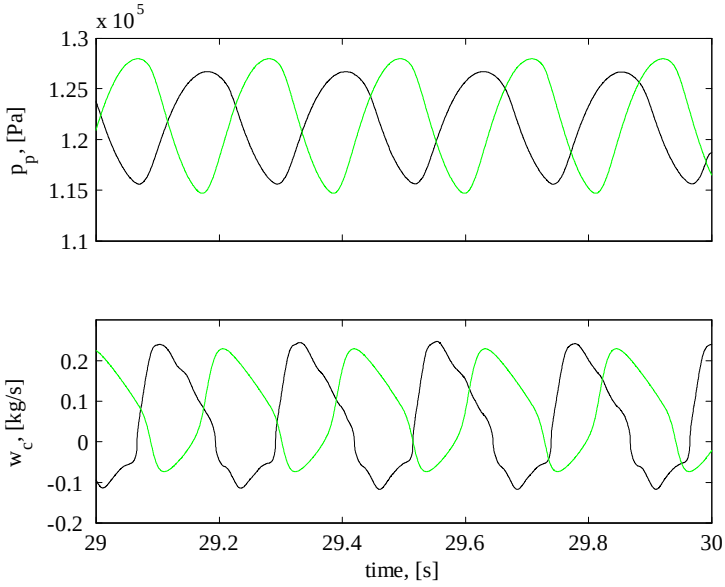

Figure C.33: $N = 25400[rpm]$

C.2.4 Speed transients to step in torque

Measured mass flow

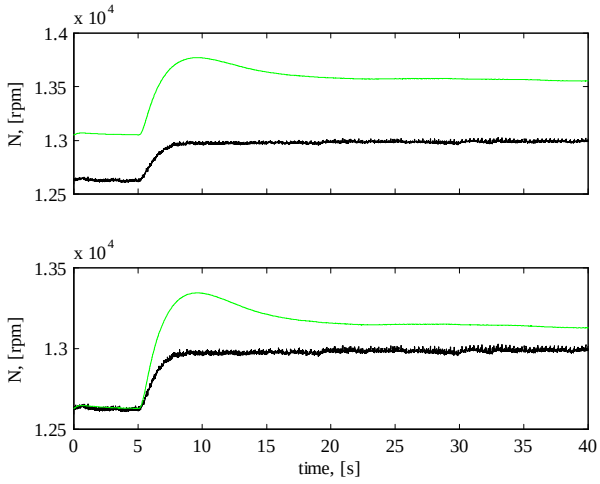

Figure C.34: Step 1 of Table 6.2

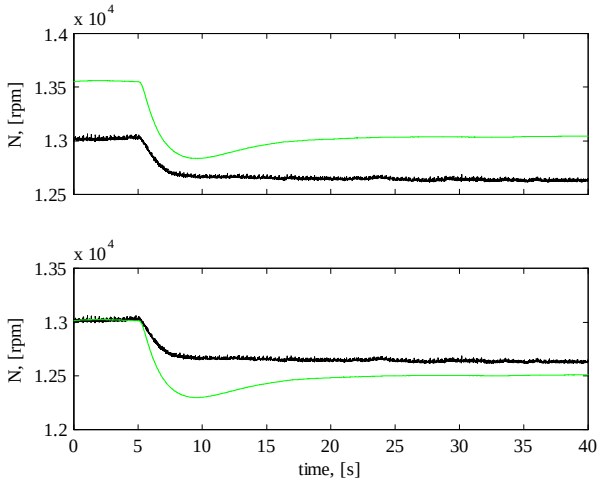

Figure C.35: Step 2 of Table 6.2

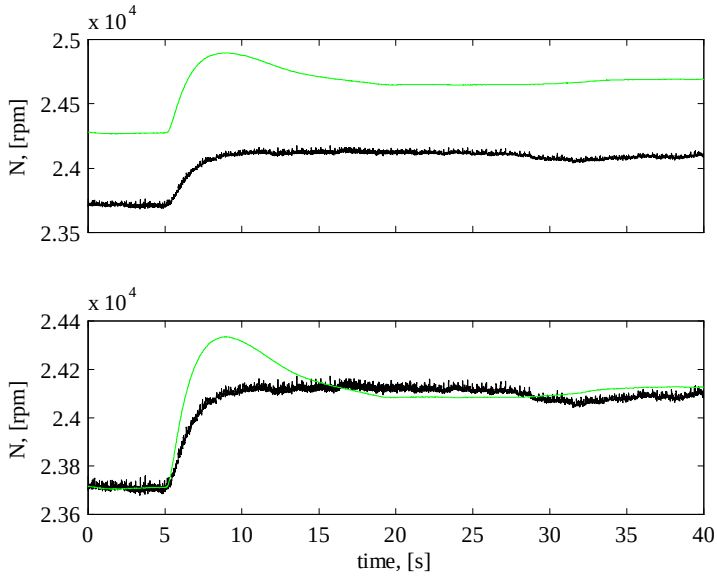

Figure C.36: Step 3 of Table 6.2

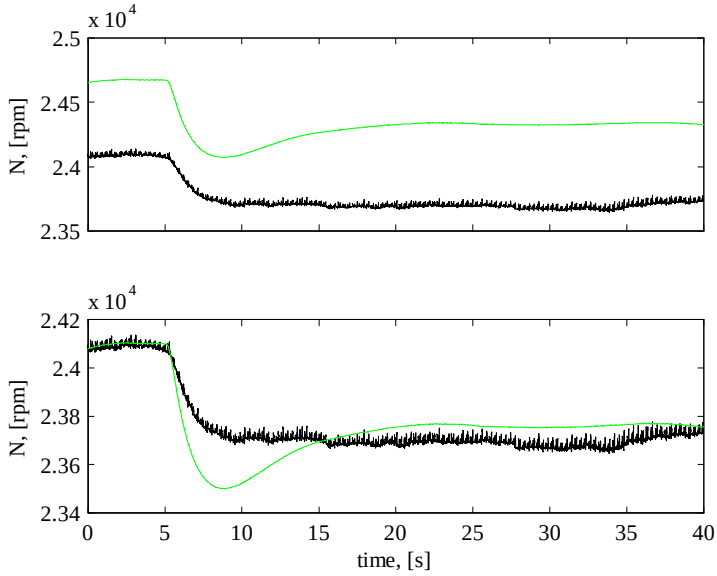

Figure C.37: Step 4 of Table 6.2

Averaged mass flow

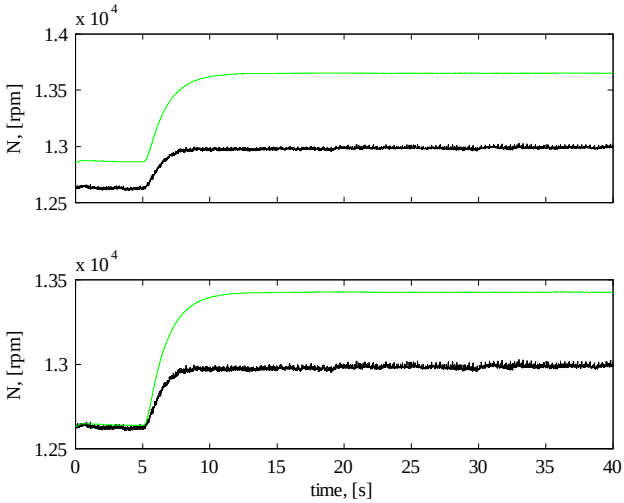

Figure C.38: Step 1 of Table 6.2

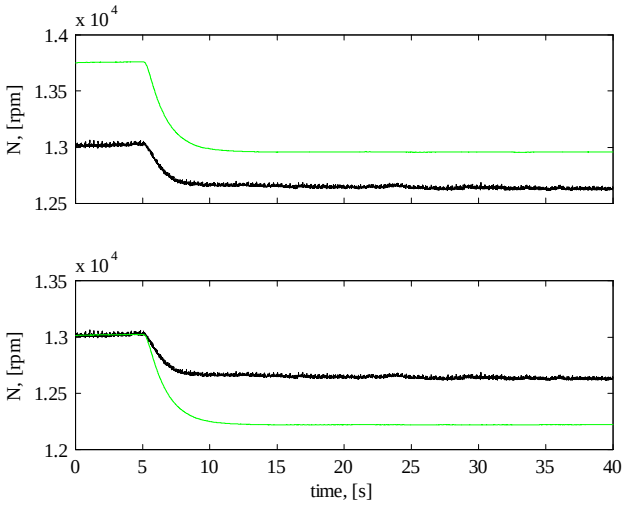

Figure C.39: Step 2 of Table 6.2

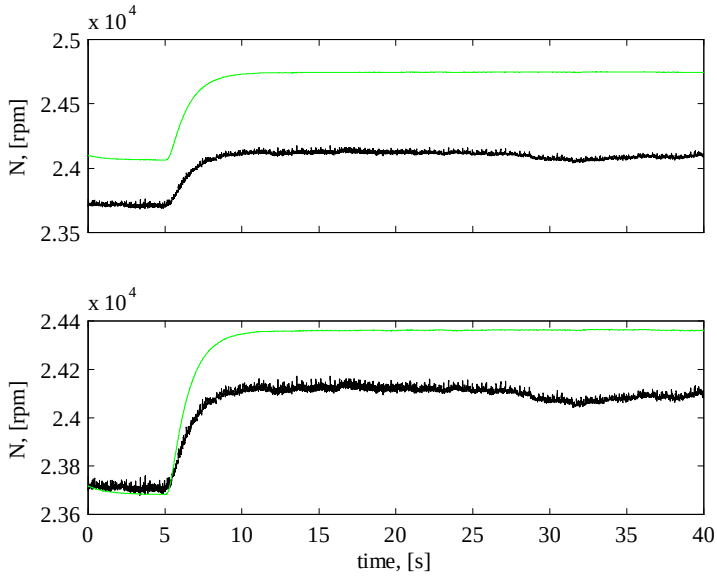

Figure C.40: Step 3 of Table 6.2

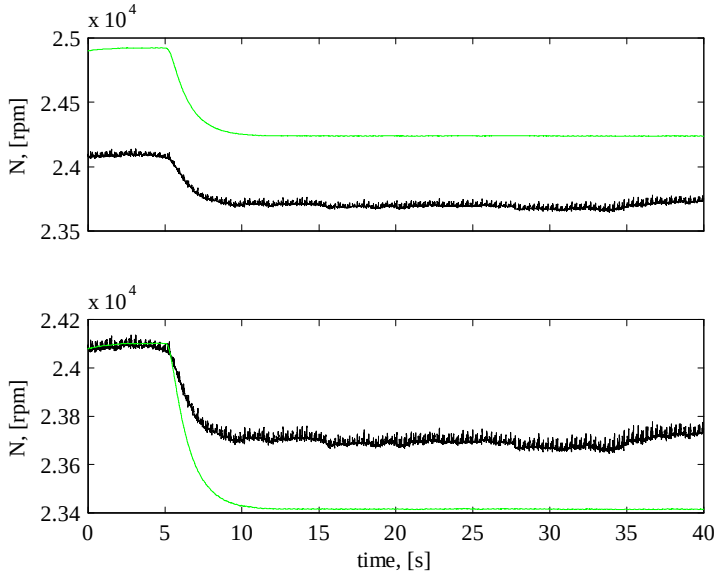

Figure C.41: Step 4 of Table 6.2

Estimated mass flow

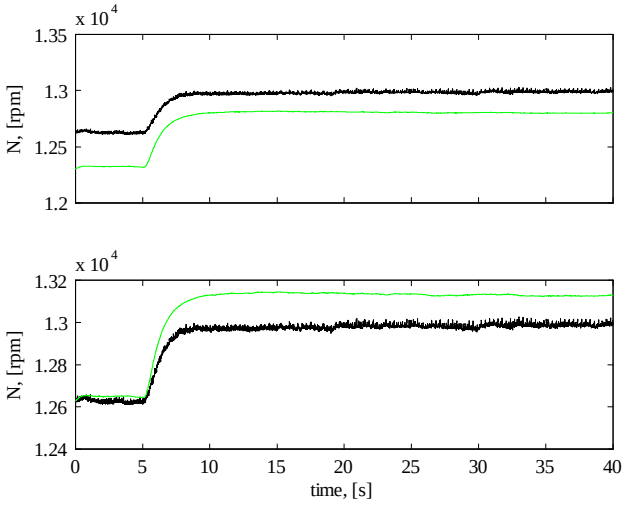

Figure C.42: Step 1 of Table 6.2

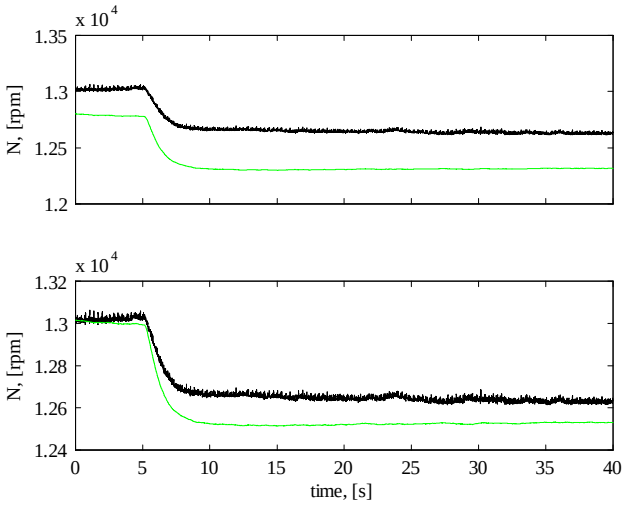

Figure C.43: Step 2 of Table 6.2

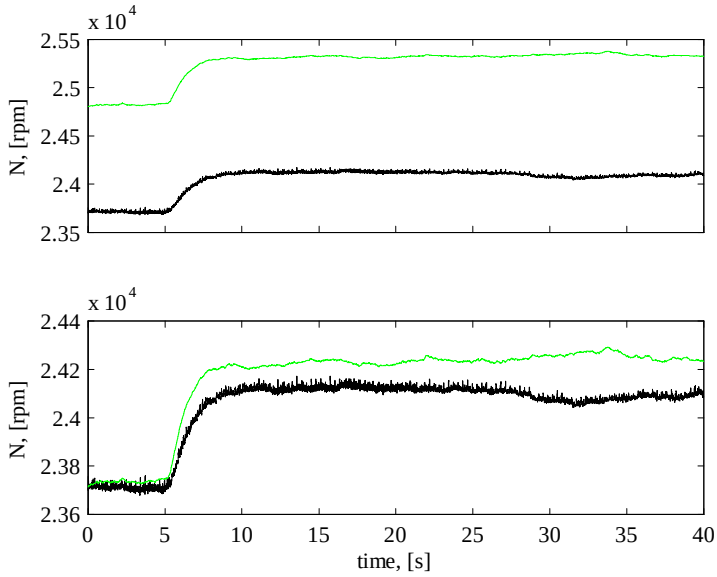

Figure C.44: Step 3 of Table 6.2

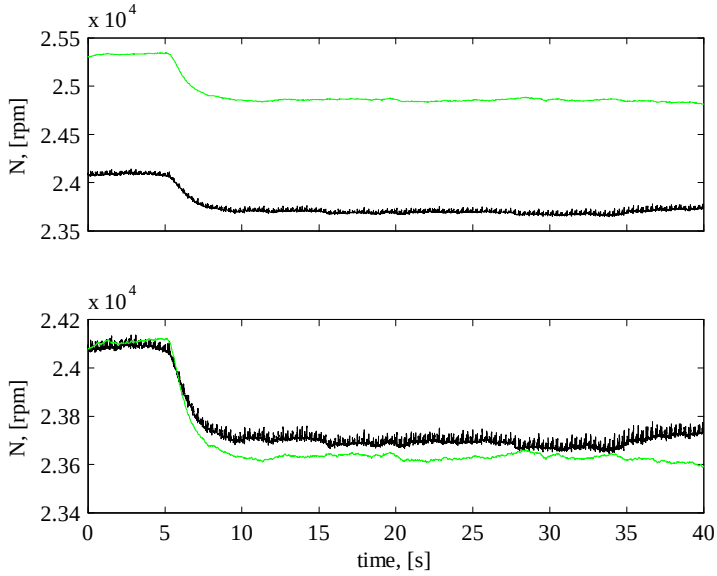

Figure C.45: Step 4 of Table 6.2

Appendix D

Figures for observer validation

D.1 Step data

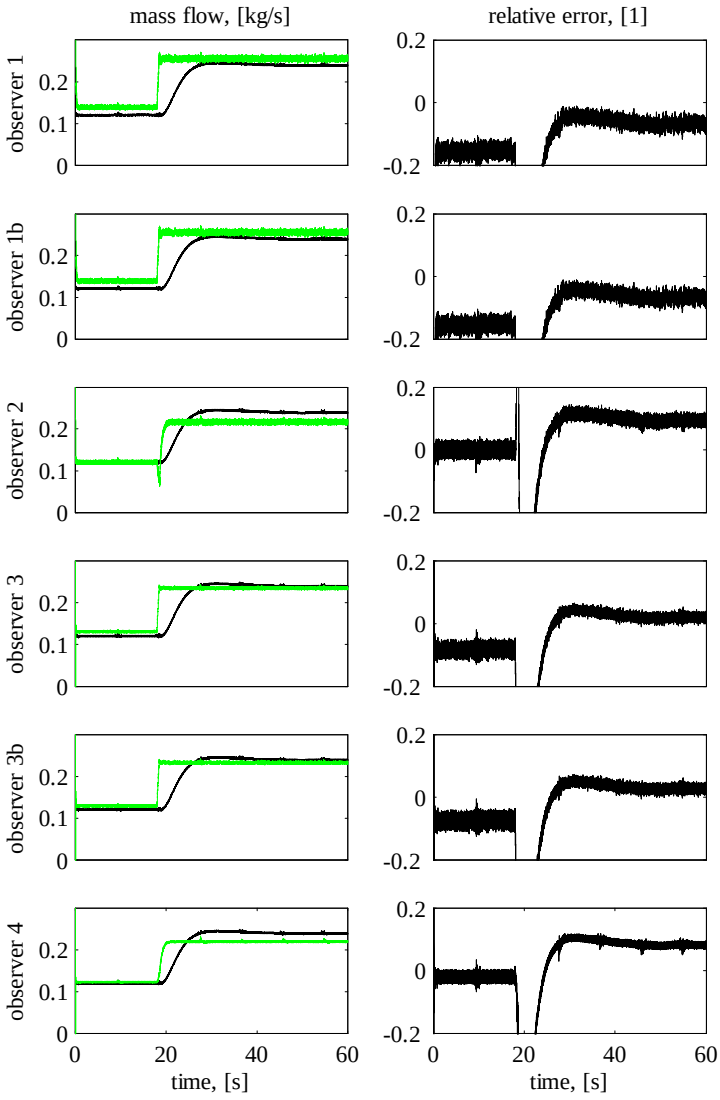

Figure D.1: Step data 1 of Table 7.2

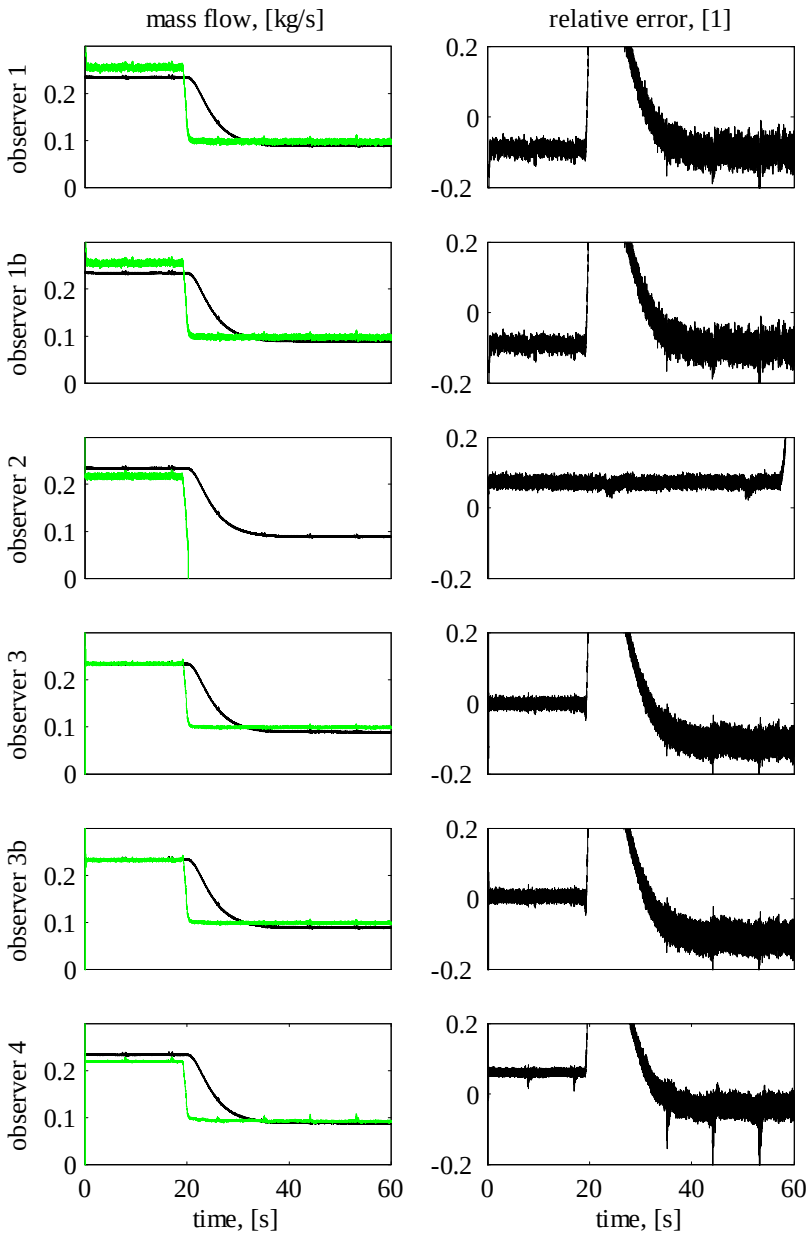

Figure D.2: Step data 2 of Table 7.2

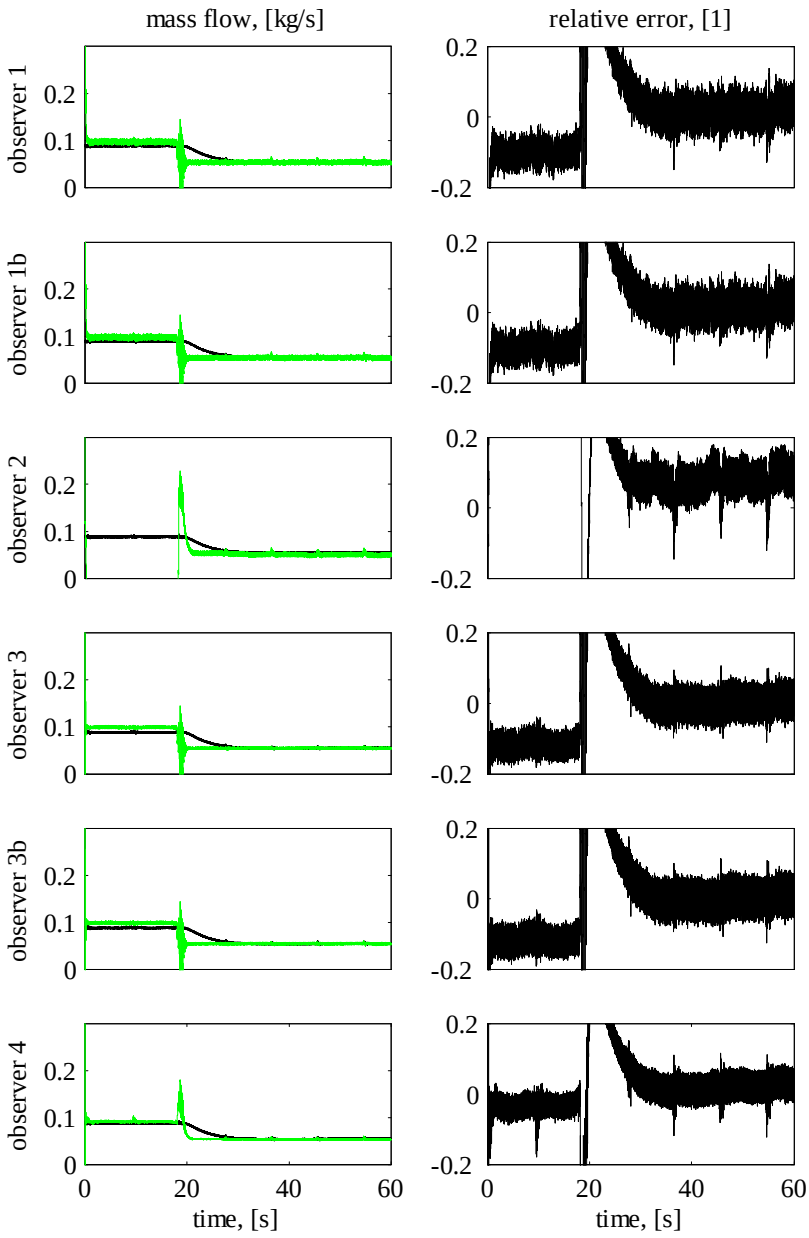

Figure D.3: Step data 3 of Table 7.2

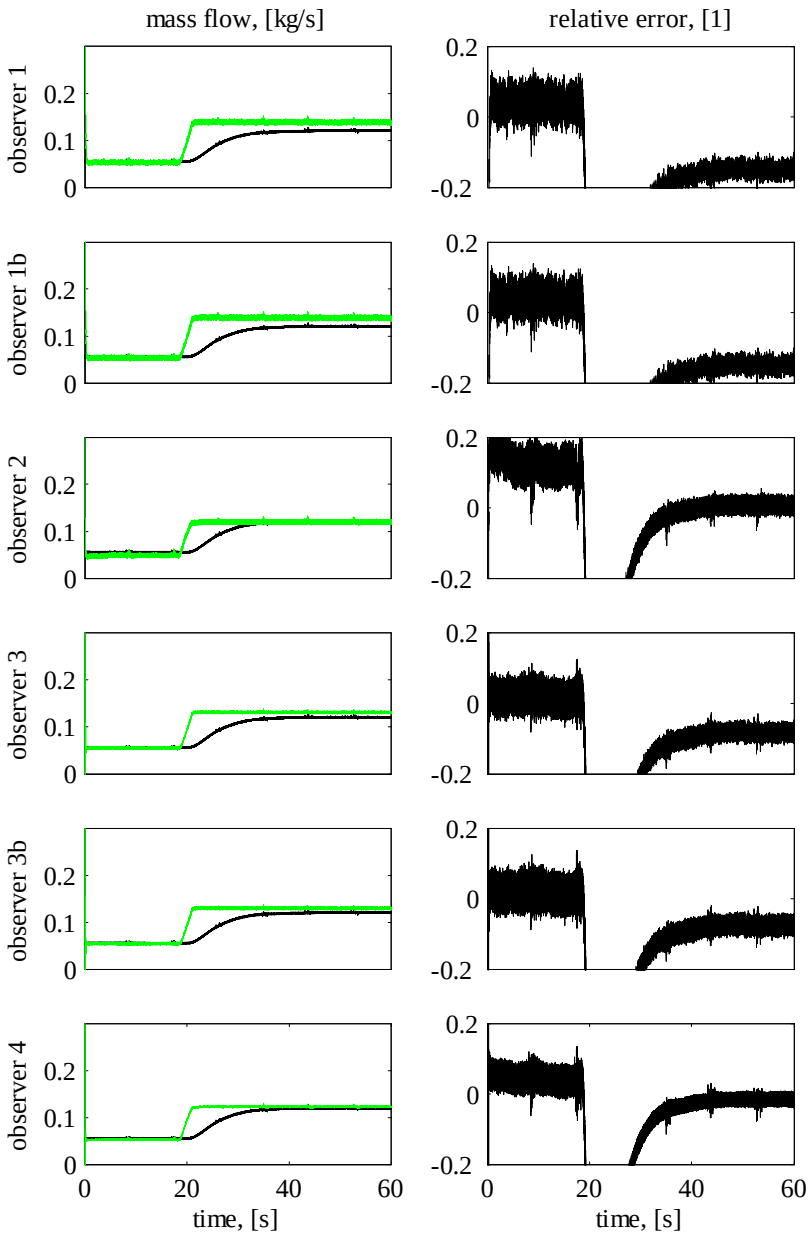

Figure D.4: Step data 4 of Table 7.2

D.2 Surge data

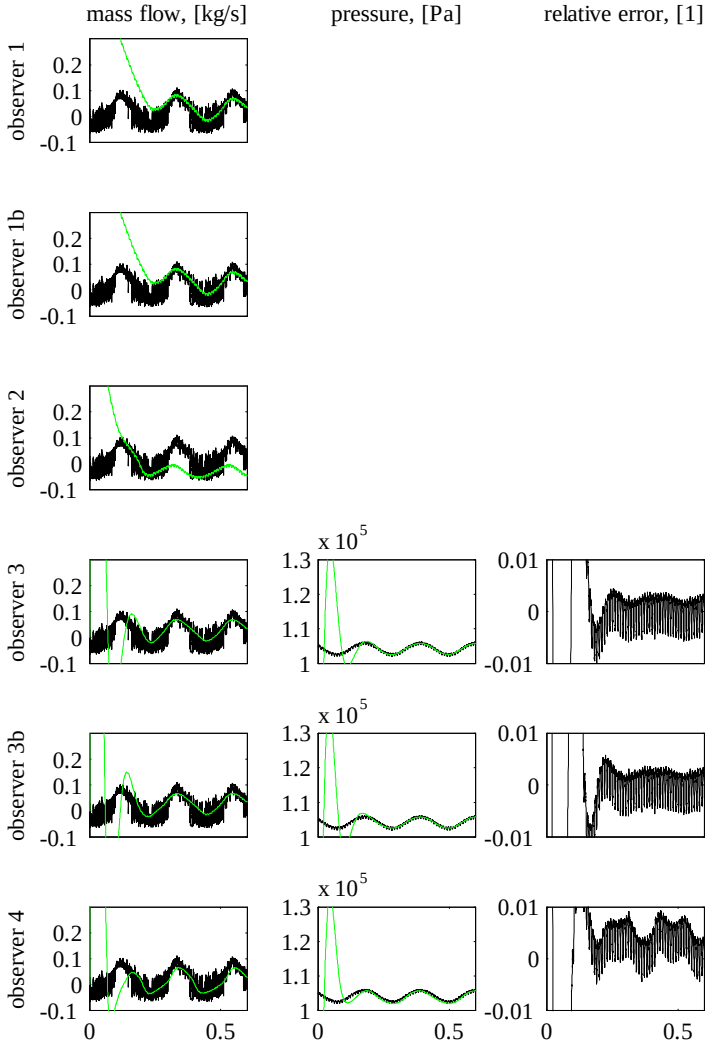

Figure D.5: Surge data 1 of Table 7.3

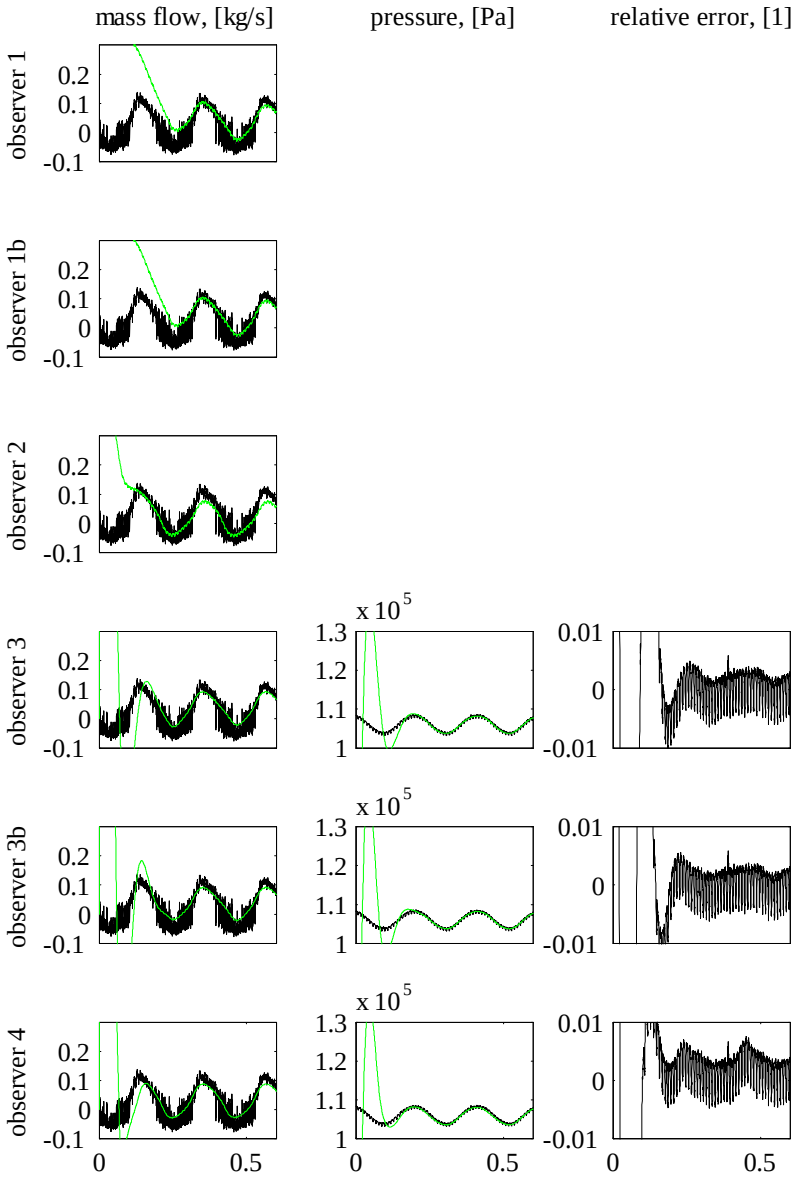

Figure D.6: Surge data 2 of Table 7.3

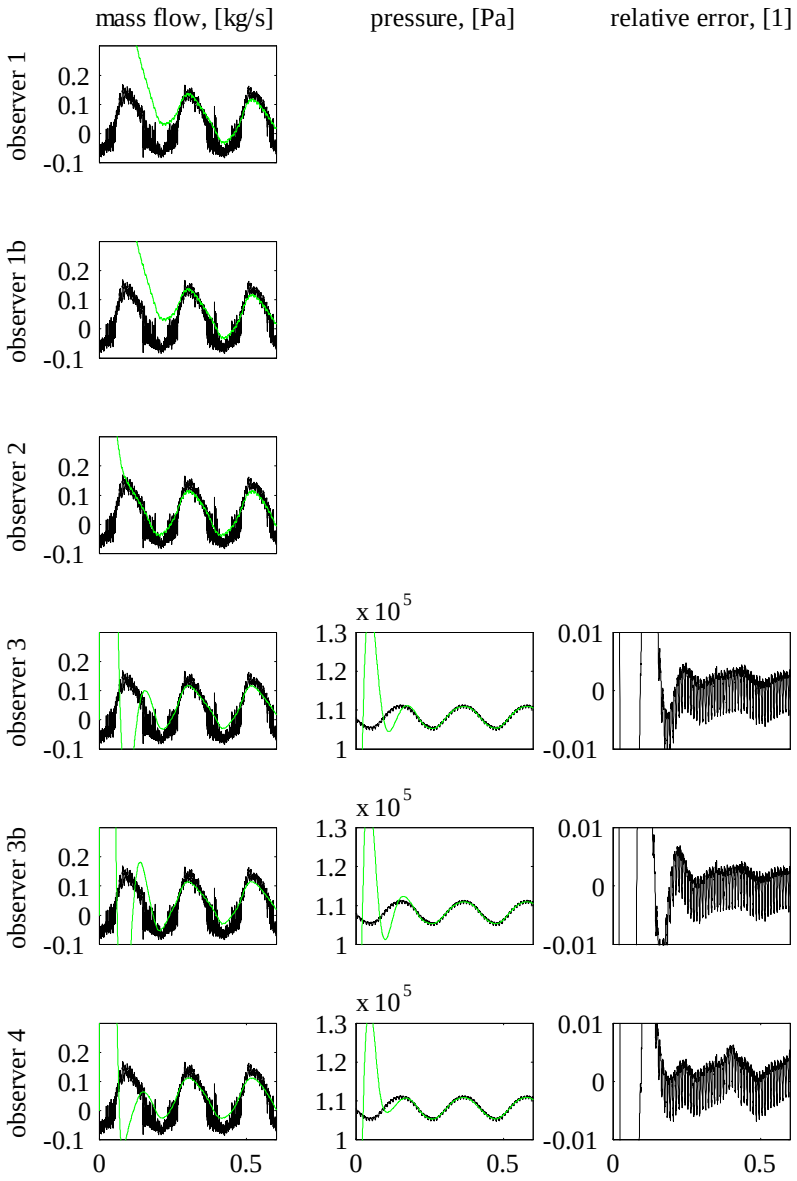

Figure D.7: Surge data 3 of Table 7.3

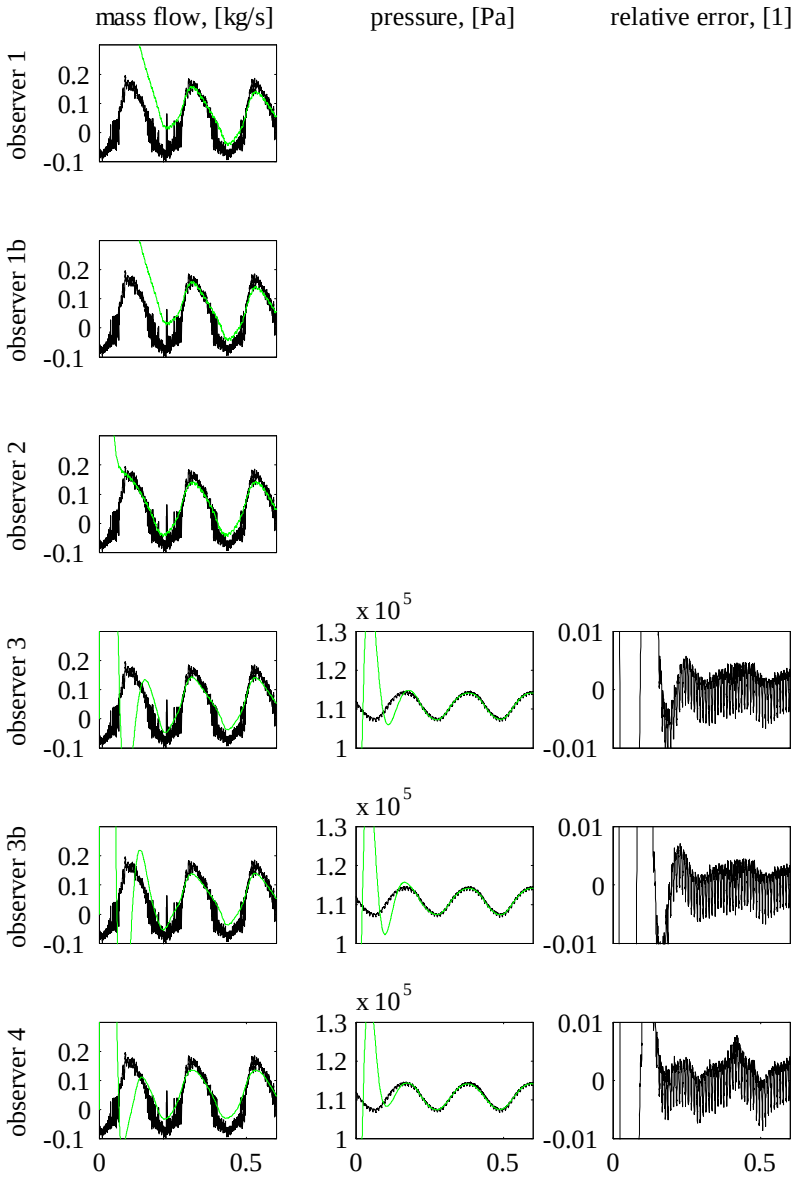

Figure D.8: Surge data 4 of Table 7.3

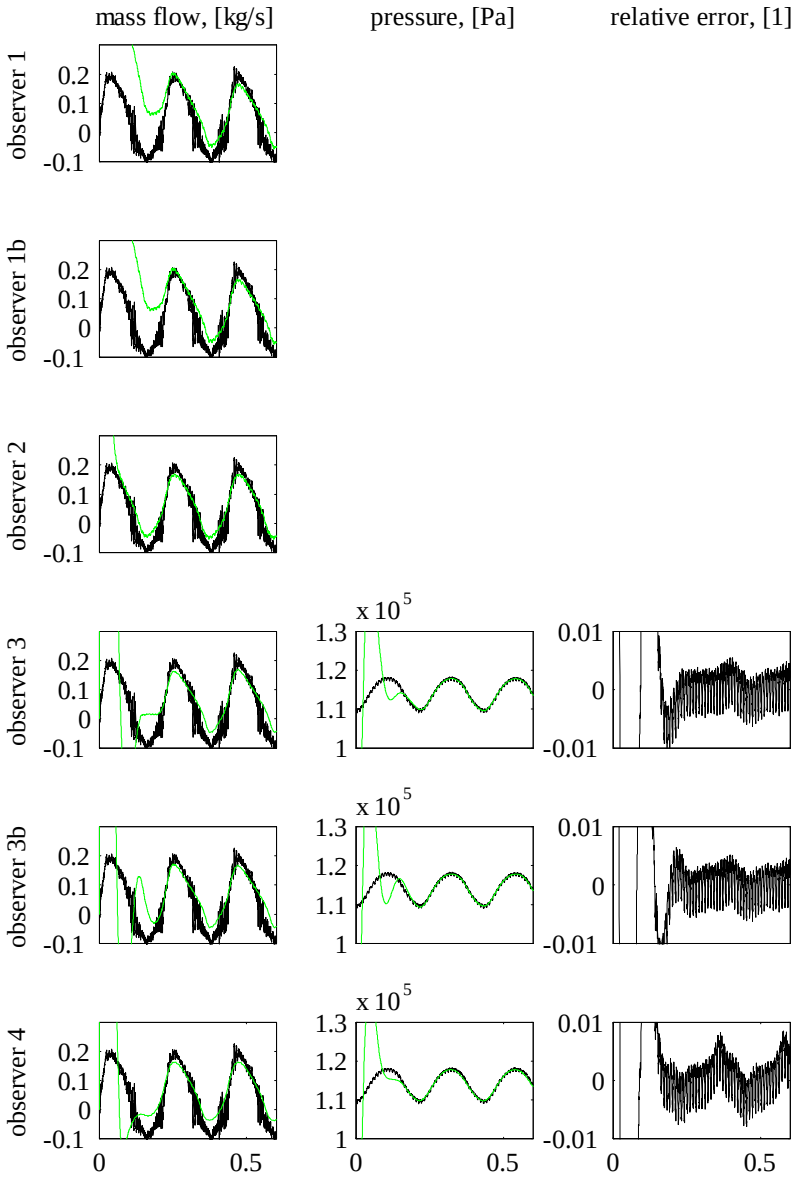

Figure D.9: Surge data 5 of Table 7.3

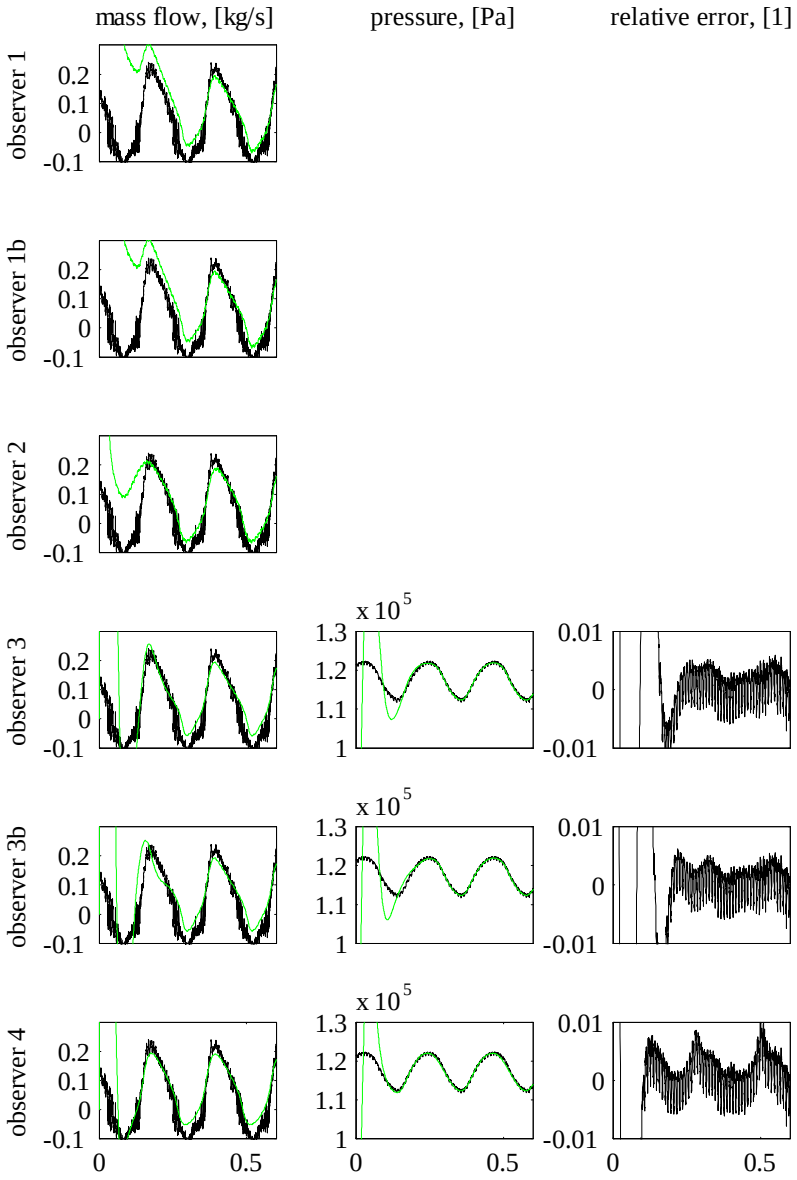

Figure D.10: Surge data 6 of Table 7.3

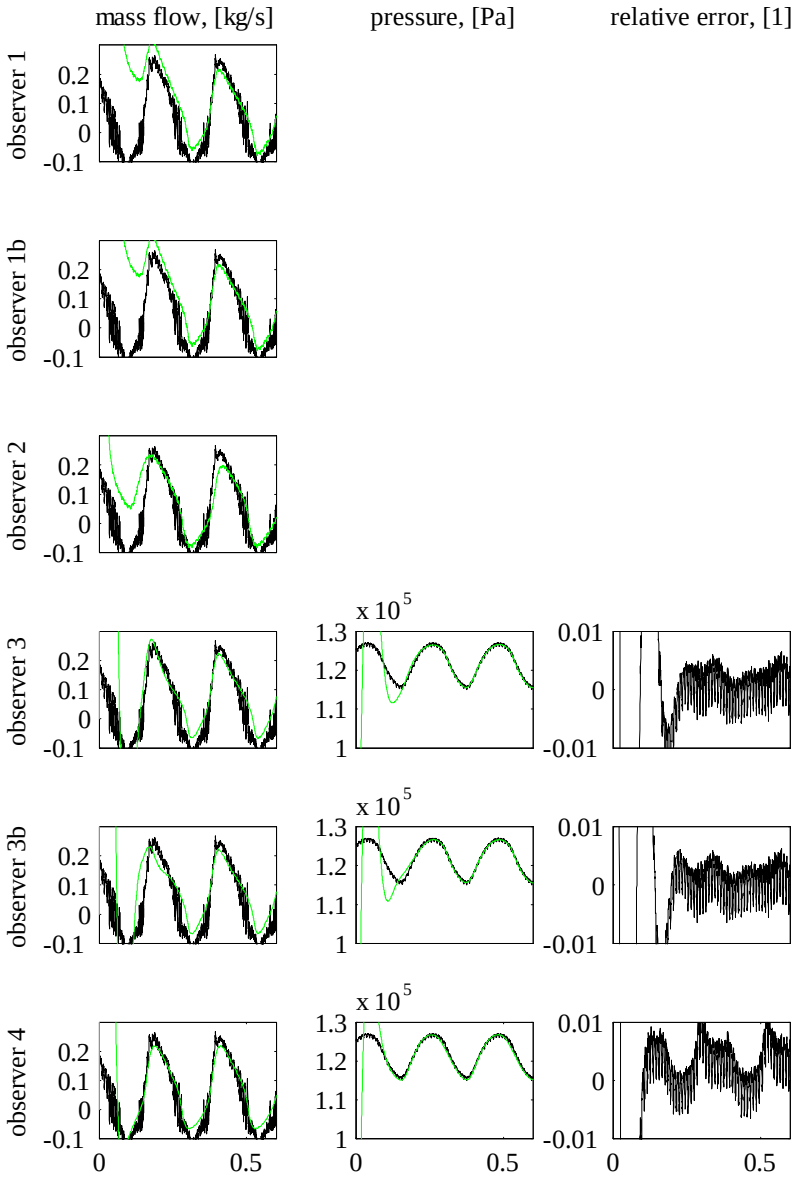

Figure D.11: Surge data 7 of Table 7.3

Appendix E

Figures for control validation

E.1 Speed control

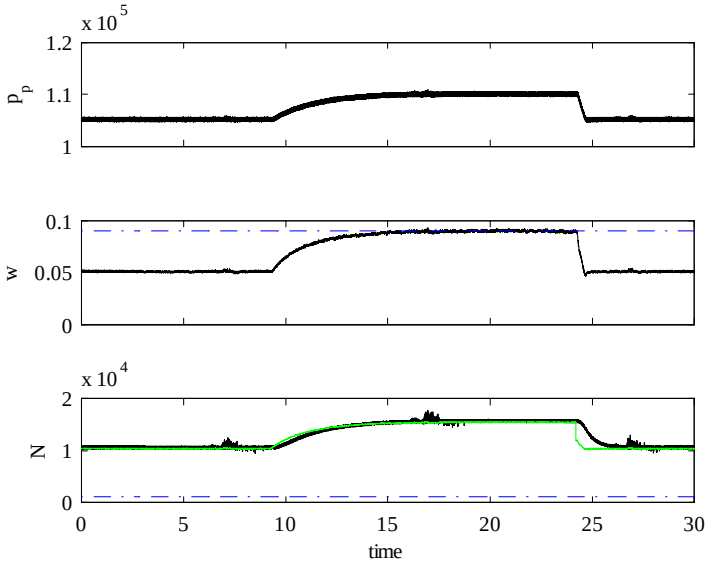

Figure E.1: Integral effect for $A_{\iota\%} = 70$

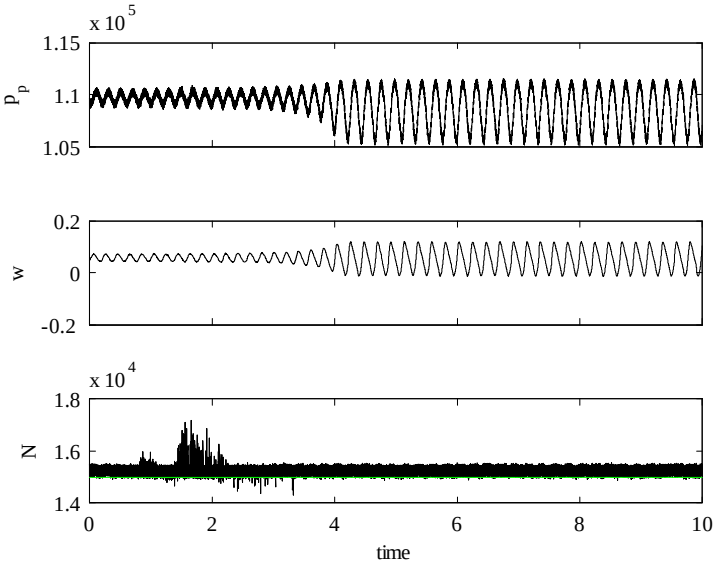

Figure E.2: Surge for $A_{t\%} = 56$

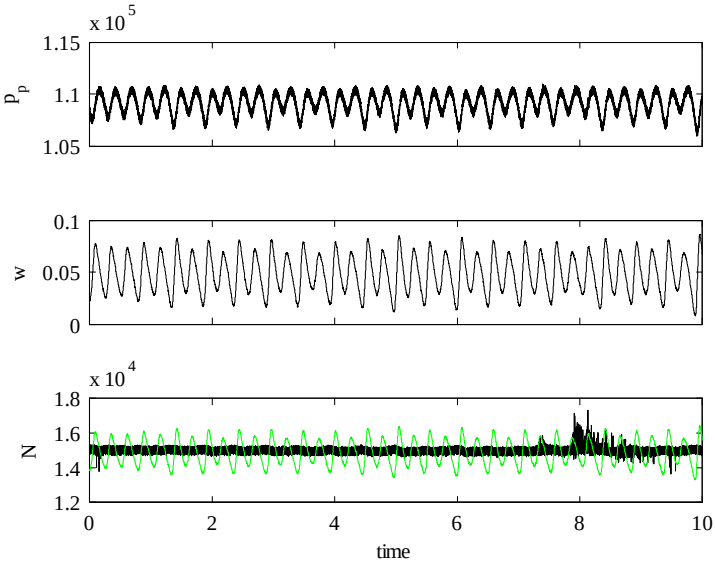

Figure E.3: Surge control for $A_{t\%} = 52$

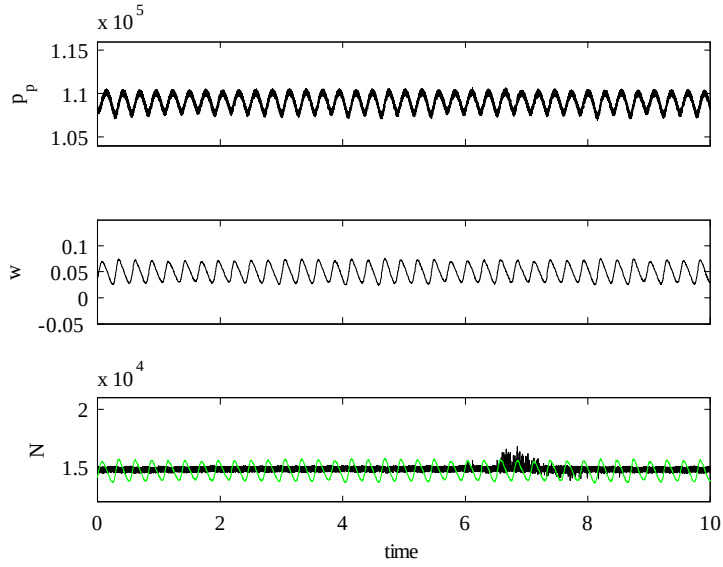

Figure E.4: Surge control for $A_{t\%} = 53$

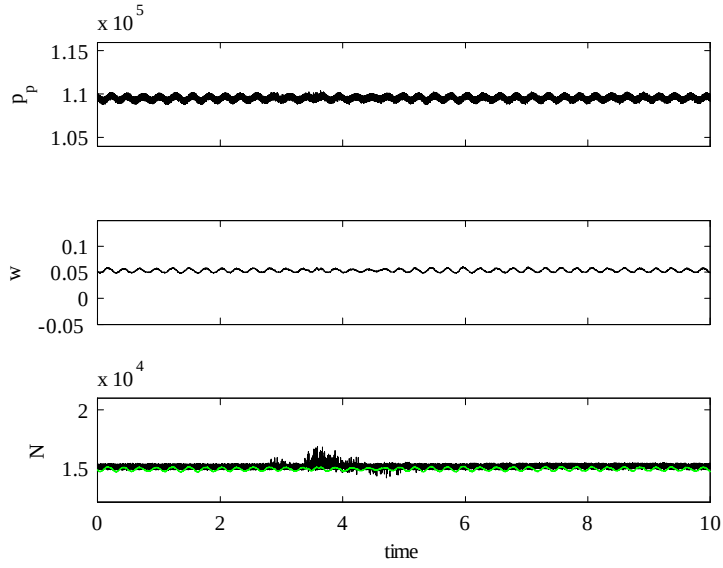

Figure E.5: Surge control for $A_{t\%} = 54$

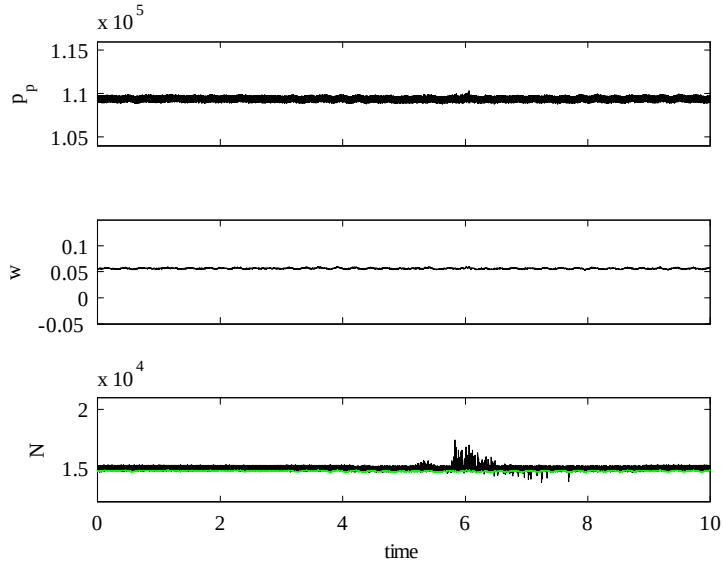

Figure E.6: Surge control for $A_{t\%} = 56$

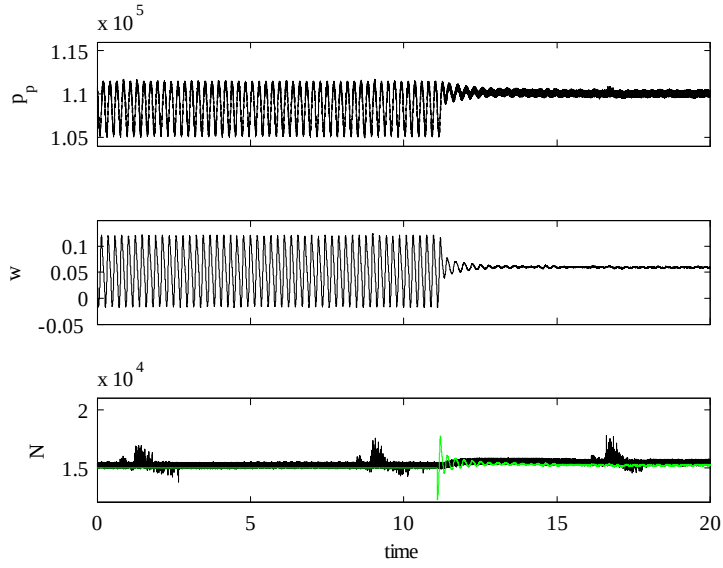

Figure E.7: Surge control for $A_{t\%} = 56$

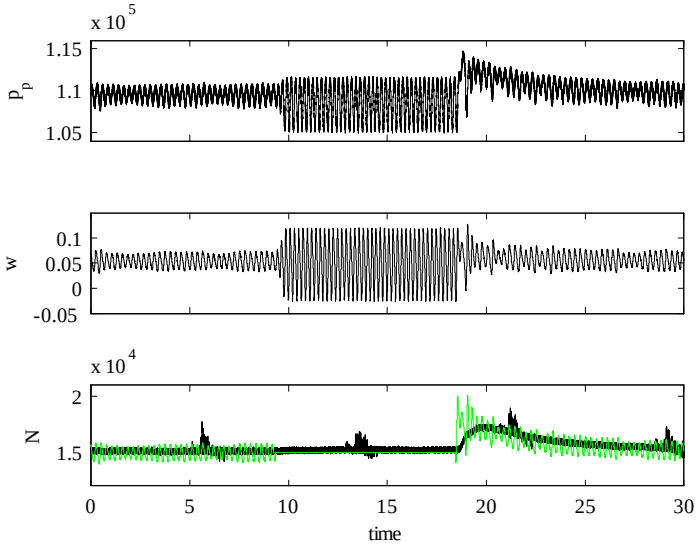

Figure E.8: Surge control for $A_{t\%} = 54$

E.2 Torque control

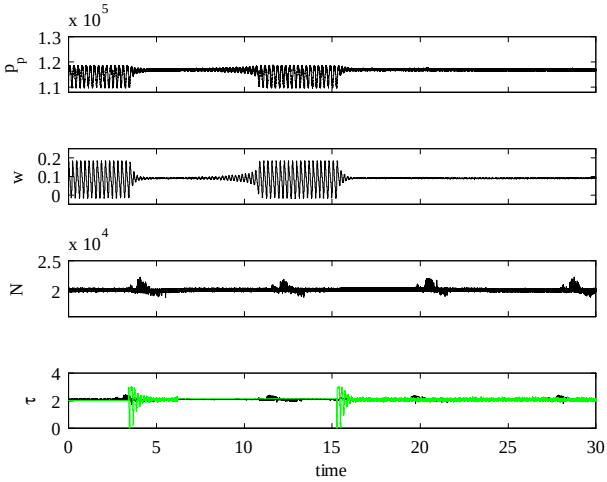

Figure E.9: Surge control for $A_{t\%} = 57$

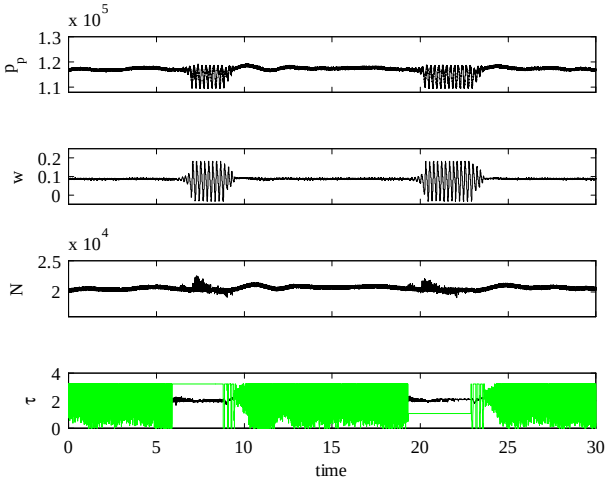

Figure E.10: Surge control for $A_{t\%} = 55$

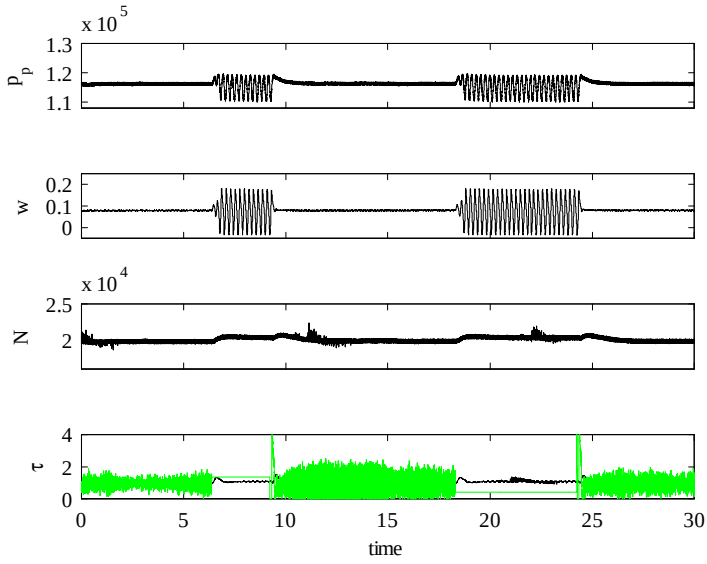

Figure E.11: Surge control for $A_{t\%} = 53$

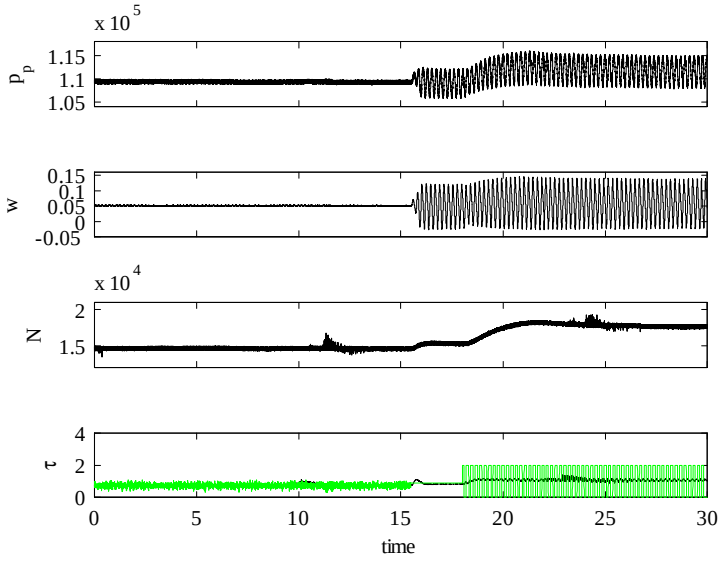

Figure E.12: Surge control for $A_{t\%} = 50$

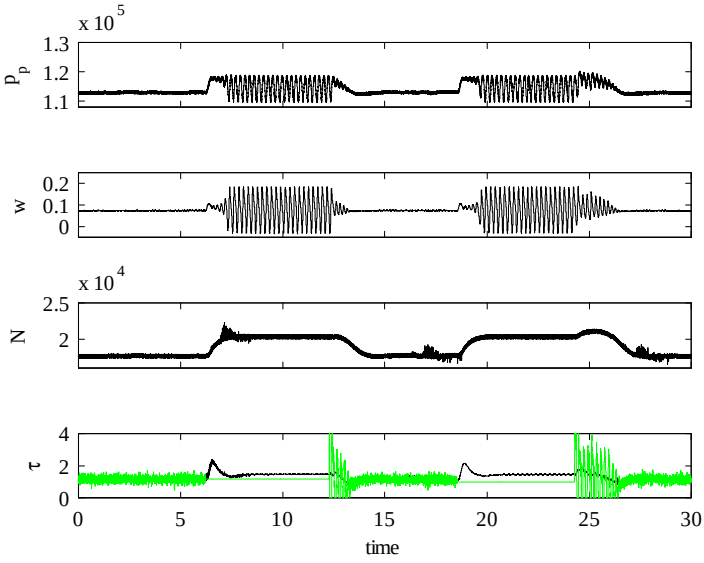

Figure E.13: Surge control for $A_{t\%} = 55$

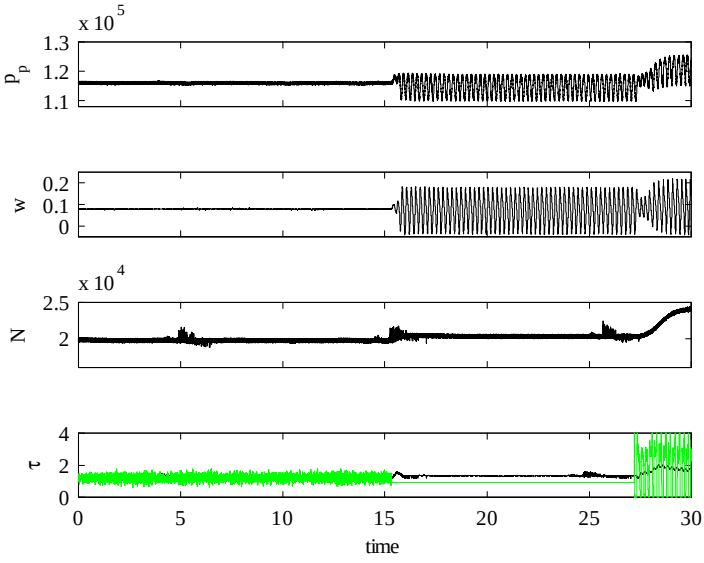

Figure E.14: Surge control for $A_{t\%} = 53$

References

[1] H. Krain. Review of centrifugal compressor's application and development. *Journal of Turbomachinery*, 127(1):25–34, January 2005.

[2] J. T. Gravdahl and O. Egeland. *Compressor Surge and Rotating Stall: Modelling and Control*. Advances in industrial Control. Springer, London, 1999.

[3] F. Willems and B. de Jager. Modeling and control of compressor flow instabilities. *Control Systems Magazine*, 19(5):8–18, October 1999.

[4] G. Gu, A. Sparks, and S. S. Banda. An overview of rotating stall and surge control for axial flow compressors. *IEEE Transactions on Control Systems Technology*, 7(6):639–647, November 1999.

[5] J. D. Paduano, E. M. Greitzer, and A. H. Epstein. Compression system stability and active control. *Annual Review of Fluid Mechanics*, 33(1):491–517, 2001.

[6] F. K. Moore and E. M. Greitzer. Theory of post-stall transients in axial compression systems: Part i - develupment of equations. *Journal of Engineering for Gas Turbines and Power, Transactions of the ASME*, 108(2):68–76, January 1986.

[7] E. M. Greitzer and F. K. Moore. Theory of post-stall transients in axial compression systems: Part ii - application. *Journal of Engineering for Gas Turbines and Power, Transactions of the ASME*, 108(2):231–239, April 1986.

[8] Z.S. Spakovszky. *Compressor Dynamic System Modeling*. Phd thesis, Department of Aeronautics and Astronautics, Massachusetts Institute of Technology, Cambridge, MA, USA, 2002.

[9] Z. S. Spakovszky. Backward traveling rotating stall waves in centrifugal compressors. *Journal of Turbomachinery*, 126(1):1–12, January 2004.

[10] W. W. Emmons, C. E. Pearson, and H. P. Grant. Compressor surge and stall propagation. *American Society of Mechanical Engineers, Meeting A-65*, 1953.

[11] E. M. Greitzer. Surge and rotating stall in axial flow compressors, part i: Theoretical compression system model. *Journal of Engineering for Power, Transactions of the ASME*, 98 Ser A(2):190 – 198, April 1976.

[12] E. M. Greitzer. Surge and rotating stall in axial flow compressors, part i: Experimental results and comparison with theory. *Journal of Engineering for Power, Transactions of the ASME*, 98 Ser A(2):199–217, April 1976.

[13] K. E. Hansen, P. Jorgensen, and P. S. Larsen. Experimental and theoretical study of surge in a small centrifugal compressor. *Journal of Fluids Engineering, Transactions of the ASME*, 103(3):391–395, September 1981.

[14] D. A. Fink, N. A. Cumpsty, and E. M. Greitzer. Surge dynamics in a free-spool centrifugal compressor system. *Journal of Turbomachinery*, 114(2):321–332, April 1992.

[15] O. Egeland and J. T. Gravdahl. *Modeling and Simulation for Automatic Control*. Marine Cybernetics, 2002.

[16] F. Willems. *Modeling and Bounded Feedback Stabilization of Centrifugal Compressor Surge*. Phd thesis, Eindhoven University of Technology, Eindhoven, The Netherlands, 2000.

[17] J. T. Gravdahl, F. Willems, B. de Jager, and O. Egeland. Modeling of surge in free-spool centrifugal compressors: Experimental validation. *AIAA Journal of Propulsion and Power*, 20(5):849–857, September 2004.

[18] H. K. Khalil. *Nonlinear Systems*. Prentice Hall, New Jersey, USA, 2002.

[19] J. T. Gravdahl, O. Egeland, and S. O. Vatland. Drive torque actuation in active surge control of centrifugal compressors. *Automatica*, 38(11):1881–1893, November 2002.

[20] A. H. Epstein, J. E. Ffowcs Williams, and E. M. Greitzer. Active suppression of aerodynamic instabilities in turbomachines. *Journal of Propulsion and Power*, 5(2):204–211, 1989.

[21] F. Blanchini and P. Giannattasio. Adaptive control of compressor surge instability. *Automatica*, 38(8):1373–1380, 2002.

[22] F. Blanchini, P. Giannattasio, D. Micheli, and P. Pinamonti. Experimental evaluation of a high-gain control for compressor surge supression. *Journal of Turbomachinery*, 124(1):27–35, January 2002.

[23] J. S. Simon, L. Valavini, A. H. Epstein, and E. M. Greitzer. Evaluation of approaches to active compressor surge stabilization. *Journal of Turbomachinery*, 115(1):57–67, January 1993.

[24] M. Van de Wal, F. Willems, and B. de Jager. Selection of actuators and sensors for surge control. *Journal of Propulsion and Power*, 18(1):84–92, 2002.

[25] J. T. Gravdahl and O. Egeland. Centrifugal compressor surge and speed control. *IEEE Transactions on Control Systems Technology*, 7(5):567–579, September 1999.

[26] A. Leonessa, W. M. Haddad, and H. Li. Globally stabilizing switching controllers for a centrifugal compressor model with spool dynamics. *IEEE Transactions on Control Systems Technology*, 8(3):474–482, May 2000.

[27] D.-C. Liaw, C.-C. Song, and J.-T. Huang. Robust stabilization of a centrifugal compressor with spool dynamics. *IEEE Transactions on Control Systems Technology*, 12(6):966–972, November 2004.

[28] B. Bøhagen and J. T. Gravdahl. Active control of compression systems using drive torque; a backstepping approach. *Proceedings of the 44th IEEE Conference on Decision and Control*, December 2005.

[29] B. Bøhagen and J. T. Gravdahl. Active surge control using drive torque: dynamic control laws. *Proceedings of the 45th IEEE Conference on Decision and Control*, December 2006.

[30] B. Bøhagen and J. T. Gravdahl. Control laws for active surge control of centrifugal compressors using drive torque. *Automatica*, May 2007. accepted for publication.

[31] M. Krstić, P. Kokotović, and I. Kanellakopoulos. *Nonlinear and Adaptive Control Design*. Adaptive and Learning Systems for Signal Processing, Communications, and Control. John Wiley & Sons, New York, USA, 1995.

[32] M. Krstić, D. Fontaine, P. V. Kokotović, and J. D. Paduano. Useful nonlinearities and global stabilization of bifurcations in a model of jet engine surge and stall. *IEEE Transactions on Automatic Control*, 43(12):1739–1745, December 1998.

[33] R. Lozano, B. Brogliato, O. Egeland, and B. Maschke. *Dissipative Systems Analysis and Control*. Communications and Control Engineering. Springer, London, 2000.

[34] O. O. Badmus, S. Chowdhury, and C. N. Nett. Nonlinear control of surge in axial compression systems. *Automatica*, 32(1):59–70, 1996.

[35] M. Arcak and P. Kokotović. Nonlinear observers: a circle criterion design and robustness analysis. *Automatica*, 37(12):1923–1930, 2001.

[36] S. P. Chaturvedi, N. A. Bhat. Output-feedback semiglobal stabilization of stall dynamics for preventing hysteresis and surge in axial-flow compressors. *IEEE Transactions on Control Systems Technology*, 14(2):301–307, March 2006.

[37] B. Bøhagen, O. Stene, and J. T. Gravdahl. A ges mass flow observer for compression systems: Design and experiments. *Proceedings of the 2004 American Control Conference*, June 2004.

[38] B. Bøhagen and J. T. Gravdahl. On active surge control of compressors using a mass flow observer. *Proceedings of the 41st IEEE Conference on Decision and Control*, December 2002.

[39] B. Bøhagen and J. T. Gravdahl. Circle criterion observer for a compression system. *Proceedings of the 2007 American Control Conference*, July 2007.

[40] X. Fan and M. Arcak. Observer design for systems with multivariable monotone nonlinearities. *Systems & Control Letters*, 50(4):319–330, December 2003.

[41] M. Arcak and P. Kokotović. Observer-based control of systems with slope-restricted nonlinearities. *IEEE Transactions on Automatic Control*, 46(7):1146–1150, July 2001.

[42] M. Arcak and P. Kokotović. Feasibility conditions for circle criterion designs. *Systems & Control Letters*, 42(5):405–412, April 2001.

[43] D. A. Fink. *Surge Dynamics and Unsteady Flow Phenomena in Centrifugal Compressors*. Phd thesis, Massachusetts Institute of Technology, June 1988.

[44] T. G. Beckwith, R. D. Marangoni, and J. H. Lienhard V. *Mechanical Measurements*. Pearson Prentice Hall, 6 edition, 2007.

[45] F. M. White. *Fluid Mechanics*. McGraw-Hill, 5th edition, 2005.

[46] J. van Helvoirt, B. de Jager, M. Steinbuch, and J. Smeulers. Modeling and identification of centrifugal compressor dynamics with approximate realizations. *Proceedings of 2005 IEEE Conference on Control Applications*, pages 1441–1447, August 2005.

[47] K. O. Boinov, E. A. Lomonova, A. J. A. Vandenput, and A. Tyagunov. Surge control of the electrically driven centrifugal compressor. *IEEE Transactions on Industry Applications*, 42(6):1523–1531, 2006.

[48] M. J. Moran and H. N. Shapiro. *Fundamentals of Engineering Thermodynamics*. Wiley, 3rd edition, 2007.